Geochemical and Petrographic Characterization of Platreef Pyroxenite Package P1, P2, P3 and P4 units at the Akanani Prospect area, Bushveld Complex, South Africa

By

Hakundwi Mandende

A thesis submitted in fulfillment of the requirement for the degree of

Magister Scientiae

In

Applied Geology

Department of Earth Sciences, Faculty of Natural Science, University of the Western Cape.

Supervisor: Dr. Abdi Mohamoud Siad

Co-Supervisors: Dr Russel Bailie and Prof. Charles Okujeni

November 2014

Geochemical and Petrographic Characterization of Platreef Pyroxenite Package P1, P2, P3 and P4 units at the Akanani Prospect area, Bushveld Complex, South Africa

Key Words

Bushveld Complex

Platreef

Akanani prospect area

Metasomatism

Platinum Group Elements

Base-Metal Sulphides

Multivariate statistics

Factor analysis

Cluster analysis

Discriminant analysis

Abstract

This study is focused on the Akanani prospect area, approximately 25 km north-west of the town of Mokopane, Limpopo Province where exploration geologists at the study area have classified the 'pyroxenitic' units into P1, P2, P3 and P4 units upward in order of succession with height based on their textures, mineralogy and colour. The primary aim of this study is to distinguish the distinctive geochemical and mineralogical characteristics that can be used to identify each unit (P1 to P4) and in so doing create major geochemical, petrographic and mineralogical variables that will help or facilitate the exploration for and recovery of PGE and BMS mineralisation. Geochemical and mineralogical variation studies were carried out on the cores from ZF044, ZF045, ZF048, ZF057, ZF078, ZF082 and M0023, located in the Platreef at the Akanani Prospect area on the farms Moordkopje 813LR and Zwartfontein 814LR. Using a combination of various multivariate statistical techniques (factor, cluster and discriminant analysis) and mineralogical studies (CIPW norm, microprobe analysis, petrography), the outcomes of the study have demonstrated that the Platreef at Akanani comprise at least four lithological units i.e. the basal pyroxenite portion referred to as the P1 unit comprises chromitite, pyroxenites and feldspathic pyroxenites with associated Cr, TiO_2, chromite, pyroxenes, hematite and Fe_2O_3, the mineralized section of the P2 unit is characterized by harzburgite, serpentinized harzburgite and in places orthopyroxenites are present consistent with high MgO and LOI contents, the feldspathic portion referred here as the P3 unit is characterized by a feldspathic pyroxenite containing higher Al_2O_3, Na_2O, K_2O, albite, hypersthene and SiO_2 and the top most portion of the P4 unit comprising CaO, Diopside, ilmenite, anorthite, apatite and P_2O_5 that can be interpreted to have formed by three separate magma pulses. Considering the possibility that the P4 unit is a hybrid melt of assimilated Platreef that interacted with intruding Main Zone magma, this reduces the number of magma pulses to two. The classification of P1, P2, P3 and P4 units of the Platreef at Akanani shows that the criteria used by mining personnel to classify the four lithological units is not definitive and therefore are not highly reliable. Although various multivariate statistical techniques were employed relatively similar elemental associations were obtained highlighiting the importance of this approach. The strongly positive correlation between sulphides, PGEs and chromite at Akanani is consistent with an orthomagmatic deposit that had been disturbed by significant hydrothermal activity, while in places a good BMS-PGE relationship is commonly associated with the main chromitite stringers in P1. Mineral and whole rock compositions of silicate rocks highlight the strongly magnesian nature of the ultramafic P2 unit. Mineral chemistry studies of chromite, orthopyroxene, olivine, clinopyroxene and plagioclase are consistent with the multi-

emplacement model. Convective exchange resulted in the enrichment of iron at the bottom of the stagnant chamber, while incompatible elements migrated upwards consistent with iron depletion with stratigraphic height. Injection of P1 magma and subsequent mixing with country rocks gave rise to the formation of chromitites and addition of plagioclase component to the intruding magma. A normal fractionation trend is suggested between P2 and P3 consistent with enrichment of MgO in P2 and enrichment of Al_2O_3, Na_2O, SiO_2 and K_2O in P3. The An% of 84.4 of plagioclase coupled with CaO enrichment in P4 is suggestive of some Main Zone influence and can be interpreted as resulting from partial melting and recrystallization of P3 in response to the intrusion of the Main Zone magma is suggested for the formation of the P4 unit. There exists a good correlation between the modal mineralogy and mineral chemistry as determined optically, the norm as determined by the CIPW norm and the whole-rock geochemical results as determined by multivariate statistics and conventional methods.

Abbreviations and Acronyms

Ab	**Albite**
AI	**Alteration Index**
ALM	**Average Linkage Method**
An	**Anorthite**
BC	**Bushveld Complex**
BIC	**Bushveld Igneous Complex**
BMS	**Base-Metal Sulphides**
CCPI	**Chlorite-Carbonate-Pyrite Index**
CIPW	**Cross, Iddings, Pirsson and Washington norm**
Cr	**Chromium**
CZ	**Critical Zone**
En	**Enstatite**
Fa	**Fayalite**
Fo	**Forsterite**
GCDKIT	**Geochemical Data Toolkit**
HFSE	**High Field Strength Elements**
HREE	**Heavy Rare Earth Elements**
IUGS	**International Union of Geological Sciences**
LGS	**Lebowa Granite Suite**

LILE	**Large Ion Lithiphile Elements**
LREE	**Light Rare Earth Elements**
LZ	**Lower Zone**
MREE	**Middle Rare Earth Elements**
MZ	**Marginal Zone**
Or	**Orthoclase**
P1 Unit	**Rock unit comprised of chromitites, pyroxenites and feldspathic pyroxenites**
P2 Unit	**Rock unit characterized by olivine-bearing rocks**
P3 Unit	**Rock layer pre-dominantly comprised of feldspathic pyroxenite**
P4 Unit	**Rock layer referred to as a melanorite**
PGE	**Platinum Group Elements**
PGM	**Platinum Group Metals**
ppm	**parts per million**
Pd	**Palladium**
Pt	**Platinum**
RGS	**Rashoop Granophyre Suite**
RLS	**Rustenburg Layered Suite**
RVS	**Rooiberg Volcanic Suite**
UZ	**Upper Zone**
Wo	**Wollastonite**
Wt.%	**Weight percent**

XRD **X-Ray Diffraction**

Declaration

I declare that “Geochemical and Petrographic characterization of the Platree Pyroxenite Package P1, P2, P3 and P4 units at the Akanani prospect area, Bushveld Complex, South Africa” is my own work, that it has not been submitted before for any degree or examination in any other university, and that all the sources I have used or quoted have been indicated and acknowledged as complete references.

Hakundwi Mandende

November 2014

Signed:……

Acknowledgements

I would like to acknowledge my primary and secondary sponsors Inkaba Ye Africa for their continued financial support throughout the production of this thesis.

This thesis embodies the number of years I have spent at the University of the Western. It comforts me through my struggles and challenges I faced throughout my academic years. Its completion has given me a glimmer of hope for a brighter future. My sincere gratitude goes to the Lord God almighty for giving me the courage, strength and motivation to complete this work. I am humbled and greatly indebted to my mentor, academic father and supervisor Dr. Abdi Siad who has guided me every step and shown undeserved patience towards me. I am very grateful to Dr. Russel Bailie and Prof Okujeni for their constructive advice and criticism of my work. I further extend my gratitude to my friends (Senzangakhona Ndumo, Adam Ramushu and Moses Magoba); family and extended family for their support and patience throughout the duration of my work. I am grateful to the technical staff (Mr Peter Meyer) and administration staff at the Department of Applied Geology for providing technical assistance that allowed the successful completion of this work.

‘This thesis is dedicated to my parents

Mr. Mpfariseni Wilson Mandende and Mrs. Christinah Matevhele Mandende’

Table of Contents

Table of Figures

List of Tables

List of Plates

Chapter 1

1.1 Introduction

The Bushveld Complex (BC), which underlies an area of more than 65,000 km^2 in north-eastern South Africa, is the world's largest layered igneous intrusion hosting many economically important ores: copper, tin, chromium, gold, vanadium, and platinum-group metals. The complex rests upon a floor of sedimentary rocks of the Transvaal System. This floor is structurally in the form of an immense oval basin, three hundred miles long and a hundred miles wide.

The Platreef forms part of the Upper Critical zone occurring at or near the base of the Northern Limb of the Bushveld Complex (Fig. 1.1). It is a 10-400m thick package of texturally heterogeneous pyroxenite, norite and gabbro-norite, containing numerous xenoliths of dolomite, calc-silicate shale (graphitic in part), quartzite and Fe- formation derived from the floor rocks (Harris and Chaumba, 2001). It represents an important resource of BMS and PGE, estimated by Vermaak (1995) to contain 6581 tonnes of PGE to a depth of 1200m. Three sectors divide the Platreef namely the Northern, Central and Southern sector. The Akanani prospect area is located in the Central sector of the Northern Limb comprising two adjoining farms (Zwartfontein 814LR and Moordkopje 813LR). The varying nature of the footwall along strike and down-dip from north to south makes it difficult for geologists to make accurate predictions on the location of mineralization. At Akanani, the Platreef rests upon granite floor with the exception of borehole ZF048 where the Platreef rests upon dolomitic floor.

Extensive Exploration activity conducted by AfriOre has been ongoing since 2004 with the aim of establishing a PGM resource with associated gold, copper, and nickel mineralization in the Platreef down-dip to a selected cut-off depth of 2000 meters in the west, being within the current depth of economic mining operations on the platinum mines in the Western Limb of the Bushveld Complex (Akanani, 2005). The main focus for this being the 9km of Platreef strike within the southern section 4km Platreef containing an inferred resource of 249 million ton (Van der Merwe, 2012). After acquiring 90% of the common shares over AfriOre in 2007, Lonmin has been conducting extensive exploration further re-evaluating the economic viability of the prospect (Van der Merwe, 2012).

This research aims at geochemically characterizing the four lithological units at the Akanani prospect area thereby determining the geochemistry of these units. This study will direct its efforts towards documenting and expanding geochemical and petrological data as well as scientific knowledge by giving a detailed geochemical and petrographical description of the Platreef pyroxenites on the farm of Zwartfontein 813LR and Moordkopje 814LR at the Akanani prospect area.

1.2 Previous work

The subjects of ore genesis, crustal contamination, fluid-rock interaction and magmatic processes have been subjects of recent focus in the Platreef (Harris and Chaumba, 2001; Ihlenfeld and Keays, 2011; Manyeruke et al., 2005). Many Authors have suggested a number of models describing how the Platreef could have formed and the processes involved in the distribution and concentration of PGE-Ni-Cu mineralization. Although these studies have added value to the already existing literature on the Platreef, the bulk of these investigations concentrated mainly on samples derived from the Sandsloot, Zwarfontein south and Overysel mine properties owned by Anglo Platinum. A limited number of studies relating to the geochemistry, petrology and mineralogy of Platreef pyroxenites at the Akanani prospect area have been published to date (Yudovskaya and Kinnaird, 2010; van der Merwe, 2012). Wagner (1926) described three distinct layers in the Platreef, which Buchanan (1979) later referred to as the A, B, and C reefs, from the base to the top based on texture and mineral mode. The A-reef occurs at the base of the stratigraphic column and is described by Lee (1996) as a heterogeneous feldspathic pyroxenite with sporadic base-metal sulphide (BMS) mineralization as well as variable grain-size. The B-reef overlies this layer and is described as a coarse-grained feldspathic pyroxenite containing between 50 and 90% orthopyroxene with the abundance of BMS mineralization and sporadic chromite-rich zones (van Der Merwe, 2012). At the top of the stratigraphic subdivision lies the C-reef which is described by Lee (1996) as a fine-grained poikilitic feldspathic pyroxenite that is depleted in BMS and PGM containing up to 70% clinopyroxene. Kruger (2010) also noted that the Platreef was divided into three units or reefs which he also termed the A, B and C reefs. He referred to the A-reef as a heterogeneous mixture of intrusive and country rocks which is in contact with the floor rocks and which changes character depending on the contact lithology. In addition, he noted that where Platreef is in contact with quartzite, there are fine-grained micro-gabbronorite chills preserved. Where sulphidic shales form the contact lithology, there is a

mixture of hornfels, sulphide-rich gabbronorites and pegmatoidal rocks that resulted from degassing and dehydration of the shales. Further North where the floor is dolomite, Kruger (2010) noted that the dolomites which include chert and thin shale bands form calc-silicate hornfels and the interaction with the magma also results in diopside-rich "parapyroxenite". Where magma interacts directly with granitic floor, the resulting partial melts formed felsic patches due to the interaction of mafic and felsic rocks. Kruger (2010) further described the B-reef as the main mineralized unit which is over 100m thick in places. He further described it as orthopyroxene-rich with abundant inclusions, xenoliths and large rafts of both the country rocks in the immediate vicinity and inclusions of chilled A-reef material and xenoliths of country rocks. According to Kruger (2010) the C-reef is a poorly mineralized websterite ranging in thickness from 0-30m.

Sections of the Platreef have been described in several papers prior to the A-B-C terminology being introduced and most of these papers describe how this subdivision is irrelevant to many parts of the Platreef (McDonald *et al.*, 2005). On the farm Drenthe 788LR, Gain and Mostert (1982) describe a basal feldspathic pyroxenite overlain by melanorites and norites, capped by a feldspathic pyroxenite. This subdivision did not match that suggested by White (1994). In the adjacent farm to the south, Overysel 815LR, Cawthorn *et al.* (1985) described the Platreef as commonly having a thin medium-grained norite at the base which grades upwards into a coarse pyroxenite with inhomogenous mineralogy, overlain by gabbro and norite. Recent work by (Armitage *et al.* 2002; Kinnaird *et al.* 2005) has also revealed limitations with the ''A–B–C'' terminology. The definitions of the reef types do not conform to the recognised IUGS classifications. Armitage *et al.* (2002) mapped faces at Sandsloot and noted that rocks corresponding to the A and C reef types were absent. Viljoen and Schürmann (1998) described the A-reef on the farm of Townlands as commonly consisting of coarse-grained norites and gabbros with minor sulphide mineralization. Furthermore, the B-reef and C-reefs were described as being pyroxenitic with the bulk of the mineralization and the highest grade found in the B-reef. The geochemical attributes that characterised the reefs has not been dealt with and remains a subject of investigation. Mitchell and Scoon (2012) identified three sub-units at the Akanani project area, and further referred to them as PU1, PU2 and PU3. According to Mitchell and Scoon (2012), the PU1 is a gabbronorite-websterite with minor feldspathic pyroxenite. The PU2 is a harzburgite with minor chromitite, while the PU3 is a feldspathic orthopyroxenite and

gabbronorite. In their study Mitchell and Scoon further described the PU1 as weakly mineralized and the most prominent lithological sub-unit and the PU2 and PU3 sub-units as containing the richest mineralization. This is in disagreement with the work of van der Merwe (2012) as well as a report published in 2006 by AfriOre, suggesting the presence of mineralization in P1 and P2, while P3 and P4 were considered barren or weakly mineralized.

The Platreef at Akanani is informally subdivided by Lonmin into 4 major lithological units (P1 to P4; from bottom to top; McDonald and Holwell 2011). Van der Merwe et al. (2012) noted that the P2 horizon was pegmatoidal in places and variably serpentinized, with increasing degree of serpentinization with depth. In this study van der Merwe et al. (2012) was able to describe the mineralogical composition of the P2 unit, but what differentiated the P2 unit geochemically from the other horizons remains a subject of investigation. In a report released in 2006 by AfriOre, the P1 unit was considered to be developed at the base of the Platreef and is locally well-developed and mineralized. The P2 horizon is well mineralized throughout, with abundant disseminated and zoned sulphides (AfriOre Limited annual report, 2006). Yudovskaya and Kinnaird (2010) noted that from the northern part of Tweefontein to the Central sector and sporadically in the Northern sector, a barren fine-grained feldspathic pyroxenite transitional to melanorite often occurs at the Platreef hanging wall contact no visible sulphides are contained within this unit and was locally referred to as the C-reef (White, 1994) or more recently as the P4 unit in the Akanani area by exploration geologists. In a study on facies variation in PGE mineralization in the Central Platreef, Yudovskaya and Kinnaird (2010) revealed that elevated PGE contents are also related to zones of massive and disseminated chromitites that occur as discontinuous layers within the top reef and at the bottom of the Platreef close to the footwall contact. The subdivision at Akanani does correspond to the A-B-C reef terminology, implying that Buchanan's (1979) subdivision of the Platreef may be applicable to certain areas of the Platreef and not a representation of the entire Platreef pyroxenite package as initially envisaged. The sequence of rock-types in the Platreef is complex, thus detailed geochemical and petrographic analysis of samples is required for the correct description of rock types. Hydrothermal fluids derived from Archaean basement has in one way or the other affected Platreef lithlogies, particularly by changing their initial $^{87}Sr/^{86}Sr$ ratios (e.g. Cawthorn et al., 1985; Barton et al., 1986). Manyeruke (2003) noted that the distribution of high-grade PGE-Ni-Cu mineralization within the Platreef was not entirely linked to floor rock composition. He further suggested that because

mineralization is localized within specific lithologies other factors must be considered. These included structural features such as faults, shear zones and post-magmatic hydrothermal activity. He also suggested that a correlation between serpentine formation and grade existed. It is the opinion of many workers (De waal, 1977; Manyeruke, 2003; Viljoen and Schürmann, 1998; Maier et al., 2007; Holwell and McDonald, 2006) that the correlation between the nature of the floor rocks and the grade of mineralization indicates an important role for floor rock assimilation and dolomite in particular, in ore genesis. The footwall at Sandsloot is dolomitic while the footwall at Zwarfontein is granitic towards the north, however the link between mineralization and alteration is not well-defined, therefore it is a possibility that the distribution of PGE-Ni-Cu mineralization is not only entirely linked to floor rock composition but the excess amount of hydrothermal activity. In a study by Holwell and McDonald (2007), the dolomite floor rock at Sandsloot released large volumes of fluids during assimilation and metamorphism, and subsequent serpentinization, whereas the largely anhydrous gneissic footwall at Overysel produced volatiles. Holwell et al. (2004) noted that characterization of the mineralization throughout the Platreef was still in its early stages, but initial results suggested that mineralization is particularly altered at localities that are underlain by dolomite (e.g Sandsloot and Zwartfonetin south). This resulted in sulphide resorption and the formation of platinum group minerals (Manyeruke, 2007). McCutcheon (2012) noted that the Platreef lithologies may have been locally modified by late-stage felsic and hydrothermal fluids, forming platinum group minerals (PGMs) such as bismuthides and arsenide-dominated PGM assemblages, primarily hosted in quartz and serpentine respectively. At other localities where the footwall is granite/granite gneiss (e.g. Townlands, Overysel) Manyeruke (2003) noted that the original sulphide assemblage was preserved. This was indicated by well-defined positive correlations between the IPGE (Os-Ir-Ru) and (Rh-Pt-Pd) and between the PGE and S (Manyeruke, 2003). If the floor rock does not entirely control the distribution and concentration of PGE-Ni-Cu mineralization, then another process must be responsible for decoupling of PGE from BMS. Holwell and McDonald (2006) noted that where the floor rock is anhydrous such as the Archaean granitic floor rock at Akanani, there is limited fluid activity and PGE behavior is controlled by the behavior of sulphide liquids, producing an intimate PGE-BMS association. This view was further supported by McCutcheon (2012) who noted that the significant PGM-BMS association within the Platreef and footwall lithologies may have been due to a downward

migrating sulphide melt that may have been responsible for the redistribution and remobilization of PGEs, predominantly Pd which migrated into the Platreef and footwall lithologies. The anhydrous nature of the granitic footwall at Akanani implies that the deposition of PGE mineralation is not controlled by hydrothermal fluids, but rather the downward migration of a sulphide liquid (Holwell and McDonald, 2006), however post-magmatic hydrothermal activity may have played a significant role in the redistribution and remobilization of PGE-BMS mineralization. Holwell and McDonald (2006) further noted that the lack of hydrothermal interaction and overprinting in the area of the Platreef that overlies the Archaean basement as opposed to the Transvaal sediments may raise the possibility that mineralization style present at Overysel is not as a result of remobilization and recrystalliation, but rather a more primary style of mineralization. Hydrothermal fluids are believed to play an important role in the re-distribution of PGEs and often creates lower Pt/Pd ratios in altered areas (McCutcheon, 2012). These findings are consistent with reports from south of Tweefontein by (Hutchinson and Kinnaird, 2005; Kinnaird, 2005; Manyeruke et al., 2005) and at Sandsloot to the North by (Armitage et al., 2002; Holwell et al., 2006).

White (1994) provided a description of the Platreef at several localities. He reported that the PGE grades in the Platreef are controlled by the nature of the floor rocks. He also noted that grades are relatively higher where the floor rocks consists of dolomite, but lower where the floor rock consisted of granite, iron-formation or shale. Kinniard et al. (2005) reported that where the footwall is Malmani dolomite (e.g. Sandsloot open pit), the PGE grade of the Platreef is typically > 4g/t where mined. Elsewhere on granite or silica-rich metasedimentary footwall rocks, the grade is typically 1-2g/t over many meters, with intersections sometimes of >10g/t. In a study by Djon and Barnes (2012) in the Roby, Twilight and the high grade zones of the Lac Iles Complex in Canada they concluded that although the BMS and PGE assemblage changed during metamorphism and late magmatic fluid circulation, the change in BMS did not change ore-grade.

The greatest challenge facing mining personell is not only the changing nature of the footwall rocks along strike, but finding a definitive criterion for characterizing these Platreef lithologies. Identifying geochemical fingerprints that can be used to accurately distinguish between barren and mineralized pyroxenites requires an understanding of geochemistry and mineralogy of these rock types. Mining companies often seek methods that can provide a quick and cost-effective

way of determining drilling targets. Siad et al. (1994) used discriminant analysis to geochemical data of lateritic soils from southwestern and central Nigeria where they successfully distinguished between barren and mineralized rock units. This approach depends upon appropriate reference groups of available geochemical data (Siad et al., 1994). They further reported that the selection of appropriate variables for the formulation of a discriminant function is an integral part of the discriminant analysis. For the better understanding of alteration systems, many researchers have used alteration indices, which were derived from major elements. Gifkins et al. (2005) noted that the degree of alteration is an indication of how completely a rock has reacted to produce new minerals and textures, and is independent of the alteration process. Alteration indices are very significant as they estimate the degree to which a rock had been altered.

1.3 Aims and Objectives

The Platreef is comprised of a 10-400m thick package of pyroxenites, feldspathic pyroxenites, norites and gabbronorites (Hutchinson and Kinnaird, 2005; Maier et al., 2007) that displays layering that cannot be correlated from core to core, even with cores drilled adjacent to one another. The succession of the Platreef lithologies has not been well defined in recent literature. White (1994) concluded that the Platreef was characterized by three reefs, the A, B, and C reef and the geochemical character of these “so called” reefs is still a subject of research.

A major concern to exploration efforts in the Platreef remains in the inability to predict the geological controls of the style and grade of the mineralization within the Platreef along strike and down-dip (Siad et al., 2012, unpublished report). In addition, because of the complexity and spurious variability of metasomatized rocks, a clear criteria for lithostratigraphic and lithogeochemical correlation of the Platreef rock succession at the Akanani prospect has not been provided (Siad et al., 2012, unpublished report).

In order to gain a further understanding of the geochemical characteristics differentiating each layer (P1-P4) a study on their geochemistry and petrography was undertaken on 53 core samples from seven boreholes (ZF044, ZF045, ZF048, ZF057, ZF078, ZF082, M0023) drilled at the Northern Platreef on the adjoining farms of (Moordkopje 813LR and Zwartfontein 814LR). With the geological background in mind the present study has three major aims.

- The first is to distinguish between the distinctive petrographical, geochemical and mineralogical characteristics that can be used to identify each layer and in so doing determine geochemical element associations characterizing each of these pyroxenite layers.
- The second is to check geochemically and petrographically the realiability and enhance if necessary, the classification of the pyroxenite layers as provided by Akanani mining personnel
- Third is to create major geochemical, petrographical and mineralogical variables that will help or facilitate the exploration for and recovery of PGE and BMS mineralisation further assisting mining personnel to locate themselves within the Platreef of the study area.
- To develop cost and time effective methods and recommend tools that can enhance the exploration for PGE-BMS mineralization.

1.4 Regional Geology

The 2050 Ma old BC in South Africa (Fig. 1.1), is the largest mafic-ultramafic layered intrusion in the world covering an area of approximately 65,000 km^2 with a thickness of 3-9km, and hosts the largest known deposits of chromium (Cr), Vanadium (V) and platinum-group elements (PGE's) (Walraven et al., 1990). The BC, as a whole, comprises four major magmatic suites: the bimodal **Rooiberg Volcanic Suite** (RVS) (Buchanan et al., 2002), the **Rashoop Granophyre Suite** (RGS) (Walraven, 1985), and the **Lebowa Granite Suite** (LGS) (Walraven and Hattingh, 1993) and the largest mafic-ultramafic layered intrusion on Earth the **Rustenburg Layered Suite** (RLS), measuring ca.65000km^2 (Barnes and Maier, 2002). The RLS may be divided into three limbs: the Western Limb (where most of the older mines are found), the Eastern Limb and the Northern Limb (where mining activity continues) (Fig. 1.1). The Western and Eastern Limbs are the best known, being the most extensive, with average strike lengths of ~200 km. The Northern Limb is partially concealed beneath younger rocks of the Waterberg Supergroup, the Far Western Limb is an eroded remnant, and the Bethal Limb is only identifiable through some gravity high, with its location confirmed by bore-core data (Eales and Cawthorn, 1996). It should

be noted that much of the literature on the BC focuses on the RLS as compared to the LGS and RGS. This is mainly due to the large economically viable deposits developed in the RLS.

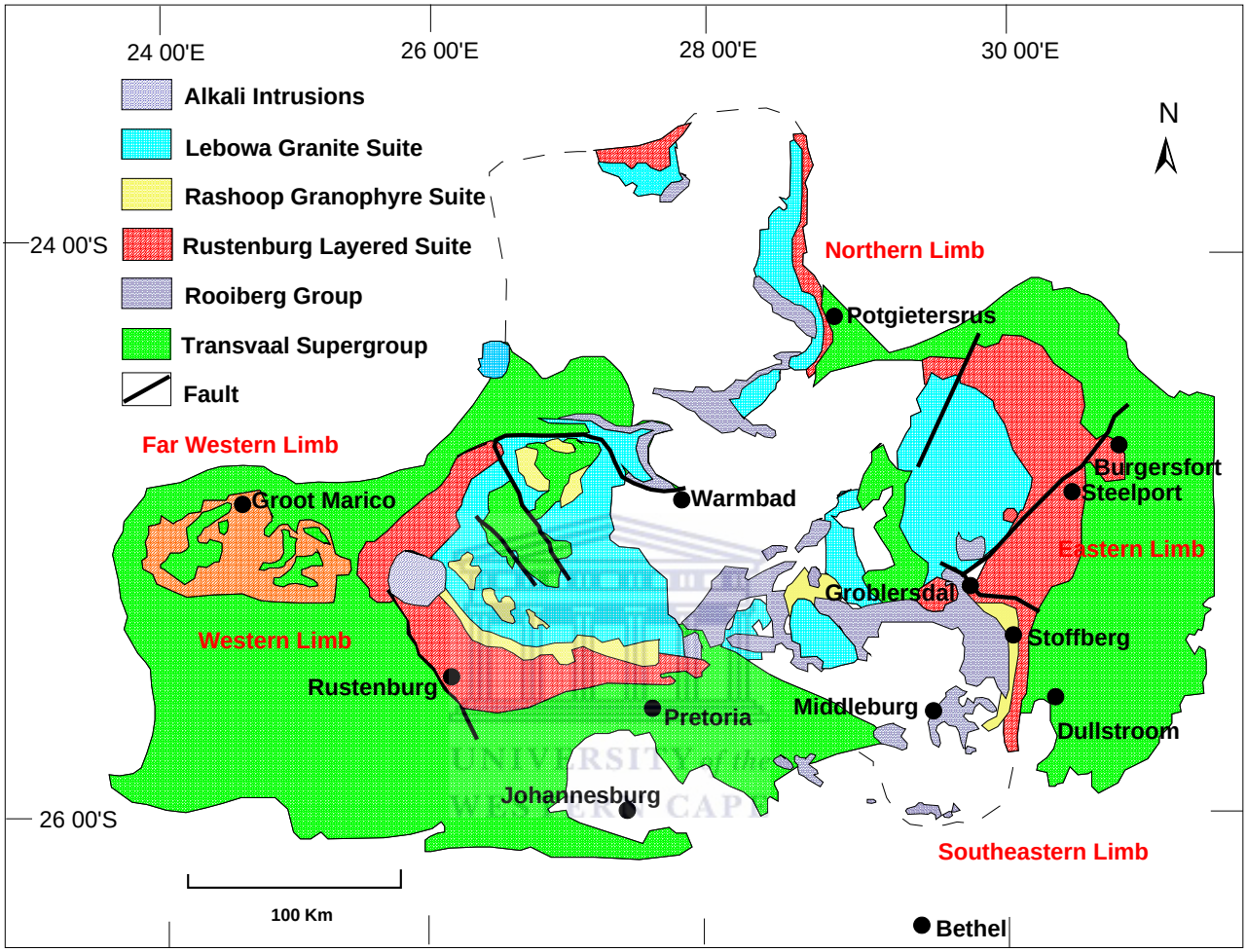

Figure 1.1: Geological map of the Bushveld Complex including the three major lobes (Northern, Eastern and Western Lobes). Map modified after Cawthorn and Lee (1998).

The Rustenburg Layered Suite (RLS) forms the largest layered intrusion (400 km by 300km in area and approximately 7km to 8km thick). Hall (1932) reported that the RLS was generally subdivided into five zones: the basal Marginal Zone, overlain by the Lower Zone, the Critical Zone (1300m to 1800m of, the Main Zone and the Upper zone (Fig. 1.2). The **Marginal Zone** is a fine-medium grained heterogeneous Gabbronoroitic unit that is generally depleted off mineralization. Its thickness ranges from (0-800m) of norites (Hall, 1932). The **Marginal Zone**

(MZ) contains variable amounts of quartz and biotite reflecting assimilation of variable floor rocks (Manyeruke, 2007). It is well developed in the Western and Eastern Limbs where it is generally referred to as "Shelter Norite"in the former and "Kolobeng Norite" in the latter (SACS, 1980). The **Lower Zone (LZ)** overlies the **Marginal Zone** and is approximately 800m wide with a maximum thickness of about 1700m in the Eastern Limb (Cameron, 1978). The **Lower Zone** is generally comprised of bronzitites, harzburgites, and dunites (Cameron, 1978). This Zone is present in the Western, Eastern and Northern Limbs of the Bushveld Complex. In the Western Limb, it is divided into four subzones namely; the Eerlyk Bronzitite (Basal Subzone) at the base, this is inturn overlain by the by the Makgobe bronzitite (Lower Bronzitite Subzone), followed by the overlying Groenfontein Harzburgite (Harzburgite Subzone) and the Tweelaagte Bronzitite (Upper Bronzitite Subzone) at the top (SACS, 1980).In the Eastern Limb, the **LZ** comprises orthopyroxenite rocks (Eales and Cawthorn, 1996) namely the Clapham Bronzitite (Basal Zone) at the base, which is inturn overlain by the Rostock Bronzitite (Lower Bronzitite Subzone); this is in turn followed by the Jagdlust Harzburgite (Harzburgite Subzone) in the middle and the Serokolo Bronzitite (Upper Bronzitite Subzone) forms part of the top portion of the **LZ** (Von Gruenewaldt et al., 1985). In the Northern Limb, the basal unit is known as the Volspruit Pyroxenite (Lower Pyroxenite Subzone) and is overlain by the Drummondlea Harzburgite (Harzburgite Subzone) and the Moorddrift Harzburgite Pyroxenite (Upper Pyroxenite subzone) that forms the top (Hulbert and Von Gruenewaldt, 1982).

Overlying the **LZ** is the **Critical Zone (CZ)** attaining a maximum thickness of between 1300-1800m. The base of the **CZ** is marked by the incoming of cumulus chromite. Two parts divides the **CZ** namely; the **Lower Critical Zone** that comprises bronzitites, chromitites, and some harzburgites; the **Upper Critical Zone** comprising incoming cumulus plagioclase which can itself be divided into two parts (Cameron, 1978) (1) a lower part comprising anorthosites, norites and minor bronzitites that occur in no systematic order and define no classical cyclic units (2) an upper part comprising UG-1 chromitite unit at the base further comprising units made up of a regular succession of rock types, consisting of some or all of chromitites, harzburgite, bronzitite, norites, and anorthosites usually occurring in that order (Cameron, 1978). The Main Zone overlies the Critical Zone with a thickness ranging from 2200-3100m (Ashwal et al., 2005). Van der Merwe (2008) interpretes the Main Zone to be overlying the **CZ** in both the Eastern and Western Limbs. In the Villa Nora Limb of the Northern Limb, the Main Zone forms the basa unit

(Barnes and Maier, 2002). In General the Main Zone comprises a succession of Gabbro-norites in which olivine and chromite are absent and anorthosites are less common (Kinnaird et al., 2005). The 2000m thick **Upper (UZ) Zone** is characterized by upto 25 magnetitite layers in four groups (Kinnaird et al., 2005). In the Eastern Limb the **Upper Zone** is Subdivided into Subzone A (Magnet Heights Gabbro-norites) at the base, Subzone B is an Ironstone Magnetite Gabbro, while Subzone C is a Luiperdshoek olivine Diorites at the top (Cawthorn and Boerst, 2006). In the Western and Northern Limb, the **Upper Zone** is not formally subdivided and therefore is referred to as the Bierkraal Magnetite Gabbro and the Molendraai Magnetite Gabbro respectively (Van der Merwe, 2012).

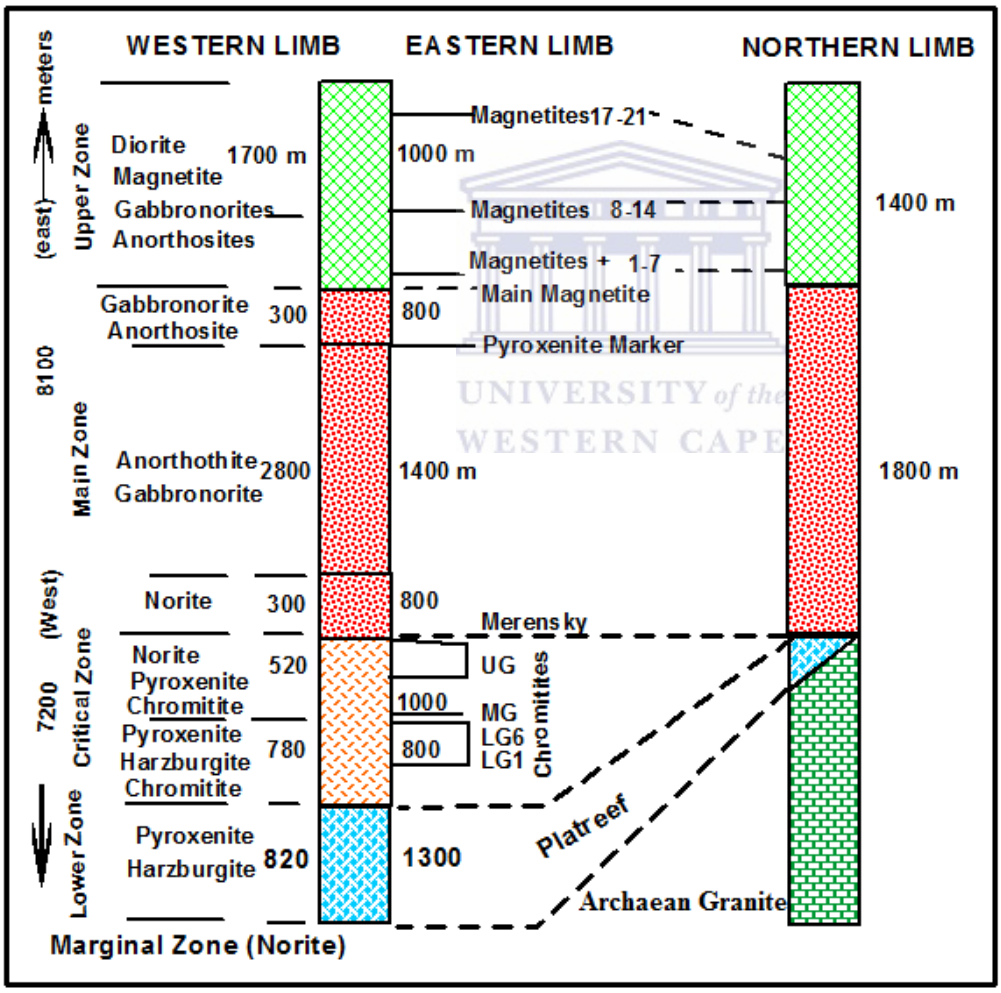

Figure 1.2: Stratigraphic sections through the Rustenburg Layered Series (after Cawthorn and Lee, 1998; White, 1994).

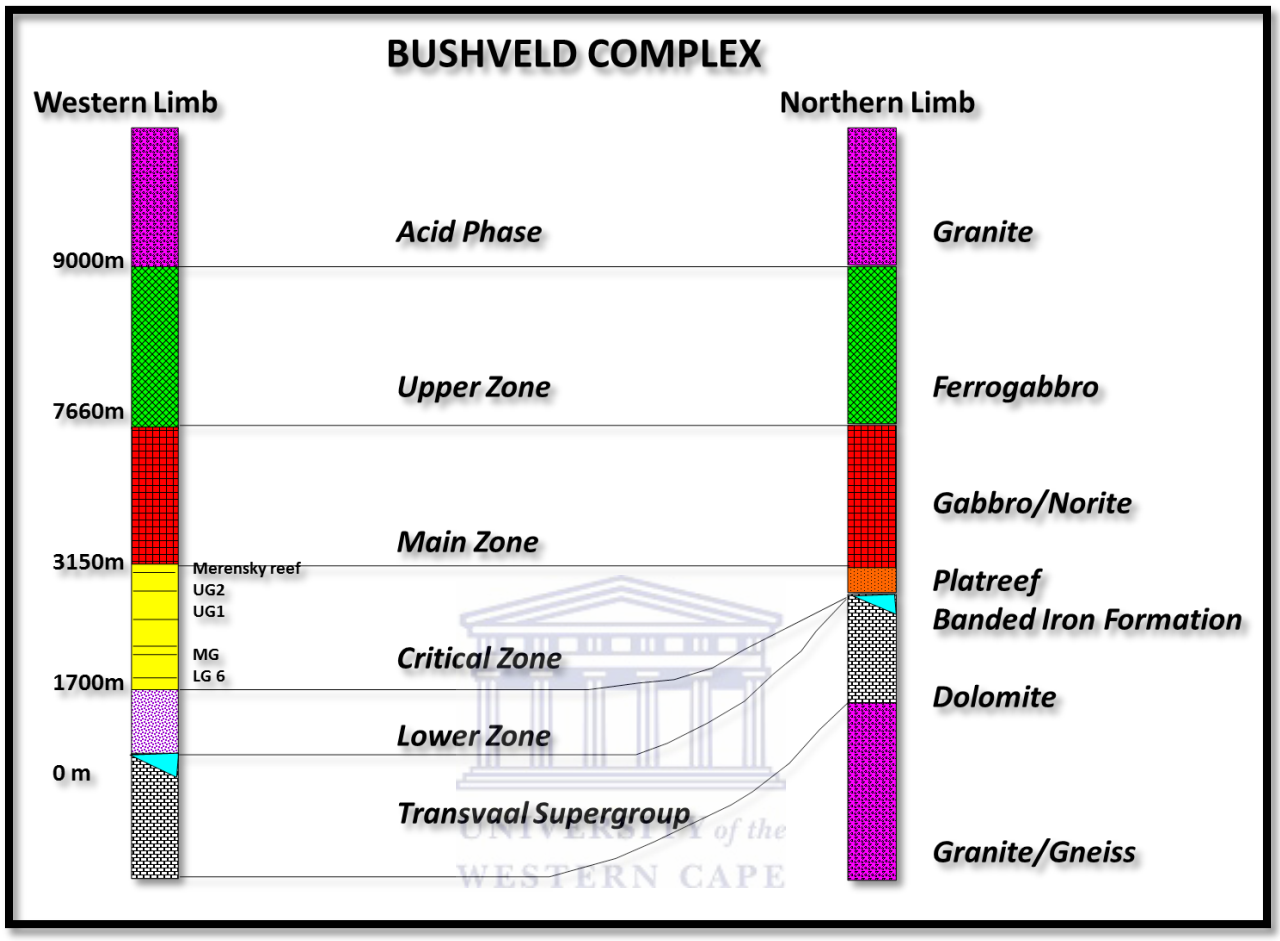

Figure 1.3: Simplified stratigraphic cross-sections of the RLS correlating the western Bushveld with the northern limb (Formerly Potgietersrust Limb) of the Bushveld Complex (Modified after White, 1994; Kinnaird *et al.*, 2005).

The three principal ore-bearing horizons of the BIC are the Merensky Reef and the UG2 chromitite layer in the Western and Eastern Limbs, and the Platreef in the Northern Limb (Eales and Cawthorn, 1996).

The Northern Limb is located in the northern part of the BC attaining a length of 110km and a maximum thickness of 15km (Armitage et al., 2002) (Fig. 1). It has three different division sectors, namely the Southern, Central and Northern sectors (Harris et al., 2005) (Fig. 1.4). The

Southern Sector comprises all of the farms from the town of Mokopane (formerly known as Potgietersrus) northwards to the farm Tweefontein where the footwall may be Penge, Duitschland or Timeball Hill Formation; the Central Sector includes, the farm Tweefontein and continues northwards until the farm Zwartfontein with a footwall of Malmani dolomite (Harris et al., 2005). The Northern Sector comprises the farms Overysel and Drenthe where the footwall is Archaean granite (Harris et al., 2005). Unlike the Merensky and UG2 reefs, the Platreef is a thick package of texturally heterogeneous zone of up to 400m of pyroxenite, norite, gabbro-norite containing large xenoliths of dolomite, calc-silicate shale (graphite in part), quartzite and Fe-formation derived from the floor rocks (Harris and Chaumba, 2001; Barnes and Maier, 2002). The Platreef rests upon the lower zone in the Southern part of the Northern lobe (on the farms of Grassvally and Rooipoort; Hubert, 1983; Maier et al., 2007), on the Transvaal Supergroup rocks between Rooipoort and Zwartfontein and on Archaean granite gneiss between Overysel and the Northern edge of the lobe (Maier et al., 2007). The Platreef displays a complex and heterogeneous lithology and mineralization patterns that distinguish its genesis from that which is proposed for the Merensky Reef and UG2 (Kinnaird, 2005).

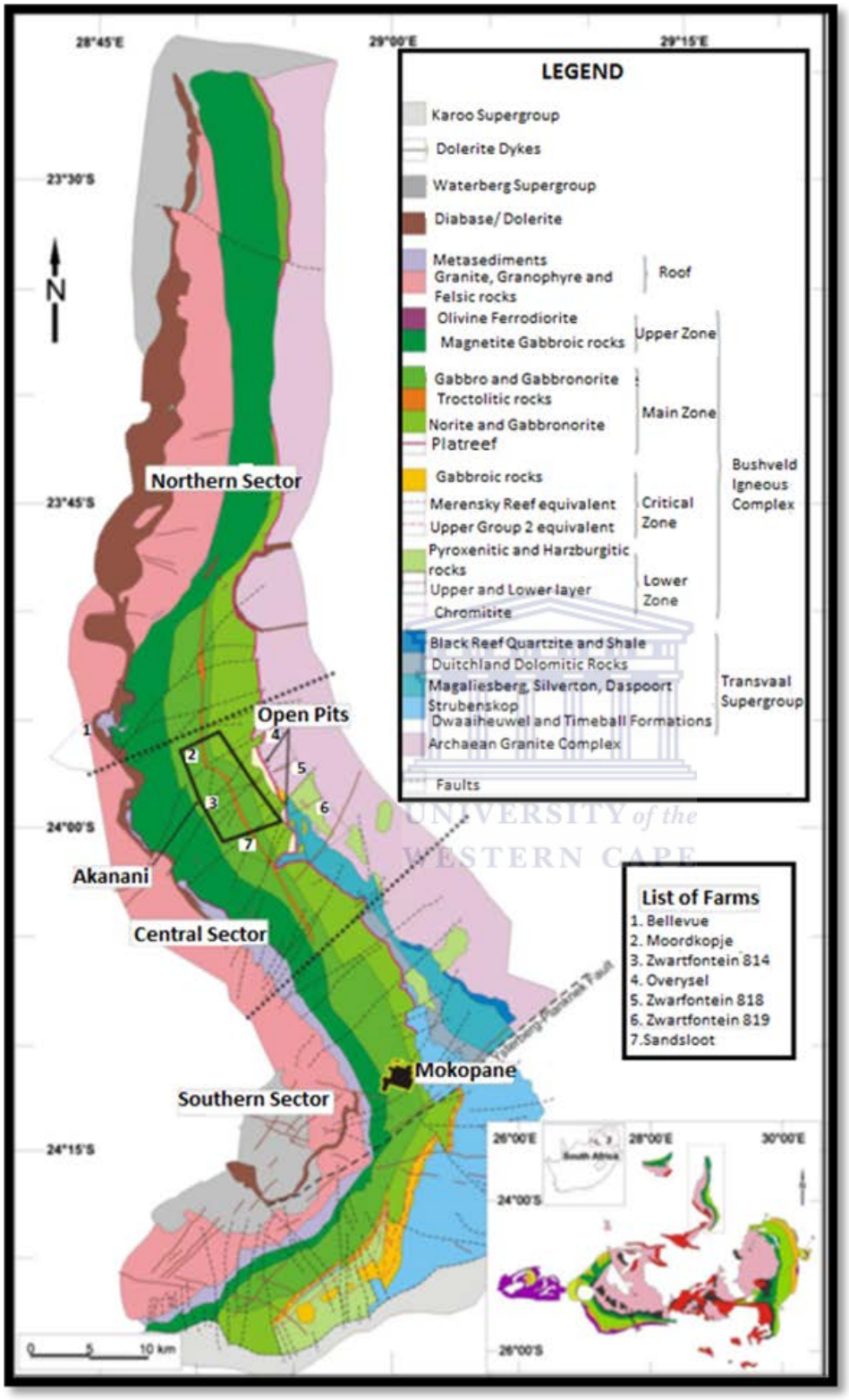

Figure 1.4: Geological map of the Platreef showing the study area (modified after Van der Merwe *et al.* 2012).

The Platreef displays varying styles of mineralization in different sectors of the Northern lobe (Manyeruke, 2007). The PGE may be concentrated at the base of the layer e.g. Tweefontein, near the top e.g. Drenthe or the PGE may be evenly distributed throughout the Platreef e.g. at Overysel (Kinnaird, 2005). The PGEs occur as PtFe, Pt_3Sn and variable Pd or Pt-tellurides, bismuthides, arsenides, antimonides, bismuthoantimonides and complex bismuthotellurides (Hutchinson and Kinnaird, 2005; Holwell et al., 2006). Sulphide mineralization (up to 20%) may occur in the form of disseminated, net-textured, sub-massive or massive chalcopyrite, pentlandite and pyrrhotite, with minor galena and sphalerite with overall grades of 0.1-0.6% Cu and Ni (Manyeruke, 2007). The Southern part of the Platreef is highly contaminated by calc-silicate xenoliths that are typically mantled by up to 20m of serpentinized pyroxenite that contains serpentinized olivine and magnetite. Higher grades of up to 4g/t (Pt+Pd) are found in the vicinity of Sandsloot, Zwartfontein and Overysel open pit mines (Naldrett et al., 2008).

1.5 Local Geology

The Akanani Project is located on the Platreef within the Central Sector of the northern limb of the Bushveld Complex, approximately 25 km north-west of the town of Mokopane (Eales and Cawthorn, 1996; Akanani Project, 2007; Van der Merwe, 2008). The project comprises two adjoining farms (Moordkopje 813LR and Zwartfontein 814LR), with a combined area of 40,950,000m^2 (Van der Merwe et al., 2012). At the Akanani prospect area, the Platreef is informally subdivided by Lonmin into 4 major lithological units (P1 to P4; from bottom to top; McDonald and Holwell, 2011; Fig. 1.5).

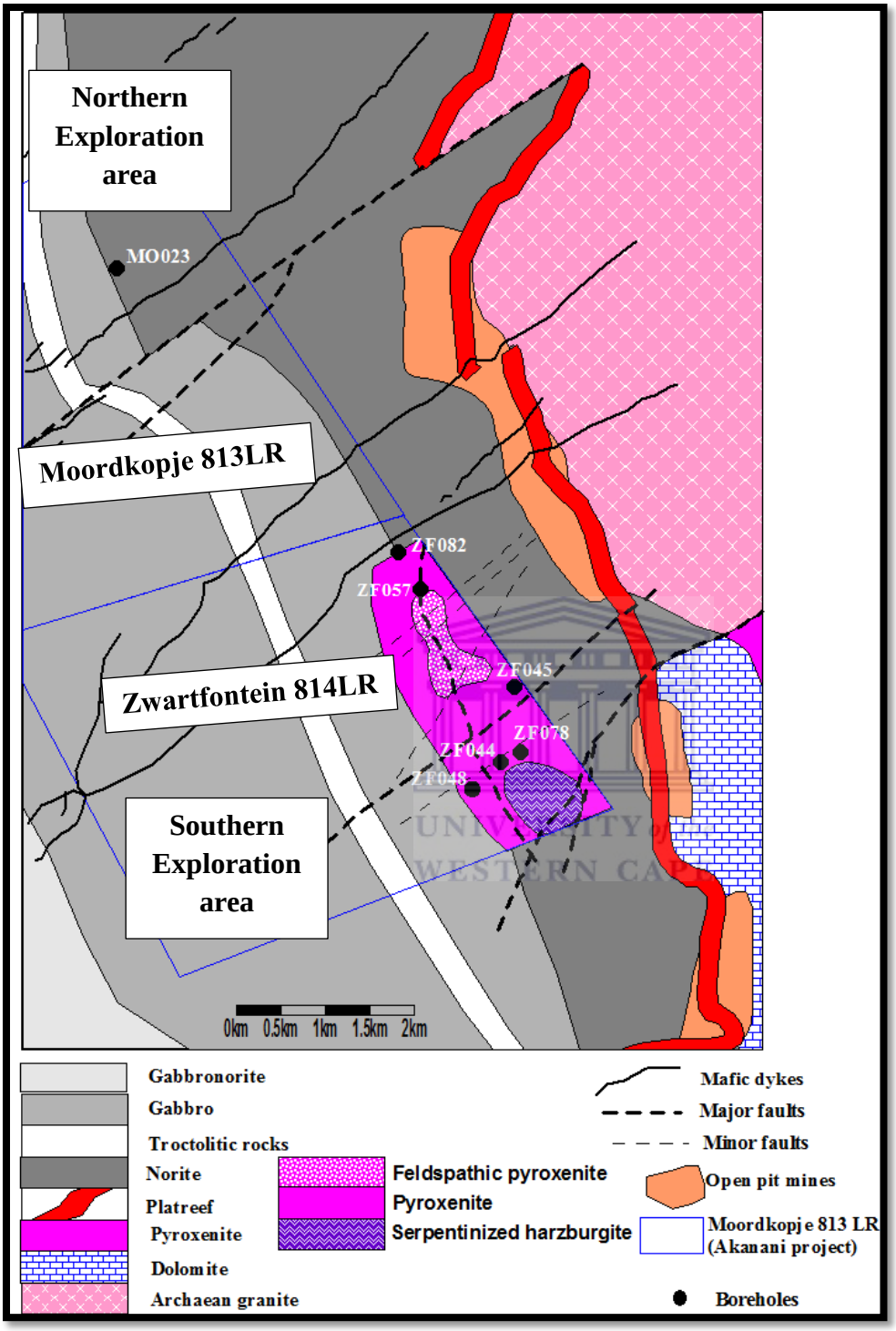

Figure 1.5: The Akanani Project on the farms Moordkopje 813LR and Zwartfontein 814LR. Northern and Southern Exploration areas indicated as well as drill cores ZF044, ZF045, ZF048, ZF057, ZF078, ZF082, MO023 (Modified from Akanani Project Interim Report, 2007; Van der Merwe, 2012).

The **footwall** of the Platreef at Akanani comprises a mixed zone consisting of chill margin granofels, pyroxenite and granite which in turn is overlain by Archaean granitoids (Van der Merwe, 2012). Inclusions of calc-silicate occur within the Platreef and this could be interpreted by the possible direction to which Platreef magma was flowing (southeast to northwest) over the Transvaal sediments onto the granitic footwall (Van der Merwe, 2012). These were intersected at a depth of 1221.76, 1281.6, 1319.99, 1327.55m respectively. At the contact between the Platreef and the granitic footwall, a fine grained granitic rock occurs. Kinnaird and Nex (2012) reported the occurrence of agmatite at the contact between the Platreef and Archaean granite on the farms Overysel and Drenthe which exploration geologist referred to as 'granofels'. More than 10m of granofels were intersected in borehole ZF078.

The **P1 unit** is a thick unit of fine-grained feldspathic pyroxenite, chromite-pyroxenite, pegmatoidal feldspathic pyroxenite, and olivine bearing pyroxenite. Mineralization in the **P1 unit** appears to be less continuous than that of the **P2 unit** and exploration is ongoing to verify mineralization continuity within this unit (Akanani project, 2007). The **P1 unit** is extensively contaminated by xenoliths of calc-silicate skarn and dolomite as well as occasional xenoliths of granite and granofelsite (van Der Merwe et al., 2012). This is inturn overlain by an approximately >20m thick serpentinized pyroxenite **P2 unit**, dominantly comprising olivine-rich lithologies. High grade mineralization is usually constrained within this geological unit, exhibiting higher grades of Ni and Cu, with an estimated grade of 4.6 g/t 3PGE (Pt, Pd, Rh) + Au, as well as 0.13 wt% Cu and 0.25 wt% Ni (Akanani Project, 2007). The **P2** horizon varies lithologically from medium to coarse-grained feldspathic pyroxenite with intervening layers of harzburgite, to highly serpentinised pyroxenites and olivine-bearing pyroxenites (Van der Merwe et al., 2012). This is in turn overlain by a barren coarse-grained feldspathic pyroxenite with poikilitic clinopyroxene (Van der Merwe, 2012) referred to as the **P3** unit. The **P4** unit is a melanorite that is located at the top of the stratigraphic succession at Akanani. It contains no PGM's, except in association with mineralized harzburgite (Van der Merwe et al., 2012). It transgresses from a fine-grained feldspathic pyroxenite to melanorites. The combined thickness of the P3 and P4 horizons amounts to less than 30m (Van der Merwe et al., 2012). Figure 1.6 below summarizes the stratigraphic subdivision at the Akanani prospect area.

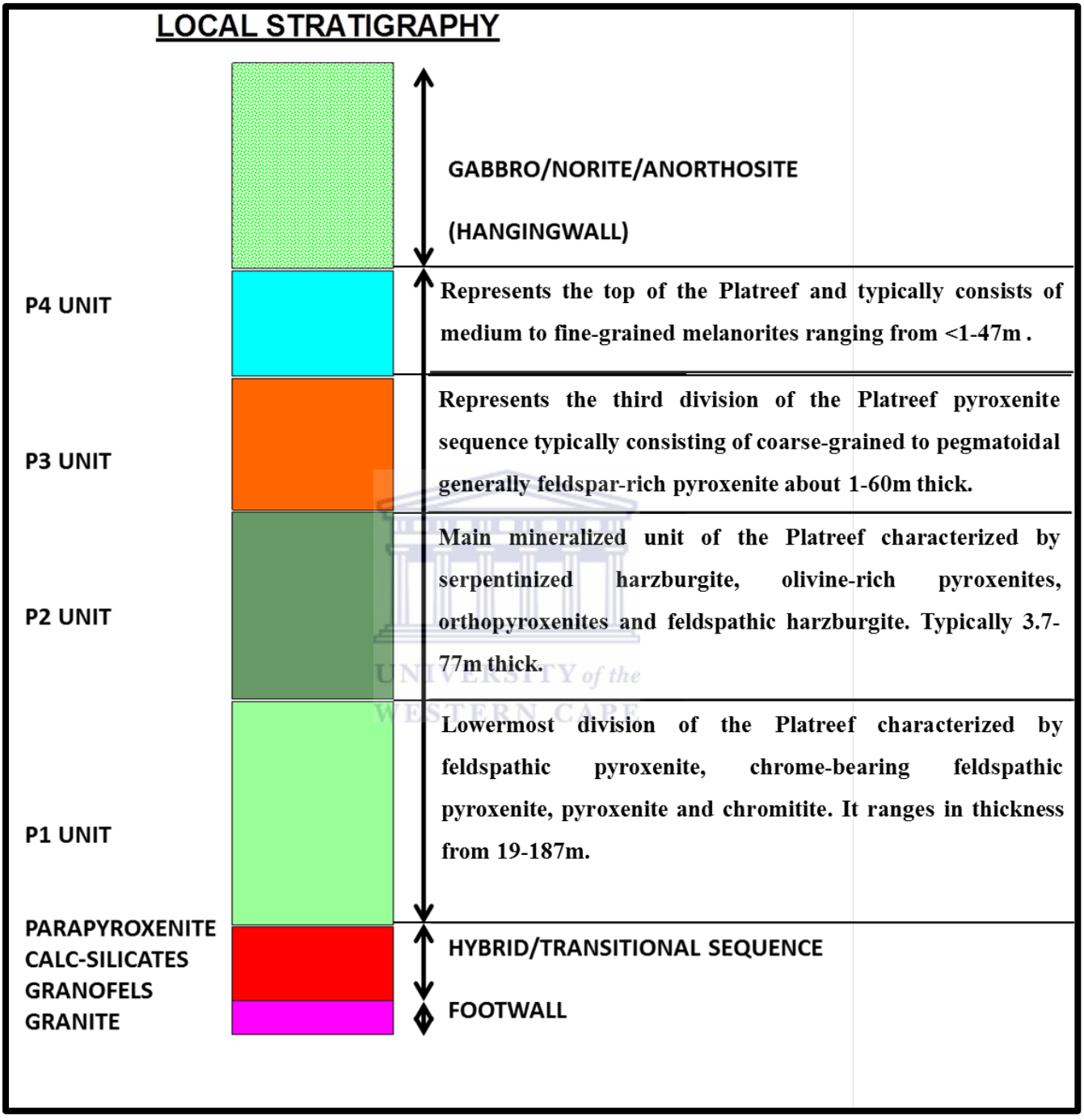

Figure 1.6: Generalised stratigraphy at Akanani prospect area.

Chapter 2

Methodology

The methodology focuses on the intergration of classical methods (petrography; mineral chemistry), geochemical and multivariate statistical techniques (factor analysis; cluster analysis; and discriminant analysis) to classify and characterize the P1-P4 units of the Platreef at the Akanani prospect area. Although the study may yield results similar to those obtained by previous researchers, it is very unique in that the methods used have not been tested for the study area anywhere in the Bushveld Complex. The first step of the study involves the selection of samples for petrographical and geochemical studies based upon the identification of the lithological grouping i.e. P1, P2, P3 and P4 units of the Platreef at the study area as logged by Lonmin mining personnel. In the second step geochemical, mineralogical, petrographical and multivariate statistical techniques were applied, inorder to check the reliability and enhance if necessary, the classification of the pyroxenite package at the study area as logged by mining personnel.

2.1 Sampling

Samples collected by the 2011 honours students from the University of the Western Cape on the farms Zwaartfontein 814LR and Moordkopje 813LR were used for petrographic and geochemical analysis. The identification of P1, P2, P3 and P4 units of the Platreef pyroxenite package was done by Lonmin mining personnel. The logging procedure included lithological variations, alterations, mineralogy, texture and sulphide mineralization.

2.2 Petrographic Analysis and Mineral chemistry

Petrographic analysis was carried out at the University of the Western Cape's microscope lab. This includes the identification of the minerals that characterize each unit (P1-P4) according to their textures, primary mineralogy, sulphide mineralization and secondary mineralogy. The mineral chemistry of each individual grain for each unit will also be studied in detail. This analysis was carried out at the University of Cape Town using an electron microprobe JEOL JXA-8100 microanalyzer. Electron microprobe analysis is chiefly used for major element analysis of minerals (Rollinson, 1993).

2.3 Geochemical data analysis

Geochemical approach used in this study is based on two different datasets. The first dataset comprises samples identified as either belonging to P1, P2, P3 and P4 units of the Platreef by Akanani mining personnel (See Appendix A), while the second dataset included unknown/unidentified samples (those not classified as belonging to either of the four pyroxenite units) that were classified and characterized through a combination of various multivariate statistical techniques (Appendix B).

- The first step of geochemical data analysis involved the characterization of P1, P2, P3 and P4 units of the Platreef as logged by mining personnel using discriminant analysis. This was done to evaluate whether or not the classification provided by mining personnel was definitive and can be used with a high level of confidence.
- In the second step a combination of factor analysis and discriminant analysis approach was used. This was used to enhance and improve the classification provided by mining personnel.
- The third approach involves the classification and characterization of P1, P2, P3 and P4 units using a combination of r-mode cluster, r-mode factor analysis and discriminant analysis.

2.3.1 Major and trace element (XRF) data analysis

Bulk analysis for major, minor and trace element compositions, namely SiO2, Al2O3, Fe2O3, MnO, MgO, CaO, Na2O, K2O, P2O5, TiO2, SO3, As, Ba, Ce, Co, Cu, Nb, Ni, Pb, Rb, Sr, V, Y, Zn, Zr, Mo, U and Th were analyzed by a Phillips 1400 X-ray fluorescence (XRF) spectrometer. All fifty three samples were measured at the geochemical laboratory of the University of the Western Cape. Oxides are expressed in weight percent (wt %) while the trace elements are expressed in parts per million (ppm) and PGE's (Pt and Pd) are expressed in parts per billion (ppb). Duplicate analyses were performed to verify that errors were <3% for major and minor elements and did not exceed a maximum of 10% error for trace elements. The following reference materials were used; STD D88, STD OREAS45CA and STDSO-18. The PGEs and BMSs were measured by Fire Assay at the geochemistry laboratory of Acme Laboratories, Vancouver, Canada. 27 samples were measured using a Thermofischer X-Series 2 with the use of the following PGE internal standard (Specpure® Alfa Aeasar Precious metal, Plasma standard

solution: Au, Ir, Os, Pd, Pt, Re, Rh, Ru @ 10g/ml with matrix 20% HCl). For Loss on ignition (LOI), a 0.5g milled sample was placed in a crucible and dried at 60ºC in an oven for 30 minutes to remove moisture. LOI was performed at 1000ºC for 45 minutes following the methods described by Potts (1987) using the Labcon® L-1200 furnace. A detailed description of the procedure is given by Potts (1987) and will therefore not be discussed here.

2.3.2 Data quality control and quality assuarance

Pellets were dried at 100˚C for 30 minutes prior to analysis to ensure the removal of moisture that could have accumulated during storage. Six samples were duplicated for major, minor and trace element compositions by XRF and used to plot a precision control scatter plot using an Excel® based programme (Appendix F). Figure 2.1 and 2.2 below shows an estimated analytical (precision) error of 5 % for MgO and 10% for Zn. Inorder to determine the heterogeneity of the sampling material as well as the analytical precision, duplicate analysis were plotted against the original analysis for major and trace element data. The results show that the data are precise as there is not much difference between the original and the duplicate. Therefore this data can be used with a high level of confidence. Comparible results between the original and the duplicate indicate that analytical variability controls precision.

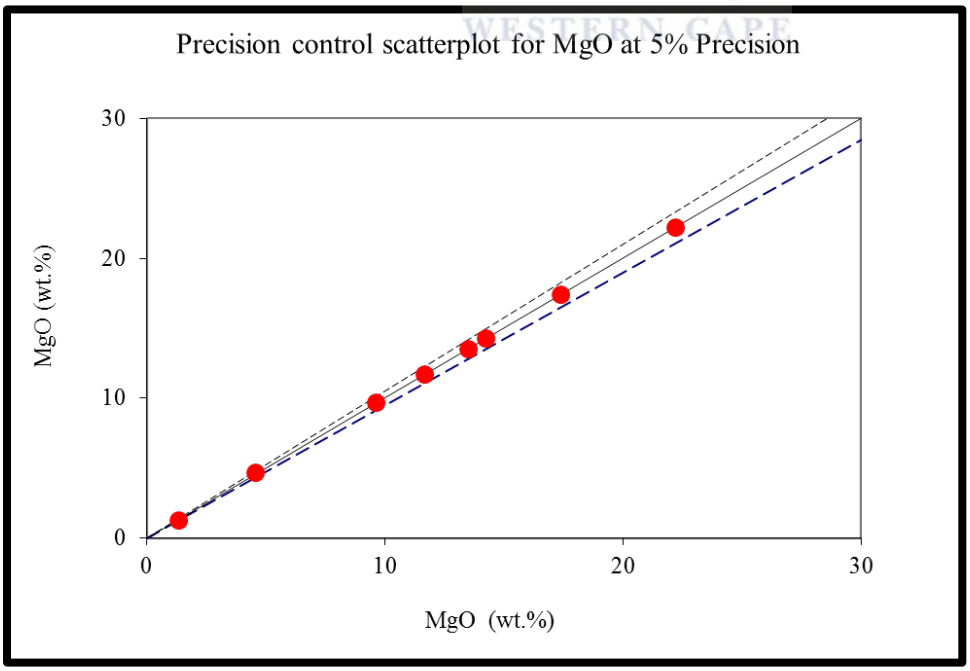

Figure 2.1: Precision scatter plot for MgO (wt.%)

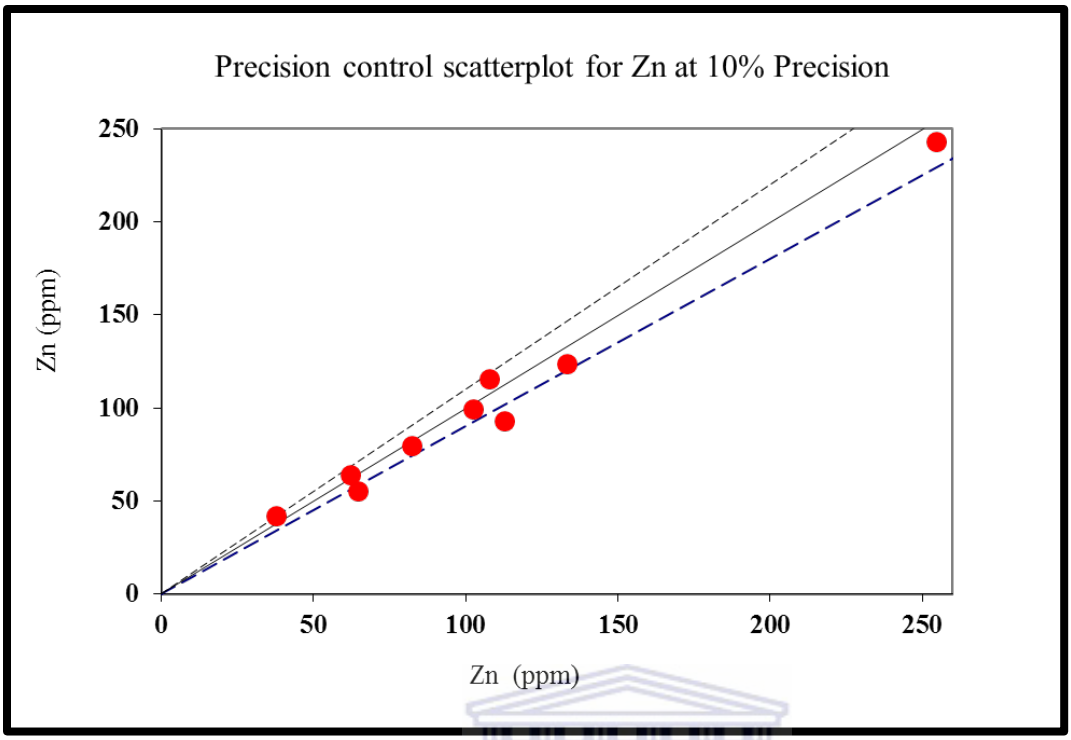

Figure 2.2: Precision control scatterplot for Zn (ppm).

2.3.3 Univariate and bivariate statistics

Geochemical variables of core-samples were analysed using IBM SPSS statistics (IBM, 2012). This software was significant for determing the descriptive statistics for core samples that provides information on the minimum, maximum, mean, standard deviation. The first step of the univariate data analysis was to examine the frequency distribution of the data set using frequency histograms as well as a statistical summary table with the minimum, maximum, mean and standard deviation. Another common approach that was used to address the skewness of data was to transform the geochemical data to a normal distribution pattern using a simple lognormal (log10) transformation inorder to see if the data will still be normally distributed.

2.3.4 Correlation Analysis

Correlation is a statistical method used to determine if a relationship between variables exists. It further provides information on the strength and direction of association between two variables (Solomon, 2013). In correlation analysis the correlation co-efficient ***r*** is a measure of the linear relationship between two variables (Cohen et al., 2013). The value of r can range from -1 to +1 and is independent of the units of measurement (Solomon, 2013). A value of r approaching 0 indicates little correlation between variables; a value approaching +1 or -1 indicates a high level

of correlation (Reimann et al., 2008). If two variables have a positive correlation co-efficient, an increase in the value of one variable implies a likely increase in the second variable while a negative correlation implies the opposite. If r = 0, then a linear relationship between the two variables does not exist although this does not mean that they are statistically independent (Reimann et al., 2008). This method has been very useful for interpreting groundwater quality data and relating them to specific hydrogeological processes (Solomon, 2013). Twenty three variables viz. SiO_2, Al_2O_3, Fe_2O_3, MnO, MgO, CaO, Na_2O, K_2O, TiO_2, P_2O_5, SO_3, LOI, Cr, Cu, Ni, Rb, Sr, V, Y, Zr, Au, Pd, Pt from six boreholes were analysed for their interrelation using bivariate correlation method with Pearson correlation co-efficient using a two-tailed test of significance in IBM® SPSS® Statistics 21. The major elements were analysed as weight percent (wt.%), while the trace element data was analyzed as parts per million (ppm). For the purpose of this study, correlation analysis was used to:

- Establish the relationship between the PGE-BMS to determine the major controls on the deposition and concentration of PGEs
- Establish the nature of the relationship between major and trace elements to determine the primary silicates characterizing each unit.

2.3.5 Multivariate Statistics

Multivariate statistics have been successfully applied to evaluate water quality data (.e.g Wu and Kuo, 2012; Solomon, 2013). Drillhole geochemical data are multivariate data involving many variables and thus multivariate statistical analysis is required for a comprehensive evaluation and interpretations to supplement the conventional methods (Solomon, 2013). Some multivariate statistical techniques such as cluster analysis, factor analysis and discriminant analysis have been widely used as unbiased methods in the analysis of water quality, air pollution in urban environments and waste recycling methods for obtaining meaningful information (Bengraine and Marhaba, 2003; Brown et al., 1996; Helena et al., 2000; Huang, 1988). Different combinations of three multivariate statistical methods have been applied to the Akanani geochemical data set to assess the relationship within the multi-element data set. The methods include:

- Cluster analysis (Hierarchical grouping of elements in a data-set based upon underlying geochemical structures)

- Factor analysis (Grouping of elements into associations that may reveal processes that govern the observed relationships)
- Discriminant analysis (A method of optimizing the geochemical distinction between P1, P2, P3 and P4 units)

Below is a detailed description of each multivariate statistical method and their procedures.

2.3.5.1 Cluster Analysis

Cluster analysis is a multivariate statistical technique that reveals the underlying structures within a data array by linking together those variables which are most highly correlated (Siad, 2012, unpublished material). In a hierarchical scheme one assumes that there are M groups of variables in an array for which M variables have been measured. At each step in the ensuing clustering procedure the two most similar variables are linked together to form a "new" variable. Strategies available for carrying out the linking procedure are described by Sokal and Sneath (1963).

The use of Pearson correlation as the measure of similarity in R-mode cluster analysis is recommended by Davis (1973). R-mode cluster analysis using Average Linkage Method (ALM) with Pearson correlation resulted in four element association groups, namely: P1, P2, P3, and P4. In the ALM, dissimilarities are averaged at each step. That is, for every updating step, we choose the average of the two distances and the two clusters of objects are then merged. Cluster analysis methods provide a means for classifying a given population into groups (clusters), based on similarity or closeness measures (Ragno et al., (2007). Detailed illustrations of the techniques used in performing a cluster analyses are given in (Davis, 1973; Templ, 2003; Templ et al., 2008).

2.3.5.2 Factor Analysis

Factor analysis is a multivariate statistical technique that allows for numerous inter-correlated samples to be reduced into fewer dimensions called factors with the least loss of information (Suk and Lee, 1999). As a multivariate statistical method, factor analysis yields the general relationship between variables by showing multivariate patterns that may help to classify the original data. With factor analysis, the sets of variables having strong associations with one another are related to underlying factors, which are called common factors. The first common

factor is related to the eigenvalue having the highest contribution to the covariance relationship. The second common factor, orthogonal to the first, has the second highest contribution to the relationship. Factor analysis was used in two ways:

- To extract training samples relevant to the four pyroxenite units based on element associations developed through R-mode cluster analysis.
- To create training samples based on factor scores relevant to the four pyroxenite units.

The geological interpretation of factors yields insight into the main processes, which may govern the distribution of geochemical samples. The extraction method used is principal component analysis, while the rotation method used for this analysis is varimax with Kaiser Normalization (Kaiser, 1958).

2.3.5.3 Discriminant Analysis

Discriminant analysis is used to device rules for assigning a new observation (x) characterized by a set of measured samples into a number of pre-determined groups (Siad et al., 1994). The aim for performing a discriminant analysis is to classify an observation or several observations into known groups. In order to understand the geochemical differences between the P1, P2, P3, and P4 layers, a linear discriminant analysis function was considered using SPSS20 (IBM, 2012). The technique used is based on previously-defined "training sets" created through the combination R-mode cluster and factor analysis, representing classes which differ in some important, observable and important characteristics (Siad, 2012, unpublished material). The detailed mathematical theory of discriminant analysis is complex and will not be presented here as this information is available in detail from most text books on multivariate statistics (e.g Tatsuoka, 1988).

The maximum number of discriminant functions is either one less than the number of groups or equal to the number of predictor variables (Siad et al., 1994). Discriminant analysis was therefore used:

- to characterize pyroxenite units identified by Lonmin mining personnel
- to classify unidentified samples to their respective pyroxenite units
- to characterize and classify training samples produced through factor analysis

- to characterize and classify training samples produced through the combination of r-mode cluster and r-mode factor analysis
- to characterize the four pyroxenite lithological units using normative data.

Since the direct discriminant function method does not show the importance of the individual geochemical variables for the description of classified groups, or their importance in the classification itself, a stepwise discriminant method should be considered (Siad et al., 1994). In this method variables are selected through a statistical test to determine the order in which they are entered or removed into the analysis. At each step the element which yielded the best classification was entered. In this way it was possible to test how many elements are necessary to describe the individual groups in the Platreef units P1, P2, P3 and P4 and also which elements have the greatest and the smallest importance in the classification.

2.3.6 Rare-Earth Element Geochemical data analysis and Normative calculations

Rare-earth element data and the normative mineralogy of that data have been processed by the Geochemical Data Toolkit (GCDKIT) software. Through this programme spider plots normalized to chondrite values will be plotted for each and every lithological unit. The complex mathematical theory describing how the programme works will not be discussed here and therefore the reader is referred to (Janoušek et al., 2011) for further understanding. The norm calculation which is embedded within the GCDKIT software was also used to describe the mineralogical character of the four lithological units. This classification is entirely chemically based (Based upon the existing geochemical data) and groups together rocks of similar bulk chemical composition irrespective of their mineralogy (Cox et al., 1993). The magma is assumed to crystallize in an anhydrous condition so that no hydrous phases (e.g. hornblende, biotite) are formed. Cox et al. (1993) simplified four basic principles to which the norm is based upon:

(a) The ferromagnesian minerals are assumed to be free of Al_2O_3. Therefore the Al_2O_3 content of the rock can be used to fix the amount of feldspar or feldspathoid in the norm, assuming that enough Na_2O, K_2O, and CaO is available to satisfy the Al_2O_3.
(b) The magnesium/iron ratio of all the ferromagnesian minerals is assumed to be the same.
(c) Several mineral pairs are assumed to be incompatible, thus nepheline and quartz for example never appear in the same norm.

The results of the norm will often show close correspondence with the modal mineralogy, in particular dry basic rocks such as gabbros which have cooled relatively slowly. The discrepancy may arise where analysis is done for rocks rich in hornblende and micas. In this case it is therefore advisable to use the norm in conjunction with petrography. It is important to note that the original purpose of the norm was not to achieve correspondence with the mode, but to try and indicate affinities which were otherwise masked by differences in grainsizes and mineralogy caused by differing water contents and cooling histories (Cox et al., 1993). There have been a number of modifications to the original norm calculations of Cross et al. (1903) known in short as the Cross, Iddings, Pirsson and Washington norm (CIPW norm) , nevertheless the most useful functions of the norm are still maintained which is the classificatory distinction between the silica-oversaturated and the silica-undersaturated rocks (Cox et al., 1993). Procedures and rules for calculating the CIPW norm are given in many older text books on igneous petrology (e.g. Cross et al., 1903) therefore will not be discussed further here.

2.3.7 Mass Balance

A quantitative determination of the degree of interaction between both the floor rock and Platreef magma at the Akanani prospect area, a technique similar to that used by Manyeruke (2003) will be undertaken using Grant's (1986) version of Gresens (1967) technique on average rock compositions. In addition the geochemical difference between the four lithological units will be determined. This includes the difference in element spectrum from P1 to P4.

Gresens (1967) quantified the absolute mobility of a component **i** in a natural system according to the formula: $\Delta M_i = fv(\rho_a/\rho_o)\, C_a^i - C_o^i$

Where **o** and **a** represent the original and the altered rock respectively, and ρ_a and ρ_o before and after alteration, ΔM_i is the mass change in component **i,** C_a^i and C_o^i are the initial and final concentrations in component **i** respectively and fv is the volume factor or the ratio of the final volume to the initial volume. Due to the complexity of Gresens' (1967) equation, this study will employ the method of Grant (1986), who proposed a simper graphical method for the solution of Gresens' equation by rearranging these equations into a linear relationship between the concentration of a component in the altered rock and that of the original. The isocon is defined by the following equation: $C_a = (M_o/M_a)\, C_o$

Where M_o is the reference mass of the original sample and M_a is the mass of the altered sample. The mass change (M_o/M_a) can be calculated by representing the concentrations in the altered rock against those in the original, which is then connected by means of a straight line through the original isocon. The components showing no gain or loss of mass are considered immobile. The components below the isocon are lost, while the components above the components above were gained during alteration. This is determined according to the following equation:

$$\Delta C_i / C_i = (M^A / M^O)(C_i^A / C_i^O) - 1$$

Where C_i^A / C_i^O is the slope of the line from the origin to the data point.

$\mathbf{C^A}$= Concentration of altered component

$\mathbf{C^O}$= Concentration of original component

$\mathbf{M^O}$= Original mass of the component

$\mathbf{M^A}$= Mass after alteration

The effects of metasomatism or the transformation of these rocks maybe very extensive to an extent that the primary mineralogical and chemical composition is not preserved and therefore the relationship between the newly formed rock and the parent rock cannot be well established. The term least altered rather than unaltered will be used in this chapter due to the fact that even the least altered samples have undergone some degree of alteration during late stage hydrothermal activity. This analysis will be carried in two ways (1) distinguish between the geochemical characteristics that can be used to identify each layer (P1-P4) (2) Reveal the gains and losses of elements occurring during metasomatism. The former will be achieved by using P2 unit as it is compositionally distinct from the other rocks and is more pristine to represent the least altered rock. In some samples the effects of hydrothermal alteration are widespread and commonly associated with high LOI. The density was used as 2.70g/cm^3 which is considered the average density of silicate rocks. The mass gains and losses as well as volume will not be quantified as this is beyond the scope of this study. The interpretation is solely based on the geochemical differences between each unit and the effects of assimilation, contamination and hydrothermal activity on element mobility and concentration. However, the determination of these processes is based upon Gressen's technique.

2.3.8 Alteration Geochemistry

Alteration indices and alteration ratios are calculated on the basis of components gained and components lost which is similar to the mass-balance principle of Greissens (1967). Two alteration indices were thus calculated using SPSS 21 to assess the alteration patterns occurring in P1, P2, P3 and P4 units of the Platreef. This includes the Ishikawa alteration index which measures the intensity of sericite and chlorite alteration; the Hashiguchi index which quantifies the enrichment of Mg relative to the depletion of Fe (Hashiguchi and Usui, 1975); the chlorite-carbonate-pyrite index which indicates the intense alteration of Fe or Mg-rich minerals such as chlorite (Large et al., 2001; Saeki and Date, 1980), the sericite index which involves the replacement of feldspars by sericite (Saeki and Date, 1980). The Rb/Sr and Ba/Rb ratios were used to indicate rocks affected by hydrothermal alteration and the effects of that link to the mineralization. The principles behind the methods are employed below.

2.3.8.1 Chlorite-Carbonate-Pyrite Index (CCPI)

Indicates the intense alteration of Fe-or Mg-rich minerals, such as chlorite (Large et al., 2001). High values of the (CCPI) indicate the intense alteration of Fe- or Mg-rich minerals, such as chlorite (Large et al. 2001; Saeki and Date 1980). This alteration index will be used in conjunction with the Ishikawa alteration index to measure the intensity of the alteration as well as distinguish between hydrothermally altered rock types and those affected by diagenetic alteration.

$$\frac{100^{*}(MgO + Fe_2O_3)}{MgO + Fe_2O_3 + Na_2O + K_2O}$$

2.3.8.2 Ishikawa Index

Measures the intensity of sericite and chlorite alteration (Ishikawa et al., 1976). It is considered useful in plagioclase-destructive hydrothermal alteration systems (Gifkins, Herrmann and Large, 2005). This alteration index is defined by the formula:

$$\frac{100^{*}(K_2O + MgO)}{(K_2O + MgO + Na_2O + CaO)}$$

The index measures two key reactions that involve the breakdown of sodic plagioclase and volcanic glass as well as their replacement by sericite and chlorite (Large et al., 2001). These reactions include:

$3NaAlSi_3O_8+K+2H= KAl_3SiO_{10}(OH)_2+6SiO_2+3Na$…….. . (1)

Albite Sericite Quartz

$KAl_3SiO_{10}(OH)_2+3H_4SiO_4+9Fe+6Mg+18H_2O= 3Mg_2Fe_3Al_2Si_3O_{10}(OH)_8+2K+28H$…..(2)

Sericite chlorite

The first reaction involves the depletion of Na_2O and CaO with the enrichment of K_2O, while reaction two involves the loss of K_2O with the subsequent gain of FeO and MgO on the basis of constant Al_2O_3 (Large et al., 2001). Values ranging between 20 and 40 are for unaltered rocks, while those ranging between 50 and 100 represent hydrothermally altered rocks (Large et al. 2001). An AI=100 represents complete replacement of feldspars and glass by sericite and/or chlorite (Large et al., 2001).

2.3.8.3 Rb/Sr and Ba/Rb ratios

Although alkali elements variation particularly Rb/Sr and Ba/Rb are generally known to characterize the degree of fractionation in plutonic rocks (Nockolds and Allen, 1953; Taylor, 1965), these ratios were used to determine rocks associated with post-magmatic alteration and their link to the mineralization. Since element pairs K-Rb, K-Ba and Ca-Sr respectively have similar ionic radii, electronegativities and ionization potentials, Rb and Ba are easily incorporated into K-minerals (K-feldspar and biotite) and Sr in Ca-minerals (Ca-rich plagioclase and clinopyroxene) (Imeokparia, 1981). Imeokparia (1981) gave the following explanation for the sensitivity of Rb, Sr and Ba to postmagmatic processes: During fractional crystallization the Rb content of the melt increases, because of the large ionic size of Rb relative to K resulting in a higher bonding energy between K and O than Rb and O. During crystallization of K-minerals from the magma, K is preferentially removed relative to Rb, while Rb concentrates in the residual melts, resulting in lower K/Rb ratios. In contrast Ba^{2+} is identical with K^+ in ionic size and may therefore incorporate in K^+ sites early crystallizing minerals. Since Ba-D bond is more covalent than the K-O bond, the substitution of barium for potassium involves a coupled

substitution of aluminium for silicon. Barium would therefore tend to remain in the solid phases during fractional melting and would be most abundant in the higher melting temperature fractions. Aqueous phases associated with magmatic activity should therefore have relatively low Ba concentrations. Sr^{2+} has a slightly higher ironic size than Ca^{2+}, causing it to be less readily admitted in the structure of Ca-bearing minerals. During post-magmatic activity Sr is depleted relative to Ca (Turekian and Kulp, 1956; Bradshaw, 1967). The suggested geochemical behavior of Rb, Sr and Ba implies that they may have greater sensitivity to magmatic processes than K and Ca. This ratio can also therefore be used in the Platreef rocks since they have been affected to some degree by post-magmatic activity especially the P2 rocks.

Chapter 3

Results

3.1 Petrography

Previous researchers (White, 1994; Lee, 1996; Holwell and Jordan, 2006) have classified rocks into A, B, C reefs. Lee (1996) described the A-reef as a heterogeneous feldspathic pyroxenite with variable grain size, while the B reef was described as a coarse-grained feldspathic pyroxenite with disseminated BMS mineralization and the C reef was referred to as a fine-grained feldspathic pyroxenite. The purpose of this chapter is to provide an overview of the petrographic observations, including mineral modes, grain sizes, textures and the alteration types of the major rock types encountered within the P1, P2, P3 and P4 units of the Platreef pyroxenite at Akanani and relate this to an overall paragenetic sequence. Furthermore, because of the complexity of the Platreef, the classification of rocks solely based on field observation and core-logging may not be as reliable; therefore the objective of this analysis is to check the reliability of rock identifications during core-logging and field observation. Prior to undertaking geochemical studies, the classification scheme of P1, P2, P3 and P4 units of 34 samples provided by the Akanani mining personnel were used as a baseline for selecting samples for petrographic analysis. The cores were selected and logged in detail more than would normally be undertaken as part of the routine logging for mining and exploration purposes. The selected samples were then analyzed microscopically in order to confirm the classification scheme as determined by the mining personnel. A total of two boreholes from the farms Zwartfontein 814LR were used in this investigation namely; ZF044 and ZF078 drilled to depths of **1335.48m** and **1343.76m** respectively in the southern exploration area. Information on the spacing between the boreholes was not readily available; however in a report released in 2007 by AfriOre it was indicated that the first 17 boreholes from the upper mineralized zone known as the P2 unit of which none of them are included in this investigation were drilled at a nominal 500 x 500m spacing along a 3.6km strike length and a width of between 0.6 and 1.4 km.

From bottom to top the stratigraphy of the two boreholes is subdivided into P1, P2, P3 and P4 by exploration geologists at the Akanani prospect area. In borehole **ZF044**, the P1 unit comprises chrome-pyroxenite, parapyroxenites, olivine-bearing pyroxenite, feldspathic pyroxenite and xenoliths of calc-silicate; P2 unit comprises olivine-bearing pyroxenite which was also logged as

a P3 lithology; the P4 unit is absent and the Platreef rocks are directly overlain by Main Zone rocks (Anorthosite at the base). The contact between Platreef and the Main Zone may be sharp very often with mottled anorthosites at the base of the Main Zone (Kekana, 2014). In borehole **ZF078**, the footwall granofels was intersected at depths of 1328.08m, this rock usually occurs at the contact between the lowermost pyroxenite and the Archaean granitic floor. The 139m thick P1 unit comprises variable thickness of calc-silicates, serpentinite and parapyroxenites, while feldspathic pyroxenite and pegmatoidal feldspathic pyroxenite dominate the P1 unit; the P2 unit is absent in this borehole. Overlying P1 is the P3 unit comprising a thin layer of pyroxenite, approximately 46 m thick; the P4 unit overlies P3 and is the top most unit of this succession; it comprises melanorites and feldspathic pyroxenite. Above this lithological subdivision of the Platreef, is the Main Zone the base of which is anorthosites. Figure 3.1 below shows the two boreholes as logged by mining personnel at the Akanani prospect area.

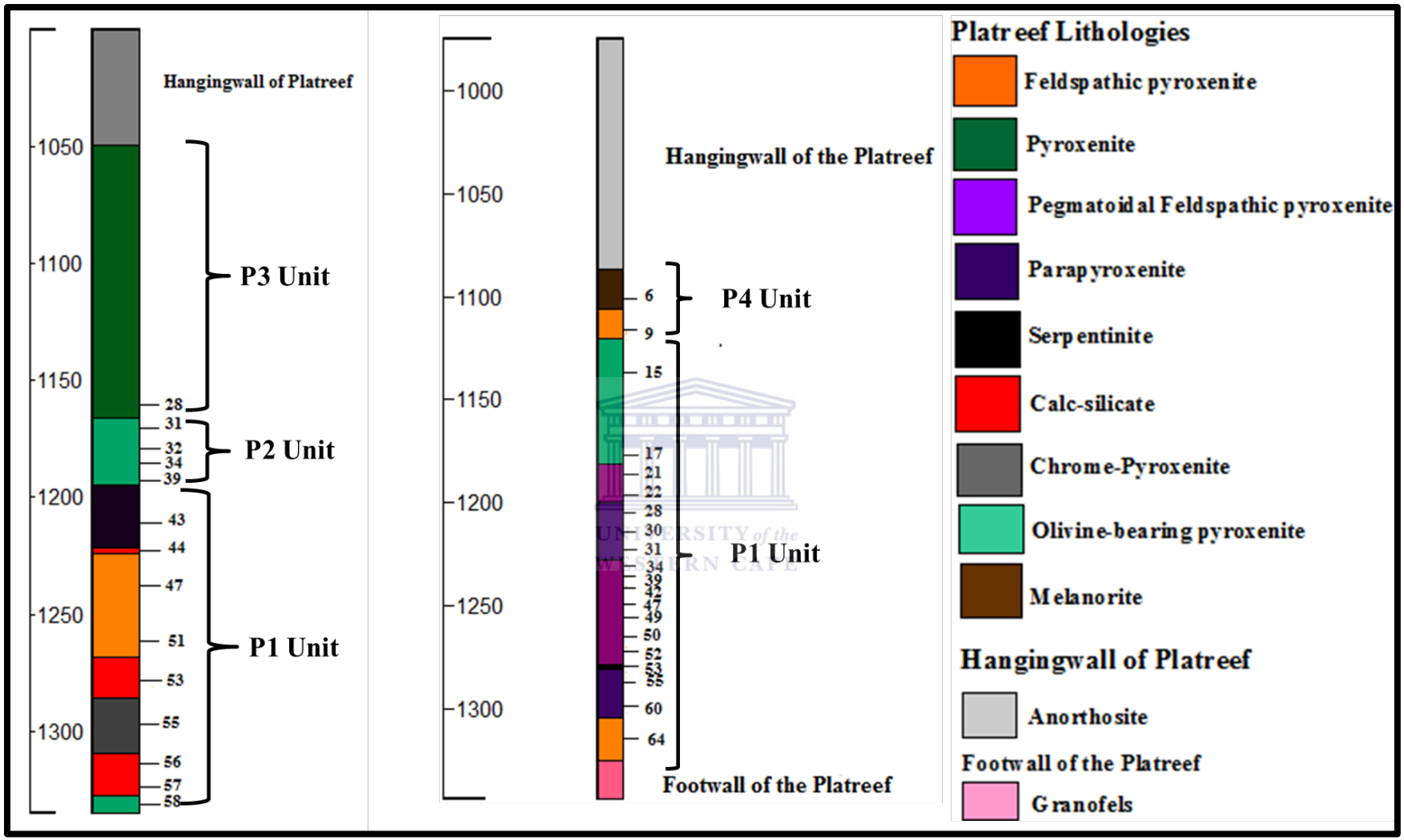

Figure 3.1: An illustration of the various rock types in boreholes in ZF044 and ZF078.

3.1.1 (P1 Unit)

The P1 unit ranges from medium-coarse grained chromitites, feldspathic pyroxenite and pyroxenites (Fig. 3.2; 3.3 and 3.4) as well as xenoliths of calc-silicate. In places the calc-silicates have interacted with Platreef magma producing a 'parapyroxenite' as referred to by mining geologist at Sandsloot. The pyroxenites and feldspathic pyroxenites within the P1 Platreef package are usually medium to fine grained. The pyroxenites and feldspathic pyroxenites immediately below the Main Zone – Platreef contact are medium grained to pegmatoidal in texture, while those occurring towards the basal portion of the Platreef were generally fine-grained (Kekana, 2014). The unit has a relatively high PGE-BMS content and anomalous PGE values are associated with areas of disseminated chromite.

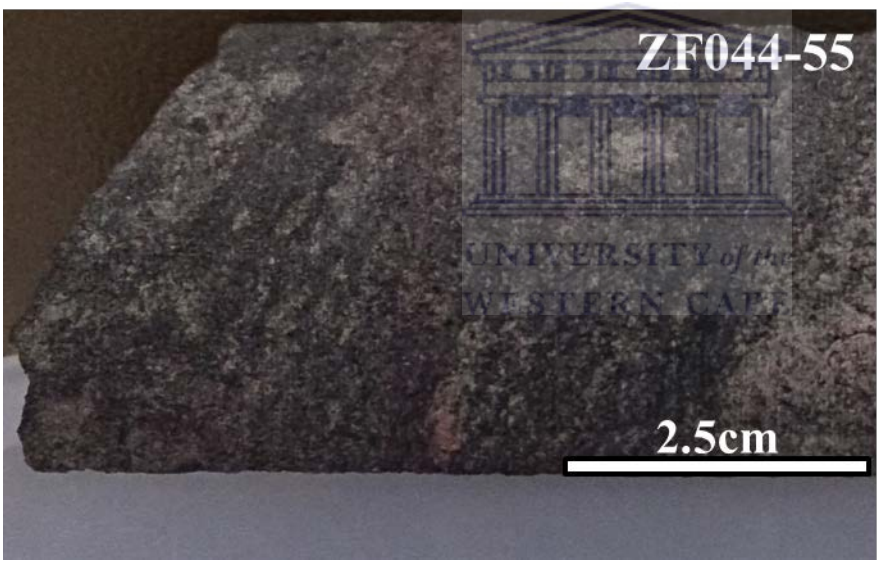

Figure 3.2: Chromitite sample in drillhole ZF044-55 at depth 1309.6m comprising interstitial plagioclase and pyroxenes with granular or sub-rounded grains of disseminated schlieren.

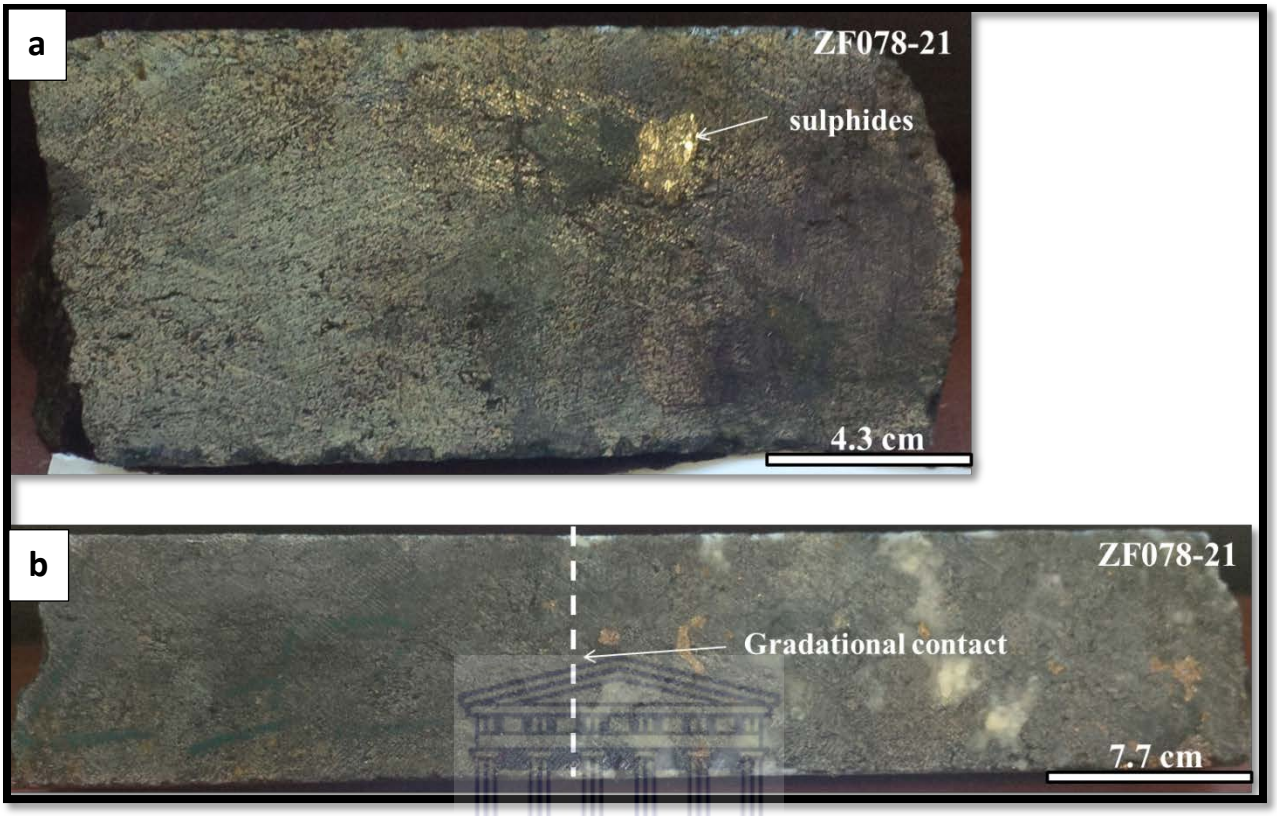

Figure 3.3: **(a)** Medium-fine grained pyroxenite with minor interstitial plagioclase and disseminated sulphides in borehole ZF078 at depth of 1186.45m **(b)** Gradational contact between feldspathic pyroxenite and pyroxenite showing progression from pyroxenite to feldspathic pyroxenite in borehole ZF078 at depth of 1186.45m.

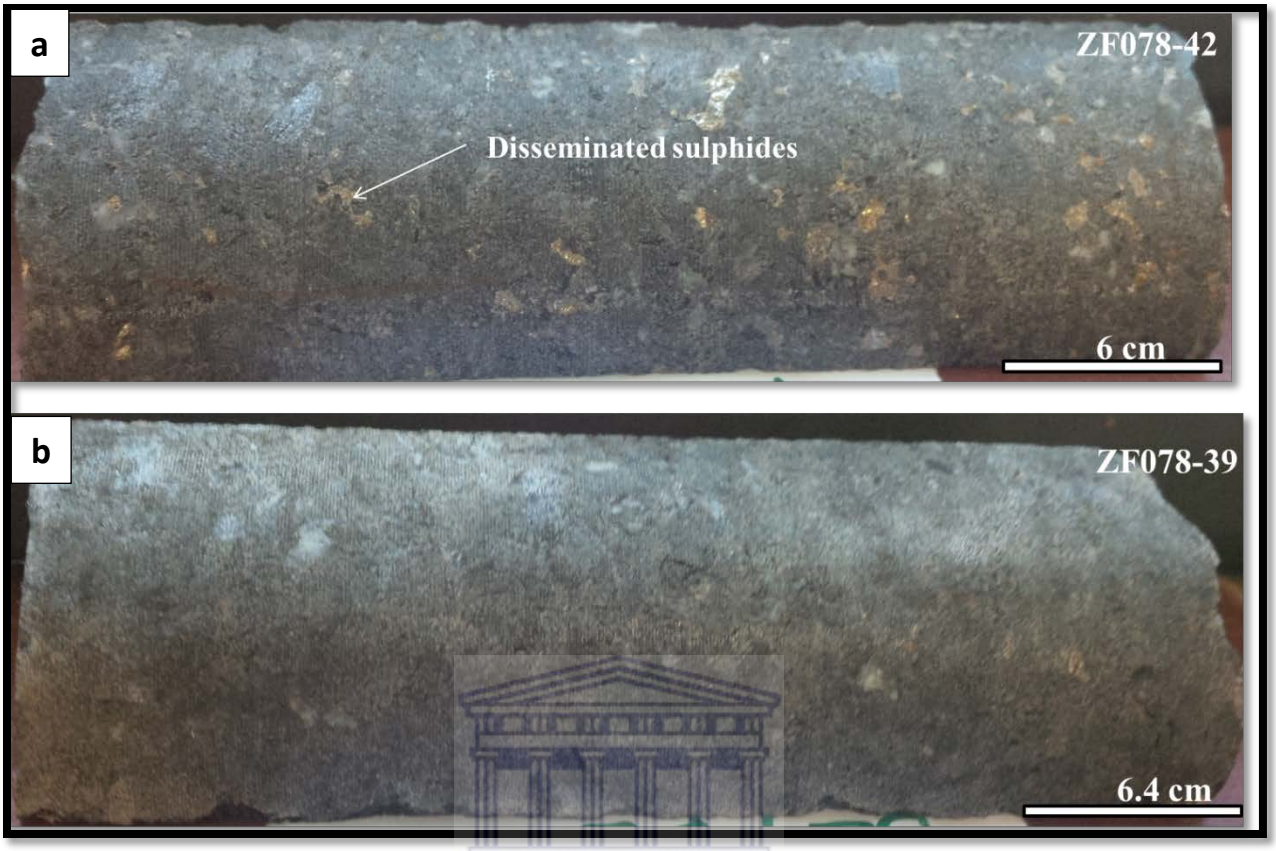

Figure 3.4: (a) Medium-fine grained pyroxenite with minor interstitial plagioclase and disseminated sulphides in borehole ZF078 at depth of 1244.39m (b) Fine-grained pyroxenite in borehole ZF078 at depth of 1238.32m.

3.1.1.1 Clinopyroxene

Clinopyroxene is a major constituent in this unit. It is present as subhedral-anhedral, coarse-grained grains ranging in size from 1-3mm (Plate 3.2a; 3.5a). It is variably altered along grain boundaries and fractures to microcrystalline alteration phases including uralite, fine-grained amphibole and sericite (less common) (Plate 3.2d). Within the clinopyroxenites (Plate 3.5c-d), the clinopyroxene is variably altered to amphibole (tremolite, actinolite)

3.1.1.2 Orthopyroxene

The orthopyroxene in the chromite-rich pyroxenite occurs mostly as coarse-grained subhedral-anhedral crystals ranging in size from 1-5mm (Plate 3.1c and 3.2c). It commonly looks to alter to microcrystalline mineral phases including fine-grained amphibole, uralite and in places sericite (Plate 3.2c; 3.5b). Alteration ranges from minor to moderate and occurs along grain boundaries

and cracks. Throughout the orthopyroxene grains, veins of fine-grained amphibole infilled with uralite often crosscut (Plate 3.1c and 3.2c).

3.1.1.3 Plagioclase

The plagioclase is interstitial occurring in between the pyroxene grains. The plagioclase occurs as a late forming mineral filling in the interstitial spaces between the pyroxenes (Plate 3.1d; 3.5a) and in places is altered to sericite. It ranges in size from 1mm-3mm exhibiting subhedral-anhedral shapes (Plate 3.2d). In some thin sections (Plate 3.4a) orthoclase occurs interstitial to the pyroxenes probably related to crustal contamination.

3.1.1.4 Chromite

Disseminated chromite is also present occurring as granular or subrounded grains on the surface of pyroxenes and plagioclase (Plate 3.1a and d; Plate 3.3a and 3.3b). In places chromite crystals (around 90%.vol) show euhedral crystal faces that range from 1mm-1.5mm in size (Plate 3.1a and b; Plate 3.3a and 3.3b).

3.1.1.5 Secondary alteration minerals and accessory minerals

In general this unit has not been affected extensively by post-magmatic processes. Alteration is generally moderate and commonly dominant along fractures, cracks and grain boundaries and hydrothermal veins occurring on the surface of pyroxene mineral grains are also present (Plate 3.5d). The transformation of orthopyroxene leads to more or less pseudomorphs of talc (Plate 3.1d). The talc is rarely orientated but rather occurs as aggregates of small particles randomly distributed. Actinolite occurs usually as an alteration product of clinopyroxene irregularly along grain boundaries of orthopyroxene and within the variable altered clinopyroxenites (Plate 3.5c). Hydrothermal veins filled with fine-grained sericite occur; this is more evident on the surface of orthopyroxene mineral grains (Plate 3.2d) and within the clinopyroxenites (Plate3.5d). Sericite is present and resulted from the alteration of plagioclase. Biotite occurs and results from the partial replacement of pyroxenes (Plate 3.2b and 3.4b). The dominant alteration phases include sericitization that mainly occurs as a result of the alteration of feldspars to a white fine-grained mica and uralitiation resulting from the alteration of pyroxenes to a fine-grained amphibole (Plate 3.5b).

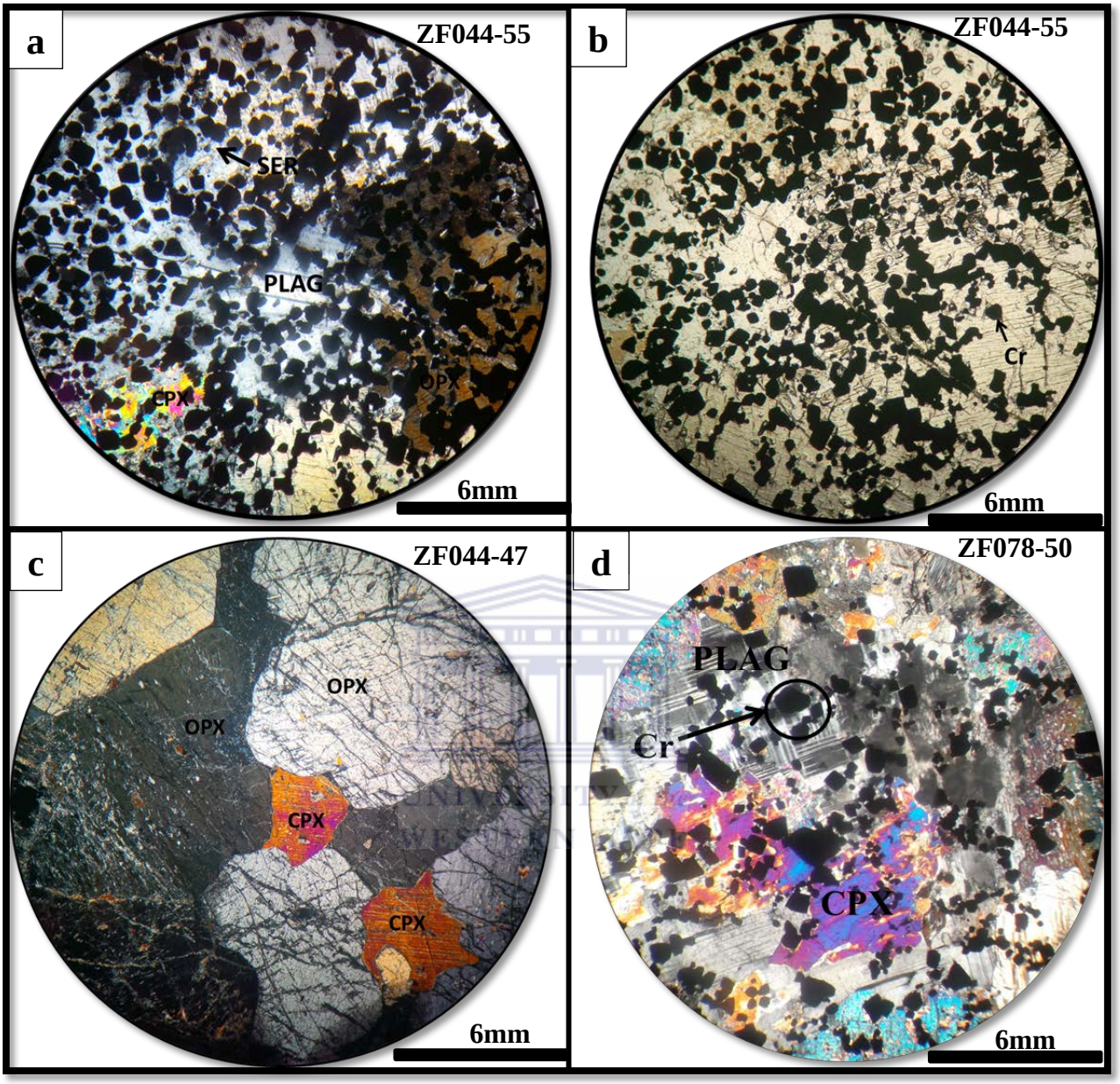

Plate 3.1: Petrographic photographs of the P1 litholgical unit present at Zwartfontein. Panels **a** and **b** are taken in both crossed nichols and crossed polars with the image on the left in plane plain polarized light and the one on the left in crossed polars. **(a-b)** Chromitite showing cumulus chromite (Cr) associated with clinopyroxene (cpx), orthopyroxene (opx) and partially altered plagioclase (plag). **(c)** Pyroxenite showing typical clinopyroxene and orthopyroxene grains that are being altered to microcrystalline mineral phases (i.e uralite). **(d)** Chrome-bearing Feldspathic pyroxenite showing euhedral-subhedral grains of disseminated chromite, clinopyroxene and interstitial plagioclase.

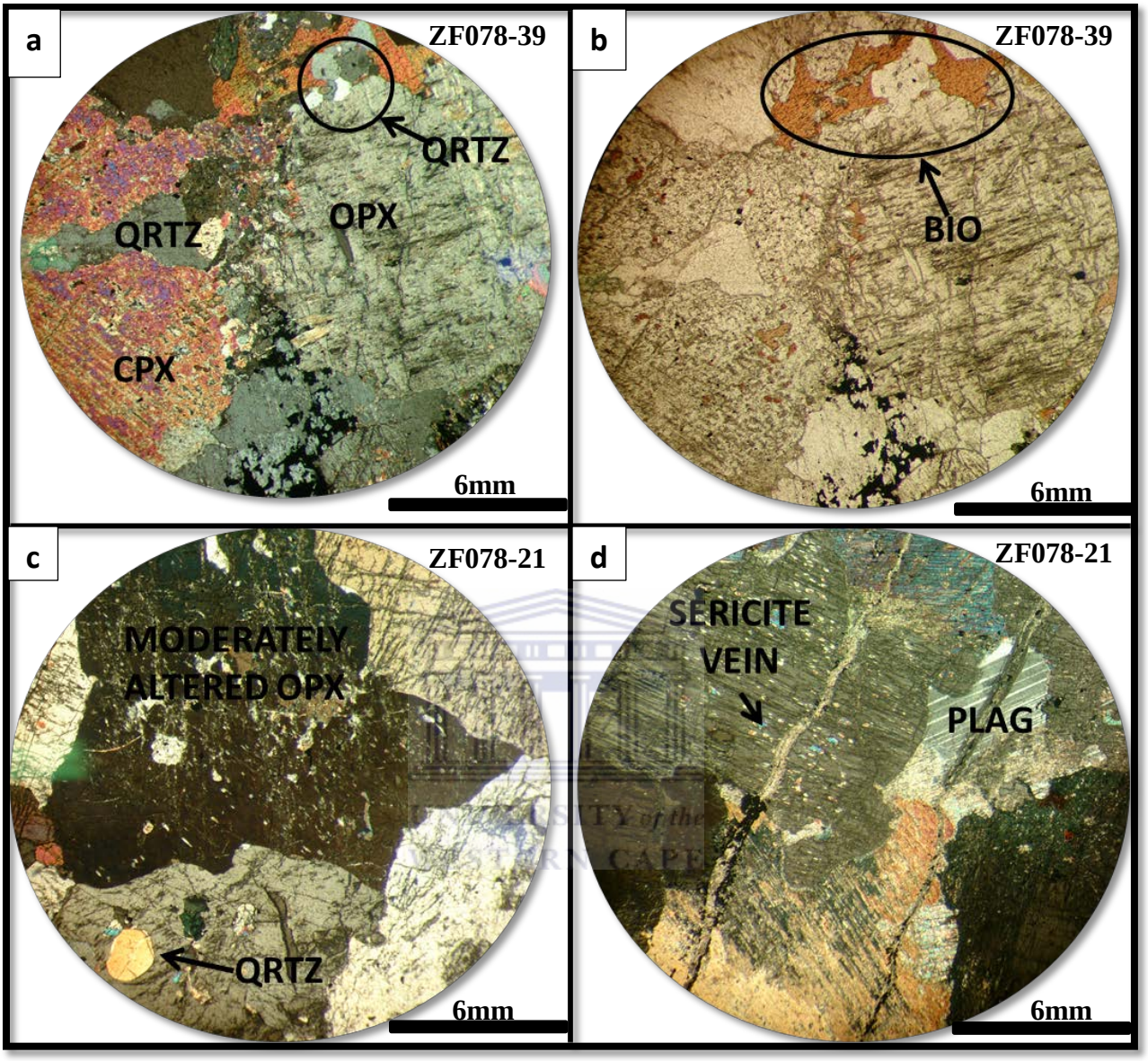

Plate 3.2: Petrographic photographs of the P1 lithological unit present at Zwartfontein. Panels **a** and **b** are taken in both crossed nichols and crossed polars. **(a-b)** Shows orthopyroxene (opx), clinopyroxene (cpx), (qrtz) quartz inclusions and biotite (bio). **(c)** Shows moderately altered orthopyroxene and quartz inclusions on orthopyroxene grains probably related to assimilation of crustal material. **(d)** Sericite vein crosscutting clin-and orthopyroxene grains (ser), moderately altered plagioclase interstitial to the pyroxene minerals.

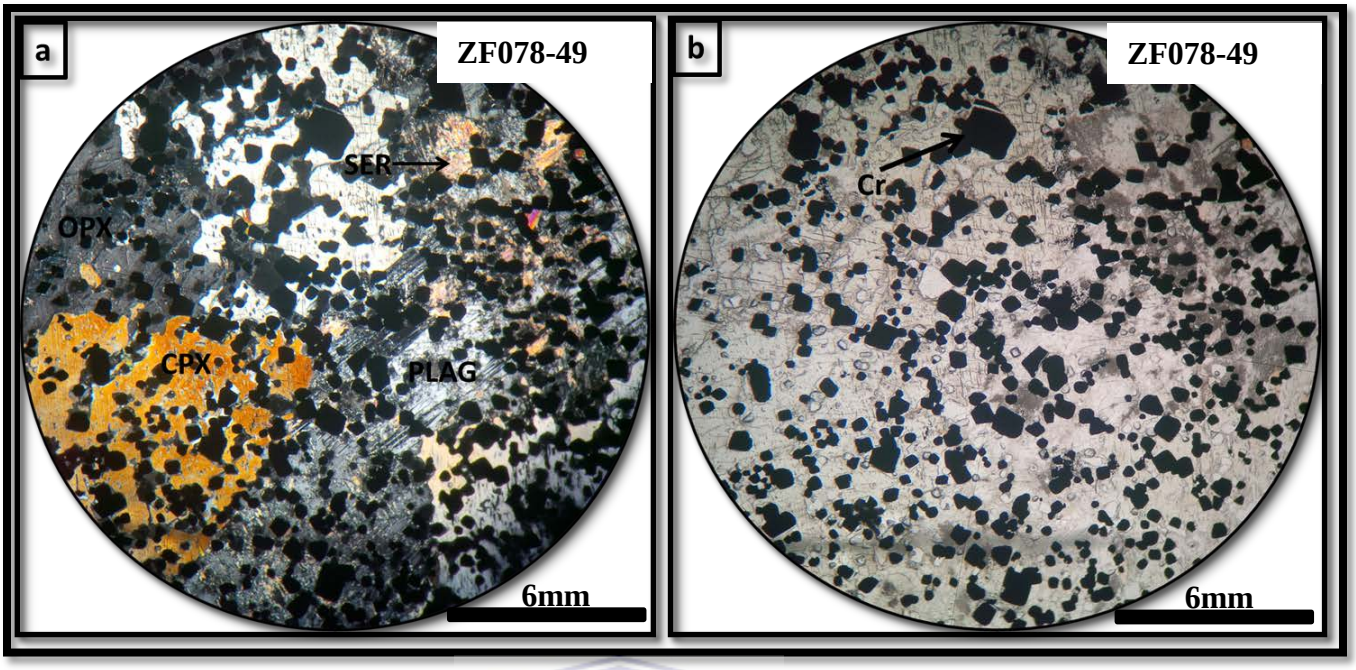

Plate 3.3: Petrographic photographs of the P1 litholgical unit present at Zwartfontein. Panels **a** and **b** are taken in both crossed nichols and crossed polars with the image on the right in plane plain polarized light and the one on the left in crossed polars. **(a-b)** Shows cumulus chromite (Cr) associated with clinopyroxene (cpx) and orthopyroxene (opx).

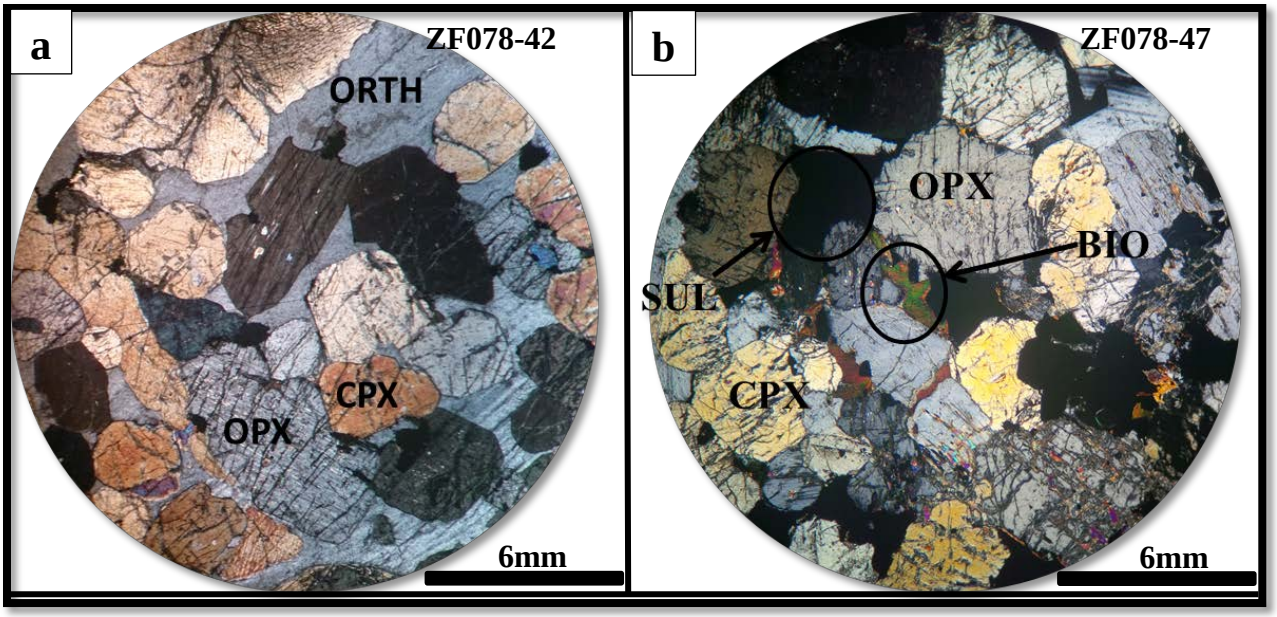

Plate 3.4: Petrographic photographs of the P1 lithological unit present at Zwartfontein. **(a)** Shows orthopyroxene (opx), clinopyroxene (cpx), and interstitial orthoclase (orth) exhibiting a medium-fine-grained texture. **(b)** orthopyroxene, clinopyroxene, secondary biotite and interstitial sulphides (sul).

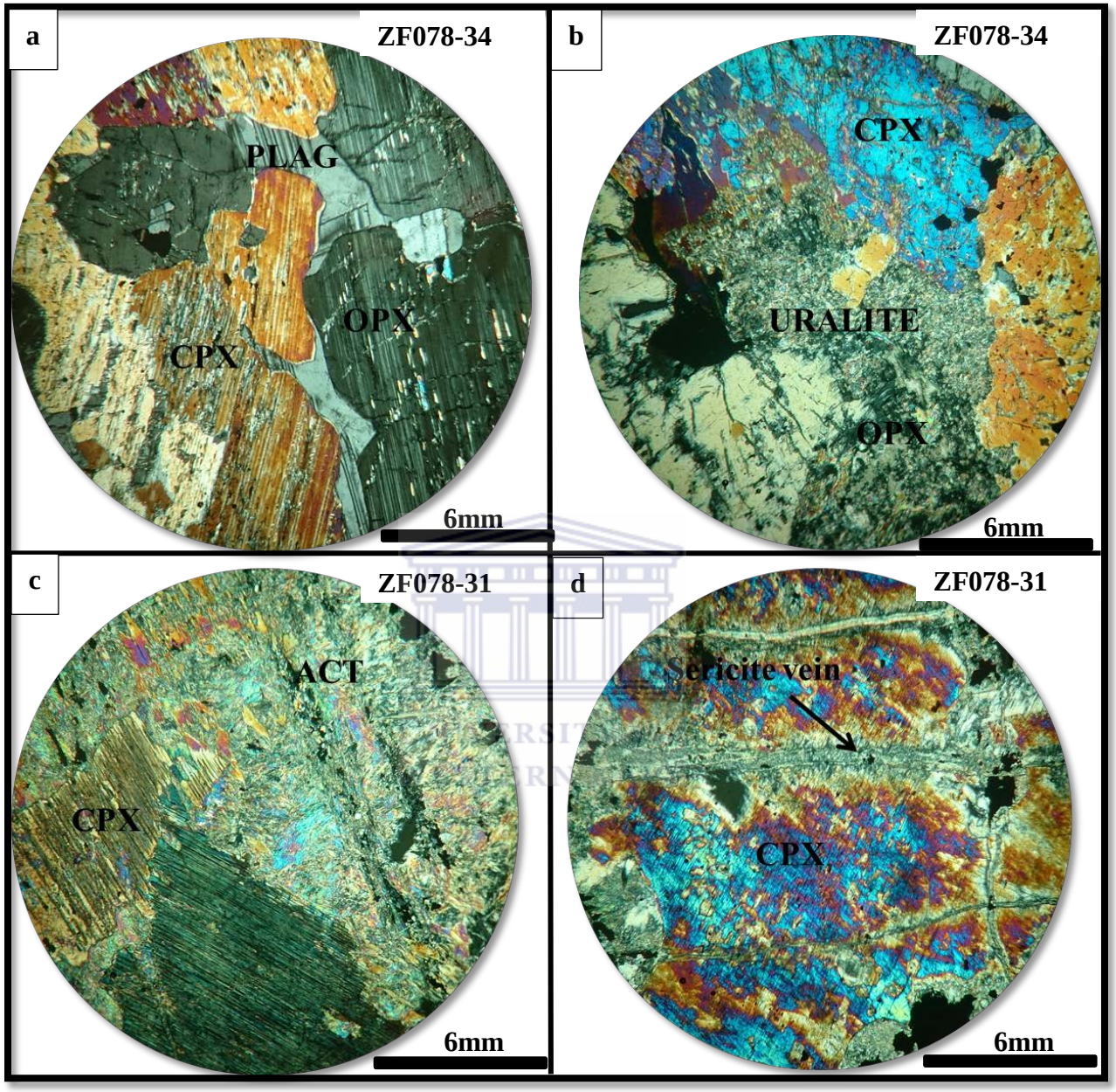

Figure 3.5: Petrographic photographs of the P1 pyroxenite unit present at Zwartfontein. **(a)** Shows orthopyroxene (opx), clinopyroxene (cpx), and interstitial plagioclase; exsolution intergrowths of clinopyroxene as very thin lamina in orthopyroxene. **(b)** Orthopyroxene altered to microcrystalline minerals (uralite and or sericite), clinopyroxene and minor interstitial sulphides. **(c)**

3.1.2 (P2 Unit)

The P2 unit is well-mineralized characterized by variably serpentinized Mg-rich lithologies (Harzburgites, serpentinized harzburgites and orthopyroxenites in places) that are medium-coarse grained (Fig. 3.5; 3.6). In places it is extensively serpentinized both laterally and vertically. The P2 unit at Akanani consists primarily of altered serpentinized olivines (50%), orthopyroxene (40%), clinopyroxene (5%) and plagioclase (<5%) by volume. In general the degree of alteration within the harzburgite exceeds that of the other lithologies (P1, P3 and P4). The common alteration types include serpentinization that occurred as a result of the alteration of olivine to serpentine and in some instances orthopyroxene also alters to serpentine, sericitization that resulted from the alteration of sodium-rich plagioclase to sericite and uralitization that resulted from the alteration of the pyroxenes to a fine-grained amphibole. Most, if not all harzburgites in the Platreef are serpentinized and they can be easily recognized where they contain black serpentinized olivine with interstitial plagioclase and green oikocrystic clinopyroxene. Where serpentinization is particularly extensive, both olivine and orthopyroxene are serpentinized and only remnant orthopyroxene is visible as oikocryst.

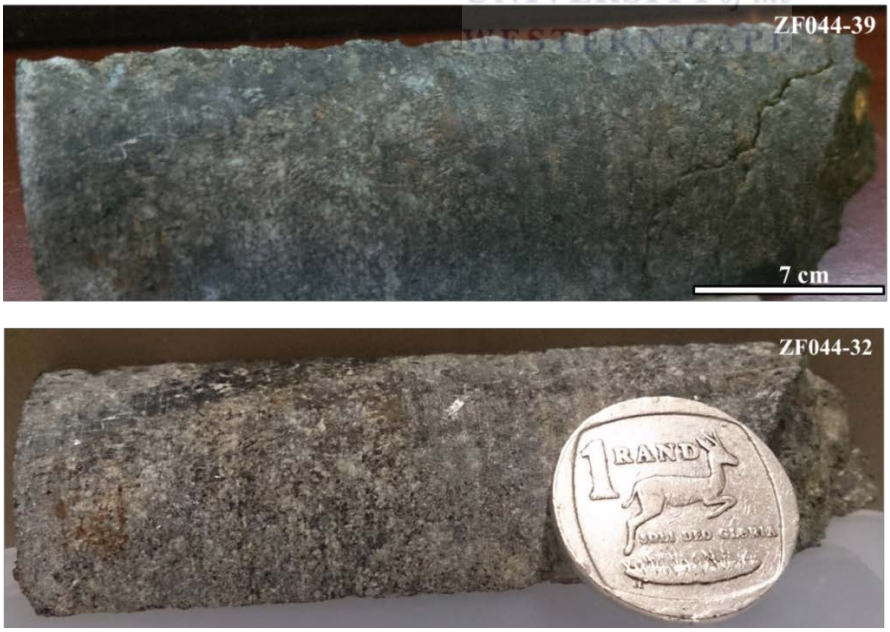

Figure 3.6: (a) Medium grained serpentinized harzburgite containing orthopyroxene (>35 %), black serpentinized olivine (>35 %) with up to 10% clinopyroxene in drillhole ZF044 at depth

1194.45m (b) Serpentinized harzburgite with black serpentinized olivine, interstitial feldspar and no visible sulphides in drillhole ZF044 at depth 1176.2m.

Figure 3.7: (a) Serpentinized harzburgite with black serpentinized olivine, interstitial feldspar with visible sulphides in drillhole ZF082-60 at depth 1511.38m. (b) Feldspathic harzburgite with minor interstitial plagioclase, variably serpentinized with cumulus olivine and orthopyroxene and oikocrysts of green clinopyroxene in drillhole ZF048-45 at depth 1513.50m.

3.1.2.1 Orthopyroxene

Orthopyroxene is, with the exception of olivine, the most common mineral in this unit. It ranges in size from 1mm-4mm exhibiting subhedral-anhedral shapes (Plate 3.6 and 3.7). In places the orthopyroxene shows fine lamellae of clinopyroxene resulting from exsolution during cooling. In places orthopyroxene grains are usually resorbed as a result of the change in composition of the magma from initially Fe-Mg rich to Ca-rich further crystallizing the clinopyroxene out. The orthopyroxenes are more resistant to serpentinization and thus presumably limiting ingress of serpentinizing fluids in the orthopyroxene-rich harzburgites. In olivine-rich granular harzburgites, the orthopyroxene is more pervasively altered to bastite pseudomorphs, and relict olivine mesh centres in serpentine are replaced by isotropic serpentine (Plate 3.5c).

3.1.2.2 Olivine

Olivine is the main component of the Harzburgite ranging in size from 1mm-2mm (Plate 3.5a; 3.7a and b). Most of the olivines are in the process of being completely replaced to serpentine, while some of the olivines have been altered completely to serpentine (Plate 3.5a and b). A radiating fracture network on the surface of olivine mineral grains is observable resulting from volume changes during transformation of olivine into serpentine (Plate 3.5a and b; 3.7a and b). Where olivine is fresh, it is usually riddled with serpentine veins (Plate 3.5a; 3.7). Fractures often occur across parallel grains (Plate 3.5). Olivine is converted to serpentine according to the following reaction:

$2Mg_2SiO_4 + H_2O + 2H^+ \rightarrow Mg_3Si_2O_5(OH)_4 + Mg^{2+}$

Olivine serpentine

3.1.2.3 Clinopyroxene

Clinopyroxene is a minor component in the harzburgites and usually occurs as inclusions in orthopyroxene or as oikocrists. It commonly exhibits subhedral-anhedral grain shapes with grain sizes ranging between 1mm-3mm. Where present it is usually altered to actinolite (Plate 3.6a and c).

3.1.2.4 Plagioclase

Plagioclase content accounts for <4% of the rock volume. In places the plagioclase look to be completely altered to sericite (Plate 3.5a).

3.1.2.5 Secondary alteration minerals and accessory minerals

Minerals that result from the alteration of primary minerals include serpentine, amphibole, actinolite, phlogopite and sericite. It is common for olivine to be transformed into serpentine under the influence of late-metamorphism, while orthopyroxene is converted to talc or tremolite In entirely serpentinized rock samples (Plate 3.5c), serpentine minerals appear under the influence of late or post-magmatic processes. Serpentine minerals cross olivines as banded network of veins. The fracture network of veins is usually filled with minute magnetite deposits (Plate 3.5a). In rocks with lower olivine content (Plate 3.6) original minerals are transformed into talc, actinolite, and tremolite along fractures and original mineral grain boundaries. Magnetite occurs as a minor constituent making up <3% of the harzburgite rocks. In places it often forms

through the breakdown of BMS (Holwell et al., 2006) and also as a possible by-product of serpentinization of olivine and orthopyroxene.

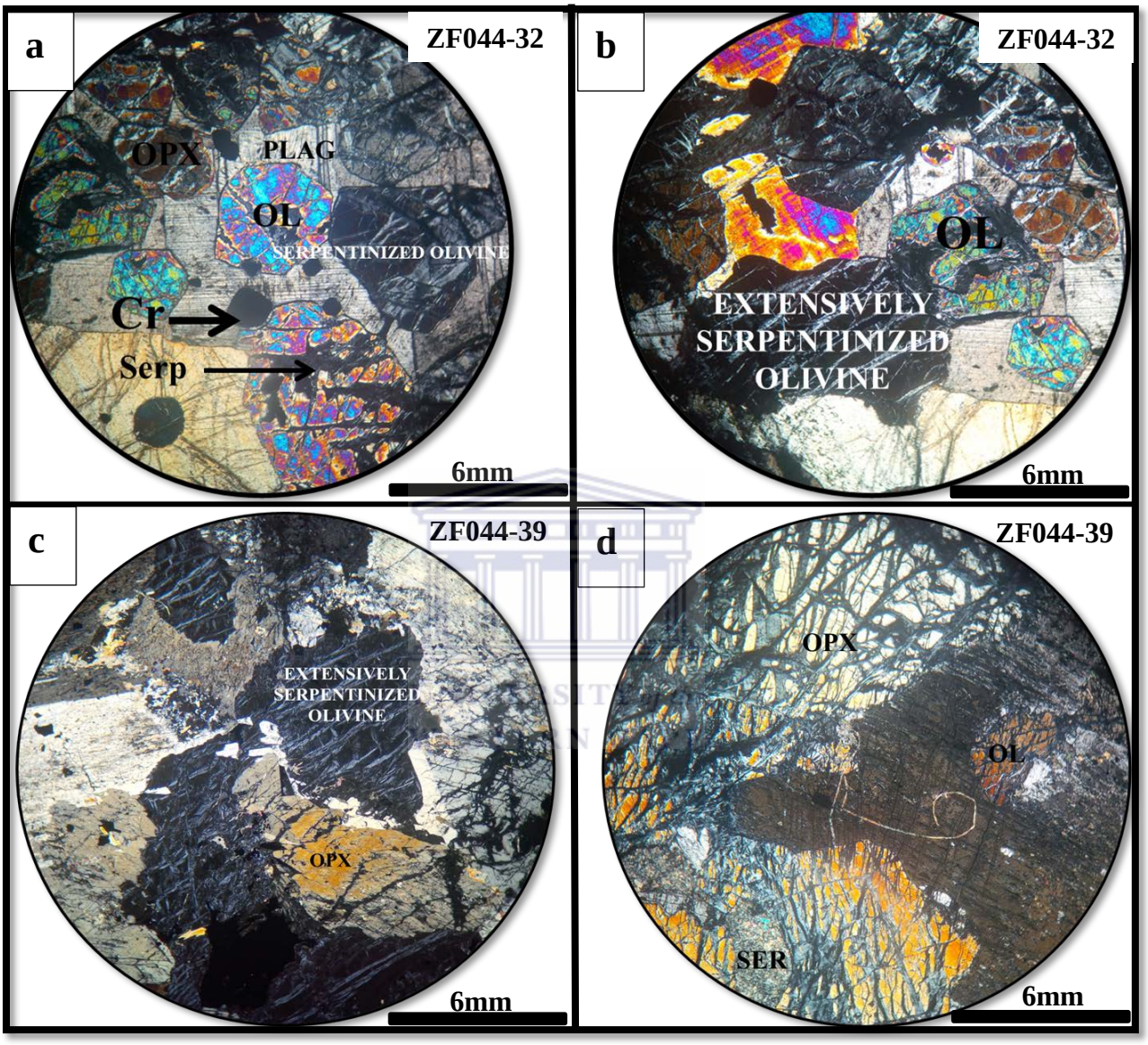

Plate 3.5: Petrographic photographs of the P2 lithological unit present at Zwartfontein. All the panels are taken in crossed polars. **(a)** Fractured orthopyroxene oikocrysts, extensively serpentinized olivine, unaltered primary Fe-Cr spinel and interstitial plagioclase. **(b)** Serpentine replacement of olivine progressed inward from internal fractures as hydrothermal fluids moved in, creating a mesh texture **(c)** Serpentine has mostly replaced primary orthopyroxene, creating bastite texture. **(d)** Sericite, and fractured orthopyroxene and olivine.

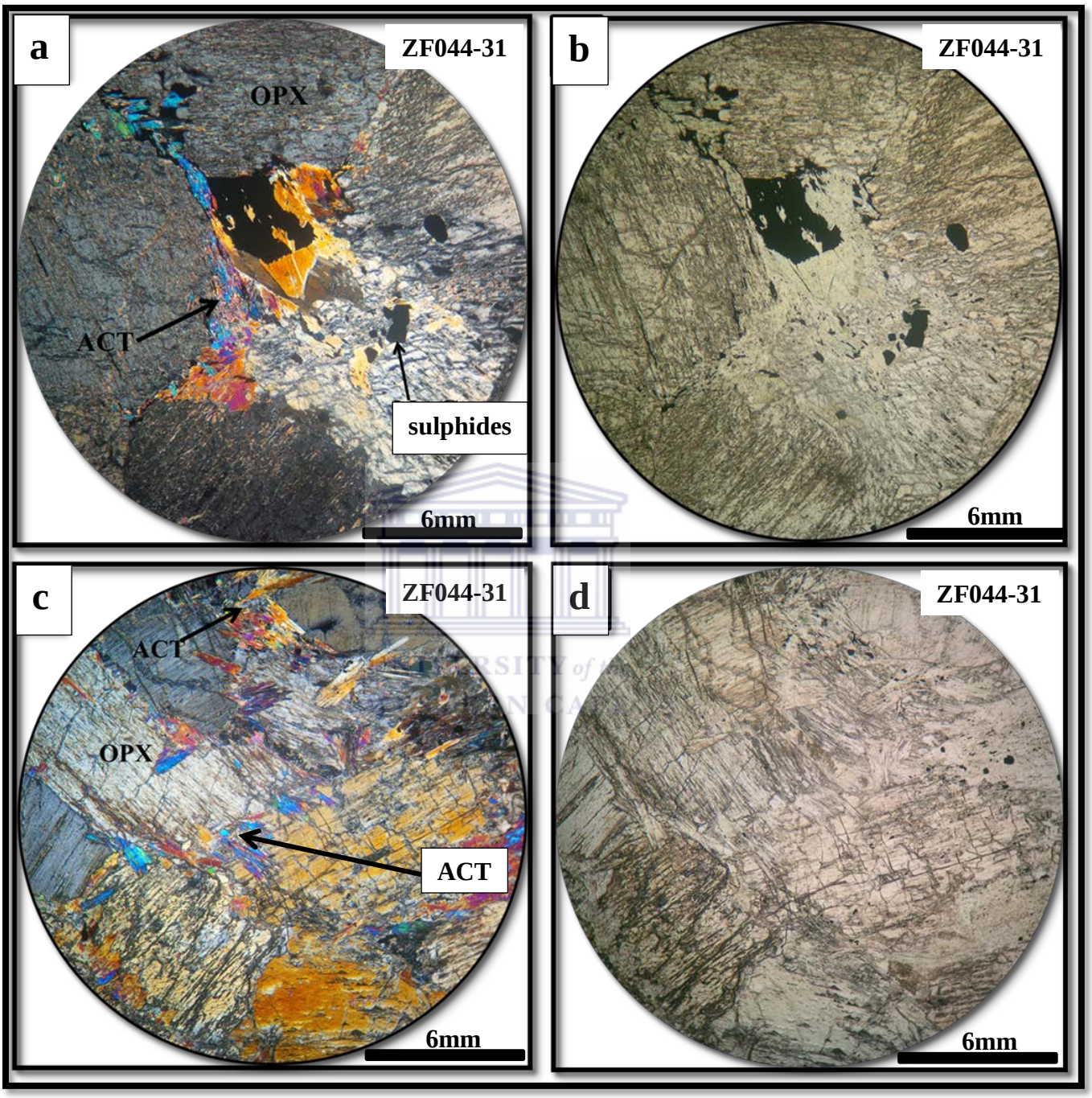

Plate 3.6: Petrographic photographs of the P2 lithological unit present at Zwartfontein. All the panels are taken in both plane polarized and crossed polarized light. **(a-b)** Orthopyroxenite comprising orthopyroxene, actinolite and disseminated sulphides. **(c-d)** Orthopyroxenite dominated by orthopyroxene and actinolite.

3.1.3 (P3 Unit)

The P3 unit of the Platreef at Akanani is a pegmatoidal-coarse grained feldspathic pyroxenite (Fig. 3.7). It is less mineralized with no significant concentration of PGE-BMS observed. It is important to note that the term feldspathic pyroxenite that describes the nature of the P1 and P3 Unit is not an internationally recognized defined rock type. However it is commonly used in the Bushveld Complex as a field and mine term which distinguishes between a pure pyroxenite and a pyroxenite with visible interstitial plagioclase. It is therefore used here to describe a pyroxenite with interstitial plagioclase. Both orthopyroxene (45%) and clinopyroxene (40%) are ubiquitous of P3 samples, while plagioclase occurs as an interstitial phase making up <11% of the rocks composition. Biotite and quartz occur as minor phases constituting approximately <5% of the rock's composition. Secondary alteration phases including amphibole and sericite that are in places very too fine-grained to distinguish occur and make up <3% of the rock volume. This unit exhibits both orthocumulate and mesocumulate texture.

Figure 3.8: **(a)** Coarse-grained to pegmatoidal feldspathic pyroxenite with cumulus orthopyroxene and intercumulus plagioclase in drillhole ZF078 at depth 1134.31m. **(b)** Coarse-grained feldspathic pyroxenite in drillhole ZF078 at depth 1174.7m.

3.1.3.1 Clinopyroxene

Clinopyroxene in the feldspar-bearing pyroxenite is present as euhedral-subhedral coarse (1mm-4mm) granular crystals (Plate 3.8a). It contains irregular exsolution lamellae of orthopyroxene (Plate 3.8c and d). In places it is variably altered to uralite and amphibole commonly along cracks and grain boundaries.

3.1.3.2 Orthopyroxene

Orthopyroxene is the second most dominant mineral phase after clinopyroxene occurring mostly as coarse-grained subhedral to anhedral crystals. The grains range in size from 1mm-5mm and in places can be larger (approximately 6mm) (Plate 3.8a, c and d). Exsolution of clinopyroxene on orthopyroxene is present, but irregular. Alteration is relatively low and occurs along grain margins and cracks (Plate 3.8d).

3.1.3.3 Plagioclase

In the feldspathic pyroxenite, plagioclase occurs as interstitial between the pyroxene grains signifying that it is a later forming mineral (Plate 3.8a, c, d). It occurs as subhedral to anhedral shapes ranging in diameter from 1mm-6mm. In places the plagioclase alters to sericite, but due to the relatively low-moderate degree of alteration this is not common.

3.1.3.4 Chromite

The three samples identified as belonging to P3 unit do not show any chromite.

3.1.3.5 Secondary alteration minerals and accessory minerals

A common feature in the feldspathic pyroxenites is the presence of veinlets of white-mica, typically <0.5mm, which crosscuts the orthopyroxene and plagioclase crystals. In general the common secondary alteration phases in the feldspathic pyroxenite are sericite and amphibole (tremolite and uralite), while the common alteration types encountered in this unit include sericitization.

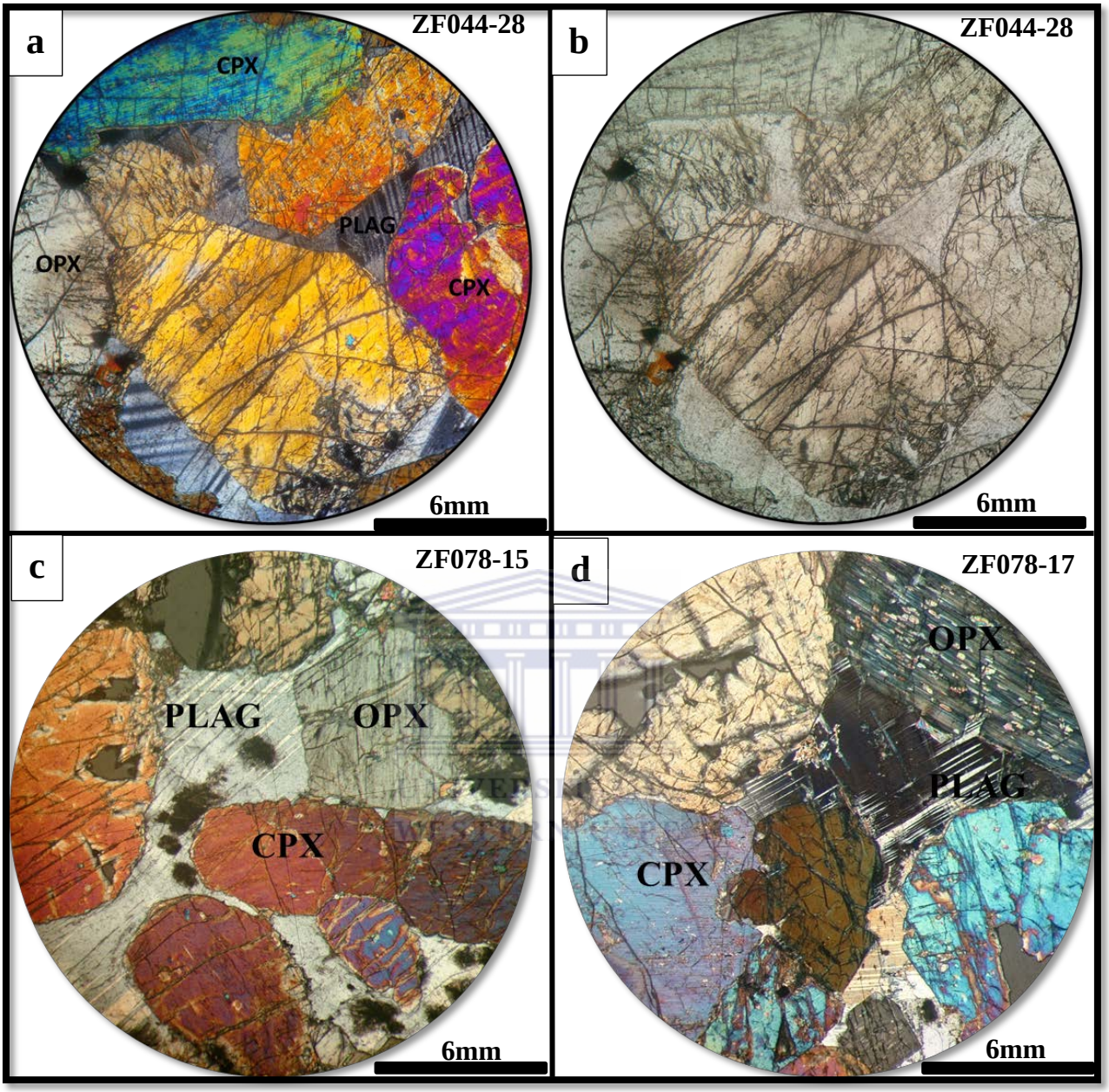

Plate 3.7: Petrographic photographs of the P3 lithological unit present at Zwartfontein. **(a-b)** Pegmatoidal feldspathic pyroxenite showing dominated by cumulus clinopyroxene (cpx), orthopyroxene (opx) and interstitial plagioclase **(c-d)** Feldspathic pyroxenite showing cumulus orthopyroxene, clinopyroxene and interstitial plagioclase. The feldspathic pyroxenites show minor alteration of pyroxenes and plagioclase to amphibole for the former and sericite for the latter.

3.1.4 (P4 Unit)

The P4 unit is classified as a melanorite and this rock type is sometimes confused with the feldspathic pyroxenite with both having relatively the same amount of pyroxene and plagioclase. The distinguishing features are that in the former clinopyroxene pre-dominates significantly, while in the latter the proportion of clinopyroxene is relatively less than that of orthopyroxene; the feldspathic pyroxenites are usually coaser-grained to pegmatoidal, while the melanorites are medium to fine-grained. In general the melanorite significantly comprises clinopyroxene (15%), orthopyroxene (35%) and Plagioclase (50%). Secondary alteration minerals will include biotite, uralite, minor sericite and hornblende. Sulphides occur in small amounts. It is important to note that sample ZF078-9 previously classified as a feldspathic pyroxenite within the P4 unit, is infact a feldspathic pyroxenite belonging to the P3 unit on the basis of petrographic observations.

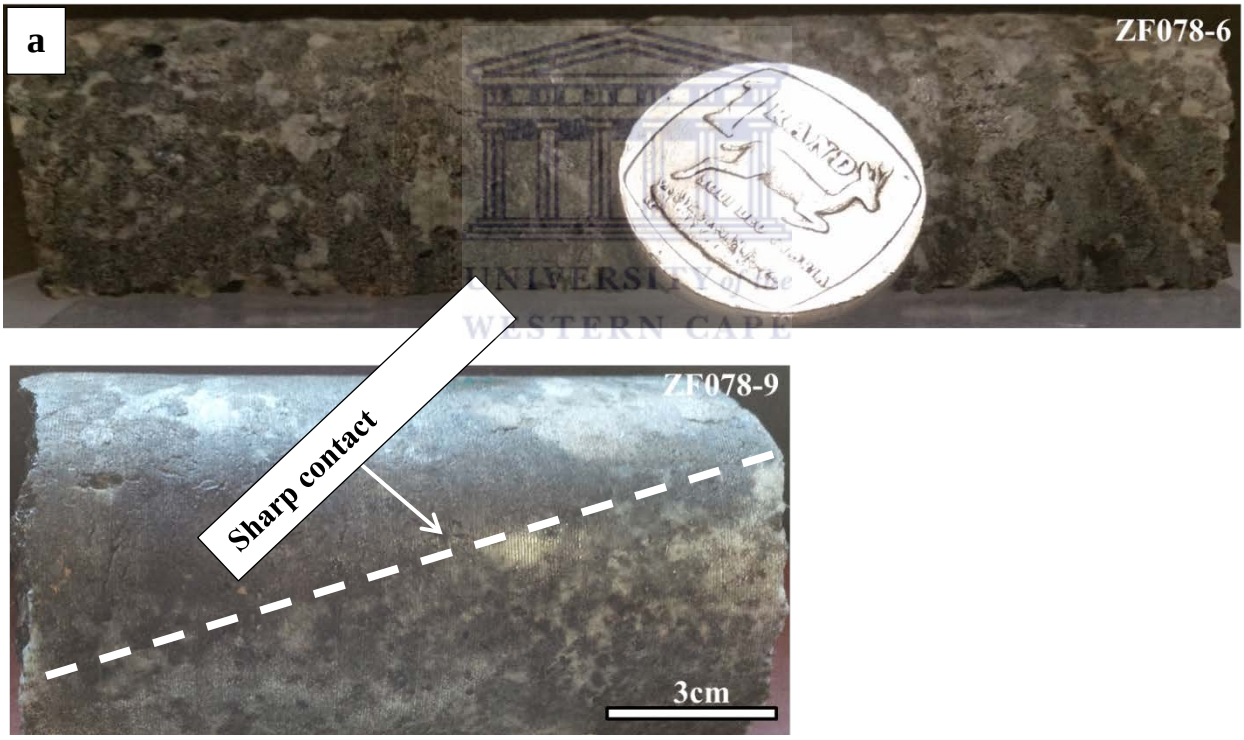

Figure 3.9: (a) medium-grained melanorite with cumulus plagioclase in drillhole ZF078 at depth 1105.57m. (b) Coarse-grained feldspathic pyroxenite in drillhole ZF078 at depth 1117.15m.

3.1.4.1 Clinopyroxene

Clinopyroxene is the least abundant cumulus mineral phase in the melanorites and this is mainly because of the relatively high CaO content associated with this unit (Plate 3.8c). The clinopyroxene exhibit subhedral-anhedral grain shapes ranging in size from 1-2mm (Plate 3.8c). Exsolution lamellae of orthopyroxene on clinopyroxene are not evident in the samples analyzed.

3.1.4.2 Orthopyroxene

Orthopyroxene is a major constituent of the melanorites making up 35% of the rock volume (Plate 3.8a-d). It usually alters to microcrystalline minerals (amphibole), especially along cleavage planes. Exsollution lamellae of clinopyroxene on orthopyroxene can be observed in some rock samples. Inclusions of plagioclase on orthopyroxene are present suggesting some Main Zone influence. Eales et al. (1991) reported inclusions of amoeboid plagioclase inside orthopyroxene grains in certain pyroxenite layers and argued for retention in the magma of plagioclase from the previous cycle.

3.1.4.3 Plagioclase

Plagioclase occurs as a cumulus mineral phase making up more than 50% of the rock volume. Alteration of plagioclase to sericite was not observed in the samples analysed. Plagioclase grains are usually 1-2.5mm in diameter while exhibiting subhedral-anhedral crystal shapes (Plate 3.8a).

3.1.4.4 Chromite

No chromite was recorded in the analysed samples.

3.1.4.5 Secondary alteration minerals and accessory minerals

This unit is the least altered unit where most of the igneous textures have been preserved. The pyroxenes are usually altered to amphibole and biotite.

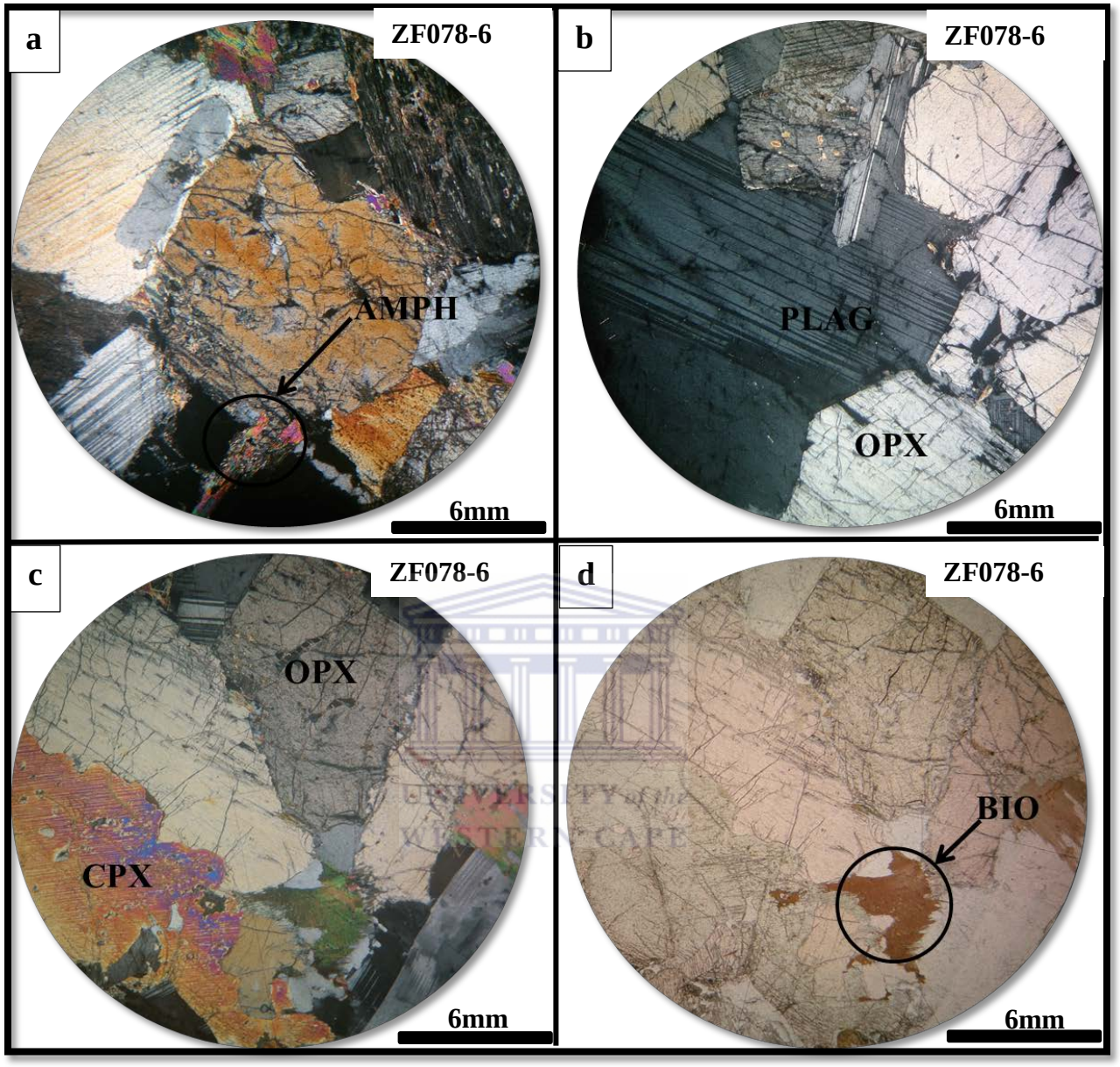

Plate 3.8: Petrographic photographs of the P4 litholgical unit present at Zwartfontein. Panels **c** and **d** are taken in both crossed nichols and crossed polarised light. (**a-d**) Melanorite with cumulus plagioclase (55%), orthopyroxene (30%) and clinopyroxene (15%), while secondary biotite and amphibole also occur probably resulting from the alteration of pyroxene.

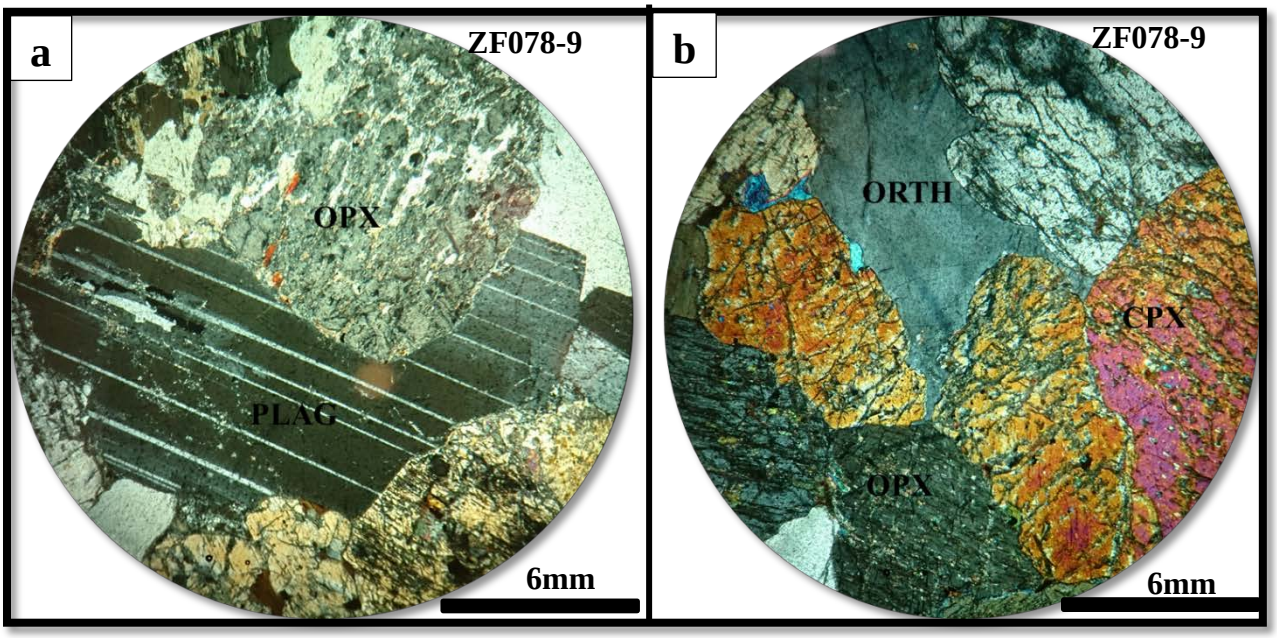

Plate 3.9: Petrographic photographs of the P4 litholgical unit present at Zwartfontein. **(a)** Feldspathic pyroxenite with large interstitial plagioclase grain and variably altered orthopyroxene grain. **(b)** interstitial orthoclase, clinopyroxene and orthopyroxene. Note: this rock was initially classified as a P4 unit rock, however on the basis of petrographic observations, this rock type should infact be classified as a P3 unit feldspathic pyroxenite.

Table 3.1 below is a summary table for the mineralogical character of the four lithological units (P1-P4).

Table 3.1: Summary of the mineralogical character of P1-P4

Platreef Unit	Primary mineral assemblage in vol (%)	Possible Alteration Products	Textures and Alteration
P1	Clinopyroxene (50%) Orthopyroxene (40%) Plagioclase (7%) Chromite (5%) where chromitite is not a major lithology.	Sericite Uralite Biotite	Interlocking textures Poikilitic Textures Minor Sericitization and Uralitization
P2	Olivine (45%) Clinopyroxene (<5%) Orthopyroxene (40%) Chromite (<5%) Plagioclase (<5%)	Sericite Serpentine	Poikilitic Texture Serpentinization relatively high Sericitization relatively low Uralitization (low)
P3	Orthopyroxene (45%) Clinopyroxene (40%) Plagioclase (>10%)	Sericite Uralite	Poikilitic textures Sericitization (dominant) Uralitizatization (Moderate)
P4	Clinopyroxene (15%) Orthopyroxene (35%) Plagioclase (55%)	Sericite Uralite Biotite amphibole	Ophitic textures Minor Sericitization Uralitization

3.2 Whole rock Geochemistry

In order to investigate the geochemical character of the mafic-ultramafic sequence of the Platreef at the Akanani prospect area a geochemical study was undertaken. This enabled confirmation of rock identifications and observations made during core-logging as well as in the field by Akanani mining personnel. Additionally other methods based on the combination of various multivariate statistical techniques were employed to develop a quick and cost effective way of differentiating and characterizing the Platreef pyroxenite layers at the Akanani prospect area. The P2 unit is believed to be the most mineralized zone (Van der Merwe, 2012). The detailed description of the methodology is given in chapter 2 and will therefore not be discussed further. A complete dataset is given in the Appendix A and B.

3.2.1 Univariate statistics

All variables of the data set from boreholes ZF044, ZF045, ZF048, ZF057, ZF078, ZF082 and M0023 were tested for normality as it is a pre-requisite before performing any multivariate statistical analysis (Fig. 3.1). Reimann and Filzmoser (2000) interpreted the strong skewness in data sets as resulting from more than one population or process that affects the normal distribution of geochemical variables. The element distributions show a skewed pattern, have outliers and originate from more than just one process (Fig. 3.1). It has always been believed that regional geochemical data sets almost never follow a normal distribution and that in most cases a data transformation (e.g. log, In, logit, square root or range) will not result in a normal distribution (e.g. Reimann and Filzmoser, 1999). Almost all the variables show no normal distribution and when transformed in log does not show normal distribution; therefore the original data was used with the assumption that the studied data show a normal or a lognormal distribution. Table 3.1 below shows the median, mean, minimum, maximum, standard deviation, untransformed data for major and trace elements. The minimum, maximum, standard deviation, untransformed data for each Platreef subdivision unit is given in the Appendix. Three outliers from P1 samples (ZF057-53; ZF078-49; ZF078-50) were removed from this analysis and were interpreted to represent chromitite samples occurring within this unit, while from the P2 unit only one outlier was detected within the data set with SiO_2 concentration of 16 wt% interpreted as an extensively serpentinized rock type probably a serpentinite.

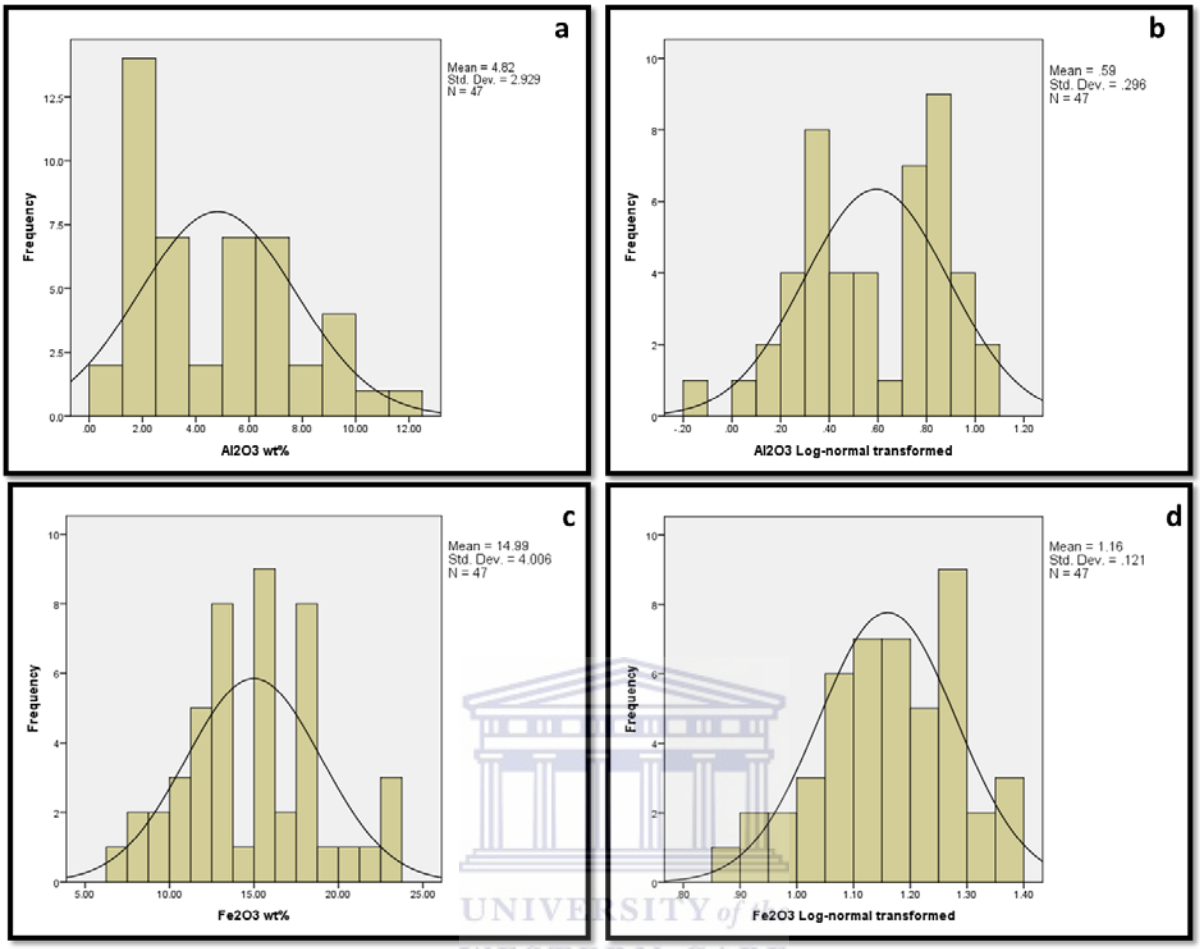

Figure 3.1: Histograms showing the normal and log-normal distribution of selected major elements. **(a-b)** Al_2O_3 (wt.%) and Al_2O_3-log normal **(c-d)** Fe_2O_3 (wt.%) and Fe_2O_3-log normal.

3.2.2 Correlation analysis

In order to determine whether a relationship between variables exists, correlation analysis was used. A summary of the results is given in Table 3.2 below. There is a positive correlation between the felsic elements (Al_2O_3, Na_2O, K_2O), while a strong positive relationship between Pt, Pd, Ni, Cu, and Au is observable which could suggest a sulphide influence on the concentration of PGEs +Au. Due to limited number of samples with PGE concentration this PGE-Ni-Cu correlation may not be a good representative of the actual relationship. There exists a strong positive relationship between TiO_2 and Cr and these elements are also related to thin layers of chromitite stringers. The mafic elements (MgO and Fe_2O_3) show a very strong negative relationship with the felsic elements (Al_2O_3, Na_2O and K_2O) indicating an increase in felsic phases (i.e. plagioclase) with decreasing mafic compositions.

Table 3.2: Correlation analysis results

Elemen	SiO2	Al2O3	Fe2O3	MnO	MgO	CaO	Na2O	K2O	TiO2	P2O5	SO3	LOI	Cr	Cu	Ni	Rb	Sr	V	Y	Zr	Au	Pd	Pt
SiO2	1																						
Al2O3	.095	1																					
Fe2O3	-.121	-.040	1																				
MnO	.400**	-.407**	-.174	1																			
MgO	-.676**	-.503**	-.214	-.059	1																		
CaO	.288*	.138	-.396**	.265	-.525**	1																	
Na2O	.452**	**.700****	.035	-.276*	**-.711****	.121	1																
K2O	.183	.549**	.027	-.071	-.446**	.070	.542**	1															
TiO2	-.150	**.608****	.573**	-.562**	-.434**	-.003	.437**	.313*	1														
P2O5	.033	.205	-.114	-.101	-.295*	.410**	.263	.192	.195	1													
SO3	-.037	.161	.429**	-.287*	-.330*	-.045	.319*	.168	.370**	.164	1												
LOI	**-.767****	-.309*	-.238	-.271	**.744****	-.338*	-.365**	-.183	-.306*	-.087	-.113	1											
Cr	-.174	.259	.528**	-.436**	-.156	-.138	.153	.010	.630**	.080	.198	-.211	1										
Cu	-.166	-.270	.261	-.038	.120	-.174	-.127	.095	-.023	-.018	.271	.134	.166	1									
Ni	-.251	-.433**	.352*	-.041	.210	-.243	-.311*	-.150	-.122	-.124	.388**	.243	.187	**.784****	1								
Rb	.158	.191	-.205	.036	-.034	-.145	.243	.331*	-.056	-.087	-.079	.049	-.236	-.329*	-.344*	1							
Sr	.283*	.252	-.020	-.132	-.315*	-.080	.612**	.193	.174	-.001	.330*	-.068	-.054	-.232	-.267	**.612****	1						
V	-.057	.307*	.480**	-.339*	-.280*	-.006	.197	.042	**.642****	.095	.131	-.312*	**.958****	.113	.128	-.285*	-.104	1					
Y	.239	.041	-.211	.229	-.341*	.434**	.268	.276*	.053	.467**	-.009	-.072	-.225	-.209	-.226	.310*	.233	-.094	1				
Zr	.065	.255	-.160	-.022	-.203	.137	.403**	.227	.205	.274	.215	.025	-.115	-.106	-.204	.476**	**.709****	-.107	.501**	1			
Au	.189	-.132	.373	.263	-.160	-.092	.044	.238	.035	.042	.133	-.339	**.739****	.572**	.435*	-.240	-.029	**.725****	-.138	.052	1		
Pd	-.062	-.349	.490**	.080	.062	-.242	-.262	-.195	-.073	-.086	.234	-.056	**.759****	.571**	**.766****	-.281	-.183	**.688****	-.195	-.103	**.741****	1	
Pt	.072	-.260	.423*	.179	-.031	-.160	-.171	-.141	-.055	-.067	.164	-.214	**.851****	.426*	.584**	-.226	-.042	**.800****	-.181	-.071	**.838****	**.931****	1

**. Correlation is significant at the 0.01 level (2-tailed).

*. Correlation is significant at the 0.05 level (2-tailed).

3.2.3 Multivariate Statistics

This section will focus on three multivariate statistical methods including factor, cluster and discriminant analysis and their combinations. Multivariate statistical methods have been applied to geochemical data of seven bore holes drilled at the Akanani area. The objective was to evaluate the mutual correlations among the various variables to reveal the distinctive geochemical character of the four Platreef lithologies. Results derived from this section can be used with a high level of confidence to differentiate between the four Platreef lithologies and further delineate areas with high/low concentration of mineralization. The initial step of this analysis involved a total number of 53 samples of which 35 were classified as either belonging to P1, P2, P3 or P4 by exploration geologists at the Akanani prospect area on the basis of field observations and core-logging. A linear discriminant analysis was applied to the 35 of the 53 available samples identified by Akanani mining personnel to check the reliability of the classification scheme. Two other methods based on the combination of different multivariate statistical techniques were employed to classify and characterize the pyroxenite layers and later the results were compared to the classification scheme provided by mining personnel.

3.2.3.1 Discriminant analysis of Lonmin classification scheme

Discriminant analysis is similar to multiple linear regression analysis in that it predicts an outcome. Given that the first step of this analysis involved 53 samples of which 35 are known and 18 are unknown, the first step will therefore involve the characterization of the known samples to determine the reliability of the classification provided by field geologists. The classification was as follows; 21 samples belonged to P1; 4 to P2; 5 to P3 and 5 to P4. The classification results are given in Table 3.3 below. The classification results gave a recognition rate of 88.6%. This means that only four out of the 35 samples were misclassified by mining personnel which translate to 11.4%. The classification allocated 20 samples to P1, 3 samples to P2, 8 samples to P3 and 4 samples to P4. The classification results proved the unreliability of the classification of P1, P2, P3 and P4 on the basis of core-logging and field observation. For example in P1, 2 of the 21 samples actually belong to P3. In P2, 1 of the samples classified as belonging to P2 belongs to P1, while in P4 1 of the 5 samples belongs to P3.

Table 3.3: classification results for the 35 known samples from the Akanani prospect area.

Platreef Subdivision			Predicted Group Membership				Total
			P1	**P2**	**P3**	**P4**	
Original	Count	**P1**	**19**	0	2	0	**21**
		P2	1	**3**	0	0	**4**
		P3	0	0	**5**	0	**5**
		P4	0	0	1	**4**	**5**
	%	**P1**	90.5	.0	9.5	.0	100.0
		P2	25.0	75.0	.0	.0	100.0
		P3	.0	.0	100.0	.0	100.0
		P4	.0	.0	20.0	80.0	100.0
a**.88.6%** of original grouped cases correctly classified.							

According to the classification results, P1 is characterized by high TiO_2, Cr, Fe_2O_3, P_2O_5, MnO and K_2O; P2 contains the highest concentration of MgO and LOI; P3 contains some concentration of SiO_2, Na_2O, Al_2O_3, while the highest concentration of the felsic elements is encountered in P4 together with CaO. Table 3.4 and 3.5 summarises the results.

Table 3.4: Three discriminant group function

	Function		
	1	2	3
Na2O	-.352*	.173	.031
SiO2	-.351*	-.114	-.291
Al2O3	-.310*	.147	.097
LOI	.413	.639*	-.005
MgO	.348	.382*	-.278
Fe2O3	.067	-.306*	.133
TiO2	-.006	-.265*	.049
P2O5	.004	-.214*	.042
Cr	.035	-.204*	.137
MnO	-.020	-.167*	-.089
K2O	-.075	-.113*	-.029
CaO	.038	-.184	.204*

Table 3.5: Function at group centroid

VAR00002	Function		
	1	2	3
P1	.465	-.549	.337
P2	3.748	1.676	-.381
P3	-1.490	-.312	-1.701
P4	-3.459	1.277	.593

The classification was further improved by creating a predicted group membership that classifies the incorrectly classified samples into their predicted group membership and the results gave a 100% classification for the training samples (Table 3.6). In this analysis, 20 samples were classified as belonging to P1, 3 to P2, 8 to P3 and 4 to P4 respectively. This method improved the reliability of the training samples as provided by mining personnel at the Akanani area.

Table 3.6: Classification results

Predicted Group for Analysis 1			Predicted Group Membership				Total
			P1	P2	P3	P4	
Original	Count	**P1**	**20**	0	0	0	**20**
		P2	0	**3**	0	0	**3**
		P3	0	0	**8**	0	**8**
		P4	0	0	0	**4**	**4**
	%	**P1**	100.0	.0	.0	.0	100.0
		P2	.0	100.0	.0	.0	100.0
		P3	.0	.0	100.0	.0	100.0
		P4	.0	.0	.0	100.0	100.0

a.**100.0%** of original grouped cases correctly classified.

After characterizing and enhancing the classification of the training samples as provided by Lonmin mining personnel, the 18 unknown samples were classified into one of the pre-defined four groups with results giving a recognition rate of 94.3%. Table 3.7 below summarizes the classification results of the new predicted group membership. Of the 53 samples, 21 were classified to P1, 3 were classified to P2, 20 to P3 and a total of 9 samples were classified to P4. Of the 21 samples classified as belonging to P1, 1 sample actually belongs to P3. In P3, 2 of the samples 20 classified as belonging to P3 belong to P1 and P4 respectively.

Table 3.7: Classification results for the 53 samples of the Platreef from the Akanani area.

Platreef Subdivision			Predicted Group Membership				Total
			P1	**P2**	**P3**	**P4**	
Original	Count	**P1**	**20**	0	1	0	21
		P2	0	**3**	0	0	3
		P3	1	0	**18**	1	20
		P4	0	0	0	**9**	9
	%	**P1**	95.2	.0	4.8	.0	100.0
		P2	.0	100.0	.0	.0	100.0
		P3	5.0	.0	90.0	5.0	100.0
		P4	.0	.0	.0	100.0	100.0
a.**94.3%** of original grouped cases correctly classified.							

The two function discriminant plot below (Fig. 3.10) seperates the mafic (P1 and P2) from the felsic (P3 and P4) components. Results show that P1 is enriched with CaO, TiO_2, P_2O_5, Cr, K_2O, while P2 has higher concentrations for Fe_2O_3, MgO and LOI, P3 and P4 is characterized by higher SiO_2, Al_2O_3, Na_2O relative to P1 and P2.

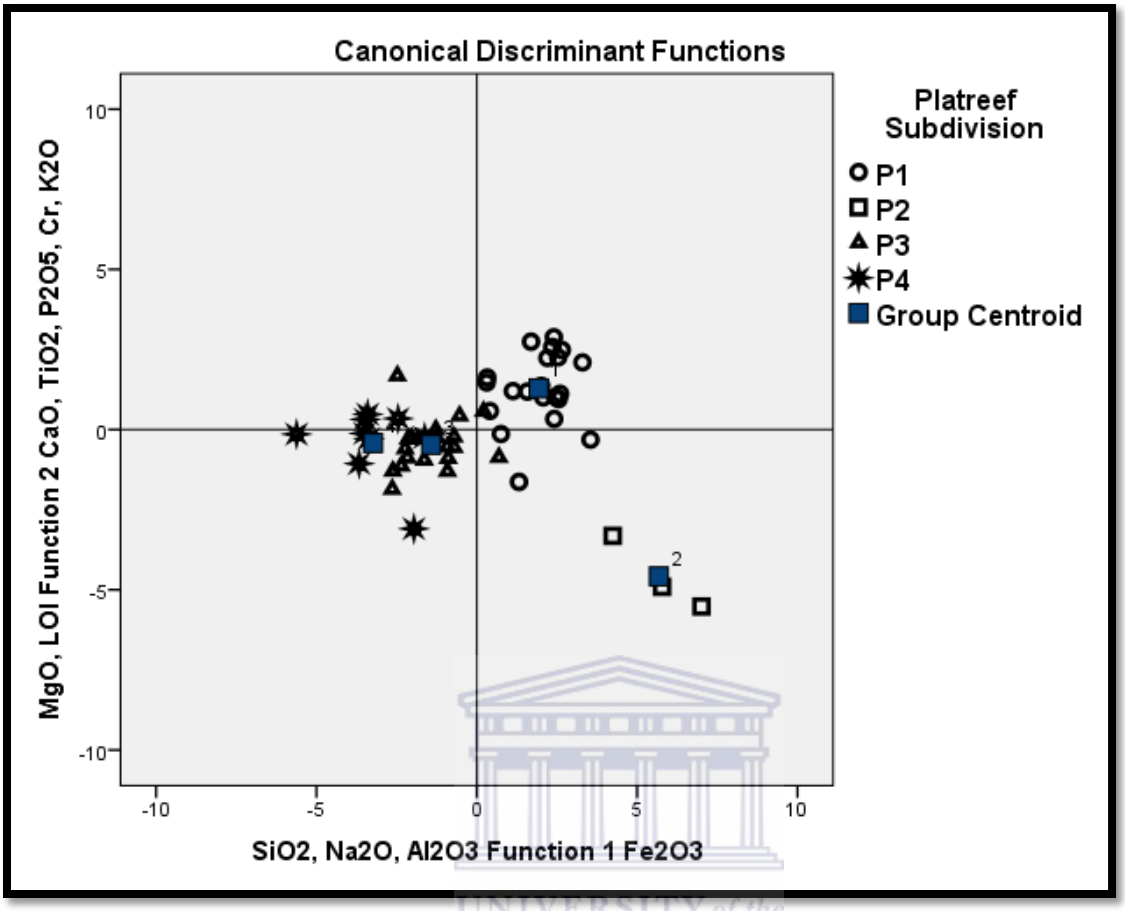

Figure 3.10: Discriminant plot for the first two functions

This data does not prove to be reliable as the incorrect classification of samples makes it difficult to determine the exact location of the mineralization and the associated rock type, For example there is no clear distinction between P3 and P4 based on this classification. Sample ZF078/15 with 46.2 wt.% SiO_2, 7.2 wt.% Al_2O_3, 14.9 wt.% Fe_2O_3, 20 wt.% MgO and 6.5 wt.% CaO is classified as within the P3 unit, while another sample ZF044/51 with 47 wt.% SiO_2, 7.8 wt.% Al_2O_3, 13.3 wt.% Fe_2O_3, 22 wt.% MgO and 6.9 wt.% CaO is classified as P4.

3.2.3.2 Classification of the pyroxenite layers - combination of factor and discriminant analysis approach

A dataset comprising 53 samples of which 25 were randomly selected from the previous dataset was therefore used with the aim of determining whether the new dataset can give the same elemental associations as those samples identified by mining personnel and to create elemental associations that can be used to identify each unit. The combination of factor and discriminant analysis approach depends upon creating reference samples (training sets) through factor analysis and characterizing these factors with discriminant analysis (Siad, 2012, unpublished material). This allows identification of the distinctive geochemical characteristics that can be used to identify each layer. A four factor score was then extracted (Table 3.10) saved and later characterized by discriminant analysis. The results for the four factors explain 81% of the total variation (Table 3.9).

Table 3.8: Factor analysis results showing the total variance.

Component	Initial Eigenvalues			Extraction Sums of Squared Loadings			Rotation Sums of Squared Loadings		
	Total	% of Variance	Cumulative %	Total	% of Variance	Cumulative %	Total	% of Variance	Cumulative %
1	4.042	36.743	36.743	4.042	36.743	36.743	2.539	23.083	23.083
2	2.320	21.095	57.838	2.320	21.095	57.838	2.533	23.027	46.109
3	1.474	13.403	71.242	1.474	13.403	71.242	2.342	21.289	67.398
4	1.160	10.546	81.788	1.160	10.546	81.788	1.583	14.390	**81.788**
5	.639	5.813	87.601						
6	.519	4.719	92.320						
7	.382	3.468	95.788						
8	.304	2.760	98.548						
9	.111	1.013	99.561						
10	.047	.428	99.989						
11	.001	.011	100.000						

Extraction Method: Principal Component Analysis.

Factor 1 is positively loaded with Al_2O_3, Na_2O, K_2O as well as TiO_2 and negatively loaded with MgO which clearly seperates mafic (P2) units to feldspathic units (P3). Factor 2 is negatively loaded with MgO and LOI which represents the extensively serpentinized P2 unit. LOI has a

higher score with the more altered P2 unit and suggests that secondary geochemical processes dominate this unit. Factor 3 is positively loaded with Fe_2O_3, Cr and TiO_2 while Factor four is represented by CaO and P_2O_5 (apatite) and has a higher score with P4. This association points to Ca-phosphate, apatite, Ca-plagioclase (anorthite) and Ca-rich pyroxene determining the values in this factor. The results are summarized in Table 3.9 below.

Table 3.9: Rotated Component Matrix

	Component			
	1	2	3	4
Al2O3	.826			
Na2O	.817			
K2O	.799			
SiO2		.920		
LOI		-.892		
MgO	-.481	-.759		
Cr			.865	
TiO2	.460		.803	
Fe2O3			.793	
CaO				.845
P2O5				.759

Using discriminant analysis the training sample were later saved and characterized. The results gave a 100% recognition rate, with five training samples correctly classified as belonging to P1, 6 to P2, 6 to P3 and 9 to P4 (Table 3.10).

Table 3.10: Classification results for the training samples

Platreef Subdivision			Predicted Group Membership				Total
			P1	**P2**	**P3**	**P4**	
Original	Count	**P1**	**5**	0	0	0	**5**
		P2	0	**6**	0	0	**6**
		P3	0	0	**6**	0	**6**
		P4	0	0	0	**9**	**9**
	%	**P1**	100.0	.0	.0	.0	100.0
		P2	.0	100.0	.0	.0	100.0
		P3	.0	.0	100.0	.0	100.0
		P4	.0	.0	.0	100.0	100.0
a.**100.0%** of original grouped cases correctly classified.							

Using the discriminant functions computed with training groups, the 27 unknown samples were classified into one of the pre-defined four groups, with a recognition rate of 100%. Table 3.11 below summarizes the classification results. Of the 53 samples, 13 samples representing P1 are enriched with Fe_2O_3, Cr, and TiO_2; 17 samples were correctly classified as P2 with the enrichment of MgO and LOI; 14 samples represented the feldspathized P3 unit which corroborates with the high Na_2O, Al_2O_3, K_2O associated with this unit, while P4 was classified by 9 samples that are highly enriched with CaO and P_2O_5. The results are summarized in Table 3.12 and 3.13 below.

Table 3.11: classification results for the predicted group membership

		Platreef Subdivision	Predicted Group Membership				Total
			P1	P2	P3	P4	
Original	Count	**P1**	**13**	0	0	0	**13**
		P2	0	**17**	0	0	**17**
		P3	0	0	**14**	0	**14**
		P4	0	0	0	**9**	**9**
	%	**P1**	100.0	.0	.0	.0	100.0
		P2	.0	100.0	.0	.0	100.0
		P3	.0	.0	100.0	.0	100.0
		P4	.0	.0	.0	100.0	100.0
a.**100.0%** of original grouped cases correctly classified.							

Table 3.12: Structure matrix of variables against function

	Function		
	1	2	3
MgO	-.341	.823*	-.018
Na2O	-.032	-.653*	.144
Al2O3	-.077	-.435*	.109
SiO2	.076	-.427*	.113
LOI	-.166	.391*	.113
K2O	.032	-.130*	-.046
Fe2O3	.118	.005	-.726*
CaO	.430	-.217	.533*
Cr	.045	-.076	-.254*
TiO2	.100	-.124	-.165*
P2O5	.132	-.005	.160*
MnO	.090	.028	-.099*

Table 3.13: Functions at Group Centroid

Platreef Subdivision	Function		
	1	2	3
P1	1.969	-.502	-2.126
P2	-1.913	2.081	.064
P3	-2.351	-2.195	.643
P4	4.428	.208	1.949

Figure 3.11 below is a discriminant plot representing the first two discriminant functions from the combination of discriminant and factor analysis. The first discriminant function has negative weights for MnO which classifies the P1 and P4 units, while Function 2 has negative weights for K_2O, Na_2O_3, Al_2O_3, SiO_2 characterizing P3 and positive weights for MgO and LOI characterizing P2.

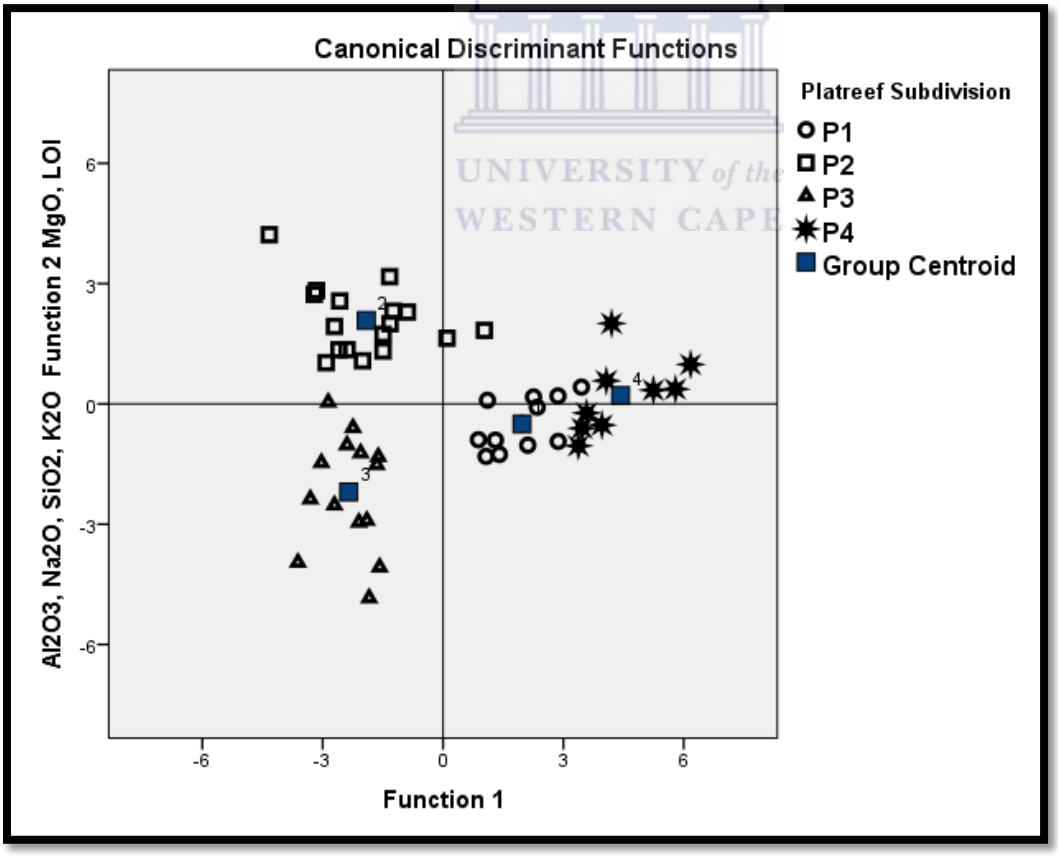

Figure 3.11: Two-function discriminant plot showing the abundance of elements in each unit (P1-P4).

Since the direct discriminant function method does not show the importance of the individual geochemical variables for the description of classified groups, or their importance in the classification itself, a stepwise discriminant method was considered. Results gave a 100% (Table 3.14) difference across the four Platreef units with MgO giving the highest percentage difference at 53.7% and Fe_2O_3 giving the second highest at 27.8% and Al_2O_3 being the lowest differentiator at 1.8 wt%. A summary of the results is given in Table 3.15 below.

Table 3.14: Summary of the classification results for stepwise discriminant analysis

Platreef Subdivision			**Predicted Group Membership**				**Total**
			P1	**P2**	**P3**	**P4**	
Original	Count	**P1**	**13**	0	0	0	**13**
		P2	0	**17**	0	0	**17**
		P3	0	0	**15**	0	**15**
		P4	0	0	0	**9**	**9**
	%	**P1**	100.0	.0	.0	.0	100.0
		P2	.0	100.0	.0	.0	100.0
		P3	.0	.0	100.0	.0	100.0
		P4	.0	.0	.0	100.0	100.0
a.**100.0%** of original grouped cases correctly classified.							

Table 3.15: Percentage difference of the three major elements discriminating between the four lithological units

Element	**Percentage difference**
MgO	53.7%
Fe_2O_3	27.8%
CaO	14.8%
TiO_2	1.9%
Al_2O_3	1.8%
Total	100%

3.2.3.3 Classification of the Pyroxenite Layers - Combination of R-mode cluster; R-mode Factor and Discriminant analysis approach

The same samples used in the previous analysis were retained inorder to compare the results of both approaches and to see if the same element associations can be obtained using a different approach. For the R-mode cluster analysis, the ALM with Pearson correlation was employed to create four element association groups, namely the mafic group (P1; Fe_2O_3, TiO_2, Cr and P2; MgO and LOI), the feldspathic group (P3; Al_2O_3, Na_2O, K_2O and SiO_2) and the melanoritic group (P4; CaO and P_2O_5 (Fig. 3.10). Figure 3.12 is a dendogram showing how the four groups were selected.

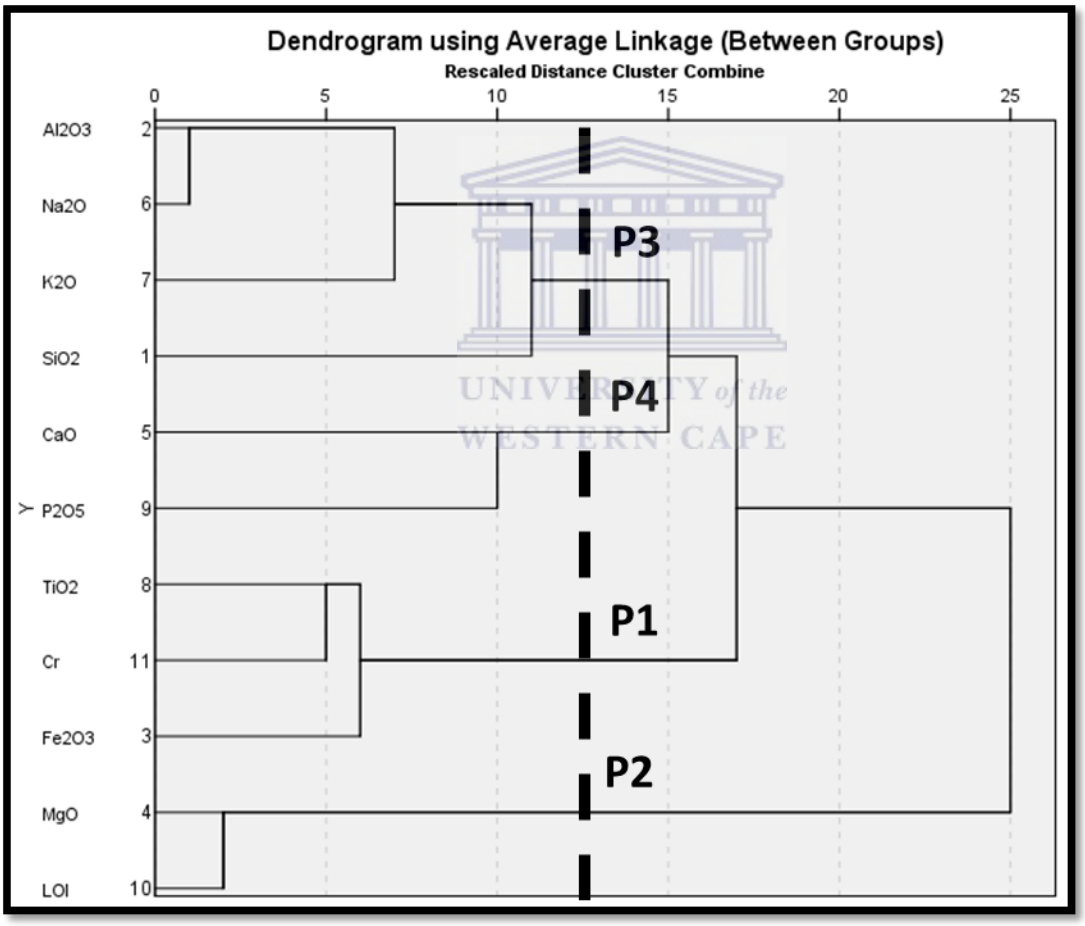

Figure 3.12: Dendogram showing the four lithological units at Akanani area

With the R-mode factor analysis training samples were selected for the four groups (P1-P4) as follows: four factor scores were extracted for each group (P1-P4) based on the element association results obtained from cluster analysis using the ALM method; factor one was

positively loaded with Fe_2O_3, Cr and TiO_2 and represents P1. The high Cr and low TiO_2 suggest that the P1 pyroxenites are Lower one-type pyroxenites. Factor two is positively loaded with MgO and LOI representing the extensively serpentinized P2; factor three is positively loaded with Na_2O, Al_2O_3, K_2O and SiO_2 representing the more feldspathic P3, while factor four is positively loaded with CaO and P_2O5 and represents P4. The results are summarized in Table 3.16 and Figure 3.13 below. Samples having high positive scores for the four factors were considered to be training samples for each group (P1-P4). The four factor scores were saved and training samples were created.

Table 3.16: Four factors scores for the four groups (P1-P4).

Component Matrix[a]	
P1	Component
	1
TiO2	.862
Cr	.841
Fe2O3	.805

Component Matrix[a]	
P2	Component
	1
MgO	.929
LOI	.929

Component Matrix[a]	
P3	Component
	1
Na2O	.937
Al2O3	.801
SiO2	.635
K2O	.531

Component Matrix[a]	
P4	Component
	1
CaO	.808
P2O5	.808

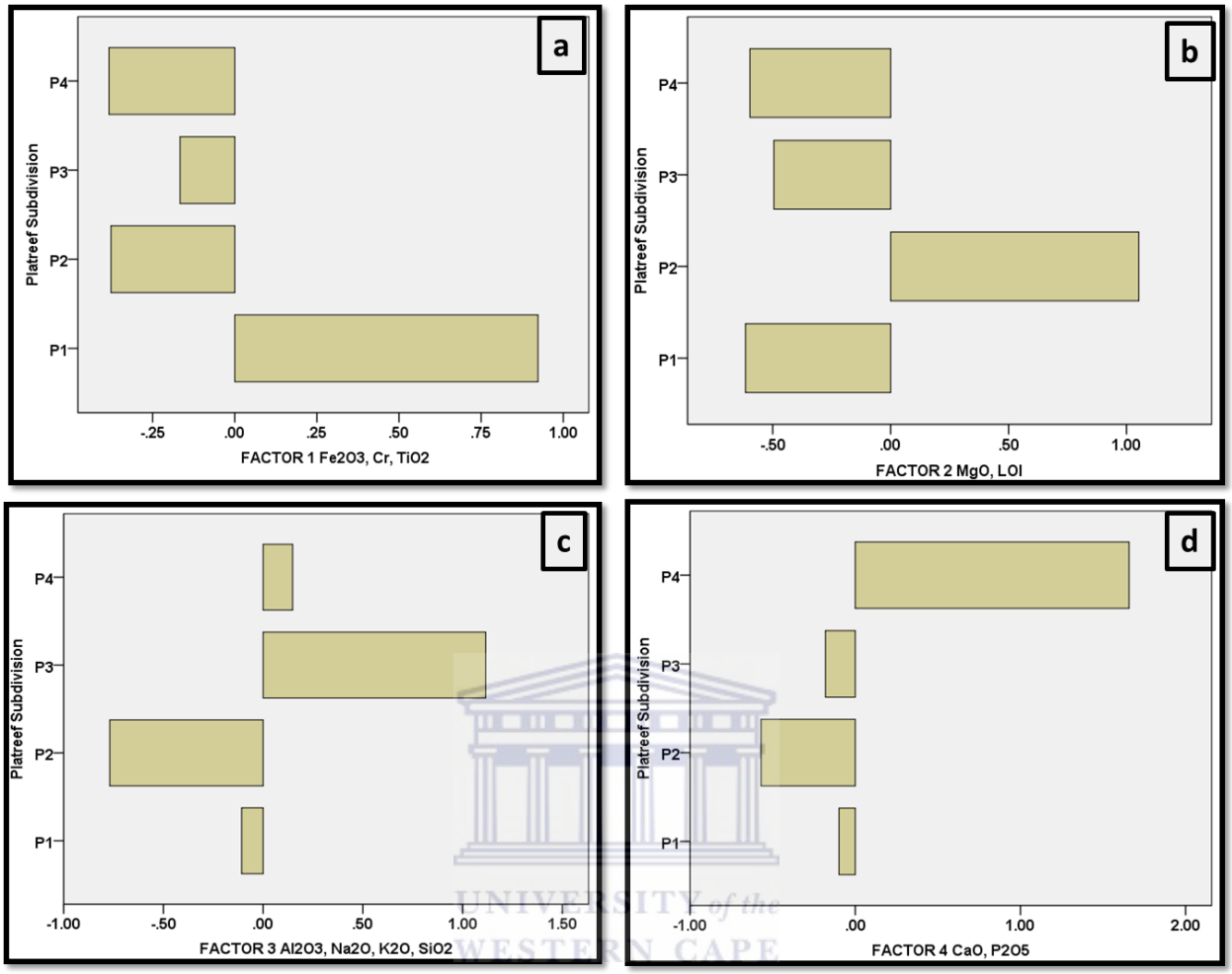

Figure 3.13: Bar graph showing the concentration of elements in each factor score representing the four lithological units at Akanani.

Using discriminant analysis, the four subgroups (P1, P2, P3 and P4) were further classified using the newly created training data set. Table 3.17 shows the results of the supervised classification using linear discriminant analysis. The training samples were correctly classified at 100% recognition rate with 5 samples allocated to P1, 13 to P2, 9 to P3 and 6 to P4.

Table 3.17: Classification results for the newly created training samples

Platreef Subdivision			Predicted Group Membership				Total
			P1	P2	P3	P4	
Original	Count	**P1**	**5**	0	0	0	**5**
		P2	0	**13**	0	0	**13**
		P3	0	0	**9**	0	**9**
		P4	0	0	0	**6**	**6**
		Ungrouped cases	8	4	5	3	**20**
	%	**P1**	100.0	.0	.0	.0	100.0
		P2	.0	100.0	.0	.0	100.0
		P3	.0	.0	100.0	.0	100.0
		P4	.0	.0	.0	100.0	100.0
		Ungrouped cases	40.0	20.0	25.0	15.0	100.0
a.**100.0%** of original grouped cases correctly classified.							

Using the discriminant functions computed with the training groups, 20 unknown samples were classified into one of the pre-defined four groups with a recognition rate of 100%. The new classification classified 13 samples to P1, 17 samples to P2, 14 samples to P3 and 9 samples to P4. Table 3.19 below shows a summary of the classification results were all the 53 samples have been allocated to their pre-defined four groups (P1-P4). The maximum number of discriminant functions is either one less than the number of groups or equal to the number of predictor variables (Siad et al., 1994). In this discriminant analysis the discriminant accuracies for the four groups are 100%, indicating that the percentage of accurate analyses is high for discriminating the four Platreef units at Akanani and thus results can be used with a high level of confidence. Table 3.20 shows the three discriminant functions of the training samples for the Akanani prospect area. The first function is positively loaded with CaO which is enriched in P4. Function 2 seperates feldspathic units (Na_2O, Al_2O_3 and K_2O) from the mafic unit (MgO and LOI), while function 3 is negatively loaded with (Fe_2O_3, Cr, TiO_2) which represent P1 and positively loaded with P_2O_5 representing P4. The increasing silica and alkaline content implies a transgression from mafic units in P1 and P2 to a more felsic unit in P3, while the high SiO_2 content in P1 may imply the assimilation of SiO_2 from the granitic footwall rocks. The three discriminant functions correctly classified the four rock units (P1-P4) by 100% as shown in Table 3.18. Figure 3.14

below shows the spatial distribution of the group membership of the Akanani prospect area resulting from the discriminant analysis.

Table 3.18: Classification results for the predicted group membership

Platreef Subdivision			Predicted Group Membership				Total
			P1	P2	P3	P4	
Original	Count	**P1**	**13**	0	0	0	**13**
		P2	0	**17**	0	0	**17**
		P3	0	0	**14**	0	**14**
		P4	0	0	0	**9**	**9**
	%	**P1**	100.0	.0	.0	.0	100.0
		P2	.0	100.0	.0	.0	100.0
		P3	.0	.0	100.0	.0	100.0
		P4	.0	.0	.0	100.0	100.0
a.**100.0%** of original grouped cases correctly classified.							

Table 3.19: Three function discriminant structure matrix

	Function		
	1	2	3
CaO	-.524*	.015	.359
MgO	.375	-.685*	-.115
Na2O	.005	.613*	.338
SiO2	-.078	.338*	.170
Al2O3	.023	.338*	.174
LOI	.147	-.307*	.085
K2O	-.007	.194*	.117
TiO2	-.089	.149*	-.110
Fe2O3	-.046	.171	-.629*
Cr	-.045	.094	-.213*
P2O5	-.126	-.020	.159*
MnO	-.058	-.005	-.118*

Table 3.20: Functions at group centroid

Predicted Group for Analysis 1	Function		
	1	2	3
P1	-1.686	.863	-2.306
P2	2.255	-2.016	-.129
P3	1.754	2.476	1.191
P4	-4.359	-1.014	1.854

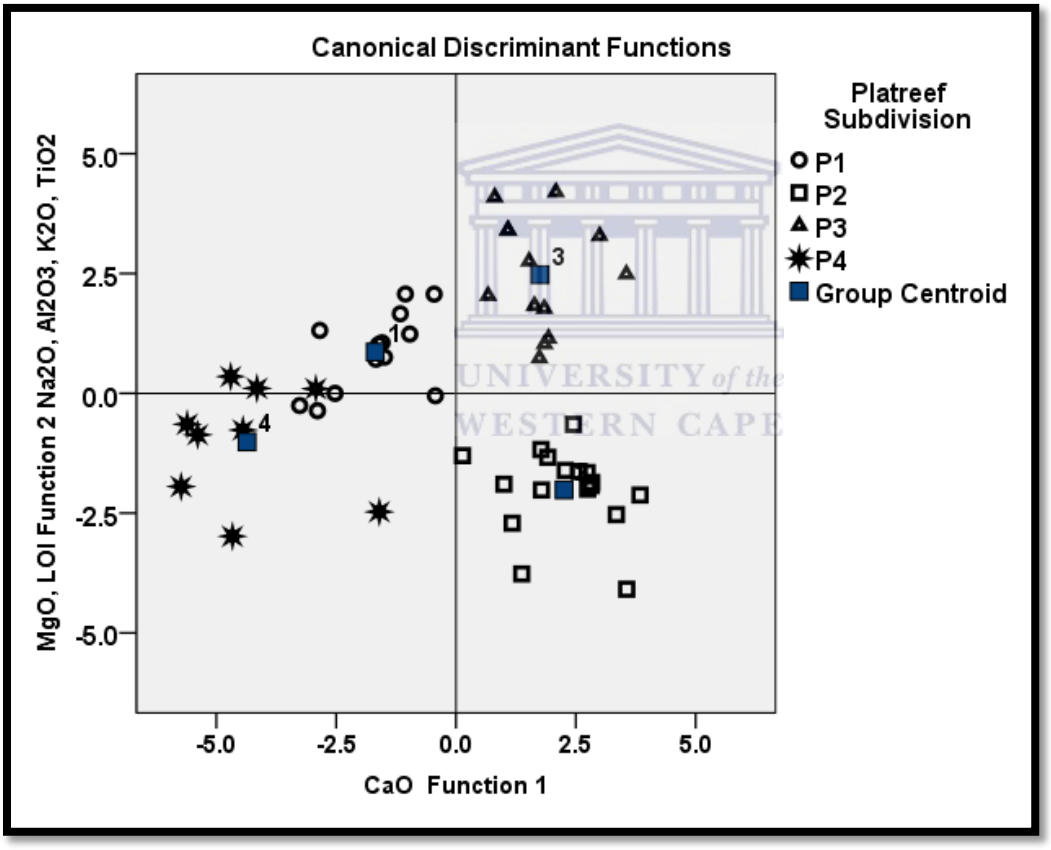

Figure 3.14: Training samples discriminant plot for the first two functions

Stepwise discriminant analysis results gave a 94.1% (Table 3.22) difference across the four Platreef units with MgO giving the highest percentage difference at 64.7% (Table 3.22) and Fe_2O_3 giving the lowest at 5.9%. A summary of the classification results is given in Table 3.21 below.

Table 3.21: Classification results for stepwise discriminant analysis using the combination of r-mode cluster, r-mode factor and discriminant analysis.

Platreef Subdivision			Predicted Group Membership				Total
			P1	P2	P3	P4	
Original	Count	P1	**12**	0	0	1	**13**
		P2	0	**17**	0	0	**17**
		P3	0	0	**12**	0	**12**
		P4	0	1	1	**7**	**9**
	%	P1	92.3	.0	.0	7.7	100.0
		P2	.0	100.0	.0	.0	100.0
		P3	.0	.0	100.0	.0	100.0
		P4	.0	11.1	11.1	77.8	100.0
a.94.1% **of original grouped cases correctly classified.**							

Table 3.22: Summary of the stepwise discriminant analysis results

ELEMENT	PERCENTAGE DIFFERENCE
MgO	64.7%
Na_2O	15.7%
CaO	7.8%
Fe_2O_3	5.9%
TOTAL	94.1%

In order to determine the relationship between the four Platreef lithologies and the PGE-BMS mineralization, the following elements (Pt, Pd, Ni, Cu, Cr and Au) were added into the analysis and the results are summarized in Figure 3.15 below. Disciminant function 1 has positive weights for Na_2O, Al_2O_3, and K_2O and positive weights for MgO separating the mafic unit P2 from the feldspathized P3. Discriminant function 2 has negative weights for CaO and P_2O_5 and positive weights for Fe_2O_3, MnO, Pt, Cr, Cu, Pd, Ni and Au separating between mafic units P1 and P2 and the less mineralized units of P3 and P4. These results suggest that P3 and P4 units are

less mineralized; while the highest tonnage and grade of PGE-BMS mineralization can be associated with P1 and P2 unit.

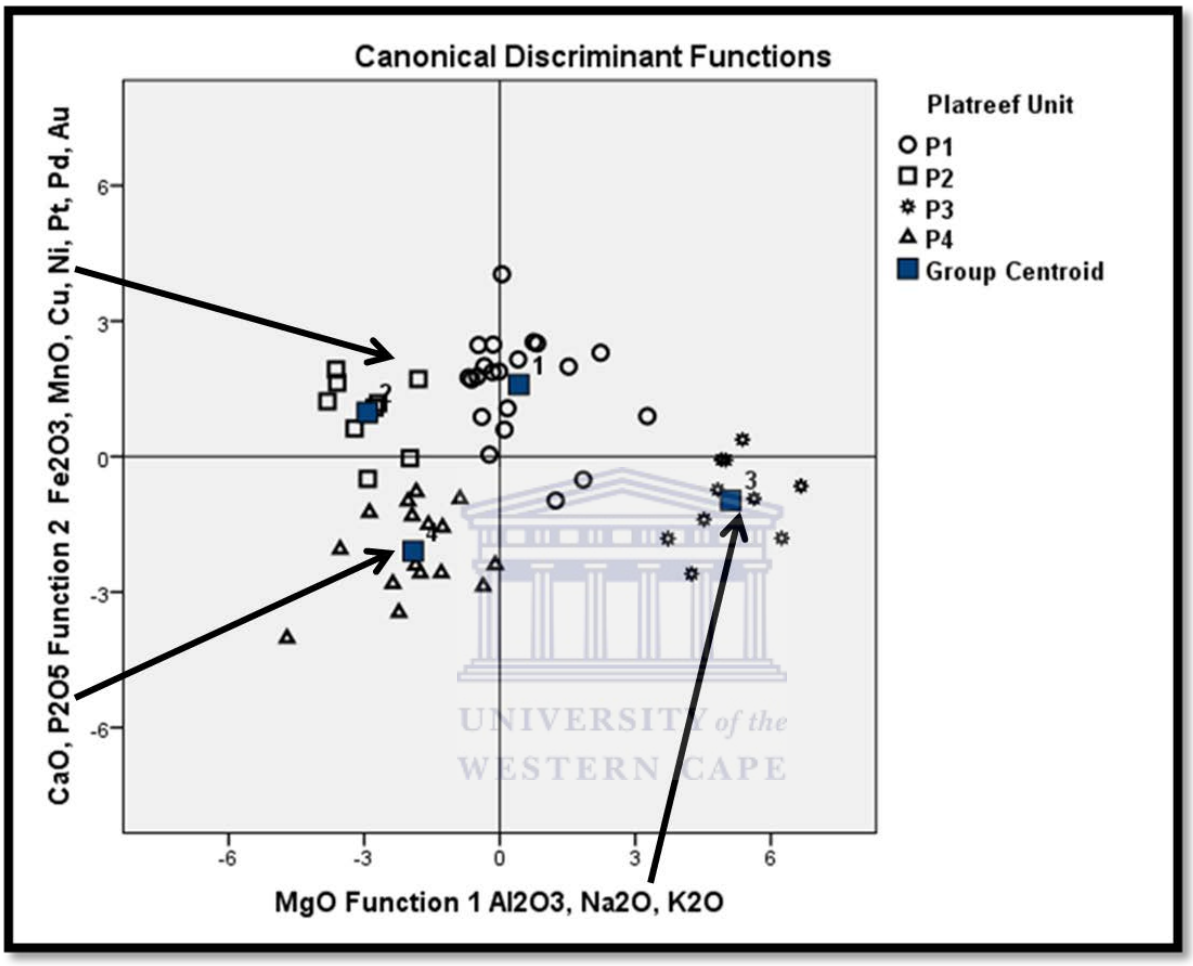

Figure 3.15: Training samples discriminant plot for the first two functions.

3.2.3.4 Scatter plots

Scatterplots are bivariate or trivariate plots of variables against each other (Härdle and Simar, 2003). They give us more insights on the nature of the relationship amongst variables of a dataset. This relationship can be in two ways (1) A downward-sloping scatter, indicating that an increase of one variable may result in the decrease of the other variable (2) An upward-sloping scatter that shows a positive relationship indicating that an increase of the variable on the

horizontal axis will result in the increase of the variable on the vertical axis (Härdle and Simar, 2003).

Figure 3.16a shows that P1 and P2 are enriched with (Fe_2O_3 + MgO), while P3 and P4 will have high Al_2O_3 content. This increase in Al_2O_3 in P3 and P4 is related to a possible increase in plagioclase relative to pyroxene. To further demonstrate the controls of modal mineralogy on rock samples, major element oxides were plotted against MgO (Fig. 3.16b, c, d). In Figure 3.16b, c, d MgO shows a negative correlation with CaO, Na_2O and Al_2O_3 probably due to an increase in plagioclase content relative to pyroxene proportions in rock.

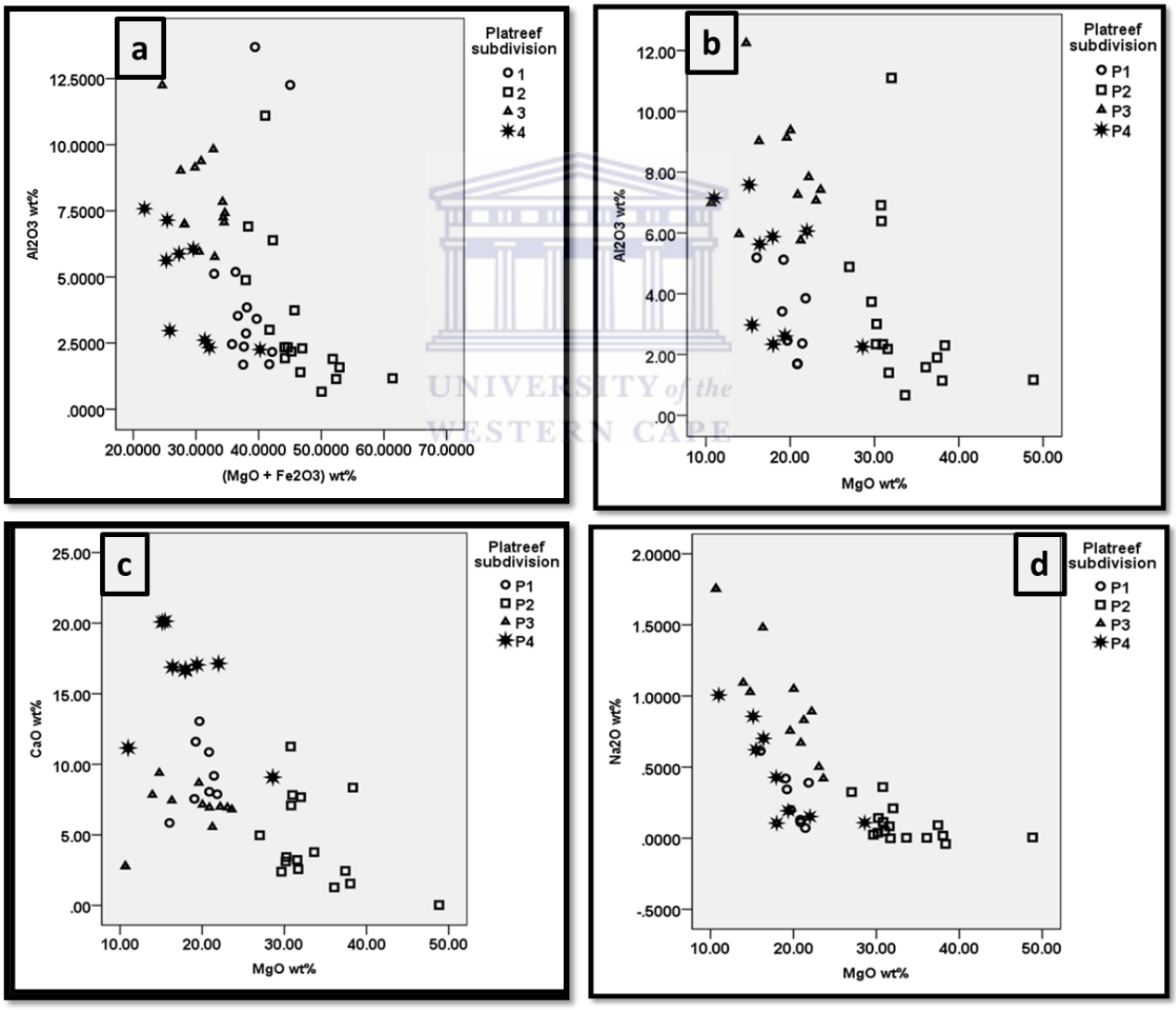

Figure 3.16: (a) Bivariate plots of whole-rock Al_2O_3 plotted against MgO + Fe_2O_3 (representing total Fe); (b-d) Bivariate plots of wt% major element oxides against wt% MgO. Increasing wt%

MgO represents increasing pyroxene and olivine relative to plagioclase proportions in rock. All MgO plots are the same scale from 10-50.

Against Fe_2O_3 and MnO, MgO (Fig. 3.17a, b, c, d) shows a positive correlation which is significantly related to increasing pyroxene relative to plagioclase proportions in rock. Fe_2O_3 proportions occur towards the base in P1 in close association with the mineralization. The concentration of MgO and Fe_2O_3, show a sharp inflection in their variation trends, which may be attributed to the early fractionation of Mg-Fe-rich phases such as olivine and pyroxene from the ultramafic magma. There is a considerable scatter developed for TiO_2 against MgO which may be caused by varying occurrences of magnetite, ilmenite and rutile through the basal mineralization. P4 samples show elevated concentrations of CaO which in part signifies the occurrence of Ca-rich pyroxene as well as the increasing CaO content of plagioclase with stratigraphic height. The LOI against MgO shows a positive relationship which signifies that most MgO-rich pyroxenes and olivines could have been variably altered to secondary phases (e.g. chlorite, serpentine, actinolite, tremolite or amphibole). This analysis is consistent with petrographic analysis.

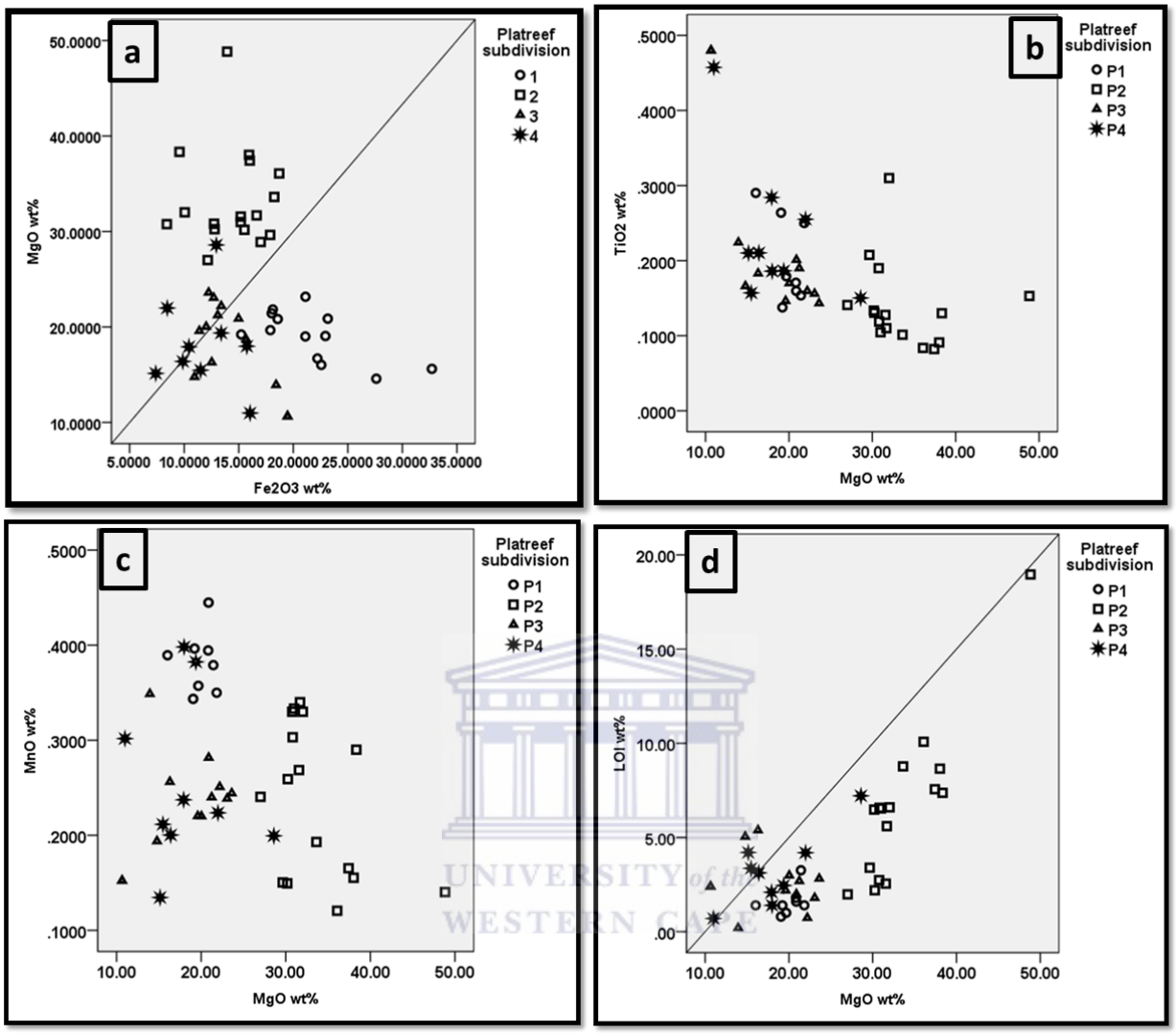

Figure 3.17: Bivariate plots of wt% major element oxides against wt% MgO. Increasing wt% MgO represents increasing pyroxene and olivine relative to plagioclase proportions in rock. All MgO plots are the same scale from 10-50.

3.2.3.5 Box Plots

In general Box plots are graphical techniques that give us an understanding of the distribution of variables (Härdle and Simar, 2003). All the major element oxides presented here are in wt% oxide. The geochemical variations of the igneous lithologies at Akanani were presented using box plots and bar graphs in order to show the distribution pattern of major elements within each lithological unit. By comparing the relative size and location of the boxes, we are also comparing the distribution patterns of variables in the data (Härdle and Simar, 2003). The advantage of

using box plots is that the important underlying structures within the data such as location, skewness, range, means and outliers are readily seen. P1 shows an enrichment of Fe_2O_3, Cr, TiO_2 and MnO (Fig. 3.18). Sample 4 and 12 have Cr concentration > 100,000 ppm and represents chromitite samples in P1. P2 shows enrichment of MgO and LOI which signifies the occurrence of Mg-rich lithologies which have been altered to varying degrees (Fig. 3.19). The sharp increase in MgO concentration in P2 with decreasing SiO_2 in its variation trend can be attributed to the early fractionation of Mg-Fe-rich phases such as olivine and pyroxene from the ultramafic magma. Sample 31 with MgO 48 wt.%, LOI contents of 18 wt.% and lower SiO_2 contents (16 wt%) represents a highly serpentinized sample which on geochemical grounds can be termed a serpentinite. In general the majority of P3 samples show an abundance of Al_2O_3 and Na_2O which may reflect the high modal proportion of feldspars in this unit (Fig. 3.20). This increase in the felsic elements (Al_2O_3 and Na_2O) suggests an incoming role for plagioclase as the dominant separate phase from the magma. P4 has the highest CaO and P_2O_5 content (Fig. 3.21). P4 has the highest CaO and P_2O_5 content (Fig. 3.21).

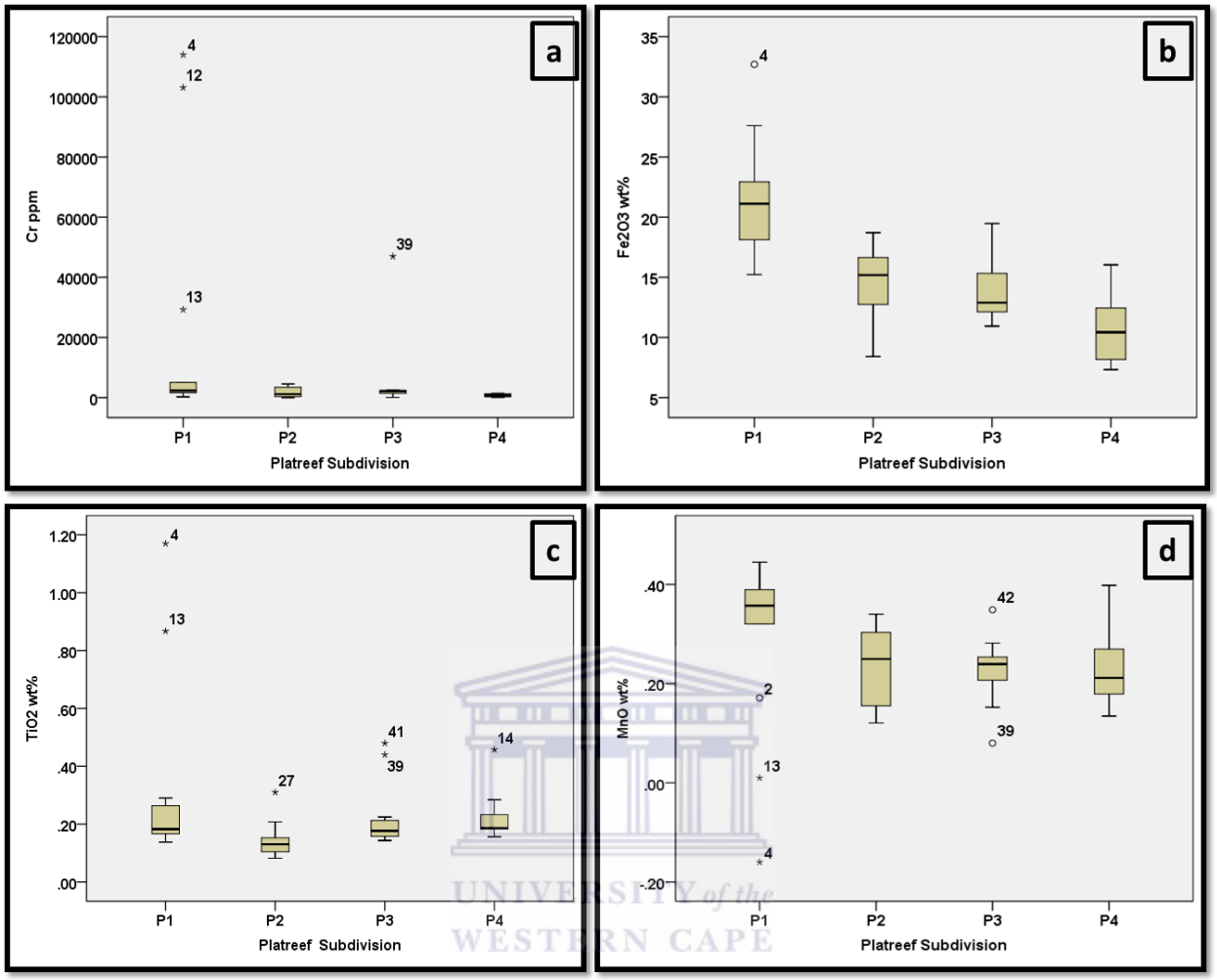

Figure 3.18: Major element abundance in P1, P2, P3 and P4 of the Platreef at the Akanani prospect area **(a-d)** Fe_2O_3, TiO_2, Cr and MnO.

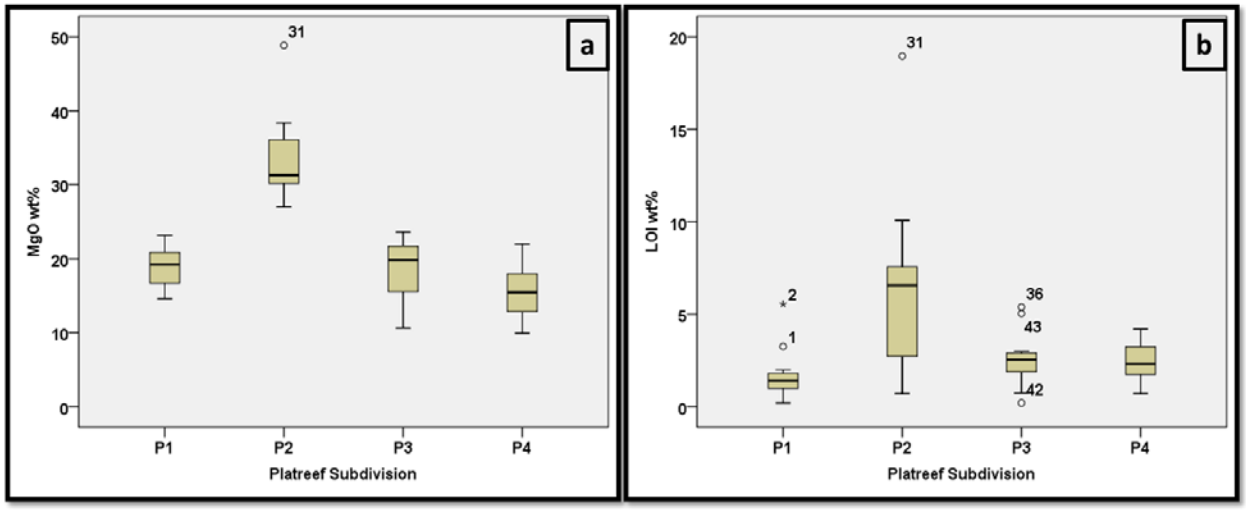

Figure 3.19: Major element abundance in P1, P2, P3 and P4 units of the Platreef at the Akanani prospect area. (a-b) MgO and LOI.

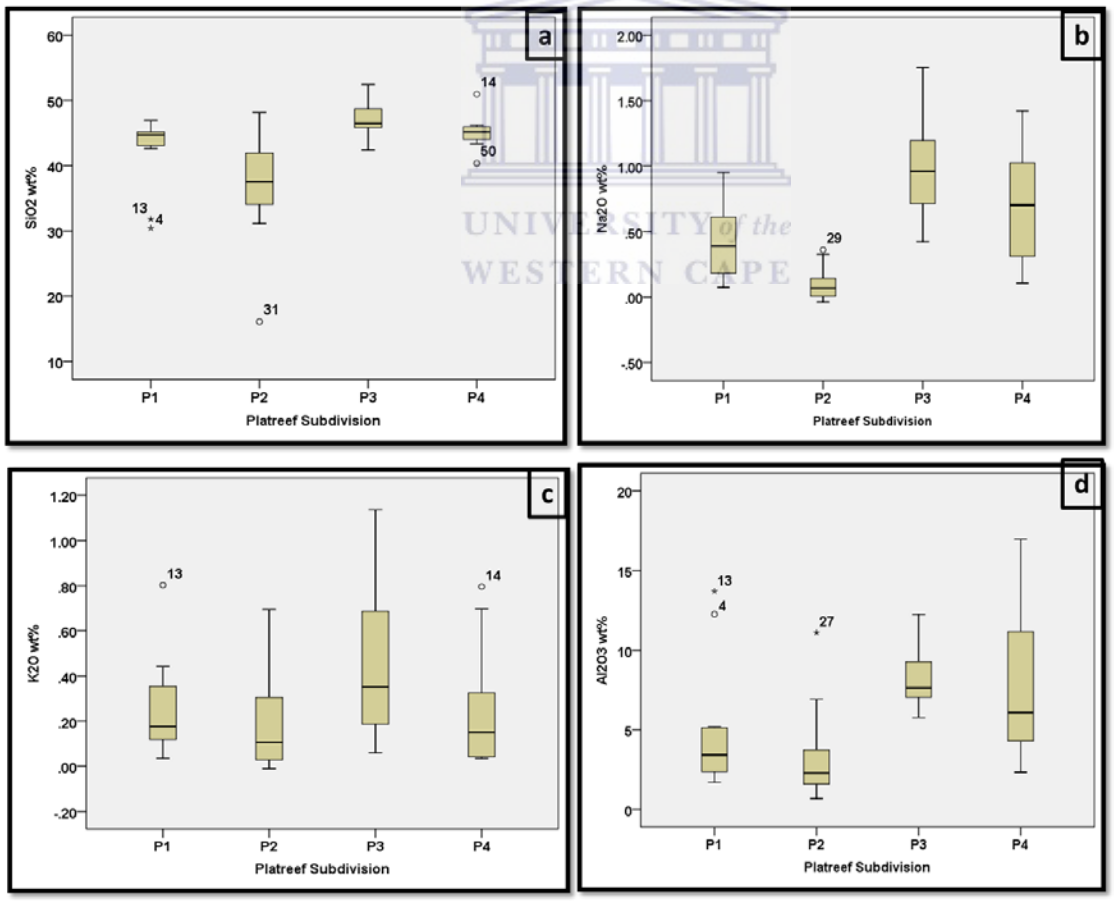

Figure 3.20: Major element abundance in P1, P2, P3 and P4 units of the Platreef at the Akanani prospect area. (a-d) SiO_2, Na_2O, K_2O, Al_2O_3.

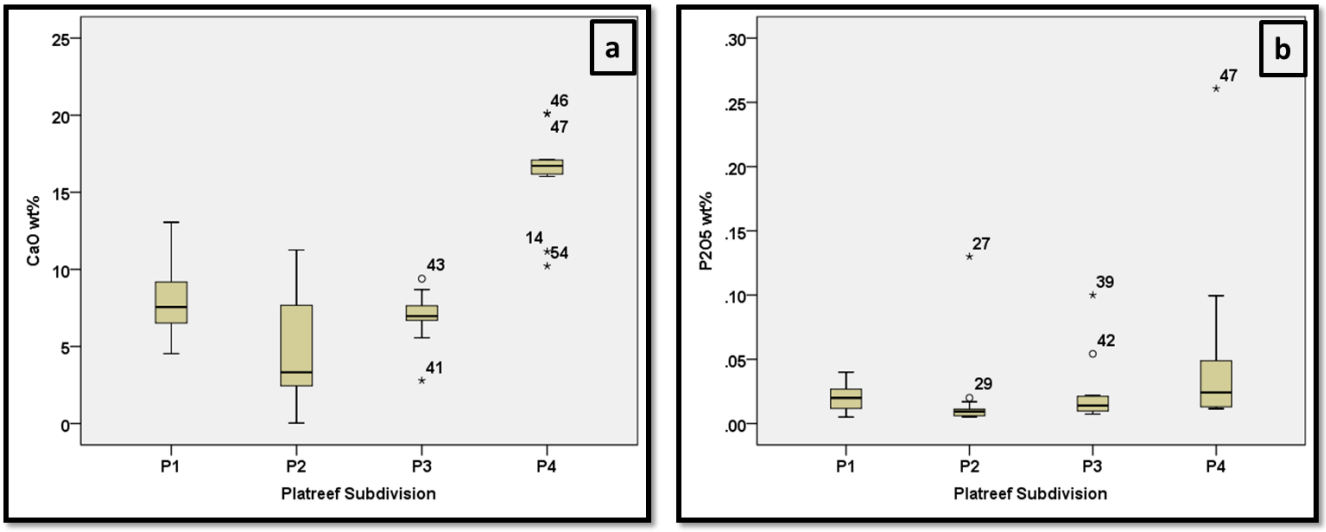

Figure 3.21: Major element abundance in P1, P2, P3 and P4 units of the Platreef at the Akanani prospect area. (a-b) CaO and P_2O_5.

3.2.4 Trace element geochemistry

Trace elements have the ability to partition into specific minerals during the crystallization of liquids (Rollinson, 1993). They are used here to predict the occurrence of specific minerals in each unit. It is important to note that this does not eliminate the use of the microscope; however where results are needed during mining and exploration to compare geochemical trends to the possible minerals occurring within a rock, this method can be employed. Abundance of trace elements in rocks is controlled by the modal proportions of the minerals present (Stevens, 2007). However, abundances may change if the rock has been subjected to to varying degrees of alteration or contamination (Stevens, 2007). **Rb, Sr, Ba, Nb, Zr, Y, Ni, Co, Cu, V** and **Cr** were used for the purpose of this analysis. Box plots were therefore used to present the change in trace element spectrum from the base of the Platreef to the top and possible link of that change to the possible minerals that occur as a result of the enrichment of certain trace elements in that unit. Table 3.21 below shows the average concentrations of trace elements in each unit. Concentrations of Pt, Au and Pd are not representative of the actual concentrations in each unit due to some samples having missing values and therefore are not included in this analysis.

Table 3.21: Variation in trace element concentrations (ppm) for different units at the Akanani prospect area

Element	P1	P2	P3	P4
Ba	32.26	70.74	92.75	63.36
Co	148.43	142.44	80.96	86.78
Cr	18112.06	2061.76	5124.14	748.59
Cu	1411.78	1622.74	1228.70	1524.52
Nb	4.83	2.75	3.32	2.56
Ni	3892.14	2952.99	1248.82	2473.21
Rb	5.14	18.92	17.32	3.21
Sr	45.79	43.52	116.18	55.37
V	186.35	68.85	107.13	102.76
Y	11.52	8.08	11.08	16.19
Zn	114.04	122.84	140.26	58.17
Zr	38.22	35.92	42.04	43.39

Figure 3.22 below shows the results in box plots for trace element concentrations in each unit. P3 shows elevated values of Sr and Ba with concentrations reaching up to 789 ppm and 720 ppm (outliers) respectively which could imply the possible occurrence of plagioclase feldspar, biotite and amphibole in this unit, while phlogopite is a possibility. Concentrations of Y in P4 are high relative to other units (38 ppm) and may reflect abundances of biotite and varying amounts of clinopyroxene. Zr is incompatible with elevated concentrations of olivine, orthopyroxene, and plagioclase and thus its low concentrations in P2 could reflect the occurrence of these minerals, while its presence in higher concentrations in other units could imply their occurrence in small amounts or the presence of trapped liquid.

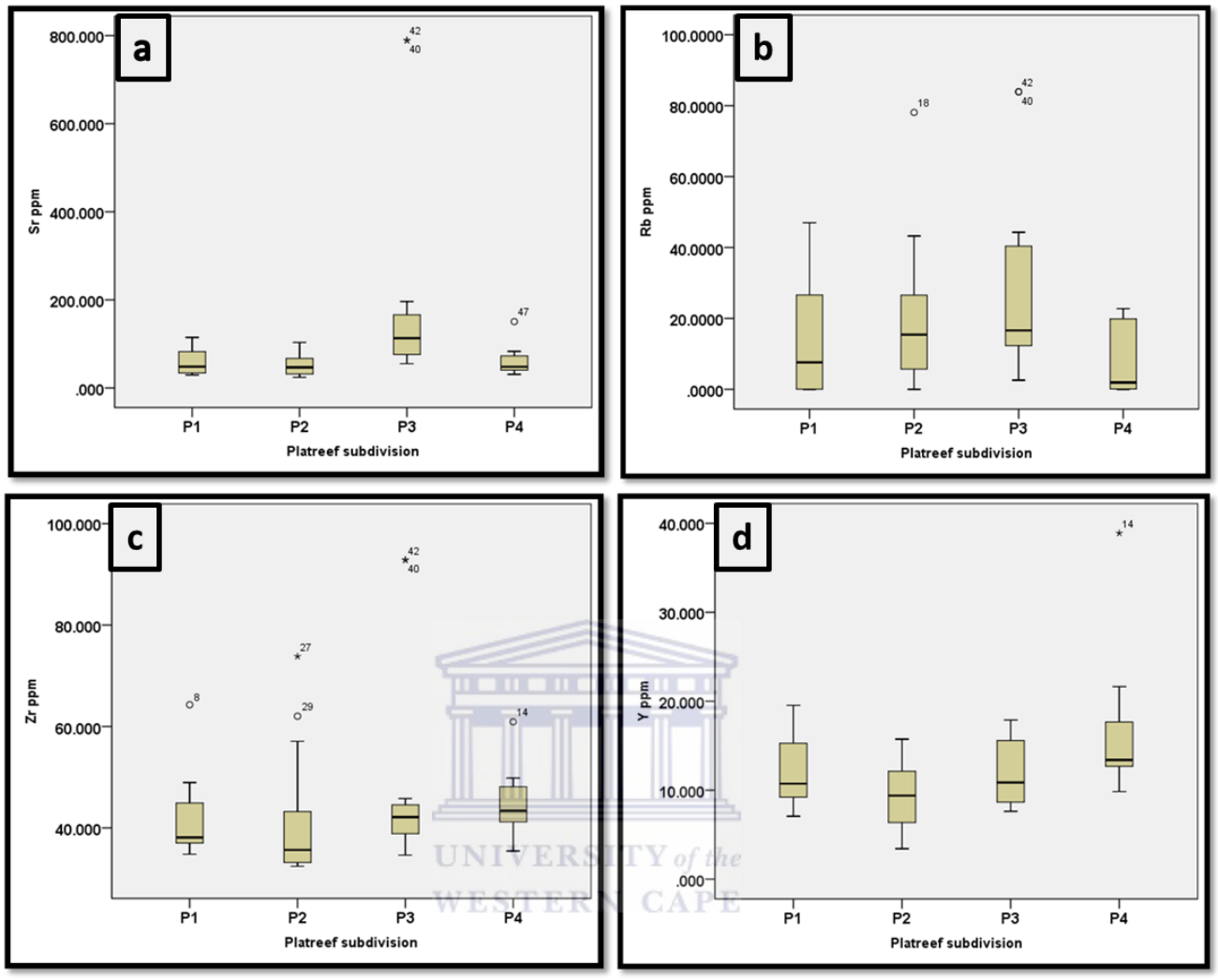

Figure 3.22: Graphical presentations of trace element distribution patterns in the four lithological units at Akanani prospect area. (a-d) Sr, Rb, Zr and Y.

High concentrations of V and Cr (Fig. 3.23a and b) in P1 and P3 could reflect the possible occurrence of oxide minerals in both units (rutile, chromite, hemaetite and magnetite).

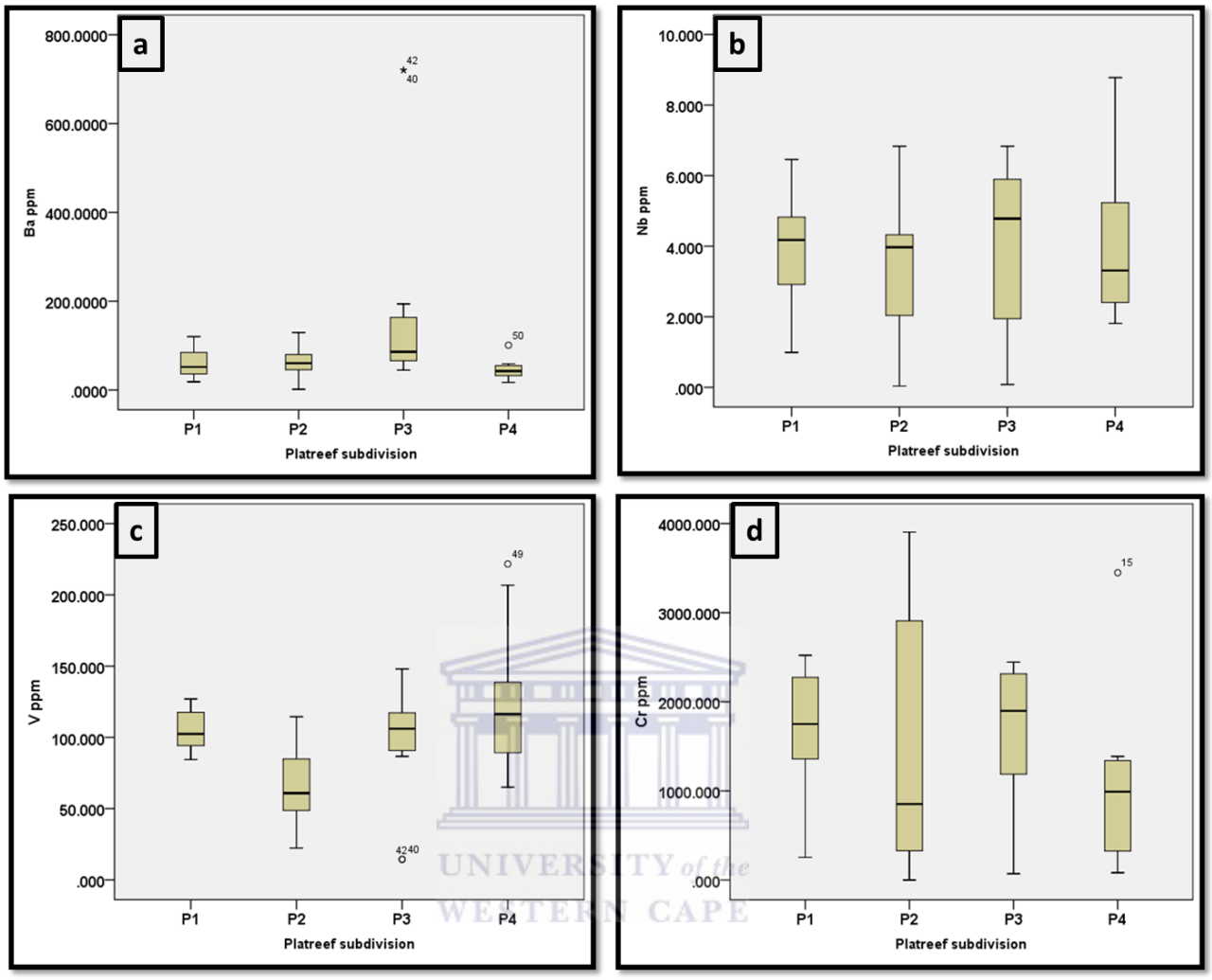

Figure 3.23: Graphical presentations of trace element distribution patterns in the four lithological units at Akanani prospect area. (a-d) Ba, Nb, V, Cr.

Higher concentrations of Ni + Cu (Fig. 3.24b) recorded in P1 and P2 which are the base of the Platreef at Akanani would reflect the occurrence of sulphides (chalcopyrite, pyrrhotite and pentlandite).

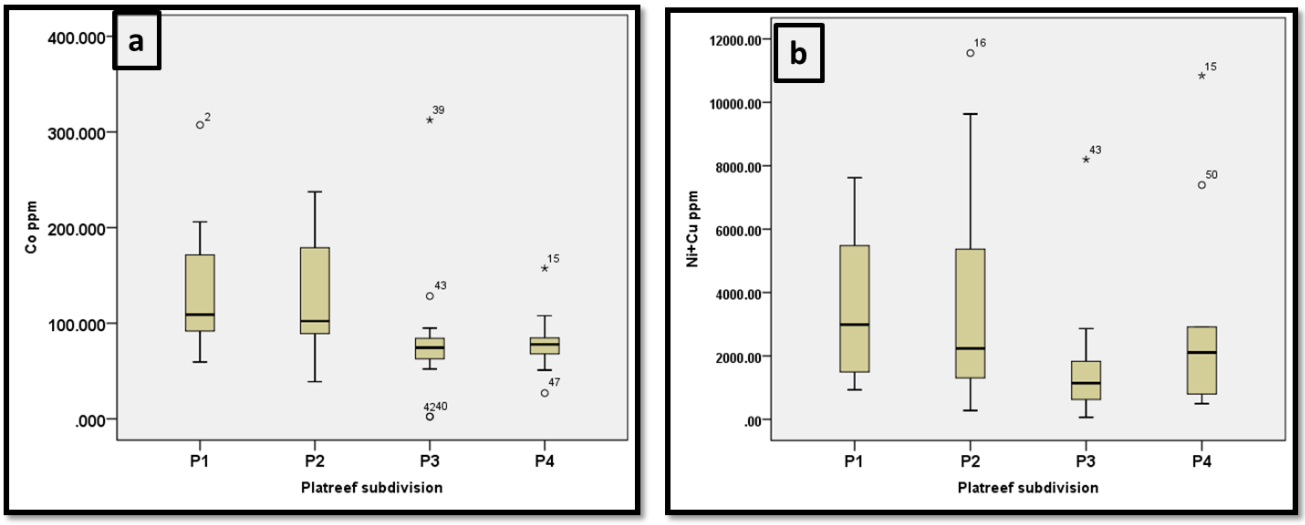

Figure 3.24: Graphical presentations of trace element distribution patterns in the four lithological units at Akanani prospect area. (a-b) Co, Ni+Cu.

3.2.4.1 Trace element ratios

Element ratios were not only selected for their compatibility and incompatibility in one phase or the other but also for their independence off modal proportions. In this section the procedure of Stevens (2007) is used.

Cr/MgO ratio was selected to determine whether single or multiple magmatic influxes played a role in the formation of P1, P2, P3 and P4 units at the Akanani prospect area. The Cr/MgO was used to indicate different sources of magma. Samples having Cr concentrations >3500 ppm were omitted from the analysis as they contained Cr-spinels following (Seabrook, 2005; Stevens, 2007). Sr and Ba are incompatible elements in all major mafic minerals and compatible in plagioclase. The ratio of Sr/Ba can thus be used to indicate fractional crystallization. Any significant break in this ratio will indicate the influx of new magma (Eales et al., 1986). Ni/Co and Ni/Cu ratios were used to mark significant peaks in mineralization for each unit. Ti/Zr and V/Zr ratio was used to determine the onset of titaniferous and vanadiferous magnetite crystallization.

There is a significant decrease from P1 (7.33) to P2 (3.91) in The Sr/Ba ratio which can suggest the influx of new magma in P2 (Table 3.23). The ratio continues to decrease in P3, however a significant break is not observed. This decrease is consistent with mineralogical changes with

stratigraphic height than influx of new magma. The Cr/MgO ratio varies with stratigraphic height; however it does increase systematically (Fig. 3.25a). For P1 rocks, the Cr/MgO ratio averages > 80, while in P2, Cr/MgO decreases to 31, which maybe consistent with introduction of olivine and probably an influx of new magma. In P3 there is sudden increase in this ratio to 90.1, while P4 displays a sudden drop in the ratio (Table 3.23). The Ni/Cu (Fig. 3.25a, b, d) shows the occurrence of high grades of sulphides in P1, which shows a decreasing trend to P3 which is less mineralized. Concentrations of Ni/Cu reach up to 4700 in P1, 4400 in P2 and < 2100 ppm in P3 are also encountered. The top most unit (P4) contains Ni/Cu ratios of up to 2300. Table 3.23 below summarises the results.

Table 3.23: Average trace and major element per lithological unit.

Ratios	**P1 Unit**	**P2 Unit**	**P3 Unit**	**P4 Unit**
	MEAN	**MEAN**	**MEAN**	**MEAN**
Cr / MgO	86.61	31.09	90.87	40.957
Sr / Ba	7.33	3.91	1.22	1.81
Ni / Cu	4769.19	4275.40	2090.77	2333.61
Ti / Zr	0.01	0.00	0.00	0.00
V / Zr	5.71	1.78	2.95	2.91

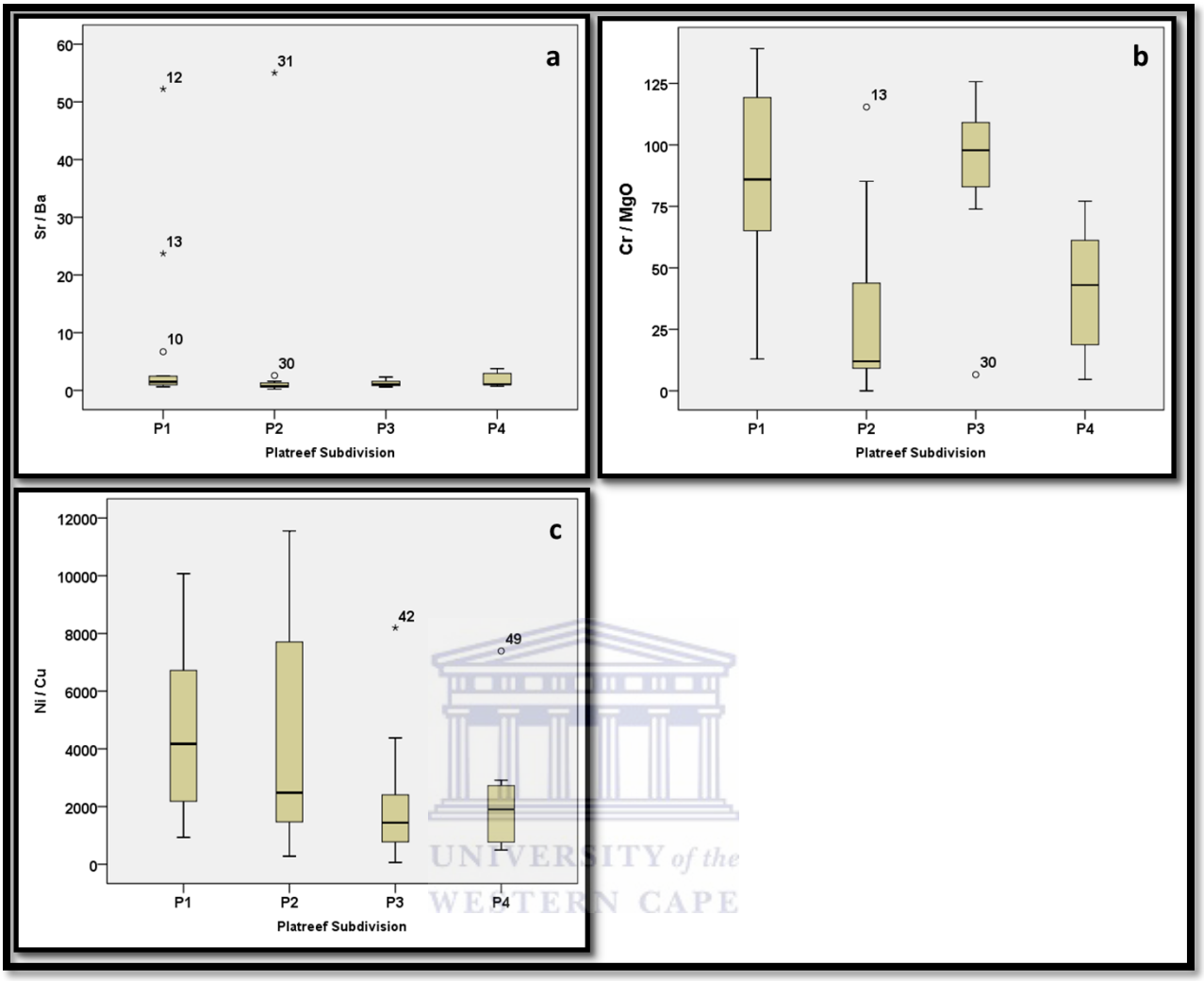

Figure 3.25: Graphical presentations of major and trace element ratios distribution patterns in the four lithological units at Akanani prospect area. (a-d) Cr/MgO, Sr/Ba, Ni/Cu

The influence of magnetite control was easily ascertained by the use of supplementary plots of Ti and V against independent fractionation index such as Zr. A lower Ti/Zr and V/Zr ratio is observed in P2 which may be suggestive of the onset magnetite fractionation during the intial stages of fractional crystallization (Figure 3.26), while a sudden peak in P3 implies the final stage of magnetite crystallization.

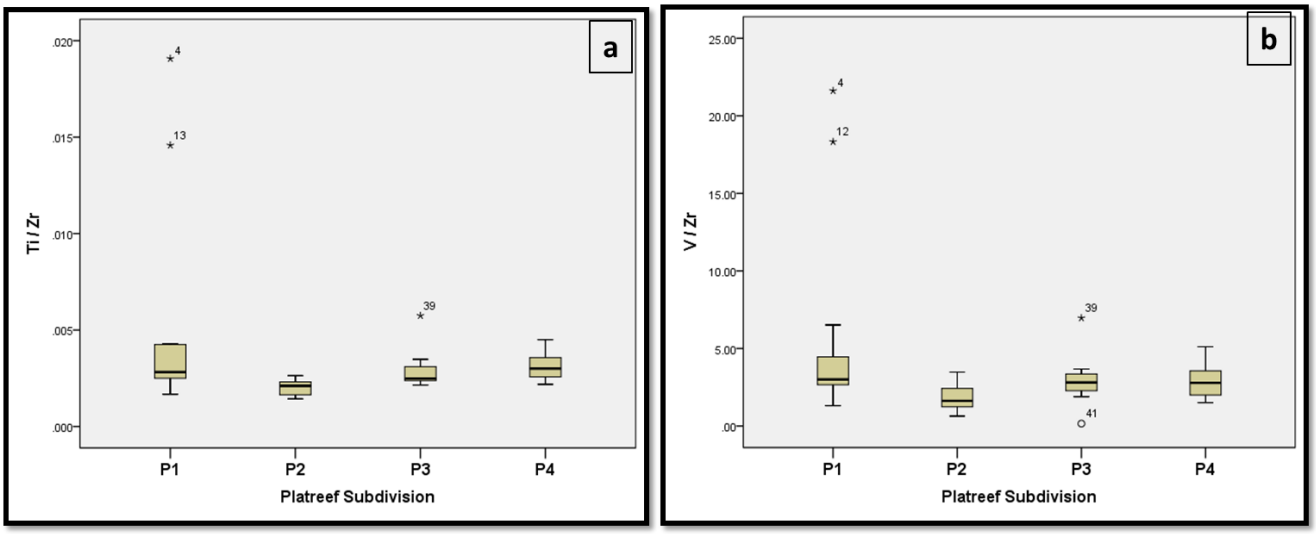

Figure 3.26: Graphical representation of the distribution of the Ti/Zr and V/Zr ratio in the four lithological units at Akanani prospect area.

3.2.5 Spider-diagrams

Rare earth elements are usually regarded as the least soluble trace elements and are relatively immobile during weathering and hydrothermal activity. This is because hydrothermal solutions contain between 5×10^2 and 10^6 times less rare earth elements than the reservoir rock through which they have passed and therefore hydrothermal activity is not expected to have a major effect on rock chemistry unless the water/rock ratio is very high (Michard, 1989). Humphris (1984) noted that REE were not totally immobile as they can be relatively mobile in exetensively altered rocks. In this section of geochemistry REEs are used to determine the degree of fractionation of LREE and HREE as well as the behaviour of the Eu anomaly in P1, P2, P3 and P4 to assess the enrichment of feldspars especially in feldspar-rich rocks of P3.

3.2.5.1 P1 Unit

There is a pronounced enrichment of Large Ion Lithiphile Elements (LILE) Rb, K and Ba (Fig. 3.27b), while Sr shows a flat pattern. The High Field Strength Elements (HFSE) Th, U, Zr, Nb, and Y are depleted relative to LILE. Ti shows a uniformly weak contrast, while P shows minor depletion. The Light Rare Earth Elements (LREE) La-Sm are enriched relative to the Heavy Rare Earth Elements (HREE) Gd-Lu testifying to the degree of fractionation (Fig. 3.27a). The $(Eu/Eu^*)_N$ which is normalized to chondrite values ranges between (0.52-0.88) for P1 samples (Appendix). The $(La/Gd)_N$ ratio ranges from 1.60-3.45 while the $(Gd/Lu)_N$ ranges from (0.44-

1.04). Likewise the $(La/Lu)_N$ ratio which is indicative of enrichment of LREE relative to HREE ranges between 1.14 and 2.65 (Appendix E).

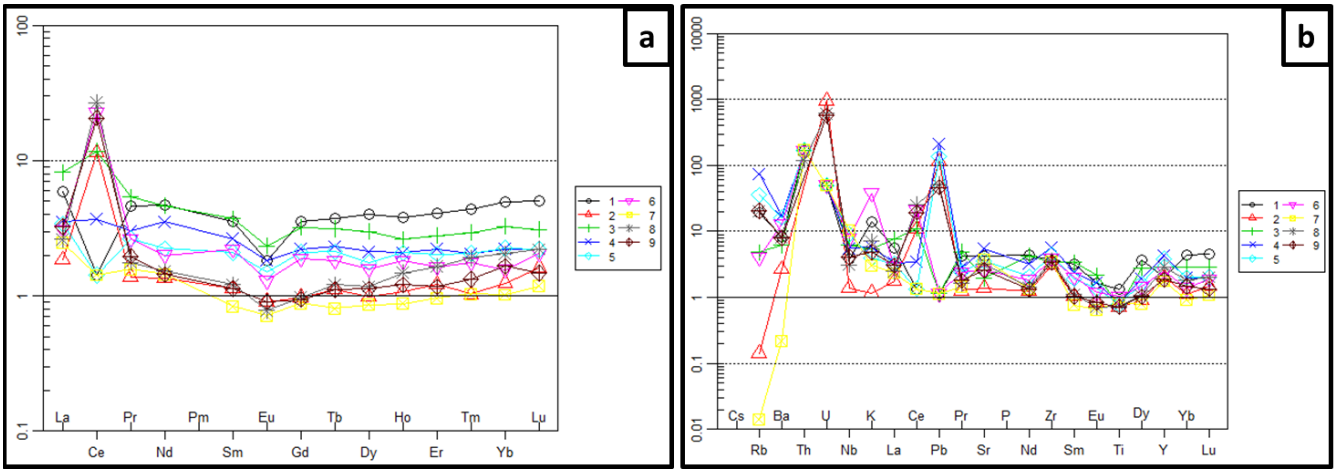

Figure 3.27: Chondrite normalized REE and Primitive mantle abundances of P1 samples at the Akanani Prospect area after (McDonough and Sun, 1995; Sun and McDonough, 1989).

3.2.5.2 P2 Unit

Comparatively there is a stronger depletion of Ba, Sr and Rb in P2 rocks which is further marked by a relatively low depletion of Th, Nb, Y, P and Ti especially for sample 12 (Fig. 3.28b). Zr on the other hand shows a positive peak for these rocks. LREEs are enriched relative to the HREEs (Fig. 3.28a), which is substantiated by the relatively low $(Gd/Lu)_N$ ratio ranging from 0.7-1.4 and the $(La/Lu)_N$ ranging from 0.80-4.39. Samples ZF044-32 and ZF078-52 have values higher than 3 for the $(La/Lu)_N$ indicating a greater degree of fractionation for these samples which are highly metasomatized. The $(Eu/Eu^*)_N$ ratio shows minor depletion with values ranging from 0.73-0.95 which is consistent with the negative Eu anomaly associated with this unit.

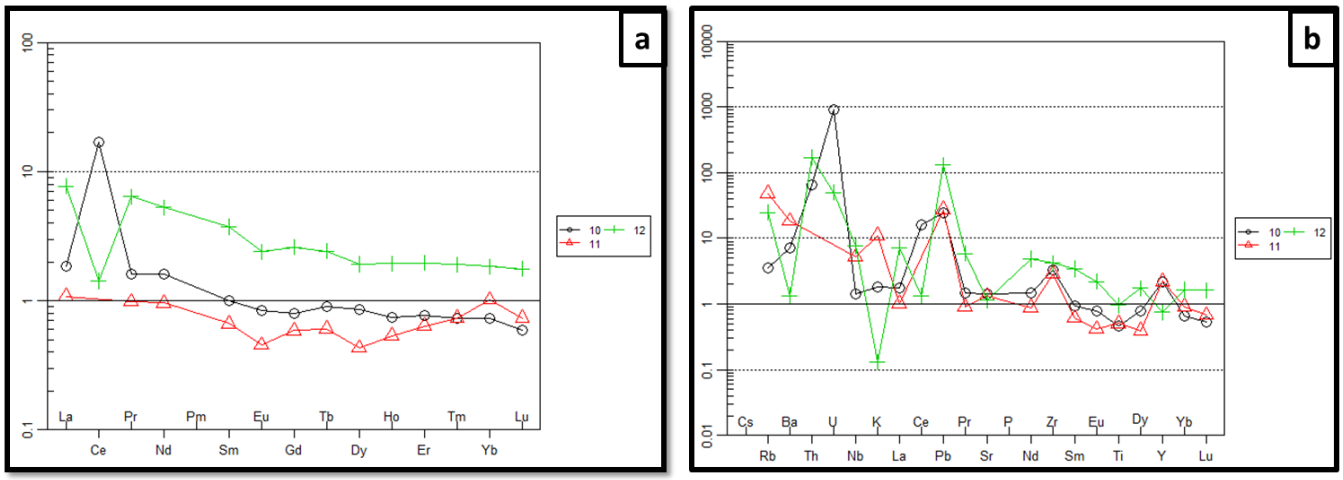

Figure 3.28: Chondrite normalized REE and Primitive mantle abundances of P2 rocks at the Akanani Prospect area after (McDonough and Sun, 1995; Sun and McDonough, 1989).

3.2.5.3 P3 Unit

The P3 rocks which are feldspathic in nature show an enrichment of LILE (Rb, K, Sr and Ba) relative to Th, and U (Fig. 3.29b). Zr and Y show enrichment in these rocks while Ti shows minor depletion. The feldspathic nature of the P3 samples is well supported by the positive Eu anomaly associated with this unit relative to its neighbouring REEs (Fig. 3.29a). K shows slight enrichment relative to K in P1 and P2. Generally LREE are enriched relative to HREEs. The $(Eu/Eu^*)_N$ ranges between 0.84 and 1.35, while the $(Gd/Lu)_N$ ratio is slightly lower ranging from 0.76-1.37 further emphasizing the enrichment of LREE relative to HREE. In contrast $(La/Lu)_N$ ratio is slightly higher relative to P1, P2 and P4 ranging from 1.7-6.71 denoting a greater degree of fractionation.

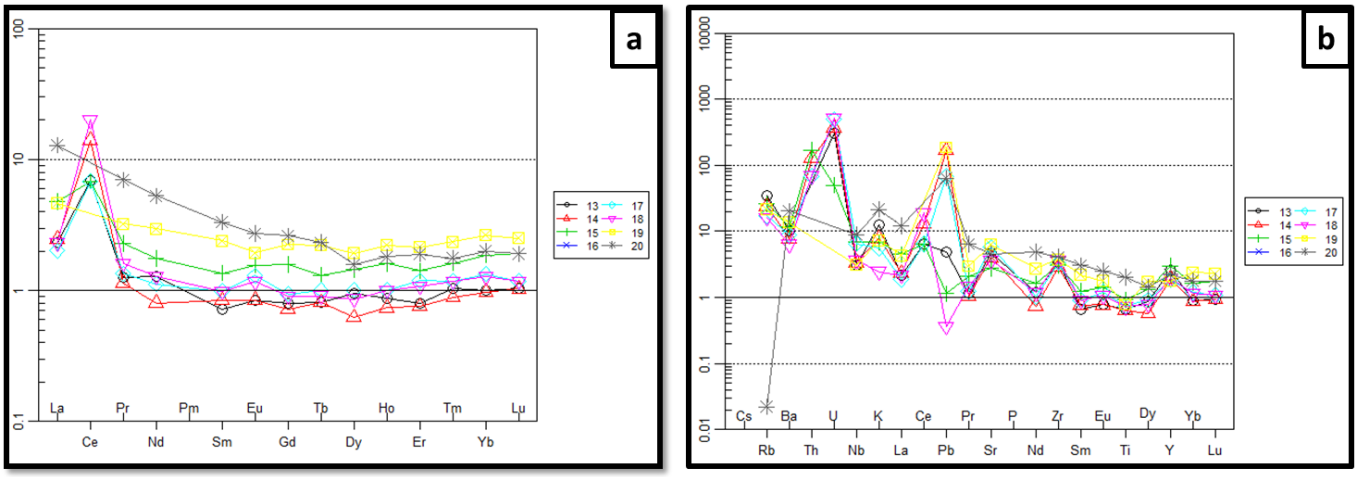

Figure 3.29: Chondrite normalized REE and Primitive mantle abundances of P3 rocks at the Akanani Prospect area after (McDonough and Sun, 1995; Sun and McDonough, 1989).

3.2.5.4 P4 Unit

A slight depletion of LILE (Ba, Rb and Sr) is noteworthy (Fig. 3.30b), while Th and U show enrichment. K contents are relatively slightly high as P and Ti show positive peaks relative to peaks in P1, P2 and P3 for the same elements. Y and Zr show a flat pattern. The Eu anomaly is negative which is consistent with the low $(Eu/Eu^*)_N$ ratio ranging from (0.47-0.88). The LREE are enriched relative to HREE which is a common phenomenon for almost all Platreef rocks at Akanani which is further highlighted by the low $(Gd/Lu)_N$ ratio ranging from (1.31-1.66). In P4 $(La/Lu)_N$ is lower with values ranging from (2.18-3.96).

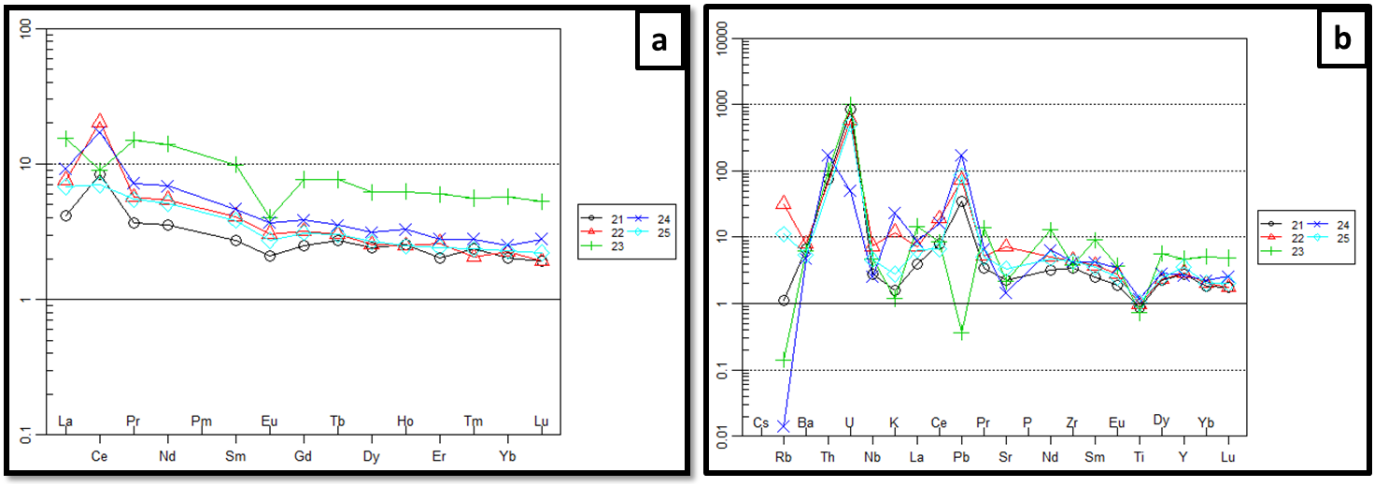

Figure 3.30: Chondrite normalized REE and Primitive mantle abundances of P3 rocks at the Akanani Prospect area after (McDonough and Sun, 1995; Sun and McDonough, 1989).

3.2.6 Mass-Balance

The interaction of rocks with aqueous fluids may cause the removal or introduction of chemical components. The interpretation is solely based on the geochemical differences between each unit and the effects of assimilation, contamination and hydrothermal activity on element mobility and concentration. However, the determination of these processes is based upon Gressen's technique.

Table 3.25 below shows the average major and trace element composition of the various rock types (P1-P4).

Table 3.24: Average major (wt.%) and trace-element (ppm) of various rock types (P1-P4) from bore-holes in Zwartfontein.

Element	P1	P2	P3	P4
Major Elements				
SiO_2	44.88	36.92	47.95	44.22
Al_2O_3	3.22	3.32	7.92	4.72
Fe_2O_3	19.56	14.31	14.22	11.75
MnO	0.38	0.24	0.23	0.25
MgO	19.86	33.58	18.08	18.21
CaO	9.25	4.44	6.61	16.1
Na_2O	0.28	0.09	1.02	0.46
K_2O	0.2	0.17	0.41	0.29
TiO_2	0.2	0.14	0.23	0.23
P_2O_5	0.01	0.02	0.02	0.06
LOI	1.58	6.63	2.55	3.19
Trace Elements				
Ba	32.26	70.74	92.75	63.36
Co	148.43	142.44	80.96	86.78
Cr	18112.06	2061.76	5124.147	748.59
Cu	1411.78	1622.74	1228.7	1524.52
Nb	4.83	2.75	3.32	2.56
Ni	3892.14	2952.99	1248.82	2473.21
Rb	5.14	18.92	17.32	3.21
Sr	45.79	43.52	116.18	55.37
V	186.35	68.85	107.13	102.76
Y	11.52	8.08	11.08	16.19
Zn	114.04	122.84	140.26	58.17
Zr	38.22	35.92	42.04	43.39

3.2.6.1 (P1) vs (P2)

From (Fig. 3.31a-d), the components Zr, Mo and Cu form a linear array through the origin. This means that the above-mentioned components are immobile and the isocon is considered to be a constant alumina isocon with the slope of the isocon at 0.94. The mobile components lost are Ba, MgO, Rb and LOI (Fig. 3.32a-b). The mobile components gained are Ni, Cr, V, Zn, Co, Sr, SiO_2, Fe_2O_3, Th, Zr, CaO, Al_2O_3, Nb, Pb, Na_2O, TiO_2, K_2O, MnO, Y and P_2O_5 (Fig. 3.32a-b).

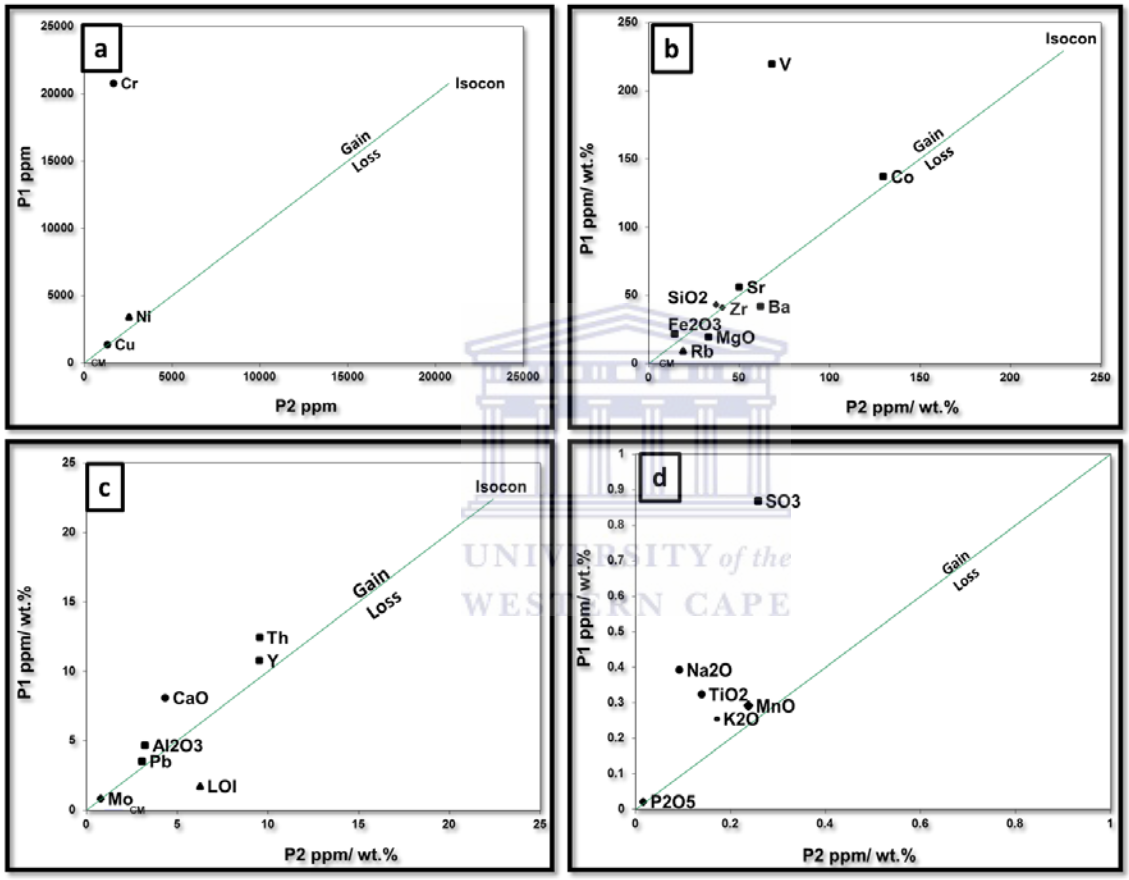

Figure 3.31: Isocon diagram showing the difference in element spectrum between P1 and P2.

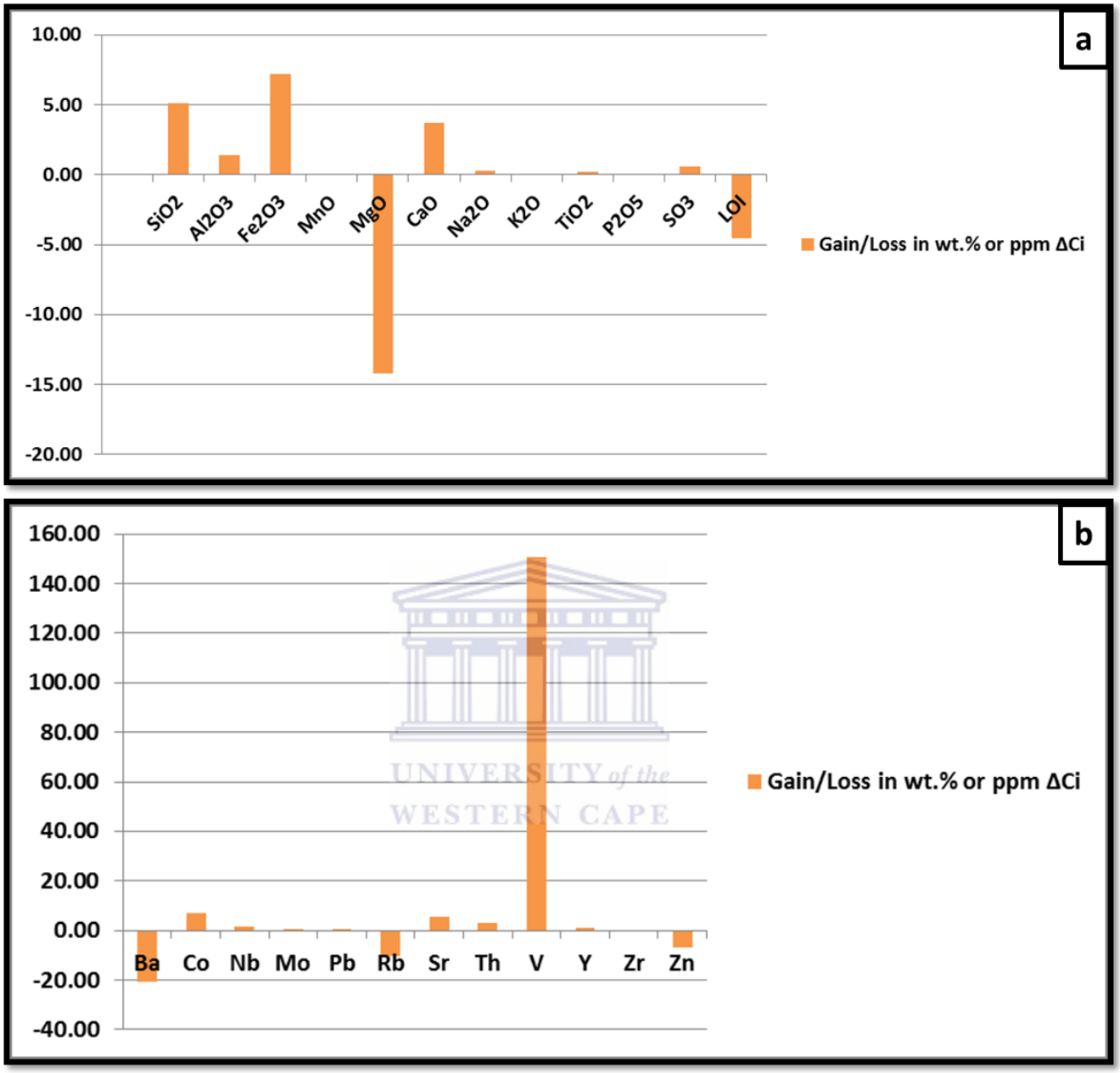

Figure 3.32: Graphical representation of components gained or lost for P1 vs P2. **(a)** Major elements lost or gained **(b)** Trace elements lost or gained. Note that P1 is considered the altered while P2 unit is considered least altered as it is the most prestine of the two.

Concentration of the components gained or lost is given in Table 3.26 below for the comparison between P1 and P2.

Table 3.25: Concentration differences in element spectrum between P1 and P2

Element	P2	P1	Gain/Loss in wt.% or ppm ΔC_i
SiO_2	37.50	42.62	5.11
Al_2O_3	3.23	4.64	1.40
Fe_2O_3	14.47	21.63	7.16
MnO	0.24	0.29	0.05
MgO	33.30	19.08	-14.23
CaO	4.36	8.07	3.71
Na_2O	0.09	0.39	0.30
K_2O	0.17	0.25	0.08
TiO_2	0.14	0.32	0.18
P_2O_5	0.02	0.02	0.00
SO_3	0.26	0.87	0.61
LOI	6.28	1.71	-4.57
Ba	62.06	41.55	-20.52
Co	129.93	136.75	6.77
Cr	1686.22	20745.09	19053.18
Cu	1335.55	1335.92	0.00
Ni	2553.70	3433.28	878.63
Nb	3.28	4.61	1.33
Mo	0.80	0.81	0.01
Pb	3.08	3.50	0.43
Rb	19.20	8.90	-10.30
Sr	50.17	55.71	5.52
Th	9.57	12.41	2.84
V	68.30	219.17	150.81
Y	9.55	10.73	1.17
Zr	40.91	40.51	-0.41
Zn	133.26	126.20	-7.09

3.2.6.2 (P3) vs (P2)

The isocon is defined by Zn, MnO and Fe_2O_3 (Fig. 3.33a-d), while Ni, Cu, Co, MgO and LOI are the mobile components lost during metasomatism (Fig. 3.33a-d; Fig. 3.34a-b). The mobile components gained are Cr, Ba, V, SiO_2, Rb, Pb, Fe_2O_3, Zr, Y, Al_2O_3, CaO, Na_2O, SO_3 K_2O, P_2O_5 and MnO (Fig. 3.33a-d; Fig. 3.34a-b).

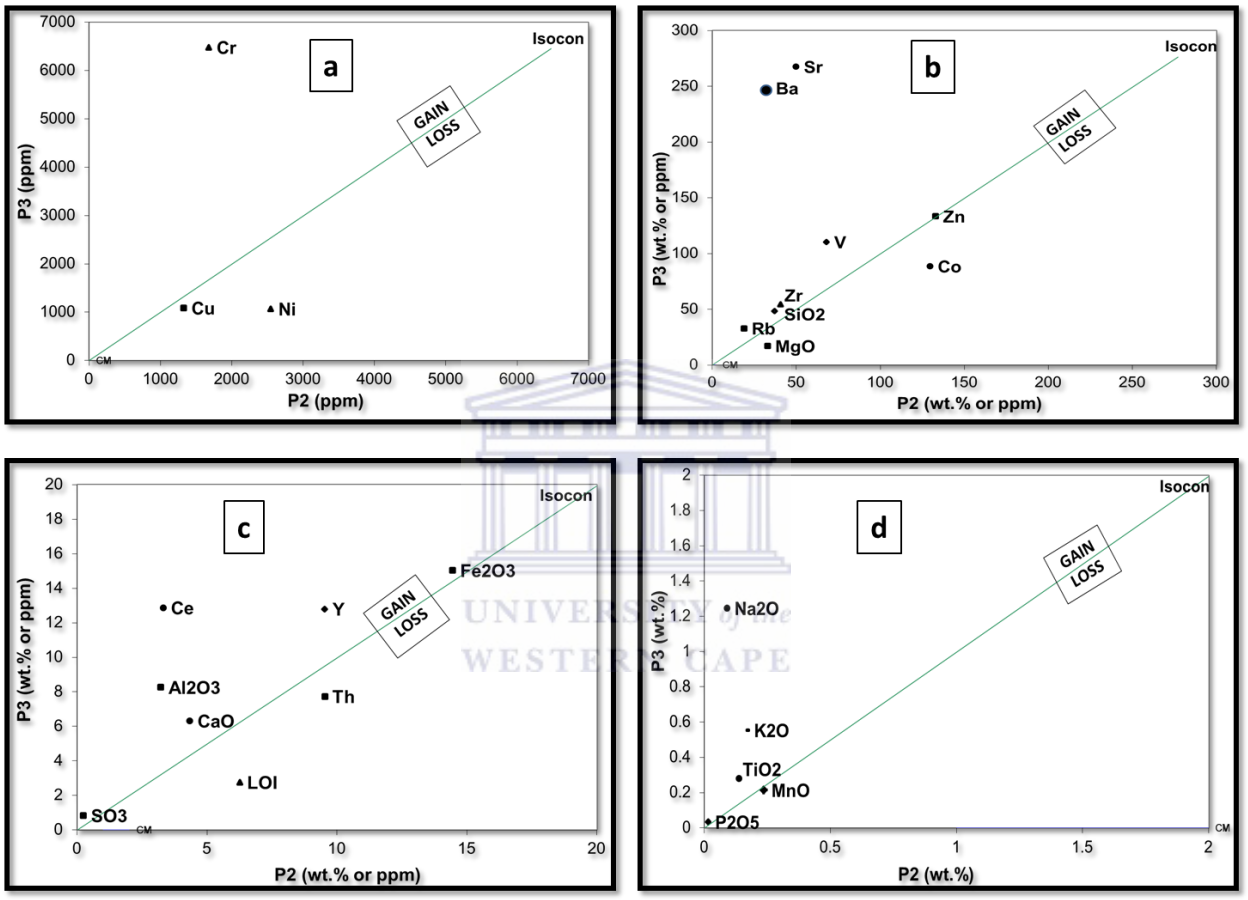

Figure 3.33: Isocon diagram showing the difference in element spectrum between P3 and P2.

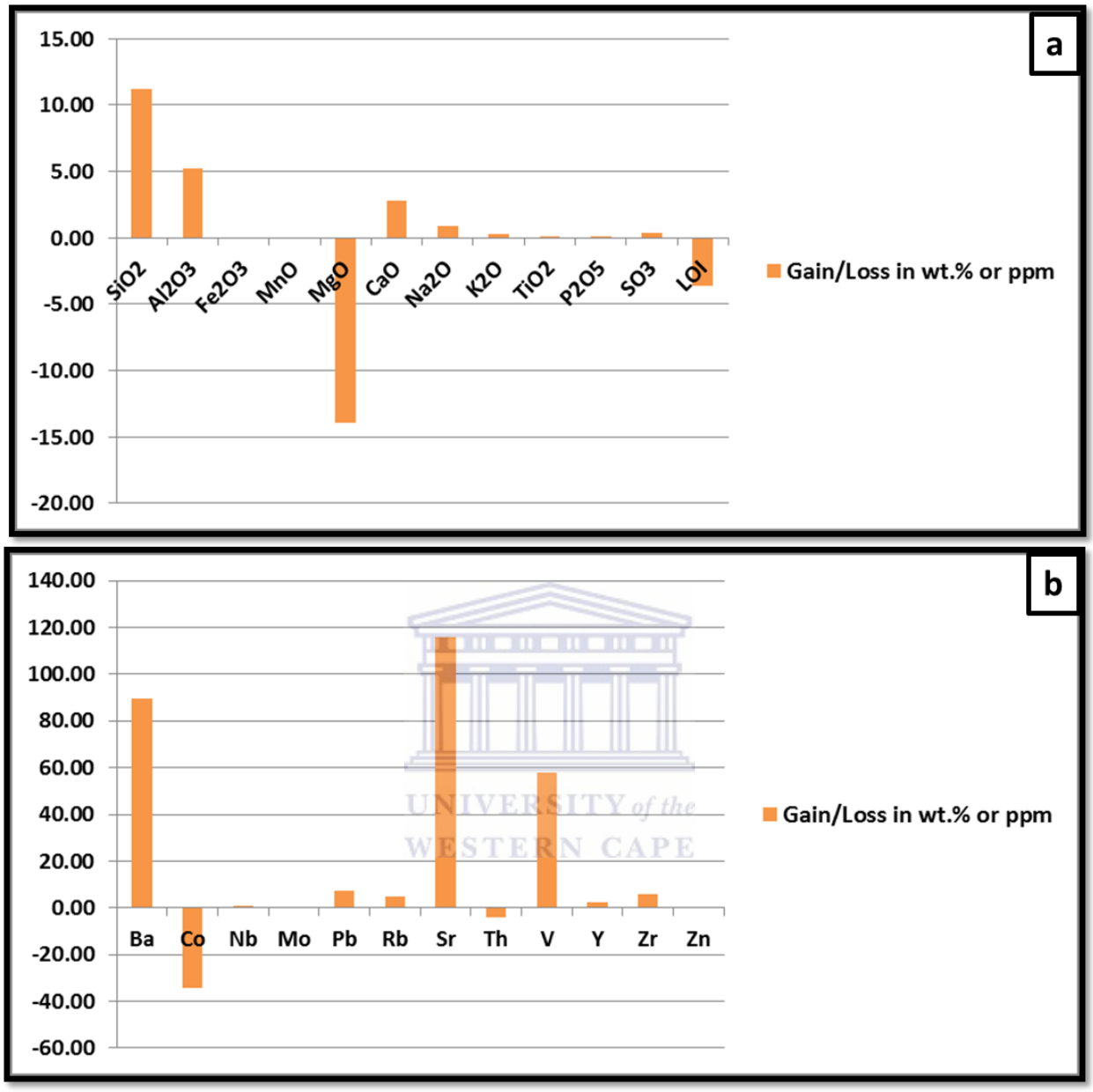

Figure 3.34: Graphical representation of components gained or lost for P3 vs P2. **(a)** Major elements lost or gained **(b)** Trace elements lost or gained. Note that P3 is considered the altered while P2 unit is considered least altered as it is the most prestine of the two.

The changes in concentrations of element spectrum for the P2 vs P3 plot is given in Table 3.27 below.

Table 3.26: Changes in concentration of element spectrum between P3 and P2

	Unaltered	Altered	Gain/Loss in wt.% or ppm
Element	**P2**	**P3**	**ΔC_i**
SiO_2	37.50	47.11	11.18
Al_2O_3	3.23	8.16	5.20
Fe_2O_3	14.47	13.90	-0.10
MnO	0.24	0.23	0.00
MgO	33.30	18.75	-13.93
CaO	4.36	6.93	2.80
Na_2O	0.09	0.98	0.92
K_2O	0.17	0.43	0.27
TiO_2	0.14	0.22	0.09
P_2O_5	0.02	0.02	0.01
SO_3	0.26	0.58	0.34
LOI	6.28	2.58	-3.62
Ba	62.06	146.56	89.38
Co	129.93	92.50	-34.36
Cr	1686.22	5545.33	4043.73
Cu	1335.55	976.86	-326.17
Ni	2553.70	1113.91	-1402.71
Nb	3.28	3.96	0.80
Mo	0.80	0.79	0.02
Pb	3.08	10.05	7.31
Rb	19.20	23.09	4.66
Sr	50.17	160.75	115.93
Th	9.57	5.45	-3.94
V	68.30	122.11	57.87
Y	9.55	11.47	2.30
Zr	40.91	45.29	5.89
Zn	133.26	128.98	0.01

3.2.6.3 (P4) vs (P2)

The isocon plot in (Fig. 3.35a-d) indicates clearly that Ni, Cu, Co, MgO, Cr, Zn, Co, Rb, Th, Fe_2O_3, Ba and SO_3 were the mobile components lost (Fig. 3.35a-d; Fig. 3.36a-b), while Zr, Sr and MnO form a linear array through the origin implying their immobility during metasomatism. The mobile components gained include V, SiO_2, Y, Al_2O_3, Pb, MnO, CaO, LOI, Na_2O, TiO_2, Mo and K_2O (Fig. 3.35a-d; Fig. 3.36a-b).

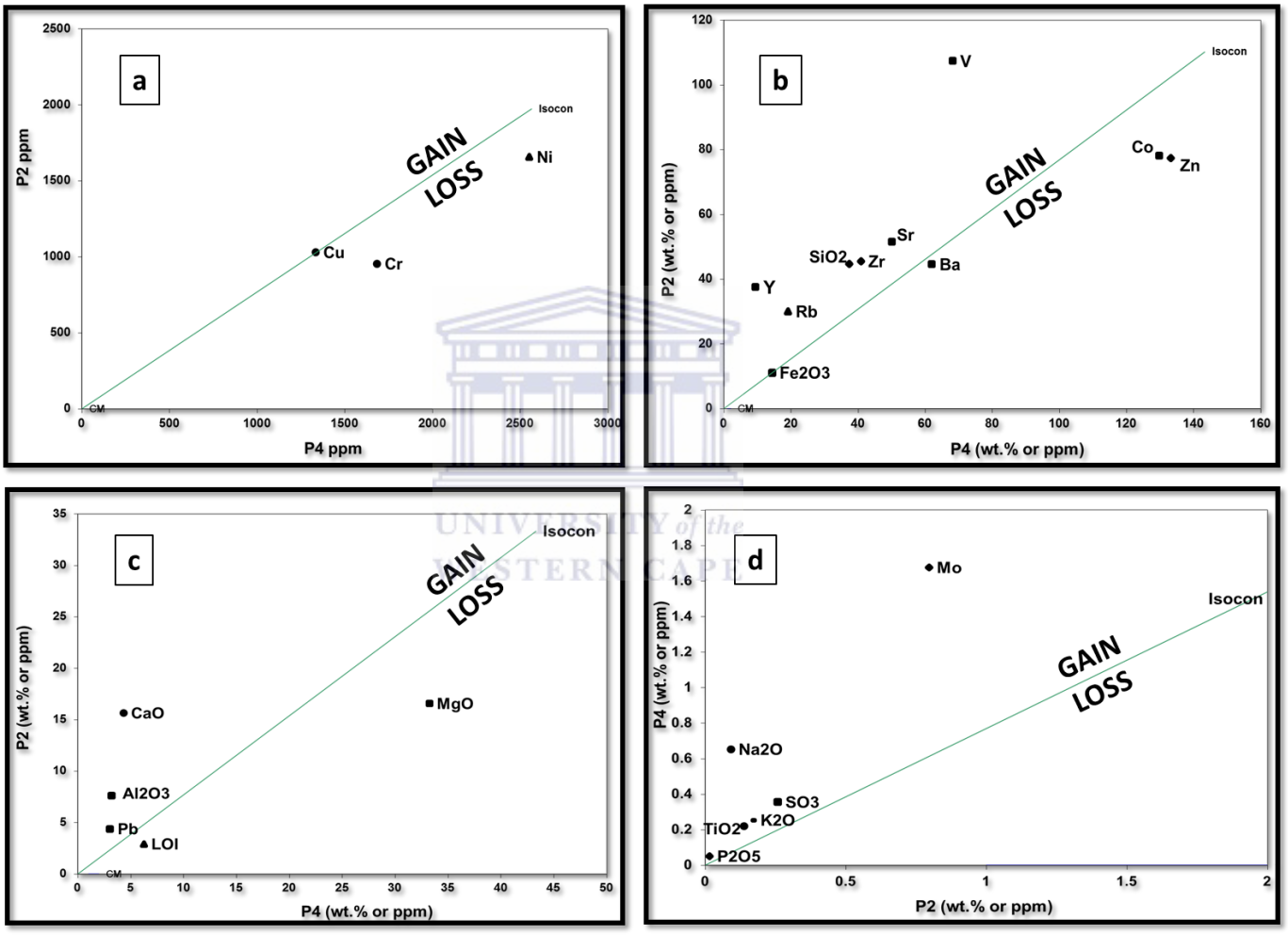

Figure 3.35: Isocon diagram showing the difference in element spectrum between P4 and P2

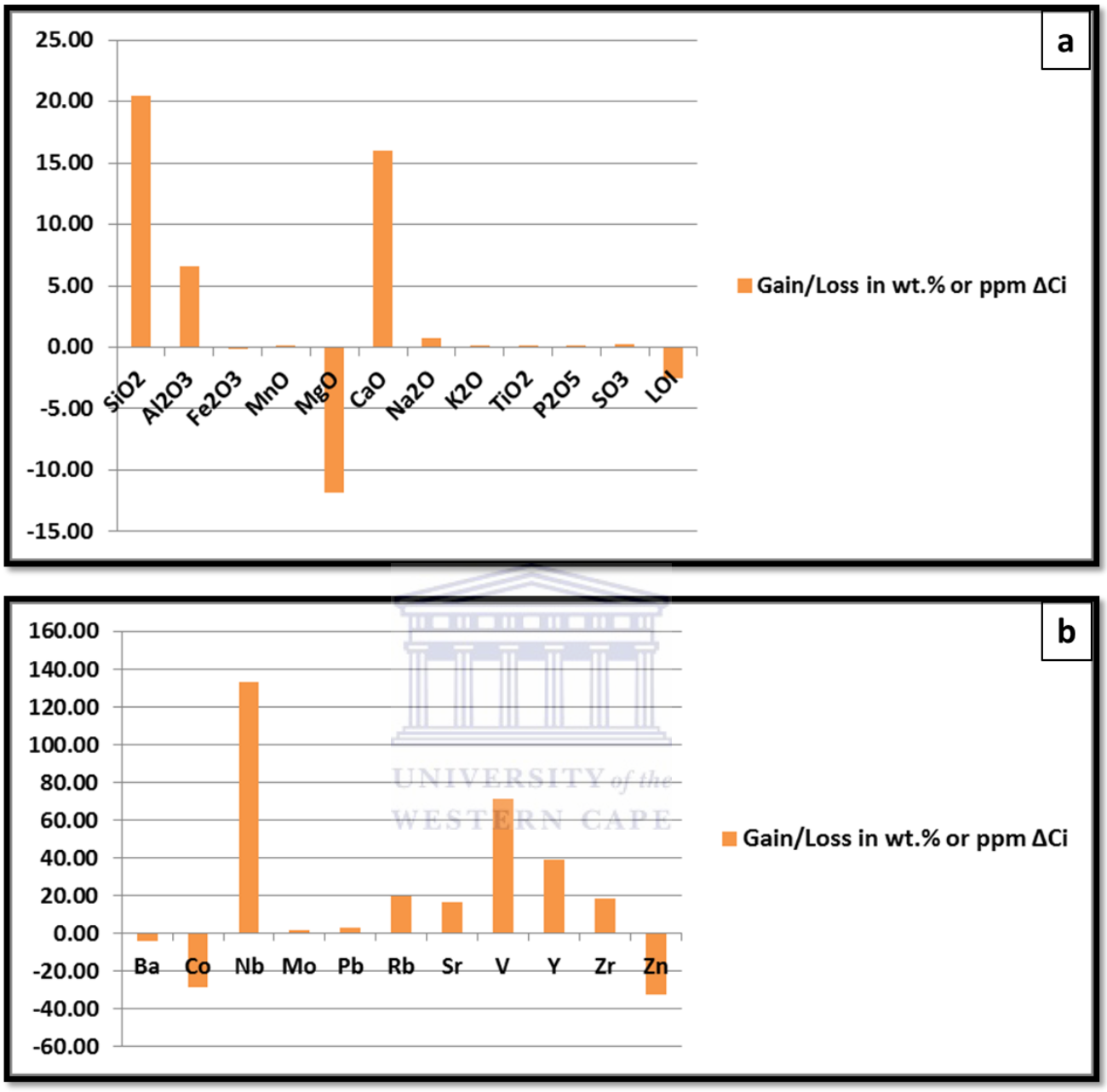

Figure 3.36: Graphical representation of components gained or lost for P3 vs P2. **(a)** Major elements lost or gained **(b)** Trace elements lost or gained. Note that P4 is considered the altered while P2 unit is considered least altered as it is the most prestine of the two.

Table 3.28 below is a summary of the concentration gains and losses for the P2 vs P4 plot.

Table 3.27: Concentrations differences in element spectrum between P4 and P2

	Unaltered	Altered	Gain/Loss in wt.% or ppm
Element	**P2**	**P4**	**ΔC_i**
SiO_2	37.50	44.58	4.66
Al_2O_3	3.23	7.57	3.93
Fe_2O_3	14.47	10.99	-4.07
MnO	0.24	0.23	-0.02
MgO	33.30	16.54	-17.66
CaO	4.36	15.62	10.42
Na_2O	0.09	0.65	0.52
K_2O	0.17	0.25	0.07
TiO_2	0.14	0.22	0.07
P_2O_5	0.02	0.05	0.03
SO_3	0.26	0.35	0.08
LOI	6.28	2.89	-3.55
Ba	62.06	44.47	-20.01
Co	129.93	77.98	-56.19
Cr	1686.22	952.68	-785.29
Cu	1335.55	1027.69	-363.69
Ni	2553.70	1655.07	-988.55
Nb	3.28	105.03	96.04
Mo	0.80	1.68	0.79
Pb	3.08	4.36	1.05
Rb	19.20	29.90	9.08
Sr	50.17	51.35	-1.61
V	68.30	107.23	33.10
Y	9.55	37.43	25.85
Zr	40.91	45.39	2.01
Zn	133.26	77.32	-60.15

3.2.6.4 Summary of the Metasomatic processes in the Platreef at the Akanani prospect area

The Platreef at the Akanani is associated with a granitic footwall that is overlain by a thick layer of pyroxenite (P1 unit). This is successively overlain by an extensively serpentinized unit (P2 unit). Further up the stratigraphic succession a thin layer of feldspathic pyroxenite (P3 unit) is intersected. The melanorites form the top most layer of the Platreef and are further overlain by anorthosites and gabbro-norites of the Main Zone. The isocon of P1 vs P2 shows an enrichment of the MgO within the P2 unit which is suggestive of the excessive serpentinization associated with this unit. The gain of some major felsic elements in P1 may also facilitate the replacement of plagioclase by sericite which is evident from the petrographic observations. The enrichment of TiO_2 in P1 is consistent with the high Cr and V concentrations associated with this unit, while the enrichment of Al_2O_3, Na_2O and K_2O may suggest some degree of contaminatin or assimilation processes related to Platreef interaction with granite footwall. The gain of Al_2O_3, Na_2O, K_2O, Rb, Pb, Ba and Sr in the isocon of P3 vs P2 may suggest that this unit may have been affected by immense feldspathization as compared to the P1 unit. The high amount of CaO gained in the P4 vs P2 isocon may suggest that the P4 unit is more calcium-rich relative to the other three units. Throughout the three lithologies, Mo remained consistently immobile. The results show that the four Platreef lithologies are significantly different with the first two units (P1 and P2) more ultramafic, while further up the stratigraphic column there is an enrichment of felsic elements in P3 unit, while P4 is more calcium-rich. The loss of base-metals in P4 vs P2 isocon plot may suggest that this unit is barren of sulphides. The gain of K_2O and LOI is representative of hydrothermal alteration. The LOI concentration in P2 ranges from 0.7 wt.% - 18 wt.% signifying how intensively altered samples from this unit are. The degree of alteration is intensive at depths between 1200m and 1550m, however the degree of alteration is not dependent on increasing or decreasing depth, but rather on the MgO and LOI contents of each sample. For example a sample from borehole ZF078 with 18 wt.% occurs at a depth of 1200m, while a sample from borehole ZF048 with 1.98 wt.% occurs at a depth of 1500m.

3.2.7 Alteration Geochemistry

This sub-chapter although in many ways similar to the subchapter on mass-balance strictly focuses on alteration indices and ratios. The ultimate goal of this section is to enhance the detection of zones of elevated geochemical anomalies of oxide or trace elements that may be reflective of mineralized zones associated with post-magmatic activity.

3.2.7.1 Ishikawa Alteration Index (AI)

For the Ishikawa alteration index, values ranging between 20 and 40 are for unaltered rocks, while those ranging between 50 and 100 represent hydrothermally altered rocks (Large et al. 2001). An AI=100 represents complete replacement of feldspars and glass by sericite and/or chlorite (Large et al., 2001). A graphic representation of the results is given in Figure 3.37. Samples from P1 show values ranging between 60-77 alteration intensity representing hydrothermally altered rocks. The P2 samples show extensive alteration with the alteration intensity value reaching 99 for a sample with 18 wt.% LOI, thus the high degree of alteration is relatively directly proportional to the concentration of LOI. For example a sample with 0.7 wt.% LOI will have alteration intensity of 49 representing a least altered rock. In the P2 unit where serpentinization seems to be the dominant alteration event, there seem to be a relationship between the mineralization and degree of alteration. For example, a sample with 18 wt.% LOI has Cu contents of 4467 ppm and Ni contents of 7715.3 ppm, while a sample with 0.7 wt.% has Cu contents of 129.2 ppm and Ni contents of 141.8 ppm (Table 3.28). For the P3 samples, alteration intensity ranges from 59-77.2 representing hydrothermally altered rocks. Alteration in this unit is not as extensive; however minor-moderate sericitization is expected due to the feldspathic nature of this unit probably related to the distruction of Na_2O and CaO with subsequent increase in K_2O (Fig. 3.38). It is important to note that the level of K_2O is dependent on the ratio of sericite to chlorite in the altered product. LOI ranges from as low as 0.2 - 5.39 wt.% reflecting the degree to which these rocks are altered. Decrease of this index in P3 from P2 may indicate a reverse of the process that occurred in P2. In this case it is possible that there is a sudden increase in K_2O with subsequent loss of MgO and Fe_2O_3 (Fig. 3.39). P3 samples could thus be associated with sericitization, while P2 samples could be associated with serpentinization this will be later confirmed by petrographic observations. P4 samples are the least altered (Fig. 3.37, 3.38 and 3.39) with alteration intensity ranging between 42-56, while LOI is relatively low ranging between 0.7- 4.2 wt (Table 3.28).

Table 3.28: Represents the minimum, maximum and mean per lithological unit of the CCPI and AI. Note: Min=Minimum, Max=Maximum

Index	P1 Unit			P2 Unit			P3 Unit			P4 Unit		
	Min	Max	Mean	Min	Max	Mean	Min	Max	Mean	Min	Max	Mean
AI	60.0	77.6	69.9	72.7	99.9	87.7	59.8	77.2	70.5	42.5	56.7	49.5
Ni	672.1	8401.3	3433.3	141.8	7715.3	2801.6	7.2	3161.6	1113.9	319.6	4611.8	1398.6
Cu	157.6	2918.4	1335.9	129.2	4467.0	1473.7	55.9	5034.7	976.9	129.3	2779.5	935.0
LOI	0.2	5.5	1.7	0.7	18.96	6.33	0.2	5.39	2.57	0.7	4.2	2.69

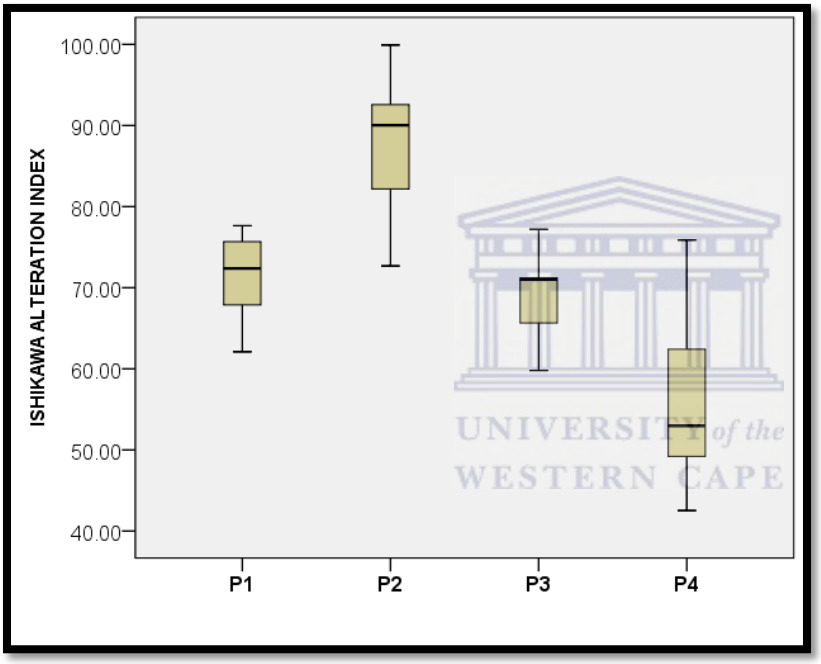

Figure 3.37: Ishikawa Alteration Index occurrence in P1-P4 indicating the intensity of the alteration.

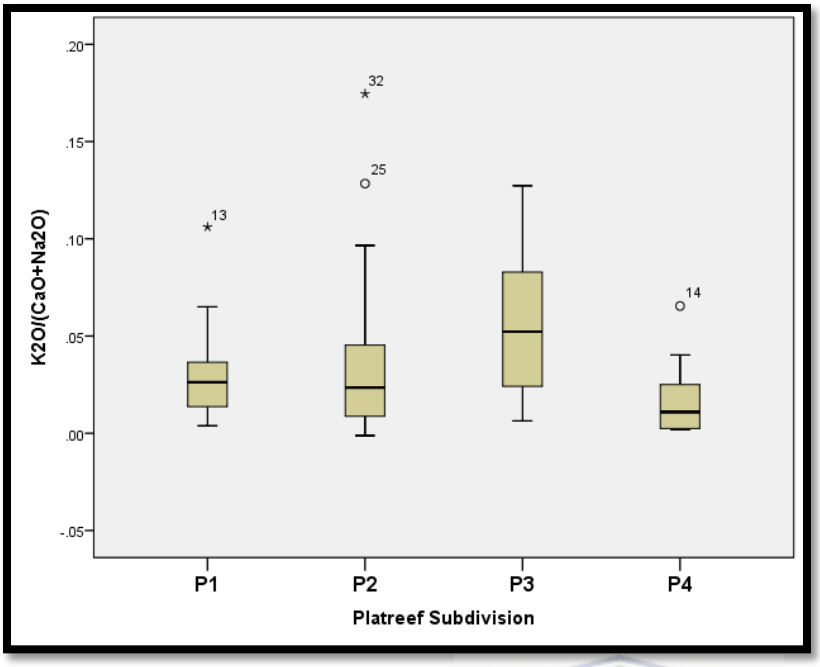

Figure 3.38: Sericitization index for the four lithological units indicating the extent and occurrence of sericitization.

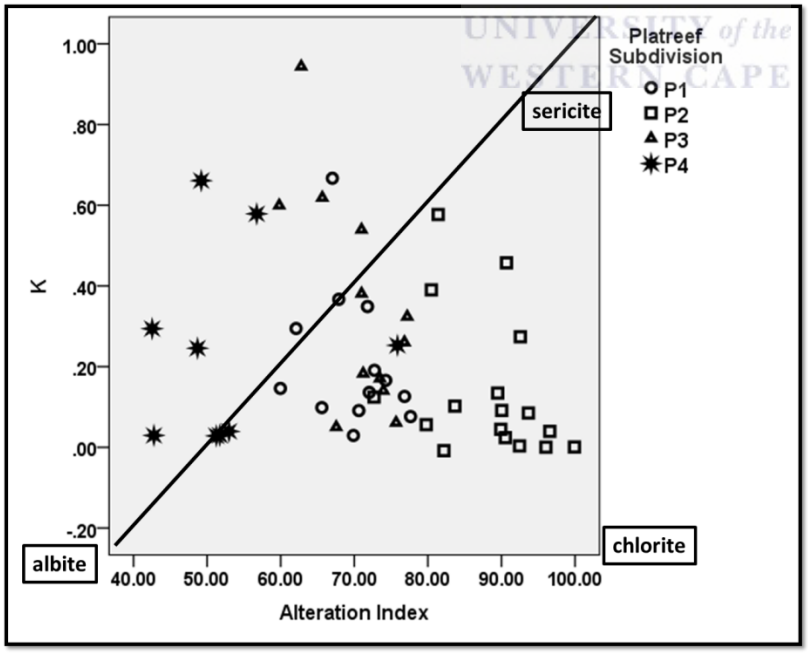

Figure 3.39: Trends of AI with K for the four lithological units (P1-P4) from the Akanani prospect area (After Large et al., 2001). Samples with an AI >60 are considered to be affected by alteration due to hydrothermal fluids.

The Ishikawa alteration index has two limitations (1) it does not take into account the alteration of carbonates which may lead to the decrease of AI even where alteration intensity is high (2) it does not enable the distinction between chlorite and sericite-rich alteration (Large et al., 2001). In order to overcome these limitations the Chlorite-Carbonate-Pyrite Index (CCPI) needs to be used in conjunction with the AI.

3.2.7.2 Chlorite-carbonate-pyrite Index (CCPI)

This index as described in the above subchapters measures the increase in MgO and Fe_2O_3 associated with the Mg-Fe chlorite development which commonly replaces albite, K-feldspar or sericite leading to the loss of Na_2O and K_2O (Large et al., 2001). This index just like the AI index has got its own limitation as it is strongly affected by magmatic fractionation and primary compositional variations in the rock (Large et al., 2001), however when used in conjuction with the Alteration Index, the limitations are reduced. Figure 3.40 below summarizes the results. P4 samples show chl-carb alteration, while some samples lie on the least altered zone. In addition the P4 samples will have fresh albite preserved with none to minor sericite, k-feldspar and chlorite development. This compositional variation relates to greenschist facies metamorphism rather than hydrothermal alteration (Large et al., 2001). P1 and P2 show relatively high values for both the CCPI and AI indices where the former reflects the breakdown of feldspars by the depletion of CaO and Na_2O which are relatively low in both layers especially P2 which is more depleted in CaO and Na_2O, while the latter reflects the intense alteration of Fe- or Mg-rich minerals such as chlorite (Gifkins, Herrmann and Large, 2005). Minerals plotting on the left hand of the CCPI axis or lower AI axis will represent diagenetic alteration. The principal change due to diagenetic alteration is the formation of alkali-rich silicate minerals such as clays, zeolites, epidote, calcite and feldspars (Iijima, 1974; Shirozo, 1974; Munha and Kerrich, 1980; Gifkins and Allen, 2001). Minerals ploting on the right hand of the CCPI axis or upper AI will represent hydrothermal alteration. The data can be classified into two major fields namely:

Field 1: The least altered rocks fall within an area bounded by AI= 15 to 65% and CCPI= 15 to 85%.

Field 2: Samples considered to have been affected by hydrothermal alteration have AI values >75 and CCPI values >85. As the CCPI and AI index increase (>85) most P2 samples move towards the ore-centre. This trend implies a direct relationship between hydrothermal activity

and sulphide ore-zone. P1, P3 and some P2 samples with AI values between 75 and 85 and CCPI values between 85 and 95 represent chlorite ± sericite ± pyrite alteration typical of chlorite-dominated footwall alteration associated with mafic and felsic volcanics.

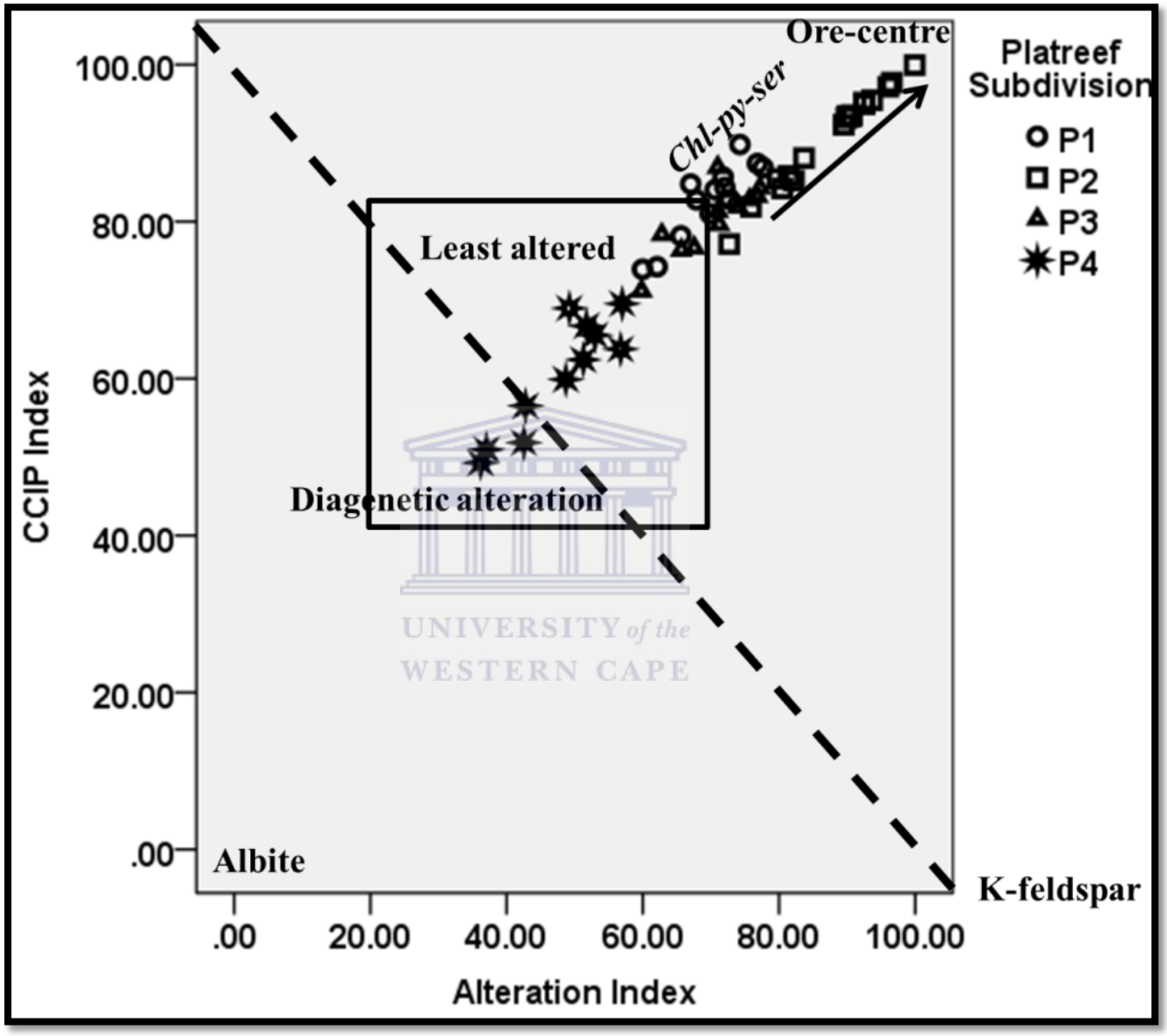

Figure 3.40: CCPI against Alteration Index box plot showing the variation in alteration for P1-P4 (After Large et al. 2001a).

3.2.7.3 Rb/Sr and Ba/Rb alteration ratios

In order to confirm the above results, the Rb/Sr and Ba/Rb ratios were used. These ratios were used as indicators for post-magmatic alteration. The Rb/Sr and Ba/Rb ratios show variable patterns and decrease where hydrothermal alteration has significantly affected the rock types. In the P2 unit were serpentinization is the dominant alteration event, the Rb/Sr ratio ranges from 0.07-1.13, while in P3 which has been affected by sericitization, the Rb/Sr ratio ranges from 0.0001-0.35. In P1 and P4, the Ba/Rb ratio is higher ranging from 1.58-6169 and 1.16-3689 respectively. It is clear that the Rb/Sr ratio is the highest were alteration is most intense, while Ba/Rb ratio is the lowest in these areas. Table 3.29 and Figure 3.41 below summarize the results.

Table 3.29: Table showing the minimum, maximum and mean values for the Rb/Sr and Ba/Rb ratio per lithology. Note: Min= Minimum, Max= Maximm

	P1			**P2**			**P3**			**P4**		
	Min	Max	Mean	Min	Max	Mean	Min	Max	Mean	Min	Max	Mean
Rb/Sr	0	0.55	0.11	0	1.13	0.41	0	0.35	0.16	0	0.27	0.07
Ba/Rb	1.58	6169	946	0.59	169.94	15	2.72	10165	854	1.16	3689	983

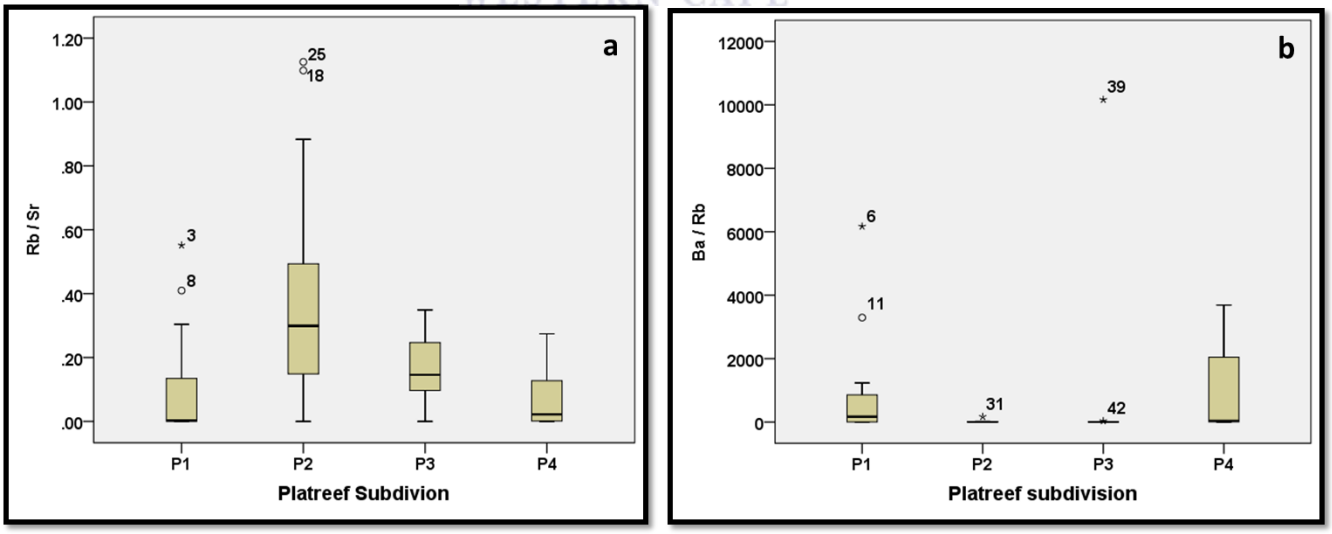

Figure 3.41: Alteration ratios used as indicators for post magmatic alteration. (a) Rb/Sr (b) Ba/Rb.

3.2.8 NORMATIVE MINERALOGICAL CALCULATIONS

The approach described in this chapter is the normative mineralogical calculation technique that quantifies the modal mineralogical composition on the basis of the available major and trace element data present for each sample analyzed. As an alternative, normative minerals provide a quantitative evaluation of mineralogical compositions that can be rapidly calculated according to each sample's unique chemical composition. Table 3.30 below represents the average mineralogical compositions in each unit at Akanani. P1 samples have relatively high hematite and magnetite which corroborates with their high Fe_2O_3 contents. Most Platreef rocks at Akanani are depleted of olivine with the exception of the "harzburgitic" P2 unit. Albite, anorthite, orthoclase and hypersthene are major components of P3 units, while diopside, apatite, and ilmenite classify P4. See Appendix C for a complete data set of the normative calculations for each sample per analysed borehole. Table 3.31 below represents the average mineralogical compositions in each unit at Akanani.

Table 3.30: Average mineralogical compositions for each unit based on normative calculations

Mineral	P1	P2	P3	P4
Orthoclase	1.50	0.53	2.53	0.96
Albite	3.31	0.44	8.30	4.18
Anorthite	9.66	7.71	16.60	16.99
Diopside	23.40	4.48	13.56	30.77
Hypersthene	30.76	22.26	34.37	5.01
Olivine	4.14	41.07	4.23	15.37
Magnetite	0.51	0.38	0.26	0.18
Ilmenite	0.33	0.26	0.32	0.38
Hemaetite	21.29	14.21	13.72	10.87
Apatite	0.05	0.04	0.06	0.12

3.2.8.1 Linear Discriminant Analysis

Using the classification results from the combination of r-mode cluster, r-mode factor and discriminant analysis, the four previously determined subgroups (P1, P2, P3 and P4) were further normalized using the CIPW norm software and classified using the training data sets. Table 3.31 shows the results of the supervised classification using linear discriminant analysis. The training

samples were correctly classified at 98.1% recognition rate (Table 3.31) with 13 samples allocated to P1, 18 to P2, 12 to P3 and 9 to P4. Table 3.32 and 3.33 show the results where P1 is characterized by Hematite and Magnetite which clearly corroborates with Fe_2O_3, TiO_2, and Cr enrichment in this unit. Olivine classifies P2 which is consistent with the high MgO associated with this unit. P3, which is more feldspathic, is characterized by albite, orthoclase, anorthite, hypersthene and quartz which are in line with the enrichment of Na_2O, Al_2O_3, K_2O and SiO_2, while the enrichment of apatite, Diopside and Ilmenite in P4 could be associated with the high CaO and P_2O_5 associated with this unit. These results are consistent with the geochemical analysis results.

Table 3.31: Classification results for normative calculations

		Platreef Subdivision	**Predicted Group Membership**				**Total**
			P1	**P2**	**P3**	**P4**	
Original	Count	**P1**	**13**	0	0	0	**13**
		P2	0	**18**	0	0	**18**
		P3	0	0	**12**	0	**12**
		P4	0	0	1	**8**	**9**
	%	**P1**	100.0	.0	.0	.0	100.0
		P2	.0	100.0	.0	.0	100.0
		P3	.0	.0	100.0	.0	100.0
		P4	.0	.0	11.1	88.9	100.0
a.**98.1%** of original grouped cases correctly classified.							

Table 3.32: Three function structure matrix for the normative calculations.

	Function		
	1	2	3
Diopside	-.271*	-.121	-.078
Ilmenite	-.190*	.002	-.082
Olivine	.367*	.029	-.511
Magnetite	.050	-.227*	.113
Anorthite	-.138	.205*	.148
Albite	-.274	.396	.642*
Hypersthene	.045	-.011	.455*
Orthoclase	-.097	.131	.371*
Apatite	-.140	.056	-.199*
Quartz	-.089	.026	.181*

Table 3.33: Functions at group centroid

	Function		
	1	2	3
P1	-1.053	-2.365	.908
P2	2.891	.010	-.664
P3	-.649	2.149	1.439
P4	-3.396	.529	-1.903

Figure 3.42 is a two function discriminant function summarizing the first two functions. Function 1 seperates ultramafic P2 (olivine) from the melanoritic P4 unit (diopside, ilmenite), while function two seperates the mafic P3 (hematite and magnetite) from the feldspathic P3 unit (anorthite).

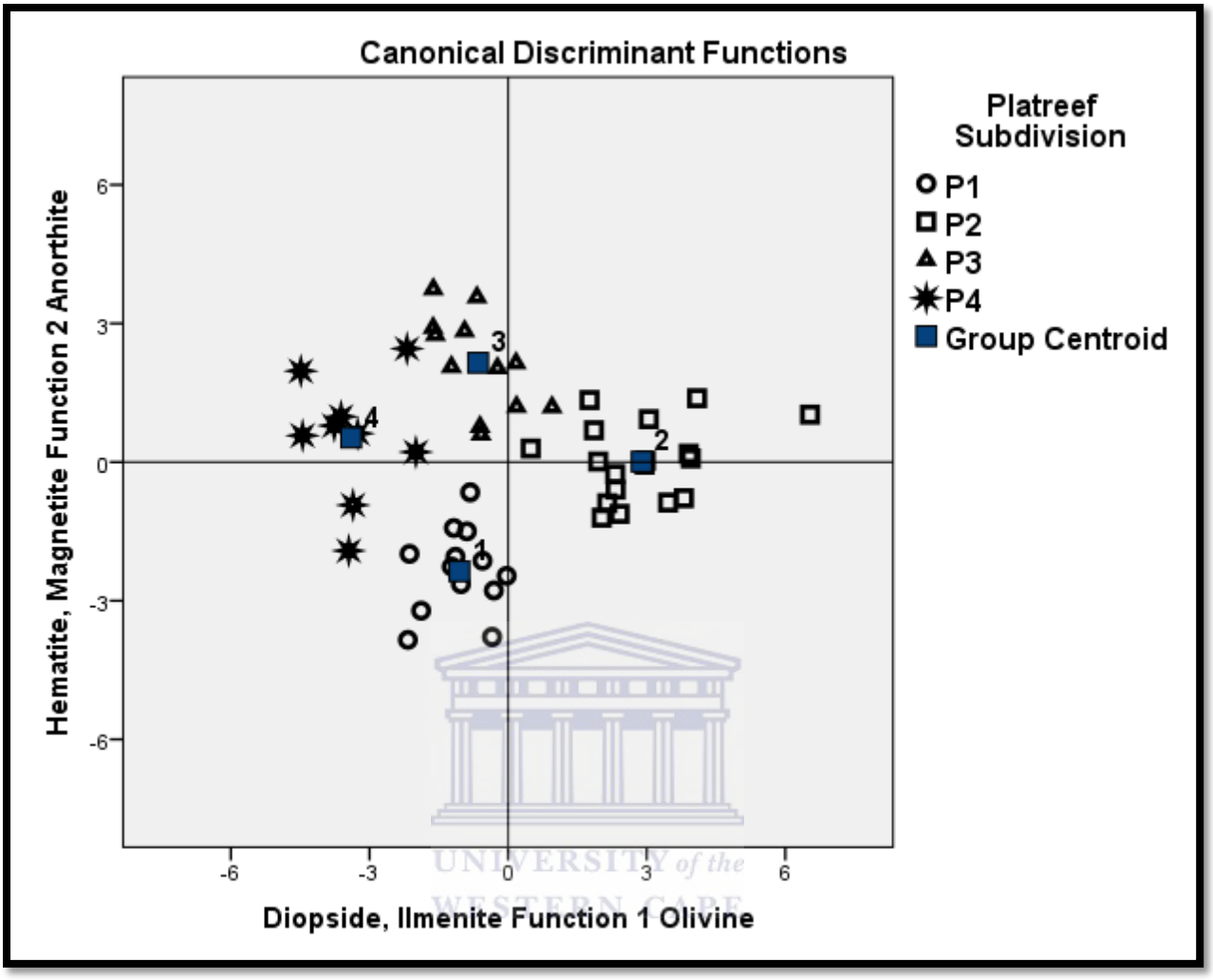

Figure 3.42: Two-function discriminant plot of the normative calculations for the first two functions.

Stepwise discriminant analysis shows that the significance normative mineralogy classifying the four pyroxenite units at recognition rate of 96.2% (Table 3.34) include albite, hypersthene, olivine, magnetite (Table 3.35). A summary of the classification results is given in Table 3.35.

Table 3.34: Classification results for stepwise discriminant analysis of the normative mineralogy

Classification Results[a]							
		Platreef Subdivision	Predicted Group Membership				Total
			P1	P2	P3	P4	
Original	Count	**P1**	**13**	0	0	0	**13**
		P2	0	**17**	0	1	**18**
		P3	0	0	**12**	0	**12**
		P4	0	0	1	**8**	**9**
	%	**P1**	100.0	.0	.0	.0	100.0
		P2	.0	94.4	.0	5.6	100.0
		P3	.0	.0	100.0	.0	100.0
		P4	.0	.0	11.1	88.9	100.0
a.**96.2%** of original grouped cases correctly classified.							

Table 3.35: Percentage difference of major normative mineralogy at the Akanani prospect area.

Normative	Percentage difference
Albite	61.5%
Hypersthene	21.1%
Hematite	7.7%
Olivine	3.9%
Magnetite	2

Multivariate statistical analysis techniques have proven to be successful in characterizing rock types either using mineralogy or geochemistry. There exist a good correlation between the modal mineralogy as determined optically, the norm as determined by the CIPW norm and the whole-rock geochemical results as determined by multivariate statistics.

3.2.9 MINERAL CHEMISTRY

This chapter aims at describing the change in the chemical composition of individual mineral grains from the base of the Platreef to the top and constrain whether a single or multiple magma injections were responsible for the formation of the Platreef at Akanani. The results obtained from this chapter will further aid in determining the extent of fluid-rock interaction and

contamination by floor rock in the Platreef at Akanani. Samples analysed here are from boreholes intersecting the granite floor (ZF044, ZF045, ZF078, and ZF057) and (ZF048). Within each sample the grains (pyroxene, plagioclase, chromite, olivine) where selected on the basis of its cumulus nature and lack of any alteration. For each analysed grain between four and eight analyses were run from the core of the grain to the outer rim. In feldspathic pyroxenite the plagioclase grains chosen were intercumulus and unaltered. A total of 16 polished thin sections were analyzed for mineral chemistry of each individual grain for each unit (5 from P1 unit of borehole ZF057-53, ZF044-47, ZF048-46, ZF078-47, ZF078-34; 4 from P2 unit of borehole ZF048-45, ZF048-48, ZF044-39, ZF048-50; 5 from P3 unit of borehole ZF078-52, ZF057-44, ZF057-46, ZF057-25, ZF078-15; 2 from P4 unit of borehole M0023-21, ZF078-31. A detailed dataset of the results is given in Appendix D in the Appendices section.

3.3.2.1 Orthopyroxene

Orthopyroxene is the most common mineral phase in the Platreef at Akanani. From P1 to P4 the chemistry of orthopyroxene varies with stratigraphic height. Where Platreef intersects granitic floor, the MgO contents of orthopyroxene in P1 averages 23.96 wt.%, while the FeO content averages 17.60 wt.%. P2 orthopyroxenes are magnesian rich showing compositions of hypersthene (En_{50-70}). These compositions are similar to those observed by Harris and Chaumba (2001) within the Platreef and also those from the Lower and Critical Zones (Eales et al., 1993). In P2 MgO increases to 28.69 wt % in core, while FeO contents decrease significantly to 9.42 wt.% in core. This increase and decrease of MgO in the presence of FeO is supported by the formula ($(Mg, Fe^{2+})_2\ SiO_2O_6$) which permits the assumption that Mg can be substituted by Fe (Van der Merwe, 2012). A decrease in MgO contents in P1 from core to rim suggests that the magma was initially Mg-rich and became Mg-poor with time and crystallization. This can further be interpreted as a normal magmatic trend and to be expected FeO shows an exception becoming marginally higher in P1. SiO_2, Al_2O_3, MgO, Cr_2O_3 contents are lower in P1 relative to P2, whereas the TiO_2, FeO, MnO and Na_2O contents are higher. A detailed summary of the results is given in Table 3.36 below.

Table 3.36: Representative compositions of orthopyroxene

Elements	P1		P2		P3		P4	
	Core	Rim	Core	Rim	Core	Rim	Core	Rim
Al_2O_3	1.09	1.11	1.54	1.62	1.65	1.16	0.65	0.68
SiO_2	54.08	53.59	56.8	56.42	54.74	55.36	52.84	51.9
TiO_2	0.12	0.19	0.04	0.06	0.14	0.11	0.2	0.14
CaO	2.07	2.4	2.5	1.28	3.04	0.66	0.77	1.28
MgO	23.96	23.84	28.69	29.59	27.81	29.03	19.34	19.07
Cr_2O_3	0.32	0.23	0.51	0.5	0.6	0.26	0.05	-
FeO	17.6	17.31	9.42	9.85	11.36	12.75	24.7	25.2
Na_2O	0.05	0.05	0.1	0.04	0.1	0.03	-	0.05
MnO	0.47	0.47	0.22	0.32	0.25	0.31	0.7	0.74
Cr	0.22	0.16	0.35	0.34	0.41	0.18	0.03	
Ti	0.07	0.11	0.02	0.04	0.08	0.07	0.12	0.08
Al	0.58	0.59	0.82	0.86	0.87	0.61	0.34	0.36
Mg	15.14	15.06	18.12	18.69	17.57	18.34	12.22	12.05
Fe	13.68	13.46	7.32	7.66	8.83	9.91	19.20	19.59
Total	99.76	99.2	99.82	99.69	99.69	99.66	99.25	99.06
Mg#	0.51	0.52	0.7	0.7	0.66	0.64	0.38	0.37
Hypersthene	100	100	100	100	100	100	100	100
En	67.84	67.58	80.2	82.11	76.47	79.2	57.31	55.88
Fs	27.95	27.53	14.77	15.33	17.52	19.51	41.06	41.42
Wo	4.21	4.89	5.02	2.55	6.01	1.29	1.63	2.7
Cr/ (Cr + Al)	0.28	0.21	0.30	0.29	0.32	0.22	0.09	0.00

The Cr content in pyroxene shows an irregular trend that does not increase systematically with stratigraphic height. Cawthorn (2007) considers Cr in pyroxene a strongly compatible element. The abundances and variability of Cr in low-Ca pyroxene provides strong evidence of two magmatic events at Akanani (Fig. 3.43). The same trend is observed for Al in pyroxene and

supports the multiple magma injection hypotheses. P4 is not consistent with introduction of new fresh magma but rather formed from partial recrystallization of P3 unit and the overlying Main Zone.

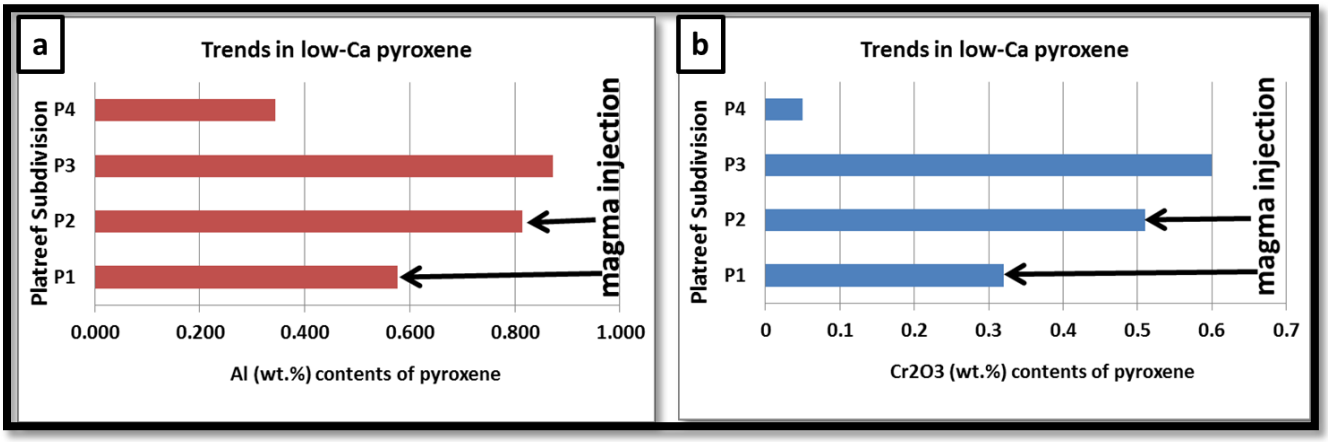

Figure 3.43: Evidence of fresh magma injection at Akanani prospect area. (a) Al contents in pyroxene (note that the Al_2O_3 oxide fraction as presented in the table above was converted to Wt. fraction of element in oxide). (b) Cr_2O_3 contents of pyroxene.

3.3.2.2 Clinopyroxene

Clinopyroxene is also a dominant mineral phase and is nearly pure diopside ($En_{>32}$ $Wo_{>37,}$ Table 3.36). Diopside is the most dominant end-member according to the CIPW norm results. Its TiO_2 and Na_2O contents are respectively 0.37 wt.% and 0.4 wt.%. In P4, hedenbergite ($CaFeSi_2O_6$) could also be present as a result of the slight enrichment of FeO in core (9.94 wt%) and the depletion of MgO to (13.59 wt%) from 13.82wt.%. In P1, the compositions of clinopyroxene are variable with high FeO and MgO, while Al_2O_3, Na_2O, K_2O contents decrease from core to rim which implies that the magma was initially enriched with those elements and were depleted with time and crystallization. The decrease in MgO contents from core to rim in P1 suggests a magmatic fractionation trend. The composition of Cr_2O_3 varies from P1 to P2 with the highest concentration in P1. The depletion Of Cr_2O_3 from core to rim in both P1 and P2 could suggest that Cr_2O_3 was the initial crystallizing phase. A summary of the microprobe results for clinopyroxene is given in Table 3.37 below.

Table 3.37: Representative compositions clinopyroxene

Element	P1		P2		P3		P4	
	Core	Rim	Core	Rim	Core	Rim	Core	Rim
SiO_2	51.75	51.97	52.02	52.04	52.1	51.95	53.53	53.07
Na_2O	0.37	0.33	0.36	0.34	0.33	0.34	0.31	0.26
TiO_2	0.2989	0.3209	0.2792	0.2831	0.5006	0.4677	0.08	0.01
FeO	8.56	9.08	6.87	6.75	4.99	4.9	9.94	9.6
Al_2O_3	2.61	1.853	3.18	2.96	2.03	2.01	0.5369	0.4817
MgO	16.43	15.54	16.75	16.62	16.01	16.1	13.59	13.82
Cr_2O_3	0.74	0.42	0.62	0.56	0.55	0.58	0.04	0.007
CaO	19.24	20.74	19.86	20.22	22.91	23.4	21.62	21.85
MnO	0.19	0.26	0.30	0.29	0.19	0.18	0.32	0.35
K_2O	0.01	0.003	0.013	0.019	0.03	0.04	0.02	0.04
Total	100.22	100.52	100.26	100.09	99.65	99.98	100.01	99.50
Diopside	72.77	80.02	71.93	75.01	87.94	86.72	87.11	88.33
Wo	37.8	41.44	37.69	39.17	46.22	45.59	44.8	45.48
En	25.32	26.99	27.24	27.54	34.25	33.9	27.25	28.01
Fs	9.65	11.59	7	8.3	7.48	7.23	15.06	14.85

3.3.2.3 Olivine

It is important to note that most Platreef rocks are depleted in terms of olivine so that only P2 unit is analysed for olivine compositions. A summary of the micro-probe results is given in Table 3.37 below. The Fo content of olivine ranges between Fo_{67} and Fo_{74} and so this olivine can therefore be referred as forsterite. Where the floor-rock is granitic, olivine compositions show a general trend of Fe-enrichment and NiO depletion which is roughly compatible with olivine fractionation. Where Al_2O_3 contents are higher, along with lower MgO and TiO_2 suggests an influence of the floor rock. For sample ZF044/39, the FeO content and MnO are higher and thus is more fayalitic. As would be expected from the relative compatibilities of Ni, Mg and Fe in olivine structure, the Ni content of olivine decreases with decreasing Fo contents. Hydrothermal

activity can affect the composition of olivine in that during actinolite alteration, olivine can be converted to a more Fe-rich variant hence the high FeO content of olivine in sample ZF044/39. Table 3.38 summarizes the results.

Table 3.38: Representative compositions of olivine in the P2 horizon of the Platreef at Akanani

Elements	**P2 (ZF048-50)**		**P2 (ZF044-39)**	
	Core	**Rim**	**Core**	**Rim**
SiO_2	39.05	39.55	38.63	38.82
MgO	42.73	42.36	39.05	38.93
TiO_2	0.01	0.06	-	-
CaO	0.05	0.02	0.09	0.06
Al_2O_3	-	-	0.03	-
Cr_2O_3	0.01	-	0.01	-
FeO	18	17.62	22.09	22.25
MnO	0.29	0.35	0.5	0.43
NiO	0.15	0.13	0.09	0.11
Cr	0.007		0.007	
Ti	0.006	0.036		
Al			0.016	
Mg	26.99	26.76	24.67	24.59
Fe	13.99	13.70	17.17	17.30
Total	100.29	100.09	100.49	100.6
Olivine	99.88	97.8	99.57	98.78
Fo	74.12	72.78	67.85	67.1
Fa	25.76	25.01	31.72	31.69
Mg#	0.61	0.62	0.54	0.54
Cr/ (Cr + Al)			0.30	

3.3.2.4 Plagioclase

CIPW norm calculations for plagioclase in P3 (ZF057-44 and ZF057-46) and P4 (ZF078-6) show relatively good matches for bytownite and labradorite (Fig. 3.44) with An% content in P3 of 67.4 wt% to 79.5 wt% (Appendix D) .

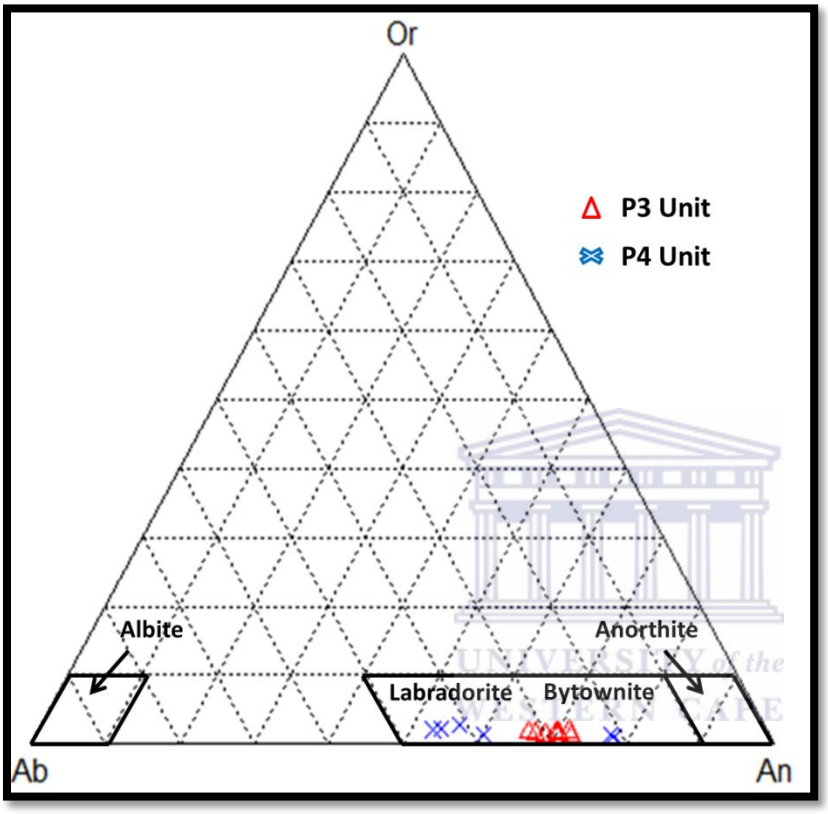

Figure 3.44: Or-Ab-An ternary diagram for plagioclase showing the variation of plagioclase composition in P3 and P4.

Microprobe data from boreholes ZF057/44 and ZF057-46 are plotted in Figure 3.43. The plots show that the grains selected are pure plagioclase separate grains. The plagioclase end-member of anorthite pre-dominates both P3 and P4 units with respective chemical compositions of $NaAlSi_3O_8$ and $CaAl_2Si_2O_8$. Orthoclase is a rare constituent; however it is present in minor concentrations. Van der Merwe (2012) interpretes its occurrence as related to footwall contamination. Al_2O_3 contents of plagioclase are relatively high in P3 averaging 31.06 wt% in core and 30.32wt% in rim. Increase in SiO_2, Na_2O and K_2O from core to rim in P3 suggests a normal fractionation trend, while an increase in MgO, CaO and FeO from core to rim and a

decrease in SiO_2, Na_2O, and K_2O from core to rim is opposite to regular fractionation trends suggesting that P3 and P4 could not have formed from the same magma.

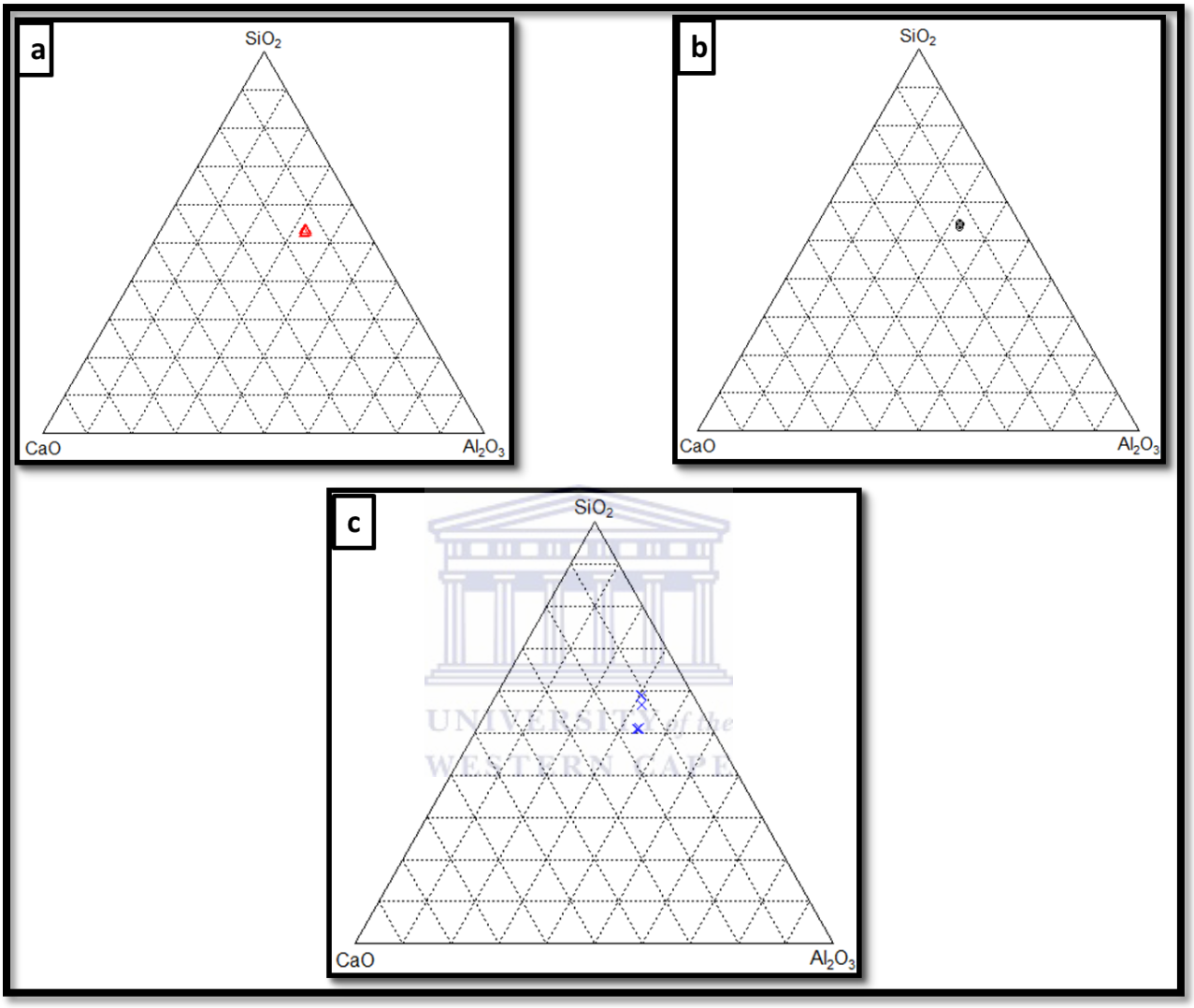

Figure 3.45: Ternary diagrams of major element oxides in plagioclase from microprobe data for P3 and P4 (a) ZF078-6 (P4 unit) (b) ZF057-44 (P3 unit) (c) ZF057-46 (P3 unit)

In P3, the feldspathic pyroxenites show An value of 67.32 in core and 63.77 in rim suggesting the intercumulus nature of the plagioclase in P3. In P4 the An% increases to 84.48 in core suggesting that plagioclase in this unit is cumulus. High An# can be attributed to contamination by Ca-rich hangingwall gabbronorites. Table 3.39 summarise the results below.

Table 3.39: Representative compositions of plagioclase for P3 and P4 unit of the Platreef

ELEMENT	P3 PLAGIOCLASE		P4 PLAGIOCLASE	
	CORE	RIM	CORE	RIM
SiO_2	51.74	52.11	49.32	47.68
Al_2O_3	31.06	30.32	32.76	33.05
TiO_2	0.03	0.025	-	-
CaO	13.3	12.42	14.88	15.5
MgO	0.0228	0.01	0.04	0.09
MnO	0.02	0.07	-	0.09
FeO	0.26	0.20	0.23	0.32
Na_2O	3.42	3.76	2.4	2.32
K_2O	0.21	0.23	0.20	0.13
Total	100.07	99.15	99.83	99.19
Or	1.28	1.30	1.28	0.83
Ab	31.34	34.93	22.30	21.14
An	67.32	63.77	76.42	78.03
An%	77.79	74.85	84.48	85.79

3.3.2.5 Chromite

Chromite, although less common at Akanani is of great importance in the Platreef because of its significant association with PGE mineralization in the Bushveld Complex (Mitchell and Scoon, 2012). Numerous small xenoliths of chromitite sometimes occur in the pyroxenite close to the top contact, a feature first noted by Holwell and McDonald (2006) and interpreted as relics of pre-existing chromitite destroyed during magmatic erosion. In addition to chromite, various Cr spinels (Mg-Al oxide) and Ti-bearing accessory phases are abundant, especially where the chromite content reaches above 29000 ppm. The Cr_2O_3 content in Fe-poor chromite ranges from 39.1-40.83 wt.% and a TiO_2 content that ranges from 1.2-1.5 wt.%, while that within the Fe-rich chromite has a lower Cr_2O_3 (28.9-29.93 wt.%) and a higher TiO_2 content (1.98-2.08 wt.%) this findings are consistent with those of Yudovskaya (2010). This compositional variation in

chromite chemistry is most related to host rock types. A summary of the results is given in Table 3.40 that follows.

Table 3.40: Representative compositions of chromite for P1 unit of the Platreef for boreholes ZF044 and ZF078.

ELEMENT	Fe-rich chromite (ZF044-55)	FeO-poor chromite (ZF078-49)
MgO	4.95	7.06
TiO_2	1.86	1.29
FeO	53.17	37.64
Al_2O_3	9.38	13.57
Cr_2O_3	29.82	40.15
NiO	0.13	0.04
MnO	0.53	0.54
Cr	20.40	27.47
Ti	1.12	0.77
Al	4.96	7.18
Mg	3.13	4.46
Fe	41.33	29.26
Cr/ (Cr+Al)	0.80	0.79
Total	99.84	100.29

To clearly show the effects of re-equilibration, analysis of different morphological types of chromites (cumulus and post - cumulus) from the disseminated chromite sample ZF044-55 in P1 unit was done (Fig. 3.46). According to Yudovskaya and Kinnaird (2010), re-equilibration causes a decrease in Mg and Al and an increase in Ti and Fe and re-distribution of Cr. In this sample an increase in TiO_2, Fe_2O_3 is consistent with decreasing MgO and Al_2O_3 content (Fig. 3.46).

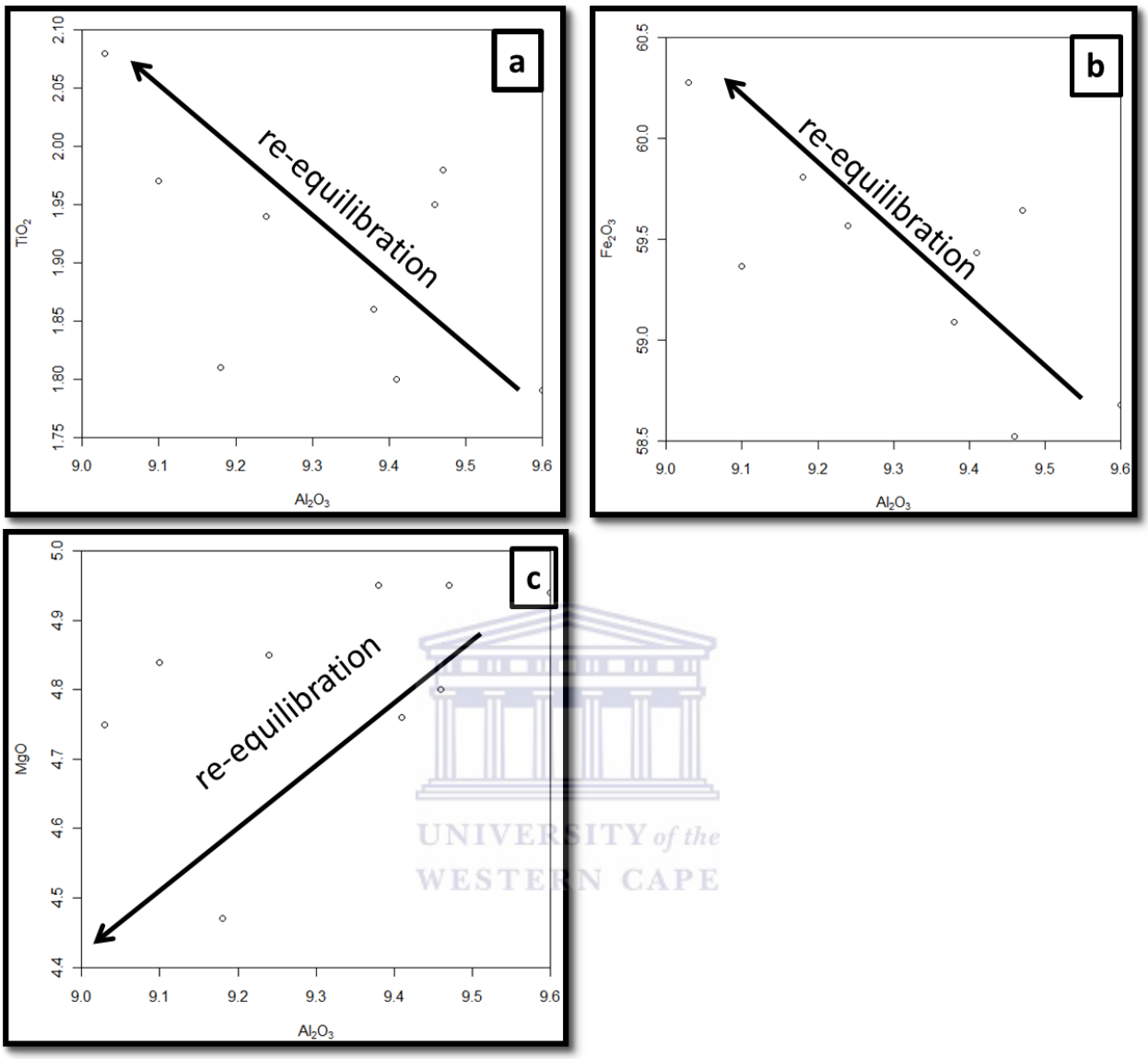

Figure 3.46: Compositional variations of the different textural types of the chromite to show an influence of post-cumulus modification on their chemical compositions. (a) TiO_2 vs Al_2O_3 wt.% (b) Fe_2O_3 vs Al_2O_3 wt.% (c) MgO vs Al_2O_3 wt.% (after Yudovskaya and Kinnaird, 2010).

3.3.2.6 Serpentine

Serpentine is the dominant hydrous Fe-Mg silicate phase present with SiO_2 content slightly above 40 wt%. The serpentine analysed here is a possible alteration product of both orthopyroxene and olivine as it occurs along cracks and fracture zones of both minerals. The serpentine analysed is FeO-poor with FeO content of serpentine ranging from 1.94-2.5 wt.%

(Table 3.41). It should be noted that the low totals of serpentine of less than 100% are due to the high LOI contents of this mineral.

Table 3.41: Representative compositions of serpentine for the P2 unit of the Platreef from borehole ZF048.

ELEMENT	Serpentine-1	Serpentine-2
SiO_2	41.81	41.29
MgO	39.65	39.72
TiO_2	0.0016	0.0148
CaO	0.0058	0.0313
Al_2O_3	0.1677	0.1391
Cr_2O_3		
FeO	1.94	2.52
MnO	0.1065	0.0573
NiO	0.09	0.0959
TOTAL	83.7717	83.8685

Chapter 4
Discussion

4.1 Introduction

The aim of this study was to distinguish between the distinctive geochemical characteristics that can be used to identify each layer and in so doing determine geochemical elements characterizing each of these pyroxenite units. If it was determined that there are three principal rock types within the Platreef (A, B, C) (White, 1994; Lee, 1996; Kruger, 2010) on the basis of modal mineralogy then the geochemical character of each reef should also be determined. The question of single continuous magmatic event or multiple magma injection is still a subject of debate (Kinnaird et al., 2005; Mitchell and Scoon, 2012; Holwell and McDonald, 2007) and an attempt is made in this study to present evidence for a multiphase magmatic event. Recently work by Harris and Chaumba, 2001; Holwell and McDonald, 2007; Pronost et al., 2008; Roelofse, 2010; McCutcheon, 2012 has linked the variable PGE-BMS mineralization in the Platreef to post-magmatic fluid activity and localised country rock contamination. The multi-element data processed by various statistical and classical methods allows for an evidence based discussion on aspects of Platreef geochemistry, mineralogy and mineralization as well as an intercorrelation of these findings with previous work on adjacent farms. This discussion will not consider in detail the mechanisms involved in the formation of the mineralization, for this will deviate from the scope of the work. The Platreef at Akanani and elsewhere is a highly complex ore-body and is extremely variable along strike on both meter and kilometer scales. This project is based on seven drill-cores (ZF044, ZF045, ZF048, ZF057, ZF078, ZF082 and M0023), therefore the cores used here may not be a representative of the ore-body as a whole. The combination of petrography and multivariate statistical methods used aided in improving the reliability of the data provided by Lonmin Limited and improving the classification of the rock types. Nevertheless, the results of this project have revealed a number of distinctive features present at Zwartfontein, some of which may have been highlighted by previous workers on this area. The classification and origin of the mafic-ultramafic rocks of the Platreef is a subject of controversy among the different workers (Kinnaird, 2005; Mitchell and Scoon, 2012). In light of the present petrographic and geochemical study a new lithostratigraphic sequence has been

proposed. Moreover, the different processes that may have resulted in the formation of this stratigraphic sequence are also discussed.

4.1.1 A, B AND C REEFS AND PU1, PU2, PU3 VS P1, P2, P3 AND P4

The Platreef at Akanani is characterized by the abundance of chromitites, pyroxenite, olivine-rich pyroxenite, feldspathic harzburgites, serpentinized harzburgites, pegmatoidal feldspathic pyroxenite and melanorite. Exploration geologists at the Akanani prospect area collectively grouped these lithologies into four distinct units namely: P1, P2, P3 and P4. This stratigraphic subdivision coincides with that of many researchers in the Platreef (White, 1994; Lee, 1996; Kruger, 2010; Mitchell and Scoon, 2012) who proposed that the Platreef is subdivided into three reefs namely A, B and C reef and PU1, PU2, PU3 respectively. Lee (1996) concluded that the Platreef consisted of a feldspathic pyroxenite with three subdivisions based on texture and mineral mode. This nomenclature was an informal stratigraphic zoning assigned to the original Platreef exploitation in order to provide datum lines for economic evaluation (Kinnaird, 2005), however this analogy did not take into account the varying nature of the footwall along strike from South to North in the Northern Limb. With the aid of geochemistry and petrography P1, P2, P3 and P4 are correlated to A, B, C reefs of White (1994) as well as the P1U, P2U and P3U of Mitchell and Scoon (2012).

The geochemical and mineralogical classification of P1, P2, P3 and P4 terminology of the Platreef sequence at Akanani is directed at correcting what is perceived to be fundamental misconceptions that the Platreef is subdivided into three reefs A, B and C. The nomenclature that is presented here is essential for mining purposes at the Akanani prospect area and cannot be used as a representation of the Platreef as a whole.

4.1.1.1 A-reef and PU1 vs P1

Lee (1996) classified the A-reef as the lower most feldspathic pyroxenite rich in base-metal sulphide mineralization. Results obtained from this study do show the occurrence of Ni and Cu in P1, however the highest tonnage is encountered in P2 unit (Van der Merwe, 2012). The classification of A-reef as a feldspathic pyroxenite disregards the occurrence of chromitite as stringers or disseminated in P1 which is usually in common association with PGE (Mitchell and Scoon, 2012). Cluster analysis results using the Average Linkage Method (Fig. 4.1) for P1 samples show a close association between PGE-BMS and Cr. However it is important to note

that the PGE-BMS relationship is based on 13 samples from P1 of which 5 had PGE concentrations above 1000 ppb and therefore results could change with increased number of mineralized samples. At Akanani, chromite grains from two chromitite layers were analysed, both from borehole ZF044 and ZF078 at depths of 1309.6 and 1264.54m respectively and occurring towards the footwall contact within the basal P1 unit. Sample ZF044-55 with Cr contents of 134596.30 ppm yielded 611.59 ppm Cu and 805.40 ppm Ni, while Pt and Pd concentrations were about 917 and 962 ppb respectively. Sample ZF078-49 with Cr contents of 103074.5 ppm yielded Pt contents of 10288 ppb and Pd concentrations of 12 788 ppb, while Cu and Ni concentrations were 2918 and 7155 ppm respectively. As a rule of thumb, iron-poor chromites are likely to have relatively high PGE-BMS grades, whereas iron-rich chromites are likely to have generally lower PGE-BMS grades. The grade of PGE associated with the chromitite tends to be at an optimum where the Cr2O3 content of chromite is 41 to 43% (Mitchell and Scoon, 2012). This may however not be true for all the chromites at Akanani, but some similarities can be derived from sample ZF078-49 to the conclusion made by Mitchell and Scoon (2012) (Table 4.1). Micro-probe analysis of different chromite grains from the disseminated chromite samples ZF044-55 and ZF078-49 in P1 unit suggests an influence of post-cumulus modifications on their chemical compositions. Yudovskaya and Kinnaird (2010) attributed the wide range of chromite compositions as influenced by late-stage magmatic processes including post-cumulus growth and re-equilibration, interaction with fluid-and sulphide-saturated magmatic liquid and contact metamorphism. At Akanani the variability of chromite composition is related to re-equilibration which lowers the Mg and Al contents of chromite thereby causing an increase in Ti and Fe and re-distribution of Cr. On the basis of petrography and geochemistry the samples previously classified as chrome-pyroxenite should be termed chromitite whose mineral chemistry is consistent with the chromitites of Mitchell and Scoon (2012).

Table 4.1: Comparison between chemical compositions of chromite samples from a study by Mitchell and Scoon (2012) and ZF078-49 from this study.

Elements	ZF001/T1	ZF078-49	ZF044-45
Cr_2O_3	43.45	40.15	40.83
Al_2O_3	14.33	13.57	13.22
FeO	24.02	37.64	37.45
TiO_2	1.21	1.29	1.46
MgO	6.93	7.06	6.98
MnO	0.22	0.54	0.58
NiO	0.21	0.24	0.04
Total	99.22	100.49	100.57

Mitchell and Scoon (2012) described the P1U (Platreef sub-unit 1) as a pervasive suite of complexly-layered medium to fine-grained gabbronorite-websterite lithologies, with minor feldspathic orthopyroxenite. Holwell and Jordaan (2006) noted that irregularly shaped intrusive fine-grained melagabbronorite are a common feature towards the base of the hangingwall and very occasionally are also seen to penetrate the Platreef. Kruger (2010) described the Platreef in contact with quartzite as having fine-grained micro-gabbronorite 'chills' preserved. Where Platreef is in contact with shales Kruger (2010) noted that a mixture of hornfels, sulphide-rich gabbronorites and pegmatoidal rocks could be observed. According to Kruger gabbronorite inclusions were absent in areas where Platreef is in contact with granitic floor as the resulting partial melts formed felsic patches with the interaction of mafic and felsic rocks. At Akanani the floor is granitic and gabbronorite inclusions were not observed in the boreholes studied instead geochemical and petrographic results suggests four major lithologies occurring within the P1 pyroxenite package (i) a chromitite (ii) a pure medium to fine-grained pyroxenite with relatively the same proportion of orthopyroxene and clinopyroxene that are usually altered to microcrystalline minerals (uralite and sericite) (iii) medium to fine-grained feldspathic pyroxenite (iv) chrome-bearing feldspathic pyroxenite. Calc-silicate xenoliths were also intersected but will not be treated as major Platreef lithologies characterizing this unit. These xenoliths have been interpreted by Harris and Chaumba (2001) as resulting from the mechanical mixture of calc-silicate material, pyroxene-rich igneous lithologies and minor serpentinites. The low Cr_2O_3 (0-0.029 wt.%) content of the clinopyroxenes suggests that these rocks could be metamorphic in origin. On the basis of petrography and geochemistry, these rocks can be called

clinopyroxenites. The term ‘parapyroxenite’, although a popular term with mining geologists at Sandsloot does not fit the description of the ‘diopsidic’ rock type intersected at Akanani. McDonald et al. (2005) defined parapyroxenite as a massive diopside-clinopyroxenite that is locally enriched in metamorphic olivine that suffered variable degrees of serpentinization. The clinopyroxenites at Akanani do not have any observable olivine and contains less orthopyroxene rimmed by alteration halo of tremolite, phlogophite, sericite veins and actinolite which provides evidence that this rock interacted with late-stage hydrothermal hydrothermal fluids.

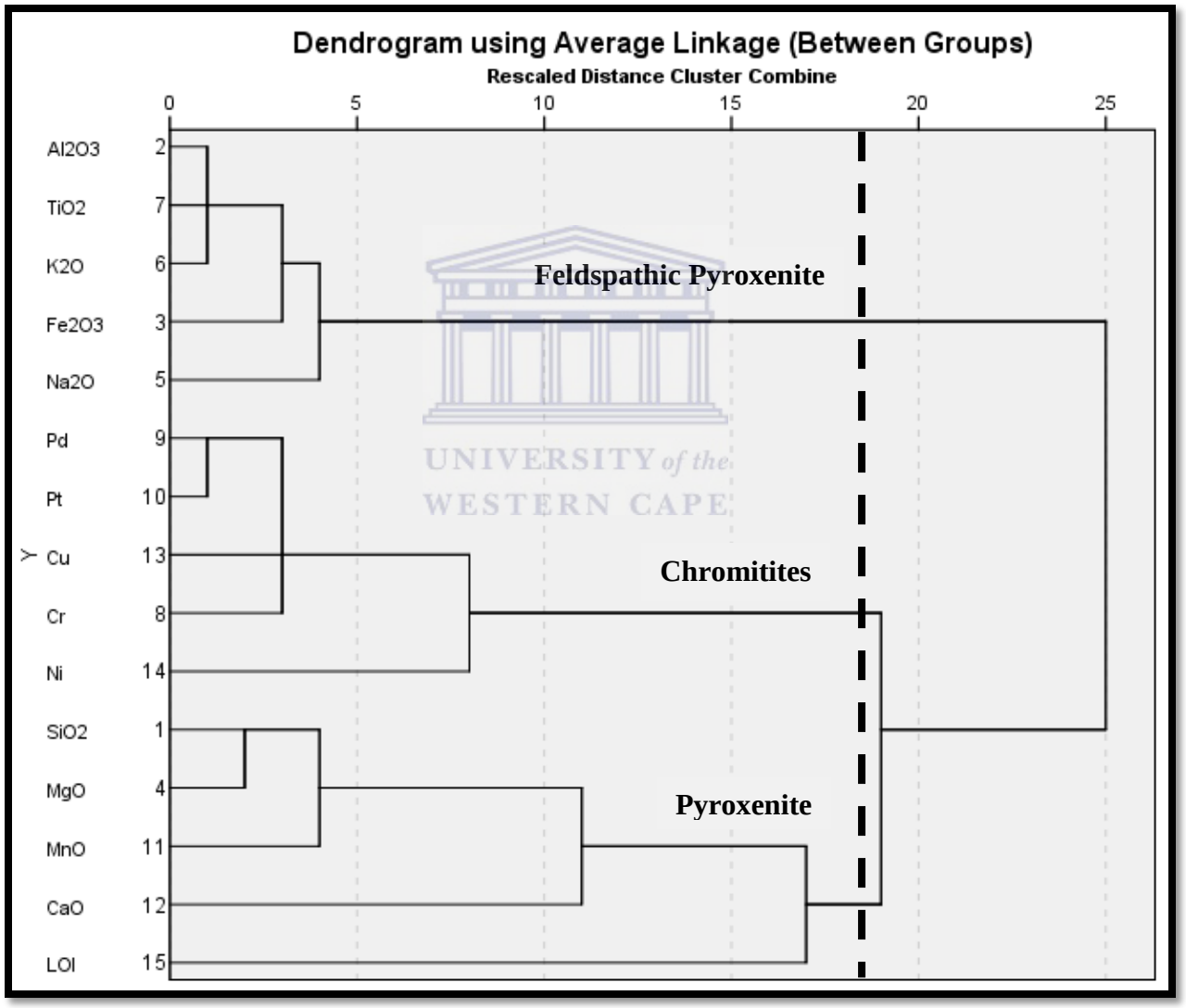

Figure 4.1: Dendogram using Average Linkage Method showing the geochemical differences between the three major lithologies in P1. Note the association between PGE-BMS and chromitites.

In this study the occurrence of gabbronorite as intrusions in the Platreef is acknowledged, however these intrusions cannot be considered major lithologies characterizing P1 at Akanani (as described by Mitchell and Scoon, 2012) as this analogy may imply that the Platreef post-dates the Main Zone which is not the case (Kinniard, 2005; Holwell et al., 2005; Naldrett, 2005; Holwell and Jordaan, 2006).

4.1.1.2 B-reef and PU2 vs P2

The geochemistry and bulk mineralogy has shown that the P2 unit which overlies the P1 unit is comprised of serpentinized harzburgite, feldspathic harzburgites and olivine-rich pyroxenite lithologies. Kruger (2010) described the B-reef as the main mineralized unit that is dominated by orthopyroxene with inclusions and xenoliths of the country rocks. Van der Merwe (2012) described the P2 unit as a well mineralized (3PGE + Au contents varying between 1 and 15g/t) medium to coarse-grained feldspathic pyroxenite with intervening layers of harzburgite. He further equated the P2 unit to the B-reef that is mined by Anglo-platinum further south of Zwartfontein where the floor is dolomitic. The degree of serpentinization also increases towards the top of the P2 horizon (Van der Merwe, 2012). Mitchell and Scoon (2012) described the PU2 as a complexly-layered medium to fine-grained gabbronorite-websterite lithologies with minor feldspathic orthopyroxenite. Although these rocks were initially classified as olivine-bearing pyroxenites by mining personnel at the Akanani prospect area, petrographic and geochemical analysis suggests that these rock are harzburgites (45% orthopyroxene and 50% olivine; 27-48 wt% MgO) as they do not contain any significant clinopyroxene to be termed olivine-bearing pyroxenites. Where olivine is present in small amounts in an orthopyroxene dominated matrix, these rocks can be termed olivine-bearing orthopyroxenites (Plate 4.1).

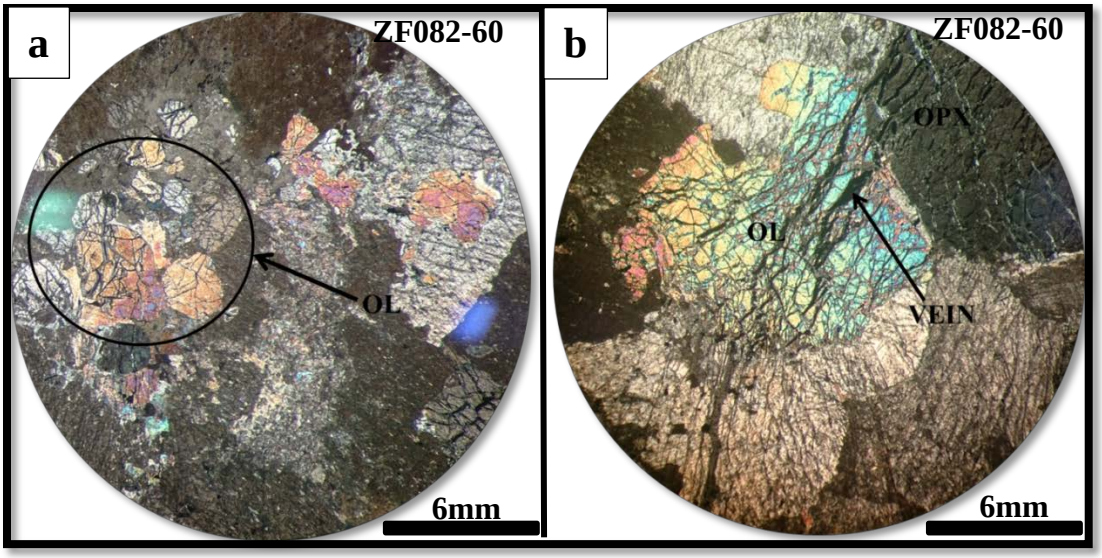

Plate 4.1: Petrographic photographs of the P2 lithological unit present at Zwartfontein. Panels **a** and **b** are taken in crossed polarized light. **(a)** Extensively altered olivine-rich orthopyroxenite sample with some olivine grains that have survived the alteration. **(b)** Fractured olivine grain with hydrothermal veins on the surface extending to nearby orthopyroxene grains. These veins are usually filled with serpentine.

The harzburgite has posed serious problems for previous researchers as there has been a lot of confusion as to whether these rocks are primary or serpentinized floor-rock xenoliths (Mitchell and Scoon, 2012). Kekanan (2014) suggested that the harzburgites at Turfspruit were rafts of serpentinized calc-silicates although texturally they appeared igneous. Micro-probe results reveal that the olivine is magmatic in origin due to its low MgO content (>38-42 wt.%; Table 3.38) than would be expected for a metamorphic olivine, however good correlation exists between the harzburgites analysed by Kekana (2014) and the harzburgites referred to here in this study (Table 4.2). Furthermore the NiO (>0.078-0.14 wt.%; Table 3.38) content of olivine is also compatible with a magmatic origin. Manyeruke et al. (2005) also analysed olivine (Fo_{79-80}) with the same composition on the farm Townlands, south of the Akanani prospect area and also Mitchell and Scoon (2012) at Zwartfontein north, while Buchanan et al. (1981) analysed igneous olivine (Fo_{75-76}). On the basis of the findings from this study the harzburgite is interpreted as a primary lithology as supported by chemical data of olivine composition and studies of Kinnaird (2010), Kekana (2014) and Mitchell and Scoon (2012). The variable NiO content of olivine (0.07 to 0.14 wt.%) may be due to the presence of pentlandite (Fe-Ni) (Filippidis, 1982; Mclnnes et al., 2001)

which crystallized during serpentinization at olivine rims (Pelletier, 2008). Van der Merwe (2012) interpreted the occurrence of pentlandite displaying higher Fe contents than normal at the Akanani prospect area as related to alteration or even the presence of Fe-rich silicates.

Table 4.2; Comparison of major element data (wt%) of the T2 Lower Harzburgites at Turfspruit and P2 harzburgite at the Akanani prospect area.

Element	Turfspruit Harzburgite	Harzburgite from this study
SiO2	43.3	38.82
Al2O3	4.01	3.30
Fe2O3	1.91	14.41
MnO	0.18	0.24
MgO	30.72	32.11
CaO	2.92	4.89
Na2O	0.26	0.10
K2O	0.13	0.19
TiO2	0.13	0.14
P2O5	0.03	0.02
LOI	7.86	5.59

This study has produced both geochemical and mineralogical evidence that reveal the occurrence of two types of harzburgites in P2. Some samples from Akanani are severely altered and in most cases the primary igneous textures are obliterated making it difficult to determine their primary origin; however these samples are referred to as serpentinized harzburgite. On the other hand some samples closely resemble the poikilitic feldspathic harzburgites described by Mitchell and Scoon (2012) and also those described from localities in the Critical Zone of the Western lobe by Manyeruke et al. (2005). The distinguishing factor between serpentinized harzburgite and feldspathic harzburgite is the high K_2O, Na_2O and Al_2O_3 content for the latter that signifies the occurrence of interstitial plagioclase and higher MgO and LOI for the former that indicates the degree of alteration (Fig. 4.2). The feldspathic harzburgites are usually olivine-rich with intercumulus feldspar, accessory spinel and oikocrysts of clinopyroxene. It is clear from the dendogram (Fig. 4.2) that the feldspathic harburgites do not carry significant PGE-BMS mineralization as the mineralization is confined to the serpentinized harzburgites. According to Mitchell and Scoon (2012) the most important component of the mineralized section of the

Platreef at Akanani is harzburgite and finding which type of harzburgite is associated with the PGE-BMS mineralization is fundamental to this study as it is to mining and exploration geologists at Akanani. This is mainly because the P2 unit is considered very well mineralized (Van der Merwe, 2012). The intimate relationship between PGE and BMS suggests that there is no apparent decoupling of PGE and base-metal sulphide concentrations as previously observed at Akanani by Mitchell and Scoon (2012).

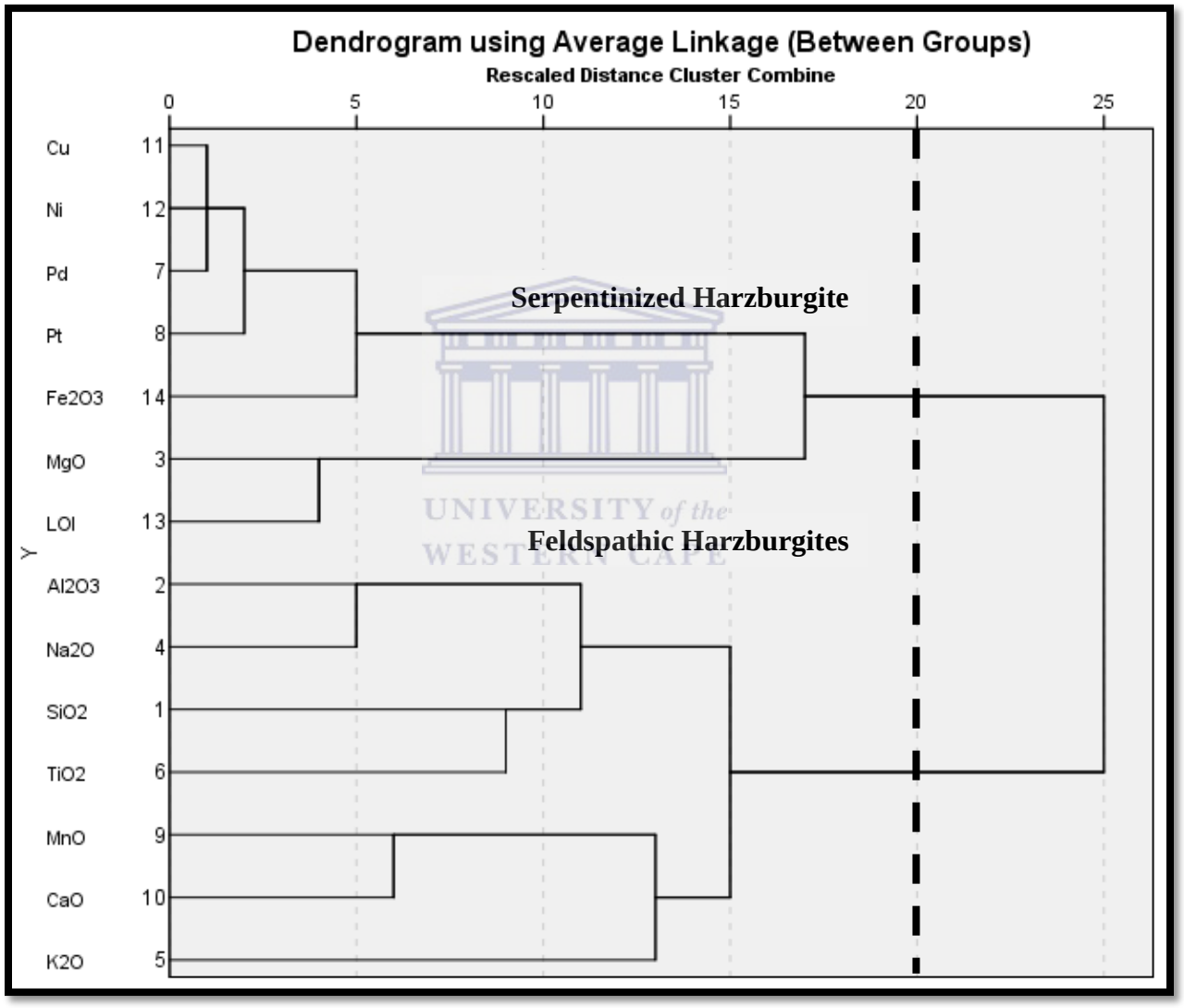

Figure 4.2: Dendogram using Average Linkage Method showing the geochemical differences between the two major lithologies in P2.

The depletion of Zr in P2 (Fig. 3.14c) further supports the abundance of olivine and orthopyroxene in this unit as this element is incompatible with olivine, orthopyroxene, clinopyroxene and plagioclase.

4.1.1.3 C-reef and Pu3 vs P3 and P4

Lee (1996) described the C-reef as a fine-grained poikilitic feldspathic pyroxenite, which lacks any BMS and PGM containing up to 70% clinopyroxene. At Sandsloot Holwell and Jordaan (2006) described the C-reef as a fine-grained feldspathic pyroxenite that is characteristically barren off mineralization. Yudovskaya and Kinnaird (2010) noted that from the Northern part of Tweefontein to the Central sector and sporadically in the Northern sector, a barren fine-grained feldspathic pyroxenite transitional to melanorite often occurs at the Platreef-hangingwall contact. They further described it as not containing any visible sulphides and equated it to the C-reef as described by White (1994) or the P4 unit in the Akanani area as described by exploration geologists. Geologists at Akanani describe the P3 as a medium-coarse grained, generally feldspar poor pyroxenite with green clinopyroxene oikocrysts. Typically the texture is poikilitic and the lack of sulphide mineralization is typical of P3 unit. On the basis of field observations, Mitchell and Scoon (2012) concluded that the PU3 sub-unit at Akanani may take the form either of pegmatoidal feldspathic websterite-orthopyroxenite-melanorite or medium/ coarse-grained feldspathic pyroxenite-gabbronorite with a microscopically glassy appearance. Van der Merwe (2012) described the P3 as typically barren consisting of medium-grained pyroxenite with Poikilitic clinopyroxene. According to Van der Merwe (2012) P4 is a medium-grained melanorite to feldspathic pyroxenite. He further interpreted its occurrence as a second intrusive event that transgressed through the upper P2 unit through the P3 and P4 units and into the Main Zone hangingwall. Geologists at Akanani have described the P4 unit as a fine to medium-grained melanorite that grades to feldspathic pyroxenite lacking any significant sulphide mineralization. Clearly from the contrasting definitions of the melanorite and feldspathic pyroxenite, the classification of P3 and P4 has proven to be challenging especially where they are both present. For the first time, this study produces geochemical and mineralogical evidence for the distinction between the P3 unit and P4 unit. The misconception that the C-reef is in fact a melanorite that has graded from a feldspathic pyroxenite is vague and misleading. Observations from this study have revealed that where the P4 is present it directly overlies the P3 and can only be distinguished because it contains cumulus plagioclase (50%) and orthopyroxene (35%) modal %,

while clinopyroxene is the least dominant cumulus mineral with 15%. The feldspathic pyroxenite is in turn coarse-grained and pegmatoidal in place (Plate 4.2) and in places pegmatoidal enriched with higher concentrations of Na_2O, Al_2O_3, SiO_2 and K_2O. The geochemical composition of the uppermost Platreef which here is referred to as P3 unit is consistent with the results of Roelofse et al. (2009) (Table 4.2). Roelofse et al. (2009) suggested the possibility that Main Zone magma may have partially molten the underlying Platreef footwall, which can further explain the hypothesis that the P4 unit occurred as a result of the interaction between the P3 unit and the overlying Main Zone. The albite composition in P3 (31.34 in core – 34.93 in rim; Table 3.39) is higher than it is in P4 (22.30 in core – 21.14 in rim; Table 3.39), while the anorthite content increases in P4 (76.42 in core – 78.03 in rim; Table 3.39) relative to P3 (67.32 in core – 63.77 in rim; Table 3.39). This increased anorthite composition and inclusions of plagioclase on orthopyroxene grains in P4 suggests some degree of contamination by Main Zone rocks that are rich in CaO relative to Na_2O. This is also evident from the increased CaO compositions in P4 unit (14.88 in core -15.5 in rim) relative to P3 unit (13.3 in core -12.42 in rim). Since the Main Zone rocks are usually depleted in MgO and Fe_2O_3, the high MgO (0.04 in core) and FeO (0.23 in core) contents of plagioclase should have been derived from the underlying feldspathic pyroxenite during partial melting of the uppermost Platreef pyroxenite by intruding Main Zone magma. These observations coupled with the greenish color of biotite which implies that these biotites are Fe-rich suggests some pyroxenite influence as the Main Zone rocks are depleted in Fe_2O_3.

Table 4.3: Comparison between the chemical compositions of the Uppermost Platreef in contact with Main Zone (Roelofse et al. 2009) and the uppermost Platreef P3 unit.

Element	P3 unit	Uppermost Platreef Pyroxenite
SiO_2	47.95	49.86
Al_2O_3	7.92	8.34
FeO	12.7	9.9
MnO	0.23	0.19
MgO	18.08	18.08
CaO	6.61	6.31
Na_2O	1.02	0.5
TiO_2	0.23	0.12

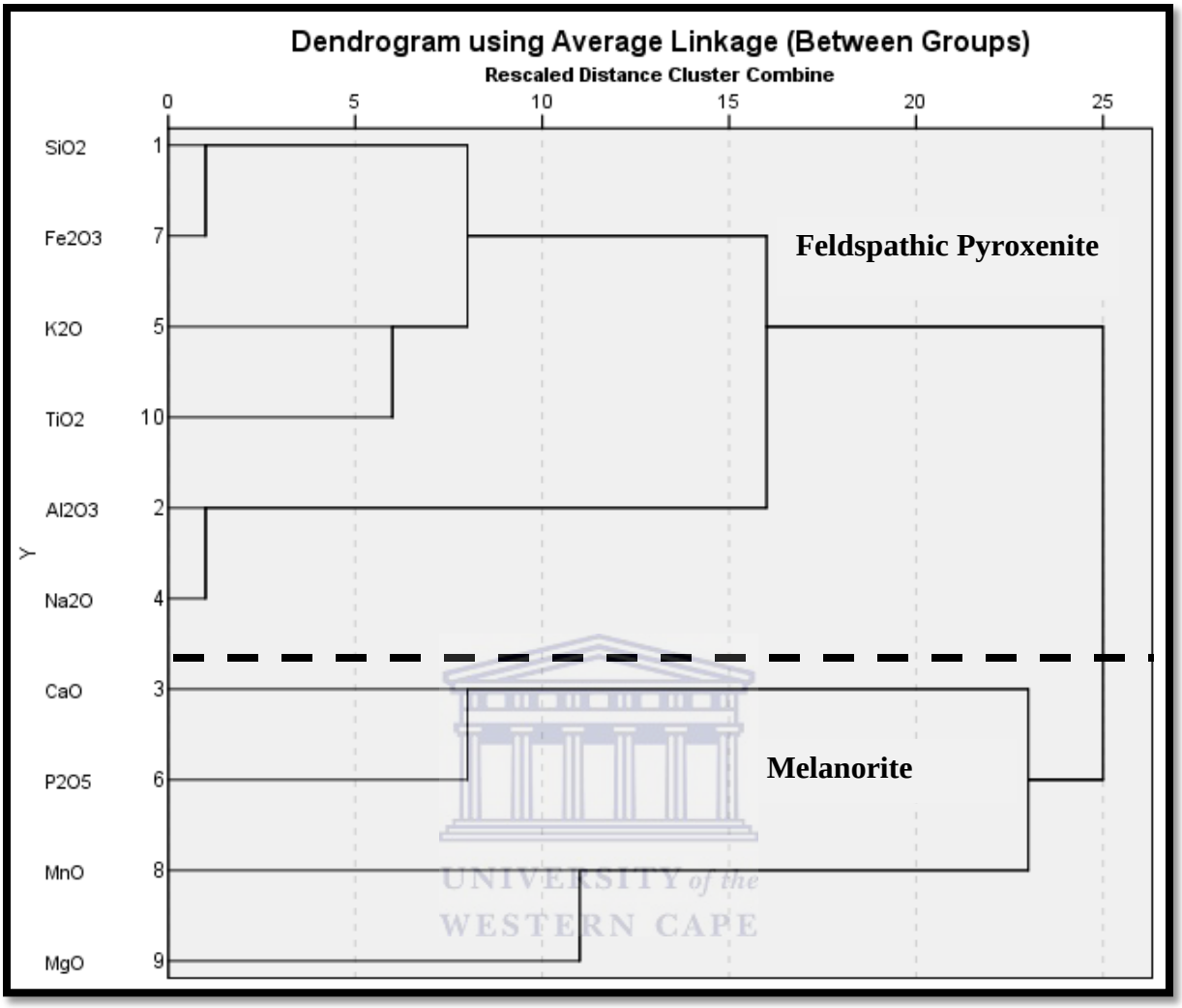

Figure 4.3: Figure: Dendogram using Average Linkage Method showing the geochemical differences between P3 and P4 units.

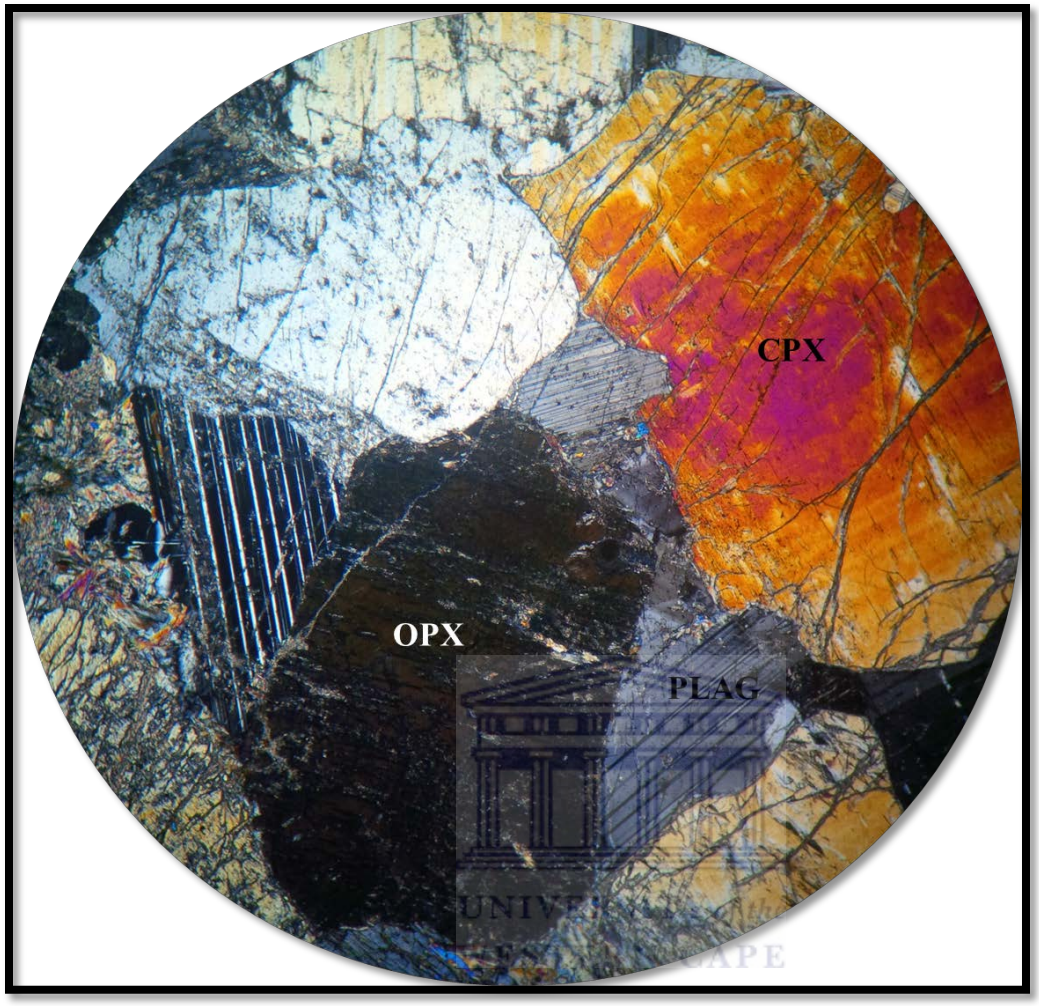

Plate 4.2: P3 Pegmatoidal feldspathic pyroxenite from borehole ZF048 sample 46 at a depth of 1524.58m.

The melanorite exhibits textural, mineralogical and geochemical affinity with the feldspathic pyroxenites and hangingwall gabbronorites of the Main Zone. For this reason it cannot be interpreted as a barren component of the Platreef sequence that was partially removed by erosion during influx of Main Zone magma as first suggested by Yudovskaya and Kinnaird (2010), but rather a representation of a later sill or late-stage residual melt or a hybrid melt of assimilated Platreef that interacted with intruding Main Zone magma as first suggested by Holwell and Jordaan (2006). The An# content (84.48) of P4 unit plagioclase in core can be attributed to contamination by Ca-rich hangingwall rocks. The conclusion that the hangingwall gabbronorites formed together with the Platreef without any significant geochemical hiatus in time and that the

magma above the Platreef contributed some of the PGEs to the reef is misleading. Infact this may not be true at Akanani as PGE and BMS mineralization are absent within the basal zones of the hangingwall and the P3 unit directly below the melanorites and this may suggest that PGE and S were not assimilated from the reef by intruding magma and that another source of and mechanism for concentration of BMS in P4 must be considered. Holwell et al. (2005) explain this as a process whereby the barren fine-grained unit which is described here as a melanorite was present continuously after the Platreef was intruded and that the Platreef-hangingwall contact is a representation of a planar contact surface which has cut down through the uppermost P3 unit and in places cut into the mineralized P2 unit, assimilating some PGEs and enough sulphur to attain sulphur saturation, further producing very localized basal zones of orthomagmatic PGE mineralization.

4.1.1.4 Summary of the stratigraphy at the Akanani prospect area

The following summary of the stratigraphic units from bottom to top at the Akanani prospect area is based on the Authors' observations and builds upon the work done by exploration geologists at Akanani; Van der Merwe (2012); Mitchell and Scoon (2012). The geochemical and mineralogical classification of the Platreef sequence at Akanani is aimed at correcting the fundamental misconception that the Platreef can be classified as A, B, C reef or PU1, PU2, PU3 in that order of succession. In order to overcome this perception the overall sequence of rocks was grouped into four layers (P1, P2, P3 and P4 unit), which were classified geochemically and petrographically to reveal the distinctive geochemical and mineralogical characteristics that can be used to identify each unit.

P1 unit is the lowermost pyroxenite of the Platreef at Akanani and is characteristically medium to fine-grained, ranging in thickness from 19 to 187m. Ocassionally granitic and granofels xenoliths are observed. Generally the lowermost Platreef unit (P1) is a high grade zone with relatively high PGE tenor and characterized by generally high Cr, TiO_2 and Fe_2O_3. Four major rock types make up this unit that is chrome-rich feldspathic pyroxenite; feldspathic pyroxenite; pyroxenite and chromitite. In places, clinopyroxenites are also present comprising predominantly metamorphic clinopyroxene (>80%).

The P2 unit overlies the P1 unit and exhibits poikilitic and cumulus texture, containing medium to coarse-grained subhedral to anhedral olivine and pyroxene crystals with plagioclase occurring interstitially between olivine and pyroxene grains. It ranges in thickness from 3.7 to 77m. This ultramafic zone is usually variably altered to varying degrees of serpentinization and is geochemically characterized by higher MgO and LOI contents. Three major rock types have been identified namely: harzburgite; feldspathic harzburgite; olivine-rich pyroxenite; orthopyroxenites and olivine-bearing orthopyroxenite. In general, the P2 rocks are usually Mg-rich and serpentinized to varying degrees.

P3 unit is characterized by high contents of Al_2O_3, Na_2O, K_2O and SiO_2 which corroborates with the feldspathic nature of this unit. This unit ranges in thickness from 1 to 60m consisting principally of medium to coarse-grained pegmatoidal feldspathic pyroxenite and in places chrome-rich feldspathic pyroxenite although this was not observed for this unit through petrographic analysis. The lack of sulphide mineralization is typical of the P3 unit, sericitization is present but not dominant and not associated with the mineralization.

P4 unit is often confused with P3 however the two are distinguishable from one another as the feldspathic pyroxenite in P3 contains interstitial plagioclase that is more albitic in composition, while the melanorite classifying P4 contains cumulus plagioclase that is more anorthitic in composition. P4 is not always present; however were present it is significantly characterized by high CaO and P_2O_5 which corroborates with increased 'anorthitic' composition associated with this unit. A summary of the suggested stratigraphic subdivision at Akanani is given in Figure 4.4 below, while Table 4.4 is a simplified summary of the expected mineralogy with stratigraphic height. The sequence of occurrence of certain rock types at Akanani contradicts the findings of previous researchers however provides an evidence based description of the Platreef at the Akanani prospect area.

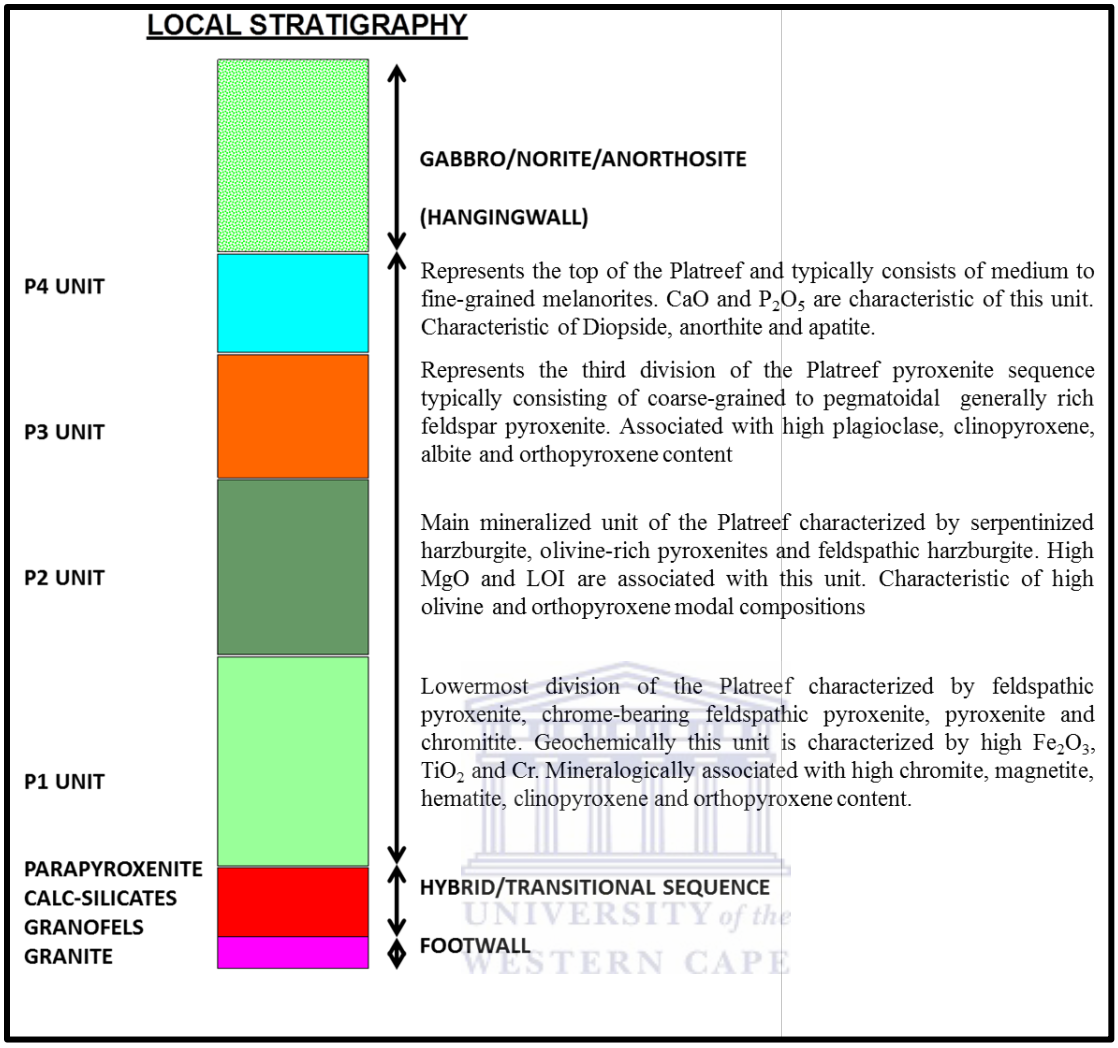

Figure 4.4: Simplified stratigraphic sequence at the Akanani prospect area.

Table 4.4: Expected composition of pyroxene (MgO + Fe_2O_3) and plagioclase (Al_2O_3) with stratigraphic height at the Akanani prospect area.

Platreef Subdivision	**MgO + Fe_2O_3 wt%**	**Al_2O_3 wt%**
P1	35- 45	2-5
P2	40- 55	<5
P3	30- 35	5 - 9
P4	20- 30	8 - 16

4.1.2 Evidence for open system fractionation at Akanani

The Platreef is a PGE-Ni-Cu bearing mafic to ultramafic package occurring in the Northern limb of the Bushveld Complex (Kinnaird, 2005). It is characterized by hangingwall of gabbro-norite, while the footwall comprises Transvaal Supergroup meta-sedimentary rocks in the south and Archaean granite gneiss in the north (Kinnaird, 2005). The Platreef has posed several puzzles to researchers one of which is the question of whether a single or multiple magma events were responsible for its formation. Although at a first glance it may seem that the Platreef at Akanani formed as a result of gravitational settling, it is however clear that no single process is responsible for the formation of the Platreef at Akanani. Over the years, it has been realized that gravitational settling cannot account for the fact that low density minerals like plagioclase where crystallized on the floor, whereas high density Fe-enriched minerals like olivine settle at the top. Mason-Apps (1998) concluded that although insitu crystallization is a dominant process, gravitational settling may still be an important factor in the formation of igneous layering. In the case of the Platreef at Akanani it is difficult to say that gravitational settling was the only process as it cannot account for the enrichment of magmatic olivine in P2 and the abundance of low density plagioclase in some P1 samples. Plagioclase is rarely the first mineral to crystallize from primitive basaltic magma, and therefore the plagioclase present in P1 unit may have accumulated as a result of assimilation hence its appearance as an intercumulus mineral.

Worst (1960) and Bichan (1969) suggested that olivine and chromite crystallized simultaneously from the magma and formed a basal layer to the cyclic units on account of its higher density subject to the process of gravitational settling. Since it is highly unlikely that plagioclase phenocrysts accumulated by gravity settling due to their small density contrasts with the parental liquid, it is therefore safe to conclude some degree of assimilation of country rock material. Marsh (2006) has questioned models that suggest that differentiated sills are constructed by fractionation of a single pulse of phenocrysts-free-magma by suggesting that stratigraphic variations in sills are caused by multiphase pulses of magma and settling or flow segregation of phenocrysts. Cox et al. (1993) noted that any reversals of a fractionation trend suggests a rise in the temperature of the magma which can be best explained as the indication of influx of new, hotter material or opening of a system. In the case of the Platreef, Kinnaird (2005) provided evidence for multiphase emplacement from boreholes drilled at Turfspruit, southern sector of the Platreef. This evidence suggested that an upward increase in Pt/Pd and Ni/Cu ratio with

stratigraphic height was not a simple fractionating trend from the bottom of the Platreef to the top otherwise the top most pyroxenite will be the most evolved, which is not the case as it contains higher Cr content (Kinnaird, 2005). On the basis of these results Kinnaird (2005) concluded that the Platreef is a complex zone of sill interfingered lithologies reflecting a multiphase emplacement. On the basis of field observations Mitchell and Scoon (2012) suggested that the PU1 formed from repeated additions of gabbroic magma and *in situ* differentiation; PU2 formed from injections of ultramafic magma, while PU3 developed from partial melting and recrystallization of the PU1 and Main Zone in response to intrusion of ultramafic magmas. There are two contrasting schools of opinions about the formation of the Platreef (i) one that favours multiphase emplacement without replenishment (Kinnaird, 2005) (ii) and one that favours multiphase, non-sequential magma replenishment (Mitchell and Scoon, 2012). These two schools of thought will be analysed on the basis of the petrographic and geochemical results obtained from this study and a model detailing the formation of the Platreef at Akanani will be developed.

4.1.2.1 Multiphase magma emplacement vs Multiple, non-sequential magma replenishment hypothesis

Processes such as assimilation, convection and gravitational settling are discussed as it is evident from the geochemical and mineralogical results that they played a major role either in the concentration of mineralization or the composition and formation of the overlying Platreef lithologies. The effects of assimilation are only briefly treated in this study. Relying upon the limited whole-rock geochemical data, petrographic observations and mineral chemistry data, one can conclude that assimilation has played a minor role and is much on a localised scale. The most difficult part of the comparison between the model proposed by Mitchell and Scoon (2012) and the one proposed in this study is the differing sequence of lithologies. Where applicable a comparison is derived.

The Platreef at Akanani is an open system that has been affected by assimilation and periodic injection of new magma. The first line of evidence is based on the processes of crystal settling, convection and assimilation in the P1 unit. The process of gravitational settling can be best explained by the enrichment of Fe, Cr and Ti in P1. It is envisaged that the earliest intrusive pulse that contributed to the Platreef formation allowed for heavy element oxides Fe, Cr and Ti

to settle at the bottom of the chamber during emplacement. At the Baima Intrusion, Zhang et al. (2013) suggested that the extreme enrichment of Fe and Ti at the base of the intrusion is related to multi-phases of magma recharge together with gravitational sorting and settling. Furthermore the unit's reaction with granite floor is evidenced by the occurrence of granofels between the granite floor and the overlying pyroxenite and enrichment of Na and Al in the lowermost pyroxenite relative to P2. Tanner et al. (2014) attributed the exponential increase in compatible elements in plagioclase within the lower most lithology of the Bellevue drill core to assimilation of felsic or metasedimentary units into fractionating mafic magma as evidenced by the occurrence of metasedimentary xenoliths. Kekana (2014) referred to the granofels at Overysel as agmatite comprising pyroxenite, amphibolite, and granite gneiss fragments within a granitic matrix that developed from the interaction between Platreef and footwall. Kinnaird (2005) noted that at Turfspruit where the floor rocks are hornfelsed shales, a significant interaction between invading pulses of magma that formed the lower two pyroxenites resulted in inhomogeneous textures, variability in composition and migration of sulphide from shale to magma. At Akanani, an indication of crustal contamination is provided by the Al_2O_3/MgO ratio because granites have higher Al over MgO and an increase in this ratio in the basal pyroxenite indicates some form of interaction with the floor although this interaction may be localised. It remains unclear how much of these ratios are changed by alteration effects or to what degree assimilation was involved. According to Spera and Bohrson (2001) the important factor that controlled the extent of magmatic contamination by country rock is not a simple function of boundary temperature, but is dependent upon the initial temperature of the country rocks, melt productivity functions and thermodynamic parameters such as heat capacity and phase charge enthalpies of relevant materials. Unpublished study by Siad et al. (2011) revealed that interaction of pyroxenite with granite floor could have brought about the elevated Al, Na and Si in both clino- and orthopyroxene and thus indicated a greater degree of floor rock contamination. The enrichment of Na further reflects increasingly sodic nature of plagioclase in pyroxenites overlying granitic floor rocks (Cawthorn et al., 1985; Harris and Chaumba, 2001), while Barton et al. (1986) attributed this to contamination by granitic country rocks. At Sandsloot it is possible that the CO_2 produced by decarbonation of assimilated dolomite enhanced the process of PGE scavenging by sulphide precipitation (Pronost et al., 2008). At Akanani assimilation of volatiles such as H_2O and CO_2 by granite floor is improbable and thus the enhanced PGE signatures in P1 and P2

cannot be due to floor rock interaction but another process. Barton et al. (1986) suggested that the Platreef at Overysel was contaminated by partial melts of the footwall granite that interacted with the lowermost pyroxenite. This could account for the relatively high concentration of felsic elements (Na, Al and K) in the lowermost pyroxenite at Akanani where the floor rock is granitic. Contamination of the magma could have occurred through partial assimilation of the country rock as the country rock would have been partially melted to produce a liquid that could mix with the magma.

Kinnaird (2005) used the CaO/Al_2O_3 as an indication of assimilation of calc-silicate by feldspathic pyroxenite which was relatively 0.6 suggesting little contamination by dolomites. There also seem to be little influence by the floor at Akanani as the Al_2O_3/MgO is relatively low, averaging about 0.4. Mitchell and Scoon (2012) noted that at Akanani interaction of the magmas with floor rocks was less intense, resulting in a lower frequency of xenoliths and a more predictable stratigraphy. This is consistent with the account given by Pronost et al. (2008) that contamination by floor is intense at Sandsloot than anywhere else in the Platreef. Platreef in contact with dolomite floor is the focus of higher PGE grades which in turn suggests that calc-silicate floor rock interaction with Platreef played a significant role in PGE deposition and concentration (Pronost et al., 2008). Although it may seem probable that dolomite interaction with Platreef was responsible for PGE concentration, Pronost et al. (2008) noted that contamination was not the primary mechanism of S saturation and PGE concentration, but rather aided in the enhancement of the processes of sulphur saturation and PGE mineralization.

On the basis of the results from this study and results from other areas in the Platreef (i.e Overysel and Sandsloot), it is easier to conclude that the Platreef at Akanani was subjected to low degrees of floor rock interaction due to the lower values of $\delta^{18}O$ value of granites estimated by Pronost et al. (2008) to be around 8-9% and that floor rock interaction did not play a significant role in PGE concentration. Furthermore the localised scale of assimilation may also be due to the fact that mafic magmas originate within the upper mantle and immediately move upwards to their final emplacement levels; therefore there may not be enough time to assimilate wall-rock (Soesoo, 2000). After the emplacement of a body of P1 magma, there was an episode of initial chilling of the magma against the country rocks, followed by the establishment of a system of convection currents and then gradually a zone of major crystallization develops on or

near the floor of the magma chamber. The significant break in the Cr/MgO ratio in P2 unit is not consistent with a single magma emplacement and can be interpreted as signifying the influx of new magma. Trace elements normalized to chrondrite and primitive mantle abundances show variable enrichment and depletion patterns for both the mafic (P1 unit) and ultramafic (P2 unit) rocks. Mafic and ultramafic rocks do not retain a similar trace element signature. For example there is enrichment of LILE (Rb, Ba and K) in P1 relative to P2 unit, reflecting a non-genetic relationship among them.

It is envisaged that the second intrusive event involved injection of new ultramafic magma, which highlights the beginning of a normal fractionation trend which continues to P3. Evidence for this hypothesis is based on major and trace element ratios and mineralogy. The magnesian nature of the P2 unit ultramafic magma demonstrated by the strongly magnesian composition of silicate rocks of this study can be attributed to the forsteritic compositions of olivine that range from Fo_{67-74} and orthopyroxene compositions of En_{55-82}. Chromite compositions are exceptionally Mg-rich especially in P3 unit and this is partly a reflection of parental magma compositions. Masson-Apps (1998) noted that post cumulus processes in the presence of an Mg-rich reactant are important in achieving the observed high magnesian compositions in olivine and orthopyroxene. This is supported by the increased MgO compositions of orthopyroxene from core (28.69 wt.%) to rim (29.59 wt.%) in P2, while in P3 orthopyroxene compositions increase from 27.81 wt.% in core to 29.03 wt.% in rim. Orthopyroxene trends at Akanani have shown to display a shift from less evolved at the base P1 unit and a gradual increase in P2 unit which maybe a representative of periods of magma influx. Orthopyroxene compositions in the P2 unit display an overall progression to more evolved compositions and can be interpreted as indication of fractionation of the primary magma source; resulting in successively more evolved magma injections (Wilson, 1982; Wilson and Prendergast, 1988).

The occurrence of magmatic olivine, orthopyroxene and minor plagioclase may mark the beginning of a normal fractionation trend from P2 to P3. Olivine, magnetite and Cr-spinel were the first early crystallizing igneous minerals. The lack of a clear Eu anomaly in the analysed P2 ultramafic rocks reflects that plagioclase played a less significant role in the partitioning of the REE between magma and cumulates assemblages. The orthopyroxene, which in turn becomes the most abundant ferromagnesian mineral, takes the role of olivine in controlling differentiation

trends of increasing SiO_2 with decreasing MgO as observed from P2 to P3 unit (Otamendi et al., 2010). Incompatible elements (Na_2O, Al_2O_3, SiO_2, K_2O and TiO_2) increase with decreasing MgO. An increase in TiO_2 may be consistent with ilmenite crystallization; however no ilmenite was encountered from the petrographic observations for the P3 unit.

Many researchers have cast doubt on the timing of the onset of magnetite crystallization with Jang et al., (2001) suggesting that the vanadium content of an evolving magma is inversely proportional to the fractionation of the oxide minerals, particularly magnetite. Therefore the onset of magnetite crystallization should be marked by a sudden decrease in V content of the evolving magma (Farla, 2004). At Akanani the V content decreases significantly in P2 until P3, marking P2 as the onset of magnetite crystallization. This in turn implies that the P2 magma had higher oxygen fugacities (Farla, 2004). Farla (2004) pointed out that higher oxygen fugacities implied the early onset of magnetite crystallization. Ferrous iron compositions of 22.09 wt% - 22.25 wt% in magmatic olivines could have reacted with oxygen of infiltrating hydrothermal fluids to form the magnetite. The decrease in V does not only mark the onset of magnetite crystallization but also the possible abundance of Ti-magnetite in P2 unit although this was not observed during petrographic analysis. There is a sharp decrease in Ti/Zr and V/Zr ratio from P1 to P2, while a significant increase is observable from P2 to P3. The increase of Ti/Zr and V/Zr from P2 to P3 could be interpreted as due to gravitative accumulation of titaniferous and vanadiferous magnetite on the magma chamber. Magnetite could have crystallized as the visible oxidation state as the magma increased from relatively reduced to oxidized. Magma then cooled and crystallized, the relative Fe^{3+} concentration increased steadily due to pyroxene removal until the magma reached the magnetite stability field. At this point, magnetite crystallized. Because magnetite is a high density mineral it then gravitationally settled out of the magma. Ti and V enrichment trends may be interpreted as resulting from magnetite fractionation and gravitational settling. Petrographic observations prove that plagioclase crystallized later after olivine and most likely after clinopyroxene. The fine-grained plagioclase crystals in P2 feldspathic harzburgite can be interpreted as unable to undergo gravitational settling probably because it was not sufficiently denser than the melt. Instead the fine-grained plagioclase crystals grew insitu on the floor of P2 unit. This plagioclase was interstitial to the olivine and pyroxene grains and probably grew under equilibrium conditions from a magma that exhibited relatively open-system conditions where CaO, Na_2O, Al_2O_3 and SiO_2 were continuously replenished due to convection. The fine-grained

texture of the plagioclase suggests that the plagioclase underwent slower growth than pyroxene. During the initial stages of crystallization, temperatures were just below the liquidus consisting of olivine crystals plus liquid. These olivines were depleted of Si and virtually free of Ca and Al (as observed from the micro-probe analysis) which are both major constituents of the liquid. In P2 Zr behaved incompatibly and was concentrated in the melt during fractionation, hence its low concentration during the initial stages of fractional crystallization. Ni which decreases significantly in P3 could have partitioned into olivine during the early stages of fractional crystallization, while decreasing in concentration with increasing fractionation. The appearance and disappearance of minerals in the stratigraphic section may reflect the normal evolution of silicate magma (Zientek, 2012). For example, cumulus olivine and chromite will appear during the early stages of crystallization in P2, whereas titanium-oxide minerals and apatite appear in P3 which is consistent with enrichment of TiO_2 and P_2O_5 (as observed from the geochemical data) with increasing fractionation. The normal crystallization trend from P2 to P3 is consistent with the sequence **olivine-Cr-orthopyroxene-plagioclase-clinopyroxene** corroborating with petrographic observations. Although chromite has been interpreted here as an early magmatic mineral, its enrichment in the P3 unit could possibly be related to infiltration of Cr-enriched fluids or hydrous melts (Edwards et al., 2000; Matveev and Ballhaus, 2002). A positive Eu/Eu^* anomaly which ranges from 0.84-1.35 supports the petrographic evidence that the P3 rocks are rich in plagioclase. The increase in Cr_2O_3 of orthopyroxene from 0.32 to 0.60 wt.% in P3 suggests a more differentiated trend of more primitive rocks towards the top of the succession. Manyeruke et al. (2005) noted that orthopyroxenes at Townlands showed an increase in Cr_2O_3 (0.07-0.37 wt.%) with stratigraphic height revealing a reversed differentiation trend of more primitive rocks at the top. On the farm Turfspruit, Kinnaird (2005) suggested multiphase emplacement of the Platreef by arguing that higher Cr content towards the top is not consistent with a simple fractionating sequence.

If the trend was a normal fractionation trend from P1 to P4 then the SiO_2 should remain relatively unchanged during the initial stages of crystallization which is not the case at Akanani. The Sr/Ba ratio was significant as an indicator for fractional crystallization as Sr and Ba are incompatible elements in all of the major mafic minerals and compatible in plagioclase (Stevens, 2007). From P1 to P2, there seem to be a sudden break with a decrease in the Sr/Ba ratio in P2 which represents influx of new magma or a geochemical hiatus (Eales et al., 1986). The pattern

remains relatively flat from P2 to P3 signifying a normal fractionation trend, while another significant break is observable in P4 suggesting an influx of new magma or geochemical hiatus (Eales et al., 1986). These findings are further supported by the Mg# which is a significant indicator for fractional crystallization (Rollinson, 1993). From P1 to P2 there appears to be an increase in the Mg#, while from P2 to P3 a decreasing trend is observable (Fig. 4.5b). During the early stages of fractional crystallization the Mg# changes due to the high Mg-Fe ratio of the liquidus of ferromagnesian minerals (e.g. abundance of olivine and orthopyroxene in P2) compared to host melt (Rollinson, 1993). Thus with continued fractionation the Mg# will decrease a trend observed in P3 consistent with the appearance of plagioclase (Fig. 4.5a). Although the variation in Mg# number can also be affected by the presence of clinopyroxene, olivine and plagioclase; nevertheless significant trends are observed and are consistent with mineralogical results.

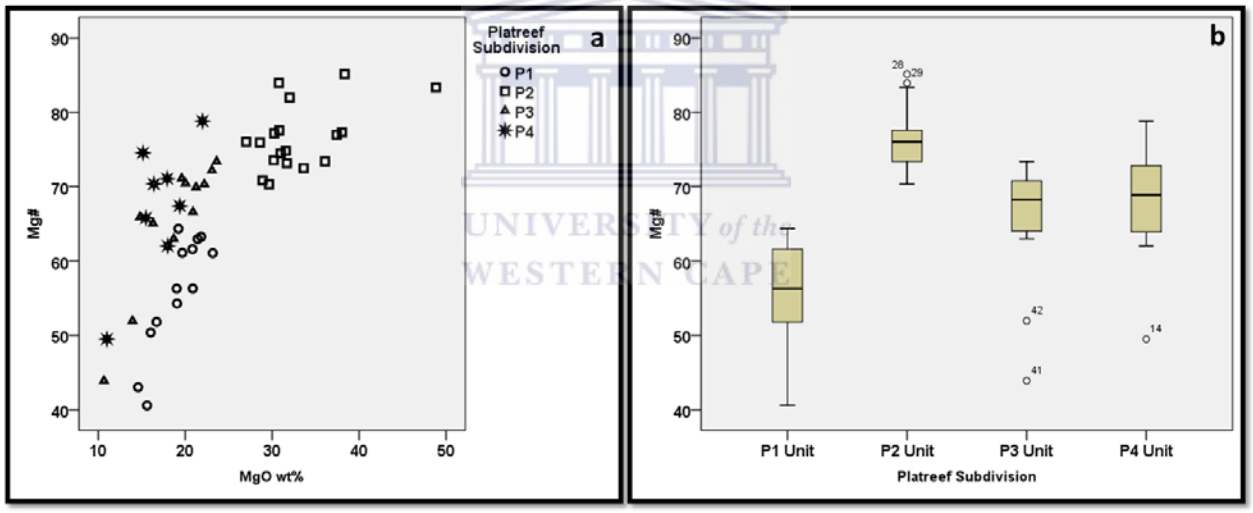

Figure 4.5: (a) Plot of whole-rock Mg# vs MgO showing low Mg# values with lower MgO consistent with appearance of plagioclase. (b) Mg# vs lithological units P1, P2, P3 and P4 of the Platreef at Akanani.

Orthopyroxene trends at Akanani have shown to display a shift from the less evolved at the base of the P1 unit and a gradual increase in P2 unit which may be a representation of periods of magma influx. Orthopyroxene compositions in the P2 unit display an overall progression to more evolved compositions as shown in Table 3.36 and can be interpreted as indication of fractionation of the primary magma source; resulting in successively more evolved magma

injections (Wilson, 1982; Wilson and Prendergast, 1988). Tanner et al. (2014) used Cr content of pyroxene to interprete three cryptic replenishment events as evidence for influxes of more primitive magma. According to Cawthorn (2007) any sudden increase in Cr concentration of pyroxene is considered the unequivocal signature of fresh magma pulses. The sudden increase in Cr concentration from P1 to P2 could suggest an influx of primitive ultramafic magma in P2 unit. The concept of replenishment of the magma chamber by periodic injection of fresh primary magma that is compositionally primitive relative to the evolved residual magma has also been suggested in the Platreef (Mitchell and Scoon, 2012) and the Bushveld Complex at large by a number of authors (Von Gruenewaldt, 1973; Molyneux, 1974; Eales et al., 1988; Scoon and Mitchell, 2012). Von Gruenewaldt (1973) and Molyneux (1974) first identified the lithological and chemical break associated with the pyroxenite marker which Klem et al. (1985) interpreted as evidence of replenishment of the chamber. At the Akanani area, Mitchell and Scoon (2012) concluded that the Platreef formed as a result of repeated injection of new magma as well as partial melting and recrystallization of existing cumulates. Tanner et al. (2014) used Cr content of pyroxene to interprete the three cryptic replenishment events as evidence for three influxes of more primitive magma. According to Cawthorn (2007) any sudden increase in Cr concentration is considered the unequivocal signature of fresh magma pulses.

The hypothesis that the PU1 sub-unit at Akanani developed from repeated intrusion of gabbroic magma injected below or partially within the semi-or wholly-crystalline lowermost part of the Main Zone does not hold true. Stevens (2007) equated the fine-grained norites and gabbro-norites at the floor of Sheba Ridge stratigraphy to the Marginal zone elsewhere in the Eastern and Western limbs. Kinnaird (2005) suggested that the earliest intrusive pulse that contributed to the Platreef package was a grey micronoritic layer, equated with the Marginal Zone of the eastern and western limbs of the Bushveld Complex. According to Kinnaird (2005) the fact that they (gabbronorites) are consistently fine-grained implies that they were intruded into the country rocks and rapidly cooled. On the basis of geochemical and petrographic observations it is suggested that the P1 unit may have formed as a first intrusive pulse chilled against the floor and wall rocks and then with further inflow reacted with and remobilised parts of the footwall, hence the occurrence of granofels xenoliths. Mitchell and Scoon (2012) suggested that the PU2 sub-unit formed from injections of ultramafic magma into the partially crystalline substrate, the latter being comprised of the PU1 sub-unit and the lowermost part of the Main Zone. In many

ways the results of this study for this respective unit are similar to those of Mitchell and Scoon (2012) in that the P2 unit is described as being ultramafic formed from a completely different magma. This ultramafic magma was injected into the pre-existing P1 unit. The steep REE pattern for P2 samples suggests that these rocks are from a different intrusive event relative to the flat pattern for P1 unit. According to Mitchell and Scoon (2012), the PU3 sub-unit formed from partial melting, recrystallization, annealing, and metasomatism of the gabbronorite-websterite in response to intrusion of U-type magmas from which the PU2 lithologies crystallized. This may be true as REE patterns for P3 samples show affinity to both P1 and P2 samples in that the P3 pattern is flat, however follow the same pattern observed in P2 (lower concentrations of MREE). Enrichment of alkali elements (Al_2O_3, Na_2O, K_2O) in P3 which are somewhat incompatible during the initial stages of crystallization can suggest assimilation of these elements during partial melting and recrystallization of P1 and P2.

If it is agreed that the processes of annealing, recrystallization, partial melting and metasomatism resulted in the formation of the PU3 unit, double diffusive convection (Irvine, 1980) could cause thermal and chemical exchange between the liquids and lead to the development of intermediate liquids (Wiebe and Wild, 1983). There is however no direct evidence of significant chemical exchange between the feldspathic P3 unit and ultramafic P2 magma.

Because this study does not consider gabbro-norite as a major lithology characterizing P1 it is suggested that if P3 formed from partial melting between P1 and P2 then the resulting lithology in this case would be a feldspathic pyroxenite. This model has three major consequences. Firstly it suggests the occurrence of gabbro-norites in P1 unit as a major lithology which is not in line with the findings of this study. Secondly it does not take into account the role of assimilation on composition of the overlying lowermost pyroxenites. Thirdly it does not take into account a fourth layer (P4 unit) that was encountered in this study, which is interpreted as resulting from the interaction or partial melting and recrystallization of the feldspathic pyroxenite and the Main Zone. It is however important to note that the P4 unit encountered in this study is not always present. Although the model proposed by Mitchell and Scoon (2012) is a possibility, there is not much evidence from this study to support it. Thus this hypothesis is neither accepted nor rejected, but further analysis of boreholes would give more insights.

4.1.2.2 Proposed model for the formation of the succession at Akanani

Combining the petrographic and geochemical data, it appears that the Platreef at Akanani formed from periodic injections of new magma. Combined with petrographic observations, geochemical data provides definitive evidence for the occurrence of open system processes in magma bodies, including replenishment by intrusion of primitive magma, assimilation of wallrock melt and cumulate formation by fractional crystallization (Spera et al., 2001).

The macro-rhythmic layering of the Platreef sequence at Akanani is considered to have been an open-system of primary magma injection and slow mixing with resident magma, followed by periods of normal fractionation that is terminated by new magma input or a geochemical hiatus. All these processes played a significant role in the emplacement of the Platreef at Akanani. The multiphase emplacement model is preferred to explain the sequence of emplacement at Akanani. Although not exactly similar to the model suggested by Kinnaird (2005) it does however prove that the Platreef at Akanani formed as a result of periodic injection of new magma. Three significant phases of events have been recognised thus far (1) one that resulted in the formation of P1 (2) one that resulted in the formation of P2 and P3 (3) one that resulted from the interaction between P3 and the Main Zone.

The initial intrusion of the Platreef magma heated footwall granites and induced partial melting along grain boundaries. The interconnectivity of the liquid resulting from the induced partial melting may have allowed for the formation of a sufficiently permeable network to allow the downward percolation of a much denser sulphide liquid through the footwall, with some felsic melt correspondingly displaced upwards to account for the felsic assimilated material at the base of the Platreef (After Holwell and McDonald, 2006). To induce partial melting of the granite floor, the intruding Platreef magma could have been hotter than the surrounding country rocks, heating them to temperatures over 800°C (Holwell and McDonald, 2006). However, for the observed melt network to be present, temperatures must have remained above 800°C throughout a sufficient volume of rock away from the igneous contact as first suggested by Holwell and McDonald (2006) at Overysel where the footwall is gneissic.

At Overysel where the floor rock is granitic gneiss, interaction of Platreef magma and footwall rocks introduced REE and SiO_2 into the basal Platreef pyroxenites (Ihlenfeld and Keays, 2011). Petrographic observations imply that the Platreef assimilated SiO_2 into the basal Platreef

pyroxenite as evidenced by the occurrence of quartz inclusions and in some places orthoclase. This magma can be equated with Lower Critical Zone magma (Kinnaird, 2005). Convection exchange played an equally important role in the formation of the Platreef. This process was mainly driven by differences between compositional densities of the main magma and interstitial liquids. During this process of convective exchange the iron-rich liquids of the main stages of differentiation tended to migrate downwards while the buoyant late-stage liquids rich in incompatible elements (Rb, Sr, Ba, U, Th) infiltrated upwards. This resulted in the enrichment of iron at the floor with simultaneous depletion of incompatible elements. The convection currents also played a significant role by supplying heat that was responsible for the local assimilation of country rocks particularly at the contacts. This is evident by the occurrence of hybrids and xenoliths of granofels at the contact between the lowermost pyroxenite and the footwall granites. Bowen (1928) stated that it was doubtful whether the presence of foreign material underlined the effects of assimilation, however highlited that it is important to acknowledge that assimilation is often required to account for the rocks found near igneous contacts. The formation of monomineralic chromitite layers comprising upto 90% of the single mineral phase chromite would require that the normal crystallization of silicate minerals (dominated by olivines, pyroxenes and plagioclase) be 'switched off' and replaced by a brief period where only the single oxide phase is on the liquidus (Robb, 2004). The crystal fractionation model (Toplis and Carroll, 1996; Cawthorn and Molyneux, 1986; Tollari et al., 2008a, Tollari et al., 2008b; Naldrett et al., 2009a, Naldrett et al., 2009b) requires that after the oxides crystallize, they are preferentially accumulated on the chamber floor because the cotectic porportions of oxides and silicates are ~1 % for chromite (Barnes, 1998b) and in the 5–30 % range for magnetite (Toplis and Carroll 1996).

In order to constrain the formation of the observed chromitite layers in P1 this study employed the model of Irvine (1975) for chromitite layers formation (Fig. 4.7). At point E the magma becomes contaminated with siliceous material by assimilation of crustal material forming the floor in this case the granitic floor at Akanani. The contaminated magmas would therefore have a composition that lies somewhere along the mixing line joining **E** to the SiO_2 apex of the ternary diagram. This composition would also lie transiently in the chromite field and result in the formation of a monomineralic cumulate layer of chromite between **H** and **G**. Due to its relatively high density, chromite would settle fairly efficiently and a single layer of near monomineralic

chromite would form (Robb, 2004). Once the magma composition reaches point **G** on the cotectic, crystallization will again be dominated by olivine, however in this case crystallization will again be dominated by pyroxene and the rocks that are in the hangingwall of the chromite layer will again contain accessory amounts of chromite (Fig. 4.6).

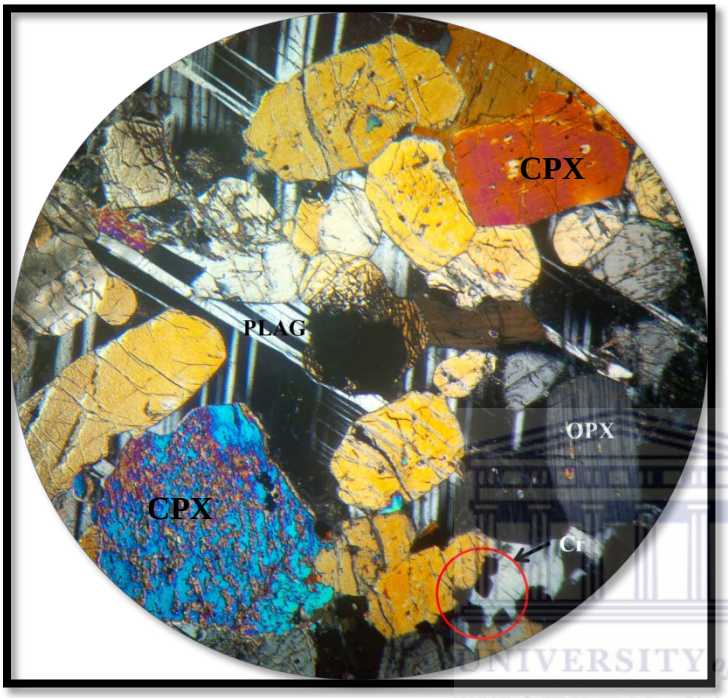

Figure 4.6: P1 Feldspathic pyroxenite with minor accessory chromite from borehole ZF078-47 at depths of 1257.57m just above the chromitite layer occurring at depths of 1264.54m.

O'Driscoll et al. (2010) proposed that addition of a plagioclase component to the intruding magma, for example, by assimilation of plagioclase-rich floor rocks, may trigger Cr–Al spinel saturation, leading to the formation of thin chromitite stringers in the Rum intrusion. This process indicates the importance of contamination of magma to igneous ore-forming processes.

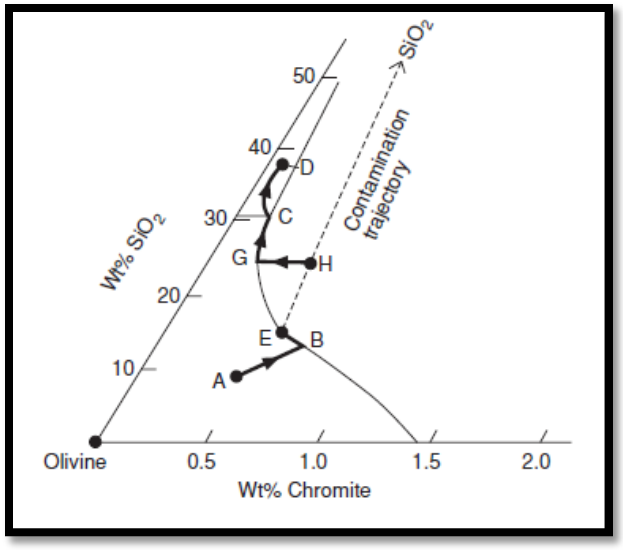

Figure 4.7: Scenario in which magma contamination occur as mechanism for promoting the transient crystallization of only chromite (After Irvine, 1977).

The second intrusive event involved injection of new ultramafic magma, which highlights the beginning of a normal fractionation trend which continues to P3. Mitchell and Scoon (2012) equated the harzburgitic lithologies of P2 to U-type magmas also identified by Sharpe and Irvine (1983) and Ealse (2002) from the Eastern and Western limbs. The sharp increase in Cr_2O_3 and Al compositions of pyroxenes from P1 to P2 suggests influx of fresh magma (Fig. 3.42). When discussing the ultra-mafic zone of the Stillwater complex of Montana, Jackson (1961) proposed that the rocks were produced by variable- depth convection. He further suggested that most of crystallization and crystal settling took place from a stagnant layer at the bottom of the Stillwater magma chamber. Periodically, this stagnant layer heated up, became stable and a convective system operating above it increased in size and swept it aside. Fresh cooler ultramafic magma now formed a new stagnant layer and started a new cycle of crystallization and settling. This analysis explains why there is a transgression from Fe_2O_3-rich layer at the bottom of the Platreef at Akanani to a more ultra-mafic layer in P2 unit. Middlemost (1975) suggested that in any magma that crystallizes from the bottom upwards, the successive layer of mineral cover up, and eventually seal off the underlying layers thus facilitating fractional crystallization. This trend is observable from the P2 unit which marks the onset of fractional crystallization to P3 unit. The occurrence of magmatic olivine and depletion of vanadium content in P2 suggests the onset of crystallization. The sudden increase in SiO_2, Na_2O and K_2O from P2 to P3 suggests a normal

fractionation trend. The abundance of olivine in the overlying P2 unit after a considerable break in oxide-crystallization in P1 unit implies that an injection of a more differentiated magma in P2 cannot be ruled out. The continued increase in Cr_2O_3 and Al contents of pyroxene from P2 unit to P3 unit represents a sympathetic shift in major element or trace element composition of pyroxene and does not imply injection of fresh magma (Eales and Cawthorn, 1996; Cawthorn et al., 1991; Cawthorn, 2007). A negative Eu anomaly coupled with a Eu/Eu^* ratio above one for some samples suggests that the parental magma that gave rise to the feldspathic pyroxenite was fractionating out plagioclase. Mafic magmas have relatively low viscosity with a density of around 2.6 g/cm^{-3}, while the density of mafic minerals is greater than 3 g/cm^{-3}. This low viscosity of mafic magmas and the high density of mafic minerals crystallizing from it suggest that minerals such as olivine and pyroxenes will typically sink in the magma, while less dense minerals such as feldspathoids, might float as they have densities less than 2.5 g/cm^{-3}. The layers that make-up the P2 ultra-mafic sequence at Akanani arise from the initial accumulation of early formed minerals (such as olivine and orthopyroxene) followed in a stratigraphic sense, by the accumulation of later formed minerals such as pyroxenes and plagioclase. Minor oxide minerals such as chromite and magnetite are also observed to accumulate among the major silicate mineral phases. In order to explain this process in detail, Irvine (1977)'s model was used (Fig. 4.8). Starting at composition **A** (Fig. 4.8) olivine is the only mineral on the liquidus. Extraction of olivine from the basaltic magma at composition **A** would result in evolution of the magma composition away from the olivine-end member composition and torwards the cotectic phase boundary at **B**. At **B** a small amount of chromite of about 1% starts to crystallize together with olivine causing the magma composition to evolve towards **C**. At **C** the SiO_2 content of the magma increases and under this conditions olivine and chromite are no longer stable and orthopyroxene begins to crystallize. Continued fractional crystallization results in the appearance of plagioclase and clinopyroxene together with orthopyroxene on the liquidus. The resulting rock is a feldspathic pyroxenite. This crystallization sequence does not lead to the formation of a chromitite layer like the one described in P1, but results in the occurrence of chromite as an accessory phase in the early formed cumulates.

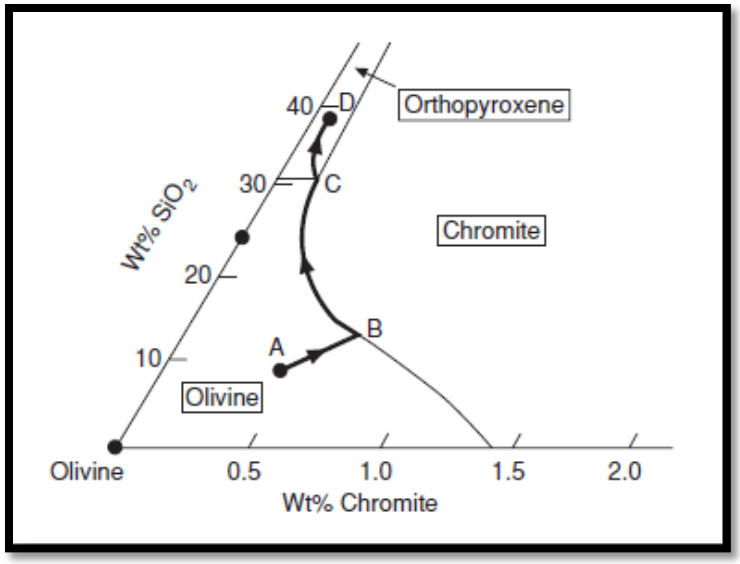

Figure 4.8: A portion of the ternary system quartz-olivine-chromite showing the nature of crystallization in a mafic magma.

The last event probably involved partial melting and recrystallization of the feldspathic pyroxenite in P3 and the intruding Main Zone magma. Kinnaird (2005) noted that the last event that preceded the Platreef was intrusion of Main Zone rocks (norites and gabbronorites) as sills and at times incorporated metasedimentary material from the top of the Platreef. Kruger (2010) noted that the C-reef which he interpreted as being the top most lithology of the Platreef was in direct contact with Main Zone rocks. It is suggested in this study that the enrichment of CaO, MgO and Fe_2O_3 in P4 and decrease in SiO_2, Na_2O and K_2O in P4 suggests some external influence during crystallization. The Platreef melanorite is ~1.82 to 28.72m thick in one of the boreholes analysed (ZF078). It often shows a gradational contact and observable major element continuities with hangingwall gabbronorite and footwall feldspathic pyroxenite that bound it. These gradational contacts and continuities provide an equally strong argument that the hangingwall gabbronorites and the feldspathic pyroxenite are definitely related to the melanorites. The work by Voordouw et al. (2009) in the Eastern Bushveld revealed sharp contacts between the hangingwall anorthosites and footwall norites, which they interpreted as providing evidence that the hangingwall anorthosite and footwall norites are not related to the UG2 melanorite. At Akanani were the anorthosite and norites bound the melanorite, there exist a

sharp contact suggesting that the anorthosite and norites at Akanani are not related to the melanorite and that the melanorite probably formed from a separate magma/intrusive event.

4.1.3 Metasomatism

The purpose of the following discussion is to provide a detailed description of the extent and continuity of metasomatism/alteration at the Akanani prospect area. Most importantly this chapter is seemingly concerned with the more important and later non-magmatic related fluid flow. It is however beyond the scope of this work to relate precious metal occurrence (PGM and Gold) to hydrothermal fluids; where necessary work done by other researchers (Van der Merwe, 2012; Kinnaird et al., 2010) will be used to substantiate the findings of this study on the subject of metasomatism which is directly linked to hydrothermal activity.

The Platreef is a complex 'sill' comprising significant concentration of PGE-Ni-Cu mineralization as such there has been so much focus on the processes that influence their concentration and deposition of mineralization. The extent, nature and timing of hydrothermal fluids are yet to be fully determined. Holwell and McDonald (2006) suggested that fluid-rock interaction was dependent on the type of floor rock and noted that where floor rock is impermeable Archaean granite gneiss hydrothermal activity was less prevalent compared to areas where the floor rock is dolomite. The influence of hydrothermal fluids on the distribution of PGE mineralization was documented in the work of Holwell and McDonald (2006) who concluded that the strong association between sulphide minerals and PGEs at Overysel is consistent with an orthomagmatic deposit that had not been disturbed by significant hydrothermal activity. They further proposed that fluid activity will have played a major role where floor rock is dolomite (e.g. Sandsloot). Armitage et al. (2002) noted that alteration, sulphur and metal mobility was much less pronounced at Townlands than at other Platreef localities further to the North, notably at Sandsloot where the PGE are largely hosted by PGM. On the basis of these results; Manyeruke et al. (2005) suggested that dolomites could have undergone pronounced devolitization relative to the shales, implying that the nature of the floor rocks plays an important role in ore-formation. Contamination by material assimilated from the floor rocks can best be considered an ore-deposit modifying process rather than a primary trigger process, this further result in the local redistribution and decoupling of PGE-BMS, and development of the lower temperature semi-metal alloy PGM assemblages (Kekana, 2014).

There is plenty of evidence that alteration and metasomatism played a role at the Akanani area this includes:

(i) Micro-fractures and a network of hydrothermal veins providing evidence for the movement of fluids especially in P2 and P3 unit.

(ii) Relatively high proportions of secondary minerals; actinolite, tremolite, phlogopite, sericite, chlorite, serpentine and magnetite. Some orthopyroxenes look to be alteration products of olivines.

(iii) Whole-rock enrichment of K_2O and LOI in units extensively affected by late-stage hydrothermal fluids

Alteration/metasomatism at Akanani area was less intense with the exception of P2 unit were serpentinization was dominant. Due to the anhydrous nature of the granite floor, one can postulate that hydraulic pressure from the fluids could have caused fracturing giving the fluids a passage through which they could flow. This is supported by the network of veins and fractures along cleavage planes of pyroxene and olivine grains. Evidently the cracks on olivine crystal provided channels for fluid penetration into the crystal. These cracks may also be picked out as trails of opaque iron oxide minerals (i.e magnetite).

The observed veins and fractures along pyroxene cleavage planes and on surface of olivine crystals generally formed at a late stage of the alteration process by crystallization of the serpentinizing fluids along fractured zones. Mason-Apps (1998) also noted that at the likely depths of serpentinization between (2 and 7km), hydraulically driven fluid flow would allow access of large quantitities of water to the rock body. At Akanani extensive serpentinization is usually developed at depths of between (1100 and 1600m) as evidenced by samples from boreholes ZF044; ZF048 and ZF078. The alteration was however not pervasive and affected only some part of the Platreef at Akanani area. Mason-Apps (1998) noted that for the pervasive serpentinization to occur, approximately ~13 wt.% is required for the hydrous reactions involvoled in the serpentinization process which is not the case at Akanani with the exception of sample ZF078/53 which is completely altered to serpentinite with LOI of 18 wt.%. At Akanani serpentinization could have taken place at lower temperatures where alteration is initiated by conditions created by the presence of intergranular water. The initial serpentinization took place rapidly producing fine-grained serpentine veins that were filled with magnetite. The magnetite

occurring along fractures of olivine probably formed during the early stages of serpentinization. This is clear from their fine-grained texture, discrete grains occurring throughout the serpentine and their very dark grey and black color. Mason-Apps (1998) noted that the extent of serpentinization was more related to volume change. In anhydrous rocks, he noted that volume change lead to more micro-fracturing and therefore increased penetration of the serpentinizing fluids. Since the granite at Akanani is considered a less permeable rock one can postulate that the increased degree of serpentinization in some P2 unit samples is most likely related to volume change that resulted in the micro-fracturing of rocks, allowing fluids enough passage way to flow. In highly serpentinized P2 unit samples there is replacement of sulphides by magnetite. In the Impala and Western Platinum mines Li et al. (2004) noted that irregardless of sample location, actinolite and tremolite always replace sulphide and orthopyroxene along their contacts. At Akanani, the initial stage of this type of replacement is marked by growth of actinolite or tremolite perpendicular to the contact between sulphide and orthopyroxene as observed in sample ZF044-31 (Plate 3.6a). Li et al. (2004) also observed that the replacement of sulphides by actinolite and orthopyroxene by tremolite in places marked the original sulphide-orthopyroxene contact. This is also observed in some samples at the Akanani prospect area (i.e ZF044-31). Sharman-Harris et al. (2005) observed an association between sulphides and biotite as well as the alteration of silicates in samples with high sulphide content in the Northern Limb. Petrographic studies at Akanani indicate an association between sulphides, actinolite and tremolite, however the degree of alteration of silicate is not dependent on the sulphide content. This sulphide-silicate relationship can be interpreted as probably due to the interaction between pre-existing silicate minerals and an immiscible sulphide liquid or a later fluid-rich phase (Sharma-Harris et al., 2005).

Many researchers (i.e Armitage et al., 2002; Holwell et al., 2006) have shown that fluid activity has played an important role on the distribution and concentration of PGEs at Sandsloot, a feature not prominent at Akanani. The hydrous nature of the footwall dolomites at Sandsloot and Zwartfontein south allowed for the release of large volumes of fluids during assimilation and metamorphism and subsequent serpentinization (Holwell and McDonald, 2006), while the anhydrous ‘granitic’ floor at Akanani produced a felsic partial melt and less volatile as first suggested by Holwell and McDonald (2006) for the granite-gneiss footwall at Overysel.

Of interest to the exploration geologist is whether or not there is an influence of hydrothermal fluids in the concentration of mineralization. Correlation analysis results for P2 mineralized unit which has also been affected by extensive serpentinization show a positive relationship between Ni, Cu, Pt and Pd thus one can suggest that the concentration of PGE is controlled by sulphides (BMS) and that hydrothermal fluids may not have played a role in the concentration of PGEs, but rather were an important mechanism for their redistribution. Van der Merwe (2012) used the correlation between PGM and BMS at the Akanani prospect area to conclude that sulphides concentrated the PGEs, with primary PGM then forming via exsollution from BMS and that most PGM were remobilized by late-stage hydrothermal activity. In the Twilight and Roby zones, Djon and Barnes (2012) noted correlations between Pt, Pd, S, Au, Ni and Cu and suggested that significant phases controlling the concentration and distribution of Pt, Pd and Au are base metal sulphides (BMS). There seem to be no direct link between the degree/intensity of alteration and the mineralization. This is evidenced by the lack of correlation between LOI and Pt, Ni, Cu, Pd, SO_3. The concentration of LOI varies in P2 and is not consistent with high grade zones (Fig. 4.9). Kennedy (1994) noted a correlation between the Cu+Ni content and alteration where serpentinization of pyroxenite is noted. At Akanani that relationship is not well defined (Fig. 4.9) within the extensively serpentinized P2 unit and this implies that hydrothermal fluids may not have played a major role in the deposition and concentration of mineralization. The lack of hydrothermal interaction and overprinting in the area of the Platreef that overlies Archaean granite basement suggests that the mineralization present could be orthomagmatic (Holwell and McDonald, 2006), although in some P2 samples the sulphides look to have been re-distributed by hydrothermal fluids as evidenced by the link between the occurrence of microcrystalline mineral phases (tremolite, actinolite, chlorite) and sulphides.

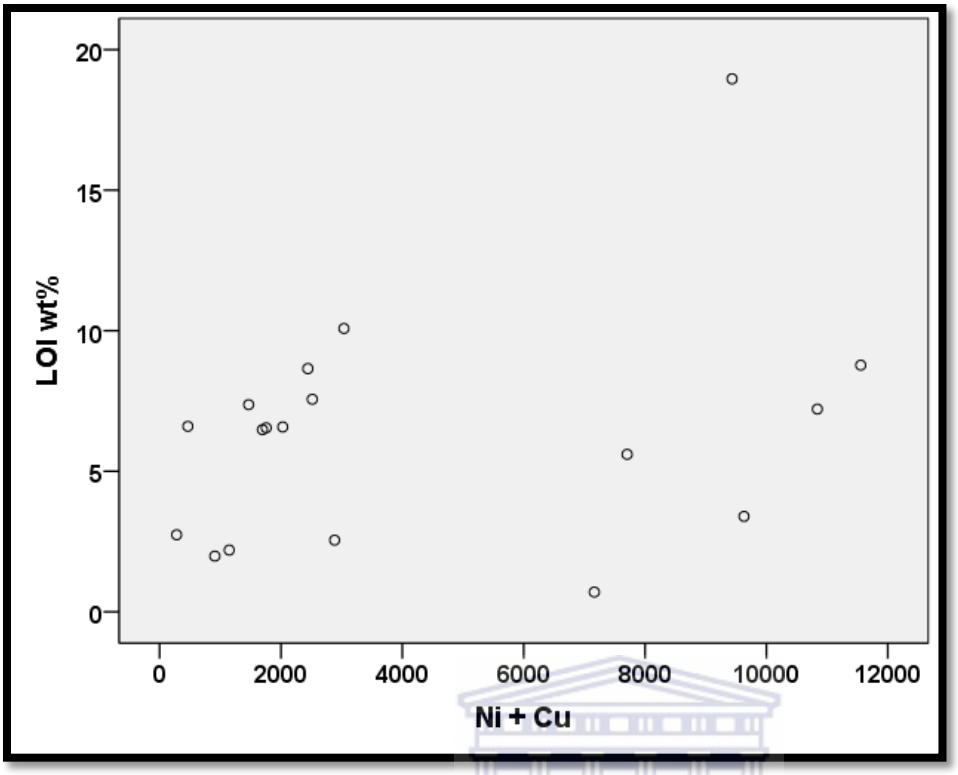

Figure 4.9: LOI vs Ni + Cu for the P2 unit at Akanani.

In contrast the alteration box plot shows that the mineralized P2 unit samples plot within and towards the ore-centre defined by Large et al. (2001) with the most altered sample plotting close to the ore-center. This trend can be due to the presence of Fe-bearing sulphides (pyrrhotite, chalcopyrite and pentlandite). It could be that the sulphides are re-distributed during extensive hydrothermal fluid flow; hence the observed increased concentration of sulphides in some extensively altered samples.

The K vs Alteration Index plot shows that altered P2 unit samples are more related to chlorite alteration, while P4 samples will be the least altered. The development of Mg-Fe chlorite alteration is typically high towards the ore-centre in both the AI vs CCPI and K vs AI plots. On the basis of these results, one can therefore suggest that P2 unit mineralization is closely related to Mg-Fe chlorite alteration as described by the reaction below. This reaction is significant because of its close association with sulphide mineralization (Ibrahim et al., 2007).

$$2KAl_3SiO_3O_{10}(OH)_2 + 3H_4SiO_4 + 9Fe^{2+} + 6Mg^{2+} + 18H_2O = 3Mg_2Fe_3Al_2Si_3O_{10}(OH)_8 + 2K^+ + 28H^+$$

Sericite Chlorite

This reaction includes the loss of K_2O and gains in FeO and MgO on the basis of constant Al_2O_3 (Ibrahim et al., 2007).

Van der Merwe (2012) noted that in borehole ZF35 of the P2 Platreef secondary silicates such as serpentine and chlorite made up 8 area % and 4 area % respectively, while base sulphides made up 2 area % with pyrrhotite being the dominant with 60% followed by pentalandite and chalcopyrite with 20% and 8% respectively. The dominance of chlorite alteration in olivine-rich rocks can be attributed to the composition of olivine which is near that of forsterite (F_{o67}-F_{o75}). Although the alteration box plot has been previously used with great success in areas associated with VHMS alteration and volcaniclastics hosting Cu mineralization (Theron, 2013), the alteration box plot is applicable to some degree at the Akanani area due to the occurrence of Fe-bearing sulphides that are associated with the mineralization. The alteration box plot was successful in linking the geochemical alteration trends and the observed alteration minerals underlying these trends and further linking those alteration trends to the mineralization. The alteration box plot results have revealed two metasomatic events, sericitization resulting from the subsequent gains in K_2O and loss of Na_2O and CaO and serpentinization associated with gains in MgO and depletion of CaO and Na_2O. These results are consistent with mass balance results. From the P1 vs P2 plot, the losses of Na, K and Fe may reflect the sericitization of feldspars particularly alkali feldspars and ferromagnesian minerals as evidenced by the occurrence of secondary biotite in P1 unit. Furthermore subsequent gains in MgO and LOI are related to serpentinization associated with the P2 unit which is consistent with petrographic observations.

It has been previously thought that the use of Rb/Sr and Ba/Rb ratios offers a more consistent guide to ore-bearing potential of granitic rocks (i.e Imeokparia, 1981). Imeokparia (1981) proposed the use of Ba/Rb and Rb/Sr as indicators and guide to post-magmatic alteration and mineralization in granitic rocks. For the first time in the Platreef it is attempted in this study to use Rb/Sr and Ba/Rb not only as an indicator for the degree of fractionation but as a guide to lithologies with higher mineralization associated with post-magmatic alteration. Ore-deposits which have associated hydrothermal alteration such as sericitization and chloritization commonly

results in the loss of CaO (Plimer and Elliot, 1980) as observed in serpentinized lithologies of P2 unit and gains in K_2O in the whole-rock as observed in sericitized lithologies of P3 unit. According to Imeokparia (1981) the ratio of Rb/Sr is similarly the lowest where alteration is associated with the mineralization. The enrichment of Rb in P2 is consistent with mass balance results and could imply that Rb was added during hydrothermal alteration as this element is expected to be incompatible during the intial stages of fractional crystallization. The high Rb/Sr ratio in P2 unit can thus be related to depletion of Ca-minerals such as plagioclase and clinopyroxene. The high Rb/Sr ratio further indicates a high degree of the melt associated with the mineralization (Imeokparia, 1981). Imeokparia (1981) noted that the Rb/Sr ratio is the highest where alteration is intense and the mineralization is present, while the Ba/Rb ratio is the lowest in these places. Although the Rb/Sr ratio is very high in P2 where alteration is intense, it is not always consistent with zones of higher mineralization. For example a sample with 6.7 wt.% LOI and a Rb/Sr ratio of 1.13 has Pt and Pd concentrations of 173 and 393 ppb. Although this ratio has proven to be significant as an indicator of post-magmatic activity, more research still needs to be done on the relationship between lower Rb/Sr and higher Ba/Rb ratios with the mineralization., hence results obtained from this study are not conclusive.

Chapter 5

Conclusion and Recommendations

1. Summary and Conclusion

The petrographic investigation is adopted first to verify the lithological subdivision at the Akanani prospect area as observed in the field and logged by mining personnel. The second approach is the attempt to create geochemical, mineralogical and petrographic variables that can be used to identify each unit, given the complexities of the stratigraphic subdivision at Akanani. Furthermore an attempt is made to determine whether these rock units are genetically related and derived from the same magma source or they evolved from more than one source.

Petrography and whole-rock geochemistry of the mafic-ultramafic Platreef sequence at the Akanani prospect area led to the recognition of four Platreef pyroxenite packages at Akanani, namely: P1 unit, P2 unit, P3 unit and P4 unit in that order of succession. The P1 unit comprises thin chromitite stringers, pyroxenites, feldspathic pyroxenites and in places chrome-pyroxenites usually occurring just above these thin chromitite layers. There is generally no agreement between the field and core-logging observations and petrographic observations. Some of the rocks previously classified as pegmatoidal feldspathic pyroxenites are infact pyroxenites in that they contain no significant feldspars and the Al_2O_3 content <3 wt%. Furthermore, what mining geologist call a chrome-pyroxenite is infact a chromitite that comprises >90 % disseminated chromite by volume. Concerning the chromitites, two main types were recognized within the P1 lithological units namely: (1) The FeO-rich (52-54 wt%) generally associated with low Cr_2O_3 (28-29.8 wt %) (2) The FeO-poor (36-37.6 wt%) which are generally Mg-rich (6.98-7.45 wt%) and Cr_2O_3 (39.1-40.38 wt%) which are more related to PGE-BMS mineralization. The Mg-rich chromitites can be interpreted as related to post-cumulus processes occurring in the presence of an Mg-rich reactant. The P2 unit is generally associated with serpentinized Mg-rich (27-38 wt%; with the exception of a sample with 48 wt% that has been completely altered to serpentinite) rocks (harzburgite, orthopyroxenites, olivine-rich orthopyroxenites, feldspathic harzburgite). These suite of ultramafic rocks were initially referred to as olivine-bearing pyroxenites, while petrographic observations has

revealed that these rocks are infact very distinct and cannot all be collectively called olivine-bearing pyroxenites as they do not all contain olivine. Further up the stratigraphic sequence the P3 feldspathic pyroxenites are intersected. The feldspar-rich pyroxenites are usually coarse-grained and pegmatoidal in places relative to those in the P1 unit that are generally fine to medium grained. The top most lithology of the Platreef pyroxenite package is a melanorite. This unit is commonly distinguishable from the other lithological units by the associated high CaO (8-20 wt%) contents. The melanorites are a complex suite of rocks and further work still need to be done to determine their origin. The petrographic observations highlight the shortfalls of core-logging and field observations as the basis of classifying the different rock types as well as the complexity of the Platreef pyroxenite package. These short comings prompted the development of element associations that can be used to classify and identify each unit. Using a combination of various multivariate statistical techniques (factor analysis, discriminant analysis and cluster analysis), four main elemental association groupings of the Platreef pyroxenite package at the Akanani area were identified namely: (1) the heavy element-rich group (Fe_2O_3, TiO_2, Cr, referred here as the P1 unit) (2) the highly serpentinized ultra-mafic unit (MgO, LOI, here referred as the P2 unit) (3) the feldspathic P3 unit (Al_2O_3, Na_2O, SiO_2, K_2O) and the melanorite P4 unit (CaO and P_2O_5). The above mentioned features lead to the suggestion of the following stages for the origin of the Platreef pyroxenite sequence at the Akanani prospect area.

(1) Initial intrusion of the Platreef magma that heated the footwall granites inducing partial melting. The occurrence of feldspathic pyroxenites dominated by quartz inclusions as well as increased values of Al_2O_3, Na_2O, SiO_2, K_2O is consistent with the process of assimilation of country rock material by addition of a plagioclase component to the intruding magma. Crustal contamination of the magma by siliceous material resulting from the assimilation of crustal material forming the granitic floor gave rise to the observed chromitite layers in P1 unit. The chrome-pyroxenites and the chrome-bearing feldspathic pyroxenites formed once the magma compositions reached the cotectic and crystallization was then dominated by pyroxene which resulted in theses rocks containing accessory amounts of chromite.
(2) The second intrusive event involved the injection of new ultramafic magma, which upon fractionation gave rise to the Mg-rich rocks in P2 unit and the feldspathic pyroxenites in

P3. The decrease in Fe_2O_3 and increase in Mg# from P1 (56) to P2 (>75) with stratigraphic height is not consistent with a single magma influx, while a sharp increase in Cr_2O_3 of orthopyroxene from 0.32 to 0.60 wt.% in P3 suggests a more differentiated trend of more primitive rocks towards the top of the succession. The occurrence of magmatic olivine, orthopyroxene and minor plagioclase may mark the beginning of a normal fractionation trend from P2 to P3. Olivine, magnetite and Cr-spinel were the first early crystallizing igneous minerals. The lack of a clear Eu anomaly in the analysed P2 ultramafic rocks reflects that plagioclase played a less significant role in the partitioning of the REE between magma and cumulates assemblages. The combination of orthopyroxene and amphibole, which in turn becomes the most abundant ferromagnesian minerals, takes the role of olivine in controlling differentiation trends of increasing SiO_2 with decreasing MgO as observed from P2 to P3 unit. Incompatible elements (Na_2O, Al_2O_3, SiO_2, K_2O and TiO_2) increase with decreasing MgO. The observations are consistent with a normal fractionating trend between P2 and P3 units.

(3) The last event probably involved partial melting and recrystallization of the feldspathic pyroxenite in P3 and the intruding Main Zone magma. Increased An % (78-85) combined with increased CaO concentrations in P4 is suggestive of hangingwall and footwall influences in the composition of the melanorite.

Using the Alteration Index (AI) against the Chlorite Carbonate Pyrite Index it was possible to confirm the dominant secondary silicate phases (sericite and chlorite) and to effectively determine those samples intensely affected by either hydrothermal or deuteric alteration. Through the alteration box plot it was possible to readily determine the direct link between the mineralization and alteration. Two fields have been defined in the alteration box plot diagram. The first relates to diagenetic alteration trends, while the second field is related to common hydrothermal alteration trends in close association with the ore. Hydrothermal alteration is especially evident in the P2 unit where most of the olivine and orthopyroxene have been altered to the secondary minerals chlorite, serpentine, phlogophite, amphibole, talc, actinolite and tremolite, as observed through petrographic analysis. It has also been revealed that actinolite and tremolite can also be alteration products of orthopyroxene and most importantly BMS, which in part provides evidence that the mineralization could have been remobilized and re-distributed by

hydrothermal fluids as evidenced by stringers and blebs of sulphides occurring in close association with the secondary silicates, especially within the P2 orthopyroxenites. Used in conjunction with petrographic studies, the alteration box plot can be a powerful exploration tool. The P2 rocks of the study area show large variations in concentration of Rb (0.01 ppm - 78.10 ppm) relative to the P1 pyroxenites which cannot be accounted for only in terms of differentiation. So, alteration must have played an important role in creating large variations in Rb content among different P2 samples. Therefore Rb is an alteration sensitive element and the sample with lowest Rb value may represent the least altered sample of the P2 unit. It is further suggested that both Rb/Sr and Ba/Rb ratios may be used as a guide to mineralization for rocks that display alteration or have no recognizable alteration. Two metasomatic events were identified through petrographic and geochemical studies including serpentinization which predominantly affected the P2 unit, while sericitization was more prevalent in the P3 unit. The first event is interpreted to be non-magmatic while sericitization was dominantly magmatic with the exception of one sample ZF044-28.

Key processes that played a major role in the formation of the Platreef at Akanani include gravitational settling as evidenced by the enrichment of TiO_2, Fe_2O_3, and Cr in the lowermost pyroxenite (P1 unit), assimilation as evidenced by the enrichment of Al_2O_3, Na_2O, K_2O in some pyroxenite samples of the P1 unit and convection which can be explained as facilitating crystal settling and assimilation by supplying heat that was responsible for the local assimilation of the country rocks. There exist a good correlation between the modal mineralogy and mineral chemistry as determined optically, the norm as determined by the CIPW norm and the whole-rock geochemical results as determined by multivariate statistics and conventional methods.

2. Recommendations

This stratigraphic subdivision at Akanani conflicts widely with the previously held view that the Platreef unit is made up of the A-B-C reefs or the PU1, PU2 and PU3 units. The proposed geochemical classification of the P1, P2, P3 and P4 units at the Akanani prospect area is directed at assisting the mining industry in evaluating new prospects as this study has simplified the complexities of the stratigraphic sequence into a generic geochemical classification of units of rocks, rather than specific lithologies.

Based on the findings of this thesis, it is recommended that the exploration geologist at the Akanani prospect area adopt the classification scheme of P1, P2, P3 and P4 units of the Platreef package as described here as a baseline for distinguishing between the four lithological units. It is further recommended that a portable XRF analyser be used during core-logging for quick and cost-effective results as the elements characterizing each unit are now known.

In light of the controls of the deposition and concentration of PGE mineralization at the study area, further investigation of samples with higher concentration of PGE is required.

As proven in this study, field observation and core-logging are not always reliable and should be accompanied by detailed geochemical and mineralogical data analysis to facilitate the correct classification of samples and thereby increase the reliability of the classification.

Chapter 6

References

References

AfrOre Limited (2006). Annual Report.

Akanani Project, (2005). AfriOre finds more high-grade zones of PGM at Akanani, AfriOre News Release, August 2005. http://www.sec.gov/Archives/edgar/vprr/06/9999999997-06-002748.

Akanani Project. (2007). The Geology and controls of Platreef mineralization at the Akanani project. Lonmin Interim Report, 49pp.

Akanani Project. (2008). Powerpoint presentation for the Lonmin Akanani visit, 4 June 2008. http://www.lonmin.com/downloads/ Akanani_Presentation.pdf. Accessed 22 February 2012.

Armitage, P.E.B., McDonald, I., Edwards, S.J., Manby, G.M. (2002). Platinum-group element mineralisation in the Platreef and calcsilicate footwall at Sandsloot, Potgietersrus District, South Africa. Appl Earth Sci (Trans Inst Min Metall B) 111:B36–B45.

Ashwal, L.D., Webb, S.J., Knoper, M.W. (2005). Magmatic stratigraphy in the Bushveld Northern Lobe: continuous geophysical and mineralogical data from the 2950 m Bellevue drillcore. *South African Journal of Geology* 108, 199-232.

Barnes, S.-J and Maier, W.D. (2002). Platinum-group elements and microstructures of normal Merensky Reef from Impala Platinum Mines, Bushveld Complex. Journal of Petrology 43, 103-128.

Buchanan, P.C., Reimold, W.U., Koeberl, C., Kruger, F.J. (2002). Geochemistry of intermediate to siliceous volcanic rocks of the Rooiberg Group, Bushveld Magmatic Province, South Africa. Contrib Mineral Petrol 144, 131-143.

Barton, J.R., Cawthorn, R.G., White, J. (1986). The role of contamination in the evolution of the Platreef of the Bushveld Complex. *Econ. Geol.* 81, 1096-1104.

Bengraine, K., Marhaba, T. F. (2003). Using Principal Component Analysis to Monitor Spatial and Temporal Changes in Water Quality. J. Hazard. Mater. 100, 179–195.

Bichan, H. R. (1969) Origin of chromite seams in the Hartley Complex of the Great Dyke, Rhodesia. In Wilson, HD. B. (Ed.) Magmatic Ore Deposits. Econ. Geol. MOllogr. 4,95-113.

Bowen, N.L. (1928). The Evolution of the Igneous rocks, Princeton Univ. Press, Prince-ton, New Jersey, USA.

Brown, S. D., Sum, S. T., Despagne, F. (1996). Chemometrics. Anal. Chem. 68, 21–61.

Buchanan, D.L. (1979). Bureau for Mineral Studies: report, University of the Witswatersrand, 4. In: Cawthorn, R.G., Eales, H.V., Walraven, F., Uken, R., and Watkeys, M.K. (2006a). The Bushveld Complex. In: Johnson, M.R., Anhaeusser, C.R., and Thomas, R.J., (Editors). The Geology of South Africa. Geological Society of South Africa, 261-281.

Buchanan, D.L., Nolan, J., Suddaby, P., Rouse, J.E., Viljoen, M.J., Davenport, J.W.J. (1981). The genesis of sulphide mineralization in a portion of the Potgietersrus limb of the Bushveld Complex. Econ Geol 76, 568-579.

Cameron, E. N. (1978). The Lower Zone of the Eastern Bushveld Complex in the Olifants River Trough. Journal of Petrology 19, 437-462.

Cawthorn, R. G. (2007). Cr and Sr: Keys to parental magmas and processes in the Bushveld Complex, South Africa. Lithos 95 (3-4), 381-398.

Cawthorn, R.G., Barton, J.M., Viljoen, M.J. (1985). Interaction of floor rocks with the Platreef on Overysel, Potgietersrus, Northern Transvaal. Econ Geol 80, 988–1006.

Cawthorn RG, Boerst K (2006) Origin of pegmatitic pyroxenite in the Merensky Unit, Bushveld Complex, South Africa. J Petrol 47, 1509–1530.

Cawthorn, R.G., and Lee, C.A. (1998). Field Excursion to the Bushveld Complex. In: 8th International platinum Symposium. Geological Society of South Africa and South African Institute of Mining and Metallurgy, 113 pp.

Cawthorn, R. G., Meyer, P. S. & Kruger, F. J. (1991). Major addition of magma at the Pyroxenite Marker in the Western Bushveld Complex, South Africa. Journal of Petrology 32, 739-763.

Cawthorn, R.G., Molyneux, T. (1986). Vanadiferous magnetite deposits of the Bushveld Complex. In: Anhaeusser, CR Maske, S (eds) Mineral deposits of Southern Africa. Geol Soc S Afr Johannesburg, 1251–1266.

Cohen, J., Cohen, P., West, S.G., & Aiken, L.S. (2013). Applied multiple regression/correlation analysis for the behavioral sciences Routledge.

Cox, K.G., Bell, J.D., Pankhurst, R.J. (1993). The Interpretation of Igneous Rocks. Chapman and Hall, 358 pp.

Cross, W., Iddings, J.P., Pirsson, L.V., and Washington, H.S. (1903). Quantitative classification of igneous rocks based on the chemical and mineral characters, with a systematic nomenclature. University of Chicago Press, Chicago, IL.

Davis, J.C. (1973). Statistics and data analysis in geology. New York: John Wiley & Sons, Inc.

De Waal, S.A. (1977). Carbon dioxide and water from metamorphic reactions as agents for sulphide and spinel precipitation in mafic magmas. *Transactions of the Geological Society of South Africa* 80**,** 193-196.

Djon, M.L.N. and Barnes, S-J. (2012). Changes in Sulphides and Platinum-Group Minerals with the degree of alteration in the Roby, Twilight and High Grade Zones of the Lac des Iles Complex, Ontario, Canada. Miner Deposita 47, 875-896.

Eales, H.V. (2002) Caveats in defining the magmas parental to the mafic rocks of the Bushveld Complex, and the manner of their emplacement: review and commentary. Mineralog Mag 66, 815-832.

Eales, H.V., Botha, W.J., Hattingh, P.J., DE Klerk, W.J., Maier, W.D. and Odgers, A.T.R. (1993). The mafic rocks of the Bushveld complex: a review of emplacement and crystallization history, and mineralization, in the light of recent data. *J. Afr. Earth Sci.* 16, 121-142.

Eales, H.V., Cawthorn, R.G. (1996). The Bushveld Complex. In: Cawthorn RG (ed) Layered intrusions. Elsevier, Amsterdam, 118–229.

Eales, H.V., Field, M., De Klerk, W.J., and Scoon, R.N. (1988). Regional trends of chemical variations and thermal erosion in the western Bushveld Complex. Miner. Mag 52, 63-79.

Eales, H.V., Maier, W.D. and Teigler, B. (1991). Mineral. Mag 55, 479-486.

Eales, H.V., Marsh, J.S., Mitchell, A.A., De Klerk, W.J., Kruger, F.J., Field, M. (1986). Some geochemical constraints upon models for the crystallization of the Upper Critical Zone-Main Zone interval, north western Bushveld Complex. Mineralogy Mag 50, 567-582.

Edwards, S.J., Pearce, J.A. and Freeman, J. (2000). New insights concerning the influence of water during the formation of podiform chromitite. *Geological Society of America Special Paper* 349, 139-147.

Farla, R.J.M. (2004). The Skaergaard Layered Intrusion, East Greenland: The mechanisms of the formation of layering and the trend of differentiation revisited. Report submitted to the Department of Petrology, Utrecht University, Netherlands.

Filippidis, A. (1982). Experimental study of the serpentinization of Mg-Fe-Ni olivine in the presence of sulfur. The Canadian Mineralogist 20, 567-574.

Gain, S.B. and Mostert, A.B. (1982). The geological setting of the platinoid and base metal sulphide mineralisation in the Platreef of the Bushveld Complex in Drenthe, north of Potgietersrus. Econ Geol 77, 1395–1404.

Gifkins, C .C. and Allen, R.L. (2001). Textural and chemical characteristics of diagenetic and hydrothermal alteration in glassy volcanic rocks: Examples from the Mount Read Volcanics, Tasmania. Economic Geology 96, 973-1002.

Gifkins, C., Herrmann, W., and Large, R.R. (2005). Altered volcanic rocks- A guide to description and interpretation: Hobart, Tasmania, Centre for Ore-deposit Research, University of Tasmania, 275.

Grant, J.A. (1986).The isocon diagram—a simple solution to Gresens'equation for metasomatic alteration. Economic Geology 81, 1976–1982.

Gresens, R.L. (1967). Composition-volume relationships of metasomatism. Chemical Geology 2, 47–65.

Hall, A.L. (1932). The Bushveld Igneous Complex in the central Transvaal. Geological Society of South Africa Memoir 28, 544.

Härdle, W and Simar, L. (2003). Applied Multivariate Statistical Analysis (2nd Ed). Springer-Verlag, Berlin, Heidelberg.

Harris, C. and Chaumba, J.B. (2001). Crustal contamination and fluid-rock interaction during the formation of the Platreef, northern limb of the Bushveld Complex, South Africa. J Petrol 42(7), 1321–1347.

Harris, C., Pronost, J. J. M., Ashwal, L. D. & Cawthorn, R. G. (2005). Oxygen and hydrogen isotope stratigraphy of the Rustenburg Layered Suite, Bushveld Complex: Constraints on crustal contamination. Journal of Petrology 46, 579-601.

Hashiguchi, H., Usui, H. (1975). An approach to delimiting targets for prospecting of the Kuroko ore-deposits; on the sulphur and magnetic susceptibility haloes. Mining Geology 25, 293-301.

Helena, B.; Pardo, R.; Vega, M.; Barrado, E.; Fernandez, J. M.; Fernandez, L. (2000) Temporal Evolution of Groundwater Composition in an Alluvial Aquifer (Pisuerga River, Spain) by Principal Component Analysis.Water Res. 34, 807–816.

Holwell, D.A., McDonald, I. and Armitage, P.E.B. (2004). Platinum-group mineral assemblages in the Platreef at Sandsloot mine, Limpopo Province, South Africa. Geoscience Africa 2004, Abstract Volume, July 2004. University of the Witwatersrand, Johannesburg, South Africa, 282-283.

Holwell, D.A., Armitage, P.E.B., McDonald, I. (2005). Observations on the relationship between the Platreef and its hangingwall. Trans Inst Min Metall B 114, 199–207.

Holwell, D.A., McDonald, I. and Armitage, P.E.B. (2006). Platinum-group mineral assemblages in the Platreef at the South Central Pit, Sandsloot Mine, northern Bushveld Complex, South Africa. Miner. Mag. 70, 83 101.

Holwell DA, Jordan, A (2006) Three-dimensional mapping of the Platreef at the Zwartfontein South mine: implications for the timing of magmatic events in the northern limb of the Bushveld Complex, South Africa. Appl Earth Sci (Trans Inst Min Metall B) 115, 41–48.

Holwell, D.A., McDonald, I. (2006). Petrology, geochemistry and mechanisms determining the distribution of platinum group elements and base metal sulphide mineralization in the Platreef at Overysel, Northern Bushveld Complex, South Africa. Minera Deposita 41, 575-598.

Holwell, D.A., McDonald, I. (2007). Distribution of platinum-group elements in the Platreef at Overysel, Northern Bushveld Complex: a combined PGM and LA-ICP-MS study. Contrib Mineral Petrol 154, 171–190.

Huang, G. H. (1988) Application of the Theory of Multivariate Statistical Inference to the Prediction of Air Pollution in Urban Environment. Proceedings of POLMET 88—International Conference on Pollution in the Urban Environment; Vincent Blue Copy Co. Ltd., Hong Kong.

Hulbert, L.J. (1983). A petrological investigation of the Rustenburg layered suite and associated mineralization south of Potgietersrus. Ph.D. thesis, University of Pretoria, 501.

Hulbert, L.J., von Gruenewaldt, G. (1982). Nickel, Copper, and Platinum mineralization in the Lower Zone of the Bushveld Complex, south of Potgietersrus. Econ Geol 77, 1296-1306.

Humphris, S.E., (1984). The mobility of the rare earth elements in the crust. In: P. Henderson (Editor), Rare Earth Element Geochemistry. Elsevier, Amsterdam, 317-341.

Hutchinson, D., Kinnaird, J.A. (2005). Complex multistage genesis for the Ni-Cu-PGE mineralization in the southern region of the Platreef, Bushveld Complex, South Africa. Appl Earth Sci (Trans Inst Min Metall B) 114:B208–B224.

Ibrahim, M.E., El-Tokhi, M.M., Saleh, G.M., Hassan, M.A., Rashed, M.A. (2007). Geochemistry of Lamprophyres associated with uranium mineralization, Southeastern Desert, Egypt. Chinese Journal of Geochemistry 26 (4), 356-365.

IBM (2012). SPSS statistics for windows (21st ed.). Armonk, New York: IBM Corp.

Ihlenfeld, C and Keays, R.R. (2011). Crustal contamination and PGE mineralization in the Platreef, Bushveld Complex, South Africa: evidence for multiple contamination events and transport of magmatic sulfides. Minera Deposita 46, 813-832.

Iijima, A . (1974). Clay and zeolitic alteration zones surrounding Kuroko deposits in the Hokiroku district, northern Akita, as submarine hydrothermal diagenetic alteration products: Mining Geology Special Issue 6, 267-289.

Imeokparia, E.G. (1981). Ba/Rb and Rb/Sr Ratios as indicators of magmatic fractionation, postmagmatic alteration and mineralization-Afu Younger Granite Complex, Northern Nigeria. Geochemical Journal 15, 209-219.

Irvine, T.N. (1975). Crystallization sequences in the Muskox intrusion and other layered intrusions—II. Origin of chromitite layers and similar deposits of other magmatic ores. Geochim Cosmochim Acta 39:991–1020.

Irvine, T.N. (1977). Origin of chromitites layers in the Muskox Intrusion and other stratiform intrusions: a new interpretation. Geology 5, 7-273.

Irvine, T.N. (1980). Magmatic infiltration metasomatism, double-diffusive fractional crystallization, and adcumulus growth in the Muskox intrusion and other layered intrusions. In: Hargreaves, (Ed). Physics of Magmatic Processes. Princeton University Press, 325-383.

Ishikawa, Y., Sawaguchi, T., Iwaya, S., Horuichi, M. (1976). Delineationof prospecting targets for Kurorko deposits based on modes of volcanism of underlying and Alteration Haloes. Mining Geology, 26 (2), 105-117.

Jackson, E.D. (1961). Primary textures and mineral associations in the Ultramafic Zone of the Stillwater Complex, Montana. U.S. Geol. Surv. Prof. Paper 358, 106p.

Jang, Y.D., Naslund, H.R. and McBirney, A.R. (2001). The differentiation trend of the Skaergaard intrusion and the timing of magnetite crystallization: iron enrichment revisited. Earth and Planetary Science Letters 189, 189-196.

Janoušek, V., Farrow, C.M., Erban, V., Trubač, J. (2011). Brand new Geochemical Data Toolkit (GCDkit 3.0) – is it worth upgrading and browsing documentation? (Yes!). The Open Congress ČGS and SGS, Monínec.

Kaiser, H.F. (1958). The Varimax criteria for analytical rotation in Factor Analysis. Psychometrika 23 (3), 187-200.

Kekana, S.M. (2014). An investigation of mineralisation controls in the upper section of the Platreef in the southern sector, on Turfspruit, Northern Limb, Bushveld Complex, South Africa. Unpublished MSc thesis, University of the Witswatersrand, Johannesburg.

Kennedy, D.C. (1994). Datamine modelling as a tool for ore reserve evaluation and mine design and the need for standardisation in data generation. Proceedings 15th CMMI congress. South African Institute Mining and Metallurgy, Johannesburg, 143-152.

Kinnaird, J.A. (2005). Geochemical evidence for multiple emplacement in the southern Platreef. Appl Earth Sci (Trans Inst Min Metall B) 114, 225–242.

Kinniard, J.A., Hutchinson, D., Schuurmann, L., Nax, P.A.M, de Lange, R. (2005). Petrology and mineralization in the southern Platreef: northern limb of the Bushveld Complex. Mineralium Deposita 40: 576-597.

Kinnaird, J., Yudovskaya, M., Nicholl, S., Naldrett, A.J., Nex, P.A. (2010). Along-Strike and Down-dip Variation in Multiphase Sills of the Platreef, Bushveld Complex. 11th International Platinum Symposium, Ontario Geological Survey, Miscellaneous Release- Data 269.

Klemm, D.D., Ketterer, S., Reichhardt, F., Steindl, J., and Weber-Diefenbach, K. (1985). Implication of vertical and lateral compositional variations across the Pyroxenite Marker and its associated rocks in the upper part of the Main Zone in the eastern Bushveld Complex. Economic Geology 80, 1007-1015.

Kruger, F.J. (2010). The Merensky and Bastard cyclic units and the Platreef of the Bushveld Complex: consequences of Main Zone magma influxes and dynamics. The 4th International

Platinum Conference, Platinum in transition 'Boom or Bust', The Southern African Institute of Mining and Metallurgy.

Large, R.R., Gemmell, J.B., Paulick, H. (2001). The Alteration Box Plot: A Simple Approach to Understanding the Relationship between Alteration Mineralogy and Lithogeochemistry Associated with Volcanic-Hosted Massive Sulfide Deposits. Economic Geology 96, 957-971pp.

Li, C., Ripley, E.M., Merino, E., Maier, W.D. (2004). Replacement of Base-Metal Sulphides by Actinolite, Epidote, Calcite and Magnetite In The UG2 and Merensky Reef of the Bushveld Complex, South Africa, Economic Geology 99, 173-184.

Lee, C.A. (1996). A review of mineralisation in the Bushveld Complex and some other layered intrusions. In: Cawthorn RG (ed) Layered Intrusions. Elsevier Science BV, Amsterdam, pp 103–145.

Maier, W.D., de Klerk, L., Blaine, J., Manyaruke, T., Baines, S.J., Stevens, M.V.A., Mavrogenes, J.A. (2007). Petrogenesis of contact style PGE mineralization in the Northern lobe of the Bushveld Complex: Comparism of data from the farm of Rooipoort, Townlands, Drenthe and Nonnenworth. Miner Deposita 43, 255-280.

Manyeruke, T.D. (2003). The petrography and geochemistry of the platreef on the Farm Townlands, near Potgietersrus, Northern Bushveld Complex. Unpublished M.Sc. Thesis, Univ. Pretoria, Johannesburg, South Africa.

Manyeruke, T.D., Maier, W.D. and Barnes, S-J. (2005). Major and trace element geochemistry of the Platreef on the farm Townlands, northern Bushveld Complex. *S. Afr. J. Geol.* 108, 381-396.

Manyeruke, T.D. (2007). Compositional and lithological variation of the Platreef on the farm Nonnenwerth, northern lobe of the Bushveld Complex: Implications for the origin of Platinum-group elements (PGE) mineralization. Unpublished PhD thesis, Department of Geology, Pretoria University, South Africa, 248pp.

Marsh, B. D. (2006). Dynamics of magmatic systems. Elements 2, 287-292.

Mason-Apps, A.D. (1998). The petrology and Geochemistry of the lower pyroxenite succession of the Great dyke in the Mutorashanga area. Unpublished MSc Thesis, Department of Geology, Rhodes University, Grahamstown, 79-120.

Matveev, S. and Ballhaus, C. (2002). Role of water in the origin of podiform chromitite deposits. Earth and Planetary Science Letters, 15, 235-243.

McCutcheon, S. (2012). Platinum-Group Mineral Assemblages in the Platreef of Tweefontein, Northern Bushveld Complex, South Africa. Unpublished MSc Thesis, Faculty of Science, University of the Witswatersrand, Johannesburg, South Africa, 127 - 128pp.

McDonald, I., Holwell, D.A. and Armitage, P.E.B. (2005). Geochemistry and mineralogy of the Platreef and "Critical zone" of the northern lobe of the Bushveld Complex, South Africa: implications for Bushveld stratigraphy and the development of PGE mineralization. Mineralium Deposita, 40, 526-549.

McDonald, I and Holwell, D.A. (2011). Geology of the Northern Bushveld Complex and the Setting and Genesis of the Platreef Ni-Cu-PGE Deposit. In: Li, C. and Ripley, E. M. eds.Magmatic Ni-Cu and PGE Deposits: Geology, Geochemistry and Genesis, Reviews in Economic Geology 17. Society of Economic Geologists, 297-327.

McDonough, W.F. and Sun, S.S. (1995). The composition of the Earth. *Chem. Geol.*, **120**, 223-253.

McInnes, B.I.A., Grégoire, M., Binns, R.A., Herzig, P.M., Hannington, M.D. (2001). Hydrous metasomatism of oceanic sub-arc mantle, Lihir, Papua New Guinea: petrology and geochemistry of fluid-metasomatised mantle wedge xenoliths. Earth and Planetary Science Letters 188, 169-183.

Michard, A. (1989). Rare earth element systematics in hydrothermalfluids. Geochimica et Cosmochimica Acta 53, 745–750.

Middlemost, E.A.K. (1975). The basalt clan, Earth-Sci. Rev., 11, 337-64

Mitchell, A.A and Scoon, R.N (2012). The Platreef of the bushveld complex, South Africa: A new hypothesis of multiple, non-sequential magma replenishment based on observations at the Akanani project, North-west of Mokopane. South African Journal of Geology 115.4, 535-550.

Molyneaux, T. G. (1974). A geological investigation of the Bushveld Complex in Sekhukhuneland and part of the Steelpoort valley. South African Journal of Geology 77, 329-338.

Munha, J and Kerrich, R. (1980). Sea water basalt interaction in Splites from the Iberian pyrite belt. Contributions to Mineralogy and Petrology 73, 191-200.

Naldrett, A.J. (2005). The Platreef: death at Drenthe; resurrection at Aurora. 2nd Platreef Workshop, Mokopane, Abstract Volume, GSSA.

Naldrett, A., Kinnaird, J., Wilson, A and Chunnet, G. (2008). Concentration of PGE in the Earth's crust with special reference to the Bushveld Complex. *Earth Science Frontiers* 15, 264-297.

Naldrett, A.J., Kinnaird, J., Wilson, A, Yudovskaya, M., McQuade, S., Chunnett, G., Stanley C. (2009a). Chromite composition and PGE content of Bushveld chromitites: part 1- the lower and middle groups. Trans Inst Min Metall B118, 131-161.

Naldrett, A.J., Wilson, A., Kinnaird, J., Chunnett, G. (2009b). PGE tenor and metal ratios within and below the Merensky Reef, Bushveld Complex: implications for its genesis. J Petrol 50, 625-659.

Nockolds, S.R. and Allen, R.S. (1953). The Geochemistry of some igneous rock series 1: Calc-Alkali igneous trends. Geochim. Cosmochim. Acta 4, 105-156.

O'Driscoll B., Emeleus, CH., Donaldson, CH., Daly, J.S. (2010). Cr-spinel seam petrogenesis in the Rhum layered suite, NW Scotland: cumulate assimilation and in situ crystallization in a deforming crystal mush. J Petrol 51, 1171–1201.

Otamendi, J.E., Cristofolini, E., Tibaldi, A.M., Quevedo, F.I., Baliani, I. (2010). Petrology of mafic and ultramafic layered rocks from the jaboncillo Valley, Sierra de Valle Fertil, Argentina: Implications for the evolution of magmas in the lower crust of the Famatinian arc. Journal of South American Earth Sciences 29, 685-704.

Pelletier, L. (2008). Li, B and Be contents of Harzburgites from the Dramala Complex (Pindos Ophiolite, Greece): Evidence for a MOR-type mantle in a supra-subduction zone environment. Journal of Petrology 49 (11), 2043-2080.

Piche, M., Jèbrak, M. (2004). Normative minerals and alteration indices developed for mineral exploration. Journal of Geochemical Exploration 82, 59–77.

Pilmer, I.R. and Elliot, S.M. (1980). The use of Rb/Sr ratios as a guide to mineralization. Journal of Geochemical Exploration 12, 21-34.

Potts, P.J. (1987). A handbook of silicate rock analysis. Blackie, Glasgow and London.

Pronost, J., Harris, C. and Pin, C. (2008). Relationship between footwall composition, crustal contamination, and fluid-rock interaction in the Platreef, Bushveld Complex, South Africa. Mineralium Deposita, 43, 825-848.

Ragno, G., Luca, M.D. and Ioele, G. (2007). An application of cluster analysis and multivariate classification methods to spring water monitoring data. *Microchemical Journal, 87*(2), 119-127.

Reimann, C., Filzmoser, P. (2000). Normal and lognormal data distribution in geochemistry: death of a myth. Consequences for the statistical treatment of geochemical and environmental data. Environ. Geol 39, 1001-1014

Reimann, C., Filzmoser, P., Garrett, R. and Dutter, R. (2008). Statistical data analysis explained: Applied environmental statistics with R. John Wiley & Sons.

Robb, L. (2004). Introduction to ore-forming processes. Blackwell publishing. 376pp.

Roelofse, F., Ashwal, L. D., Pineda-Vargas, C. A. and Przybylowicz, W.J. (2009). Enigmatic textures developed along plagioclase-augite grain boundaries at the base of the Main Zone, Northern Limb, Bushveld Complexçevidence for late stage melt infiltration into a nearly solidified crystal mush. South African Journal of Geology 112, 39-46.

Roelofse, F. (2010). Constraints on the magmatic evolution of the lower Main Zone and Platreef on the Northern Limb of the Bushveld Complex as inferred from the Moorkopje drill core. Johannesburg: PhD thesis, University of the Witwatersrand, 155 p.

Rollinson, R.H. (1993). Using Geochemical data: Evaluation, Presentation and Interpretation. Longman Group, 352pp.

SACS (1980). Stratigraphy of South Africa. Part 1 In: L.E. Kent (Compiler), Lithostratigraphy of the Republic of South Africa, Handbook Geological Survey of South Africa, 8, 690pp.

Saeki, Y. and Date, J. (1980). Computer application to the alteration data of the footwall dacite lava of the Ezuri Kuroko deposits. Akita prefecture. Mining Geology, 30, 241-250.

Seabrook, C.L. (2005). The Upper Critical and Lower Main Zones of the Bushveld Complex. Ph.D. Thesis, University of the Witwatersrand, Johannesburg, South Africa.

Scoon, R.N. and Mitchell, A.A. (2012). The Upper Zone of The Bushveld Complex At Roossenkal, South Africa: Geochemical Stratigraphy and Evidence of Multiple Episodes of Magma Replenishment.South African Journal of Geology 115.4, 515-534.

Sharman-Harris, E.R., Kinnaird, J.A., Harris, C. and Horstmann, U.E. (2005). A new look at sulphide mineralization in the northern limb, Bushveld Complex. *Applied Earth science (Transactions of the Institute of Mining and Metallurgy B),* 114**,** 252-263.

Sharpe, M.R., Irvine, T.N. (1983). Mixing relations of two Bushveld chilled margin rocks and implications for the origin of chromitites. Carnegie Inst Geophys Lab Yearbook 82, 295-300.

Shirozo, H. (1974). C lay in altered wall rocks of the Kuroko type deposits. Society of Mining Geologists of Japan, Special Issue 6, 303-311.

Siad, A.M. (2012). Geochemical characterisation of BMS and PGE mineralised layers within platreef: Combination of R-Cluster, R-Factor and Discriminant analysis approach. Unpublished report.

Siad, A.M., Matheis, G., Utke, A., & Burger, H. (1994). Discriminant analysis as a geochemical mapping technique for lateritic covered areas of southwestern and Central Nigeria. *ITC Journal*, (1), 7-12.

Siad, A.M., Mwenze, T., Okujeni, C., Bailie, R. (2012). Geochemical Classification and Characterization of Metasomatized rocks within the Platreef at Sandsloot farm, Bushveld Complex, South Africa: A multivariate statistical technique approach. 9th Annual Inkaba yeAfrica and Khure Africa Conference.

Siad, A.M., Okujeni, C., Bailie, R. Mwenze, T., Andrews, M. (2011). The influence of the floor rock composition and crustal contamination on sulphide mineralization in the Platreef, Bushveld Complex, South Africa: Multi-element geochemical Approach. 11th International Platinum Symposium, Platreef workshop Mokopane.

Soesoo, A. (2000). Fractional crystallization of mantle-derived melts as a mechanism for some I-type granite petrogenesis: An example from Lachlan Fold Belt, Australia. Journal of the Geological Society of London 157, 135-149.

Solomon, H.G. (2013). Application of multivariate statistics and Geographic Information Systems (GIS) to map groundwater quality in the Beaufort West area, Western Cape, South Africa. Unpublished MSc Thesis, Faculty of Science, University of the Western Cape, Cape Town, South Africa.

Sokal, R.R., and Sneath, P.H.A. (1963). Principles of numerical taxonomy. San Francisco, California: Freeman.

Spera, F.J., and Bohrson, W.A. (2001). Energy-Constrained open-system Magmatic Processes I: General Model and Energy-Constrained Assimilation and Fractional crystallization (EC-AFC) formulation. Journal of Petrology 42 (5), 999-1018.

Stevens, F.J. (2007). Geology and Mineralization of the Sheba's Ridge Area, Eastern Bushveld Complex, South Africa, Unpublished MSc Thesis, Faculty of Science, University of the Witswatersrand, Johannesburg, 82-95.

Sugiono, S.R.A. (2008). PLSR Modelling of the Whole-Rock Geochemistry Using Reflectance Spectra for the Panorama Hydrothermal System, Western Australia. Unpublished MSc Thesis, International Institute for Geo-Information Science and Earth Observation Enschede, ITC, Netherlands.

Suk, H., Lee, K.K. (1999). Characterization of a Groundwater hydrochemical system through multivariate analysis: Clustering into Groundwater zones. Groundwater 37(3), 358-366.

Sun, S.-S and McDonough, W.F. (1989). Chemical and isotopic systematics of oceanic basalts: implications for mantle composition and processes. In: Saunders, A.D., Norry, M.J. Eds. , Magmatism in Ocean Basins. Geol. Soc. Spec. Publ., London, 313–345.

Tanner, D., Mavrogenes, J.A., Arculus, R.J., Jenner, R.J. (2014). Trace Element Stratigraphy of the Bellevue Core, Northern Bushveld: Multiple Magma Injections Obscured by Diffusive Processes. Journal of Petrology 55 (5), 859-882.

Tatsuoka, M.M., (1988). Multivariate Analysis: Techniques for educational and Psychological Research. Macmillan, New York, 479pp.

Taylor, S.R. (1965). Application of trace elements data to problems in petrology. Phys. Chem. Earth 6, 133-213

Templ, M., 2003. Cluster Analysis applied to Geochemical Data. Diploma Thesis, Vienna University of Technology, Vienna, Austria, 137pp.

Templ, M., Filzmoser, P., & Reimann, C. (2008). Cluster analysis applied to regional geochemical data: Problems and possibilities. Applied Geochemistry *23*(8), 2198-2213. http://dx.doi.org/10.1016/j.apgeochem.2008.03.004.

Theron, L.M. (2013). Phase Relationships and Pt Solubility In Sulphide Melt In The Fe-Ni-Cu-S System At 1 ATM: Implications For Evolution Of Sulphide Magma In The Merensky Reef, Bushveld Complex, South Africa. Unpublished MSc Thesis, University of Stellenbosch, Cape-Town, South Africa.

Tollari, N., Baker, D., Barnes, S-J. (2008a). Experimental effects of pressure and fluorine on apatite saturation in mafic magmas, with reference to layered intrusions and massif anorthosites. Contrib Mineral Petrol 156, 161–175

Tollari, N., Barnes, S-J., Nabil, H., Cox, R.A. (2008b). Trace elements concentrations in apatites from the intrusive suite of Sept-Îles, Canada—implications for the genesis of nelsonites. Chem Geol 252, 180–190.

Toplis, M.J., Carroll, M.R. (1996). Differentiation of ferro-basaltic magmas under conditions open and closed to oxygen: implications for the Skaergaard intrusion and other natural systems. J Petrol 37, 837–858.

Turekian, K.L. and Kulp, J.L. (1956). The Geochemistry of strontium. Geochem. Cosmochim. Acta 10, 245-296.

Van der Merwe, F. (2012). MLA-based mineralogical investigation of PGE mineralization at Lonmin's Akanani platinum group metal project, Northern limb of Bushveld Complex, Unpublished MSc Thesis, University of Johannesburg, South Africa.

Van der Merwe, M.J. (2008). The geology and structure of the Rustenburg layered suite in the potgietersrus/mokopane area of the Bushveld Complex, South Africa. Miner Deposita 43, 405–419.

Van der Merwe, F., Viljoen, F., Knoper, M. (2012). The mineralogy and mineral associations of platinum group elements and gold in the Platreef at Zwartfontein, Akanani Project, Northern Bushveld Complex, South Africa. Miner Petrol 106, 25-38.

Vermaak, C.F. (1995). The platinum-group metals—a global perspective. Council for Mineral Technology, Randburg, 247 pp.

Viljoen, M.J, Schürmann, L.W. (1998). Platinum-group metals. In: Wilson MGC, Anhaeusser CR (eds) The mineral resources of South Africa. Council for Geoscience, Pretoria, 532–568.

Von Gruenewaldt, G. (1973). The upper and main zones of the Bushveld Complex in the Roossenekal area, eastern Transvaal. South AfricanJournal of Geology 76, 207-227.

Von Gruenewaldt, G., Sharpe, M.R., and Hatton, C.J. (1985). The Bushveld Complex: Introduction and review. Economic Geology, 80, 803-812.

Voordouw, R., Gutzmer, J., Beukes, N.J. (2009) Intrusive origin for Upper Group (UG1, UG2) stratiform chromitites seams in the Dwars River area, Bushveld Complex, South Africa.

Wagner, A. (1926). The Platinum Deposits and Mines of South Africa. Oliver Boyd, 366p.

Walraven, F., 1985. Genetic aspects of the granophyric rocks of the Bushveld complex, *Econ. Geol*. 80**,** 1166–1180.

Walraven F, Armstrong RA, Kruger FJ (1990) A chrono-stratigraphic framework for the north–central Kaapvaal Craton, the Bushveld Complex and Vredefort structure. Tectonophysics 171, 23–48.

Walraven, F. and Hattingh, E. (1993). Geochronology of the Nebo Granite, Bushveld Complex. South African Journal of Geology 96, 31-41.

White, J.A. (1994). The Potgietersrus prospect-geology and exploration history. Proceedings, XVth CMMI Congress, Johannesburg, South African Institute of Mining and Metallurgy, 3:173–181.

Wiebe, R.A. and Wild, T. (1983). Fractional crystallization and magma mixing in the Tigalak layered intrusion, the main Anorthosite complex, Labrador. Contributions to Mineralogy and Petrology 84, 327-344.

Wilson, A.H. (1982). The geology of the Great 'Dyke', Zimbabwe: the ultramafic rocks. 1. Petrol 23, 240-292.

Wilson, A.H., and Prendergast, M.D. (1988). The Great Dyke of Zimbabwe-I: tectonic setting, stratigraphy, petrology, structure, emplacement and crystallization. In: Prendergast, M.D., and Jones, M.J. (Eds), Magmatic Sulphides- The Zimbabwe Volume. Inst. Min. Metall., 1-20.

Worst, RG. (1960) The Great Dyke of Southern Rhodesia. Bull. Geol. Surv. Sth. Rhod. 47,234. Pp.

Wu, E.M.Y. and Kuo, S.L. (2012). Applying a Multivariate Statistical Analysis Model to Evaluate the Water Quality of a Watershed. Water Environment Research, 84 (12), 75-85.

Yudovskaya, M.A., Kinnaird, J.A. (2010). Chromite in the Platreef, Bushveld Complex, South Africa: Occurrence and evolution of its chemical composition. Miner Deposita 45, 369-391.

Zhang, X.Q., Song, X.Y., Chen, L.M., Yu, S.Y., Xie, W., Deng, Y., Zhang, J.F., Gui, S.G. (2013). Chalcophile element geochemistry of the Baima layered intrusion, Emeishan Large Igneous Province, SW China: implications for sulfur saturation history and genetic relationship with high-Ti basalts. Contrib Mineral Petrol 166, 193–209.

Zientek, M.L. (2012). Magmatic Ore Deposits in Layered Intrusions—Descriptive Model for Reef-Type PGE and Contact-Type Cu-Ni-PGE Deposits. U.S. Geological Survey Open-File Report 2012–1010, 48 p.

Appendices

Appendix A: XRF data from the study area as classified by mining personnel

The whole-rock major and trace element data is given in the Tables 3-10 below for samples from borehole ZF044, ZF045, ZF057, ZF078, ZF082, MO023, MO019 and MO009. The unit and rock type short codes used to describe each geochemical sample are also given in Table (1) and Table (2) below. The samples provided below were logged by mining personnel at the study area.

Table 1: List of rock types short codes used to describe geological samples from the study area

Rock Type Short Code	Description
FP	Feldspathic Pyroxenite
P	Pyroxenite
PP	Parapyroxenite
PFP	Pegmatoidal Feldspathic Pyroxenite
CS	Calc-silicate
CP	Chrome-Pyroxenite
CSP	Calc-silicate Pyroxenite
MN	Melanorite
NC	Not Classified

Table 2: List of unit short codes used to describe geological samples from the study area according to Akanani personnel.

Unit Short Code	Description
P1 Unit	Lowermost division of the Platreef characterized by feldspathic pyroxenite, pegmatitic feldspathic pyroxenite, calc-silicate, parapyroxenite and serpentinite.
P2 Unit	Main mineralized unit of the Platreef characterized by pyroxenite, serpentinized harzburgite, serpentinized pyroxenite and feldspathic pyroxenite
P3 Unit	Represents the third division of the Platreef pyroxenite sequence typically consisting of medium to coarse graine generally poor feldspar pyroxenite
P4 Unit	Represents the top of the Platreef and typically consists of medium to fine-grained melanorites to feldspathic pyroxenite

Table 3: Whole rock element geochemistry of samples from borehole ZF044.

Borehole	ZF044	ZF044	ZF044	ZF044	ZF044	ZF044	ZF044	ZF044	ZF044	ZF044	ZF044	ZF044	ZF044
Sample #	28	31	32	34	39	43	44	47	51	55	56	57	58
Unit	P3 Unit	P2 Unit	P2 Unit	P2 Unit	P2 Unit	P1 Unit	P1 Unit	P1 Unit	P1 Unit	P1 Unit	P1 Unit	P1 Unit	P1 Unit
Lithology	OP	OP	OP	OP	OP	PP	PP	FP	FP	CP	CS	CS	OP
SiO2	47.45	38.52	33.91	45.44	36.52	43.99	29.28	45.00	47.31	35.46	46.79	43.35	44.13
Al2O3	7.07	2.26	0.66	4.29	2.34	2.61	1.70	2.37	7.84	19.18	6.41	7.58	2.97
Fe2O3	12.70	12.94	18.26	9.65	15.19	13.39	4.15	18.03	13.39	17.10	14.24	7.39	11.50
MnO	0.24	0.20	0.19	0.18	0.33	0.38	0.27	0.38	0.25	0.00	0.21	0.13	0.21
MgO	23.07	28.59	33.62	18.78	30.99	19.37	19.87	21.43	22.19	13.51	20.31	15.14	15.48
CaO	6.94	9.08	3.78	18.00	7.82	17.04	32.89	9.18	6.99	9.13	7.58	20.08	20.13
Na2O	0.50	0.11	0.00	0.52	0.05	0.19	0.00	0.07	0.89	1.27	0.95	0.86	0.62
K2O	0.07	0.30	0.05	0.08	0.07	0.05	0.01	0.04	0.17	0.91	0.24	0.35	0.04
TiO2	0.16	0.15	0.10	0.23	0.10	0.19	0.10	0.15	0.16	0.86	0.22	0.21	0.16
P2O5	0.01	0.01	0.01	0.03	0.01	0.01	0.00	0.01	0.01	0.05	0.05	0.06	0.26
SO3	0.00	0.62	0.64	0.47	0.03	0.33	0.02	0.08	0.06	0.14	0.58	0.63	1.13
LOI	1.80	7.21	8.77	2.33	6.55	2.45	11.82	3.26	0.73	2.66	2.42	4.20	3.36
As	-40.86	-34.92	-37.65	-41.34	-36.22	-35.80	-44.50	-42.24	-38.82	-37.31	-33.73	-33.12	-40.26
Ba	44.86	59.21	50.43	37.63	67.34	46.40	103.50	18.61	60.99	17.54	80.13	55.10	42.76
Ce	-67.30	-116.12	28.54	-23.51	-49.04	-28.09	-38.95	-38.51	-22.83	44.53	1.41	34.08	-29.94
Co	94.91	157.40	237.37	54.02	102.12	67.92	2.83	59.50	79.89	99.92	116.05	26.91	84.67
Cr	2247.56	3448.64	1857.11	446.41	1357.56	990.33	0.14	1910.39	2445.09	134596.30	1996.11	324.26	249.20
Cu	166.64	3823.08	3838.68	405.92	357.72	671.02	74.13	419.64	353.93	611.59	1011.71	368.03	1123.05
Mo	0.77	0.79	0.81	0.83	0.80	0.83	0.79	0.78	0.78	0.83	0.82	0.81	0.73
Nb	2.60	6.69	1.03	3.28	4.23	1.95	0.22	0.99	4.64	6.88	4.50	5.24	3.31
Ni	657.83	7016.69	7715.32	459.21	1398.89	1018.70	22.74	672.12	955.87	805.40	1938.30	363.99	1789.17
Pb	0.03	0.03	1.74	6.06	0.03	2.46	5.31	8.09	4.79	0.03	0.03	5.16	0.03
Rb	10.19	19.86	2.25	7.08	4.80	0.71	6.00	0.09	10.94	0.09	11.21	20.08	0.09
Sr	76.75	40.36	30.37	70.76	52.53	47.97	155.36	29.48	120.34	79.87	100.19	150.56	45.45

Th	-11.76	-10.29	-11.00	-5.68	-3.77	-12.95	-15.88	-8.16	-11.62	-14.06	-4.12	-6.25	-17.04
U	-21.74	-34.94	-38.11	-21.33	-29.60	-35.75	-14.68	-40.35	-20.91	-80.55	-27.59	-24.79	-42.21
V	148.00	89.21	65.50	93.54	53.44	104.59	6.52	92.63	102.49	835.11	96.99	76.93	65.00
Y	8.92	9.84	9.76	16.21	9.02	12.68	19.51	9.21	8.39	6.77	11.83	13.27	21.64
Zn	113.52	88.82	102.95	101.51	101.79	76.81	142.05	72.97	117.26	265.52	115.82	74.99	43.57
Zr	40.26	41.18	36.88	48.84	35.77	39.04	46.91	34.82	37.48	39.50	49.77	49.82	43.00
Au			117	12	33	129		47	73	32		<5	45
Pd			6317	129	325	526		361	153	962		16	276
Pt			1457	141	280	384		316	109	917		<5	114

Table 4: Whole rock element geochemistry of samples from borehole ZF078.

Borehole	ZF078	ZF078	ZF078	ZF078	ZF078	ZF078	ZF078	ZF078	ZF078	ZF078	ZF078	ZF078	ZF078	ZF078	ZF078	ZF078	ZF078	ZF078	ZF078	ZF078
Sample #	**6**	**9**	**15**	**17**	**21**	**22**	**28**	**30**	**31**	**34**	**39**	**42**	**47**	**49**	**50**	**52**	**53**	**55**	**60**	**64**
Unit	**P4 Unit**	**P4 Unit**	**P3 Unit**	**P3 Unit**	**P1 Unit**	**P1 Unit**	**P1 Unit**	**P1 Unit**	**P1 Unit**	**P1 Unit**	**P1 Unit**	**P1 Unit**	**P1 Unit**	**P1 Unit**	**P1 Unit**	**P1 Unit**	**P1 Unit**	**P1 Unit**	**P1 Unit**	**P1 Unit**
Lithology	**MN**	**FP**	**P**	**P**	**PFP**	**PFP**	**PP**	**PP**	**PP**	**PFP**	**PFP**	**PFP**	**PFP**	**PFP**	**PFP**	**PFP**	**S**	**PP**	**PP**	**FP**
SiO2	46.22	46.92	46.33	45.81	42.63	44.48	40.37	44.67	43.96	45.17	50.03	45.01	43.72	44.73	31.78	41.95	16.07	38.06	43.93	52.44
Al2O3	14.74	5.19	7.26	5.12	1.70	2.46	6.06	2.34	1.95	1.69	5.96	3.53	3.42	2.16	13.70	3.74	1.17	4.51	3.35	7.00
Fe2O3	10.97	22.57	14.98	15.22	23.16	17.90	8.44	15.74	13.95	18.57	18.42	22.21	22.94	21.12	27.61	17.88	13.94	13.23	14.70	19.47
MnO	0.21	0.39	0.28	0.40	0.44	0.36	0.22	0.40	0.27	0.39	0.35	0.38	0.34	0.32	0.01	0.15	0.14	0.18	0.32	0.15
MgO	14.76	16.02	20.89	19.21	20.87	19.66	21.98	17.98	17.04	20.83	13.93	16.70	19.05	23.17	14.58	29.64	48.84	14.42	21.07	10.65
CaO	10.22	5.85	6.94	11.60	8.06	13.05	17.14	16.71	18.05	10.86	7.84	7.50	7.55	6.52	6.91	2.39	0.03	22.63	13.76	2.79
Na2O	1.04	0.61	0.67	0.34	0.11	0.20	0.15	0.11	0.13	0.13	1.09	0.61	0.42	0.18	0.66	0.02	0.01	0.16	0.25	1.75
K2O	0.15	0.42	0.21	0.35	0.16	0.18	0.70	0.04	0.04	0.12	1.14	0.44	0.11	0.09	0.80	0.00	0.00	0.00	0.10	0.46
TiO2	0.16	0.29	0.20	0.14	0.16	0.18	0.26	0.19	0.17	0.17	0.22	0.20	0.26	0.18	0.87	0.21	0.15	0.29	0.20	0.48
P2O5	0.01	0.03	0.02	0.01	0.01	0.01	0.03	0.02	0.01	0.01	0.05	0.03	0.01	0.03	0.02	0.01	0.01	0.07	0.02	0.02
SO3	0.01	0.21	0.11	0.34	0.98	0.46	0.23	0.27	0.55	0.19	0.74	1.26	1.30	1.09	2.93	0.53	0.97	2.02	0.83	2.27
LOI	1.39	1.40	1.99	1.39	1.60	1.00	4.19	1.40	3.79	1.80	0.20	2.00	0.80	0.40	0.20	3.39	18.96	3.99	1.40	2.40
As	1.92	1.92	1.92	1.92	1.92	1.92	1.92	1.92	1.92	1.92	1.92	1.92	1.92	1.92	1.92	1.92	1.92	1.92	1.92	1.92
Ba	13.40	56.66	81.57	55.52	42.85	120.34	33.20	32.56	45.93	113.06	90.34	7.71	29.64	1.53	1.53	9.35	1.53	31.28	1.53	720.29
Ce	21.42	2.38	11.42	2.38	19.72	6.18	28.65	2.38	2.38	2.38	38.02	2.38	18.89	2.38	27.55	2.38	2.38	2.38	2.38	19.63
Co	91.51	101.38	78.15	160.42	100.97	65.30	72.89	77.90	90.60	91.73	128.31	149.58	171.46	205.96	177.38	102.20	98.92	102.93	220.48	2.35
Cr	1232.08	2229.90	2043.51	1590.87	1439.63	254.76	1340.06	1386.50	1854.88	1276.13	1751.67	4742.45	2521.75	103074.50	29262.24	0.01	474.56	333.65	13011.19	69.96
Cu	726.42	568.50	1290.11	2382.65	1676.94	387.74	996.20	933.56	347.56	1129.41	5034.67	1876.44	1892.45	2918.41	1286.67	4467.03	3403.74	1439.72	10203.30	55.90
Mo	0.83	0.78	0.75	0.83	0.81	0.87	0.84	0.84	0.82	0.85	0.82	0.82	0.81	0.82	0.81	0.83	0.89	0.80	0.85	0.81
Nb	4.78	2.76	4.92	4.40	4.50	3.95	1.81	2.51	3.34	6.46	5.59	2.49	5.15	7.34	2.52	5.39	4.25	3.41	7.50	6.08
Ni	917.38	1331.03	1571.97	4189.81	2119.81	1794.20	1545.43	1176.42	1168.71	3259.11	3161.60	4843.61	5728.84	7155.07	2886.29	5163.65	6030.00	1928.62	7572.49	7.16
Pb	0.08	0.08	0.08	0.32	0.08	15.20	12.32	0.08	0.08	9.54	0.08	0.87	5.59	0.08	0.08	9.29	8.06	0.08	12.55	56.74

Rb	9.54	12.09	16.48	0.01	3.08	46.99	0.01	0.01	1.44	22.74	2.57	0.01	0.01	0.01	0.01	15.77	0.01	1.86	23.72	83.91
Sr	63.11	89.79	57.90	34.33	41.30	114.70	30.73	34.62	35.27	74.78	55.05	51.60	33.68	79.89	36.27	24.03	84.17	57.17	82.57	789.17
Th	14.47	14.47	14.47	14.47	14.47	14.47	14.47	14.47	14.47	14.47	14.47	14.47	14.47	14.47	14.47	14.47	14.47	14.47	14.47	14.47
U	1.05	1.05	1.05	1.05	1.05	1.05	1.05	1.05	1.05	1.05	1.05	1.05	1.05	1.05	1.05	1.05	1.05	1.05	1.05	77.06
V	202.69	126.92	116.86	101.45	114.86	84.42	116.35	131.95	93.84	95.84	94.82	174.40	103.34	712.03	232.39	30.49	88.80	115.71	254.86	14.40
Y	17.18	9.23	13.75	7.06	13.04	19.55	12.04	13.40	8.97	17.53	11.33	8.65	10.04	8.01	5.80	3.42	12.36	13.74	14.37	17.89
Zn	170.69	169.34	93.15	118.32	93.15	67.68	106.79	57.31	91.32	3.00	113.42	114.86	101.51	248.71	216.81	110.73	36.36	129.47	93.15	114.38
Zr	38.67	40.91	34.63	37.29	38.27	64.29	47.53	35.46	37.64	48.94	43.31	39.15	36.77	38.85	35.66	47.16	57.08	49.61	50.81	92.83
Au					165.66					113.25	976.60		358.45	1398.23	77.16	114.29		584.22	1664	
Pd					2032.32					2588.47	1782.30		4142.57	12787.61	353.30	4342.86		3053.30	9831.47	
Pt					1684					2256	1493		2977	10287	158.38	2118		720	7200	

Table 5: Whole rock element geochemistry of samples from borehole MO019.

Sample ID	MO019-34	MO019-46	MO019-47
Unit	**NC**	**P3 Unit**	**NC**
Lithology	**P**	**FP**	**CS**
SiO2	50.52	48.19	42.77
Al2O3	6.60	7.76	6.64
Fe2O3	20.43	12.02	10.23
MnO	0.37	0.22	0.19
MgO	12.56	21.40	23.29
CaO	6.28	8.06	12.09
Na2O	0.86	0.91	0.22
K2O	0.41	0.16	0.24
TiO2	0.21	0.18	0.23
P2O5	0.10	0.01	0.02
LOI	1.61	1.09	4.08
Total	99.94	100	100
SO3	0.0580	0.0020	0.0002
As	1.93	1.93	1.99
Ba	104.99	43.97	35.99
Ce	41.41	6.81	0.20
Co	80.82	85.86	60.47
Cr	743	3,257	1,770
Cu	235.62	138.42	94.70
Mo	0.96	0.79	0.80
Nb	2.36	5.07	3.27
Ni	441.03	608.53	695.93
Pb	0.03	3.14	0.28
Rb	12.40	15.83	24.44

Sr	79.95	98.53	98.27
Th	14.37	14.37	14.36
U	0.02	0.02	0.05
V	143.54	130.05	83.31
Y	21.07	9.35	9.69
Zn	197.69	102.08	103.24
Zr	90.10	42.35	48.14
Au			
Pd	53.00	101.00	12.00
Pt	45.00	178.00	8.00

Table 6: Whole rock element geochemistry of samples from borehole MO023.

Sample ID	MO023-21	MO023-37	MO023-39	MO023-42	MO023-46	MO023-47	MO023-50
Unit	**P3 Unit**	**P4 Unit**	**NC**	**NC**	**NC**	**NC**	**NC**
Lithology	**P**	**FP**	**FP**	**P**	**PFP**	**PFP**	**PFP**
SiO2	50.97	49.25	48.52	48.91	48.01	47.69	49.27
Al2O3	7.15	11.47	4.70	4.92	8.13	7.74	7.11
Fe2O3	16.04	10.99	16.26	14.75	11.35	12.71	14.11
MnO	0.30	0.20	0.30	0.29	0.25	0.25	0.26
MgO	10.99	18.12	24.58	25.23	23.04	23.02	21.80
CaO	11.16	8.13	4.18	4.61	7.23	6.74	5.92
Na2O	1.01	1.12	0.48	0.53	0.51	0.57	0.76
K2O	0.80	0.33	0.21	0.15	0.38	0.24	0.40
TiO2	0.46	0.16	0.16	0.15	0.14	0.14	0.23
P2O5	0.10	0.02	0.01	0.01	0.01	0.01	0.02
LOI	0.70	0.20	0.40	0.40	0.91	0.80	0.10
Total	99.66	99.99	99.79	99.94	99.97	99.91	99.99
SO3	0.29	0.01	0.21	0.06	0.03	0.08	0.01
As	-33.98	-41.97	-39.18	-43.77	-37.41	-37.19	-41.26
Ba	26.39	71.01	56.77	55.65	70.00	54.05	55.91
Ce	44.80	-61.78	-89.63	-68.89	-23.21	-46.87	-38.35
Co	82.65	75.33	110.54	98.63	72.10	81.58	83.25
Cr	383.91	2,250	2,691	2,310	3,391	3,100	2,229
Cu	479.29	175.65	441.84	390.20	234.52	362.68	215.73
Mo	0.89	0.77	0.80	0.78	0.76	0.76	0.82
Nb	8.78	4.50	2.21	2.90	2.19	2.41	4.33
Ni	319.62	689.15	1,713	1,122	828	1,041	753
Pb	4.36	2.31	-7.25	3.31	-0.70	11.94	3.77
Rb	22.76	16.88	12.85	13.03	22.28	15.27	17.22

Sr	82.95	115.13	66.89	54.75	97.49	85.05	74.70
Th	-10.65	-6.56	-20.50	-5.94	-6.48	-21.83	-5.81
U	-38.33	-10.93	-25.87	-24.09	-12.97	-15.56	-21.42
V	206.75	104.93	131.85	129.26	105.63	112.59	133.40
Y	38.90	9.67	13.22	8.54	11.59	8.65	12.48
Zn	167.80	114.29	143.01	136.58	78.64	95.74	119.19
Zr	60.92	38.87	40.73	38.00	38.84	32.27	51.60
Au			48.53	36.47	48.73	48.63	36.59
Pd	32.26	48.34	1,027	109.42	93.40	117.53	
Pt	8.06	100.70	703.74	166.16	178.68	324.21	12.20

Table 7: Whole rock element geochemistry of samples from borehole MO009.

Sample ID	MOO09-25	MOO09-28	MOO09-48
Unit	**NC**	**NC**	**NC**
Lithology	**P**	**P**	**P**
SiO2	47.44	46.65	47.75
Al2O3	8.80	10.56	8.52
Fe2O3	12.66	10.67	11.82
MnO	0.24	0.21	0.23
MgO	20.03	21.59	22.07
CaO	8.25	7.55	6.58
Na2O	0.81	0.71	0.86
K2O	0.22	0.11	0.11
TiO2	0.19	0.13	0.16
P2O5	0.02	0.01	0.01
LOI	1.30	1.80	1.90
Total	99.95	99.99	100.01
SO3	0.0052	0.0002	0.0079
As	-36.98	-45.19	-41.55
Ba	52.89	70.37	61.15
Ce	-22.49	-33.91	-19.24
Co	71.87	77.22	72.30
Cr	2,031.42	1,885.58	2,749.97
Cu	167.95	191.93	188.74
Mo	0.79	0.79	0.79
Nb	0.10	2.02	2.25
Ni	625.09	700.29	712.64
Pb	1.26	1.26	1.67
Rb	16.84	16.88	12.87

Sr	87.72	100.49	93.87
Th	-19.39	-13.13	-7.23
U	-18.47	-12.24	-15.14
V	144.45	105.24	111.70
Y	11.53	6.81	10.53
Zn	134.37	142.63	123.80
Zr	41.95	38.89	40.02
Au			
Pd	20.47	88.89	16.36
Pt	61.41	113.13	28.63

Table 8: Whole rock element geochemistry of samples from borehole ZF057.

Sample ID	ZF057-36	ZF057-44	ZF057-46
Unit	**NC**	**NC**	**NC**
Lithology	**FP**	**FP**	**FP**
SiO2	47.11	50.10	46.65
Al2O3	7.53	5.76	9.38
Fe2O3	13.35	13.07	12.01
MnO	0.26	0.24	0.22
MgO	22.74	21.24	20.03
CaO	6.30	5.56	7.14
Na2O	0.63	0.83	1.05
K2O	0.03	0.39	0.22
TiO2	0.14	0.19	0.17
P2O5	0.01	0.01	0.02
LOI	1.89	2.69	2.99
Total	99.99	100.08	99.88
SO3	0.00	0.02	0.10
As			
Ba	45.81	70.98	94.60
Ce			
Co	83.23	74.43	72.65
Cr	3,268	2,379	2,163
Cu	137.57	267.05	518.84
Mo	0.79	0.78	0.79
Nb	3.39	1.68	2.21
Ni	638.52	706.45	1,192.13
Pb	0.66	0.66	13.33
Rb	6.54	15.71	13.68

Sr	88.84	87.19	132.93
Th			
U			
V	114.05	141.63	99.61
Y	8.17	13.84	7.98
Zn	119.86	149.84	165.50
Zr	36.76	42.56	42.23
Au		12.12	186.61
Pd		40.40	1,692
Pt	154.00	80.81	2,260

Table 9: Whole rock element geochemistry of samples from borehole ZF045.

Sample ID	ZF045-27	ZF045-29	ZF045-30	ZF045-44	ZF045-46
Unit	**NC**	**P4 Unit**	**NC**	**NC**	**NC**
Lithology	**P**	**FP**	**P**	**P**	**P**
SiO2	45.96	48.00	45.93	46.20	43.10
Al2O3	5.63	11.16	5.73	9.02	2.86
Fe2O3	9.87	8.33	13.43	12.52	21.10
MnO	0.20	0.19	0.26	0.26	0.17
MgO	16.39	13.51	22.33	16.30	19.01
CaO	16.88	14.13	7.65	7.44	5.37
Na2O	0.70	1.49	0.54	1.48	0.41
K2O	0.30	0.41	0.25	0.74	0.15
TiO2	0.21	0.17	0.16	0.18	0.17
P2O5	0.02	0.02	0.01	0.01	0.04
LOI	3.12	2.23	3.48	5.39	5.55
Total	99.29	99.62	99.77	99.54	97.93
SO3	0.71	0.38	0.23	0.46	2.07
As	0.85	0.85	1.91	1.91	1.91
Ba	100.91	112.61	69.82	194.05	27.19
Ce	9.21	6.20	55.86	16.37	36.37
Co	107.76	72.24	101.93	67.75	307.31
Cr	1,006	808	1,894	1,205	5,060
Cu	2,779	2,298	716	1,035	1,419
Mo	0.80	0.78	0.77	0.79	0.81
Nb	2.41	3.38	0.44	5.72	6.84
Ni	4,612	2,508	1,819	915	8,401
Pb	0.32	23.03	0.07	5.22	0.07
Rb	8.82	20.05	20.38	44.29	0.16

Sr	72.69	152.39	86.72	196.26	40.39
Th	14.43	14.43	14.41	14.41	14.41
U	0.23	0.23	0.09	0.09	0.09
V	138.70	116.04	95.15	86.66	95.70
Y	14.26	15.47	8.61	17.33	13.97
Zn	54.14	93.43	88.25	159.16	101.60
Zr	48.12	52.55	41.53	45.79	36.93
Au	24	315	77	35	33
Pd	393	1,943	835	114	3,459
Pt	173	1,046	592	47	1,374

Table 10: Whole rock element geochemistry of samples from borehole ZF045.

Sample ID	ZF082-40	ZF082-52
Unit	**NC**	**P4 Unit**
Lithology	**N**	**FP**
SiO2	45.30	45.28
Al2O3	11.05	11.45
Fe2O3	13.75	12.84
MnO	0.23	0.23
MgO	19.59	15.60
CaO	7.82	10.74
Na2O	0.71	0.95
K2O	0.11	0.18
TiO2	0.16	0.17
P2O5	0.02	0.02
SO3	0.36	0.32
LOI	0.80	2.03
Total	99.90	99.81
As	0.85	0.85
Ba	56.50	66.81
Ce	6.20	6.20
Co	109	88
Cr	1,467	902
Cu	1,541	1,239
Mo	0.79	0.76
Nb	2.16	2.89
Ni	3,443	2,365
Pb	0.11	10.17
Rb	10.12	9.34

Sr	92.16	109.95
Th	0.01	0.01
U	0.23	0.23
V	95.69	116.90
Y	6.16	9.28
Zn	82.58	99.30
Zr	38.99	42.46
Au	85	639
Pd	806	5,824
Pt	471	3,426

Appendix B: XRF data from the study area as classified by the author using multivariate statistics

The whole-rock major and trace element data is given in the Tables 13-18 below for samples from borehole ZF044, ZF045, ZF057, ZF078, ZF082 and MO023. The unit and rock type short codes used to describe each geochemical sample are also given in Table (11) and Table (12) below. The samples provided below were logged and classified geochemically by various multivariate statistical techniques (i.e cluster analysis, discriminant analysis and factor analysis).

Table 11: List of rock types short codes used to describe geological samples from the study area

Rock Type Short Code	Description
FP	Feldspathic Pyroxenite
P	Pyroxenite
FP	Feldspathic Harzburgite
SH	Serpentinized Harzburgite
C	Chromitite
H	Harzburgite
MN	Melanorite
S	Serpentinite

Table 12: List of unit short codes used to describe geological samples from the study area based upon geochemical data analysis

Unit Short Code	Description
P1 Unit	Lowermost division of the Platreef characterized by feldspathic pyroxenite, chrome-bearing feldspathic pyroxenite, pyroxenite and chromitite. Geochemically this unit is characterized by high Fe_2O_3, TiO_2 and Cr
P2 Unit	Main mineralized unit of the Platreef characterized by serpentinized harzburgite, olivine-rich pyroxenites and feldspathic harzburgite. High MgO and LOI are associated with this unit
P3 Unit	Represents the third division of the Platreef pyroxenite sequence typically consisting of coarse-grained to pegmatoidal generally rich feldspar pyroxenite
P4 Unit	Represents the top of the Platreef and typically consists of medium to fine-grained melanorites. CaO and P_2O_5 are characteristic of this unit.

Table 13: Whole rock element geochemistry of samples from borehole ZF044.

Sample ID	ZF044-47	ZF044-31	ZF044-32	ZF044-39	ZF044-51	ZF044-28	ZF044-43	ZF044-57	ZF044-58	ZF044-1	ZF044-16
Lithology	**P**	**SH**	**SH**	**SH**	**FP**	**FP**	**MG**	**MN**	**MN**	**MN**	**MN**
Unit	**P1**	**P2**	**P2**	**P2**	**P3**	**P3**	**P4**	**P4**	**P4**	**P4**	**P4**
SiO2	45.00	38.52	33.91	36.52	47.31	47.45	43.99	43.35	44.13	45.61	45.17
Al2O3	2.37	2.26	0.66	2.34	7.84	7.07	2.61	7.58	2.97	16.66	16.96
Fe2O3	18.03	12.94	18.26	15.19	13.39	12.70	13.39	7.39	11.50	7.32	7.89
MnO	0.38	0.20	0.19	0.33	0.25	0.24	0.38	0.13	0.21	0.15	0.16
MgO	21.43	28.59	33.62	30.99	22.19	23.07	19.37	15.14	15.48	9.92	9.99
CaO	9.18	9.08	3.78	7.82	6.99	6.94	17.04	20.08	20.13	16.33	16.03
Na2O	0.07	0.11	0.00	0.05	0.89	0.50	0.19	0.86	0.62	1.42	1.18
K2O	0.04	0.30	0.05	0.07	0.17	0.07	0.05	0.35	0.04	0.15	0.12
TiO2	0.15	0.15	0.10	0.10	0.16	0.16	0.19	0.21	0.16	0.18	0.18
P2O5	0.01	0.01	0.01	0.01	0.01	0.01	0.01	0.06	0.26	0.01	0.01
LOI	3.26	7.21	8.77	6.55	0.73	1.80	2.45	4.20	3.36	2.26	2.31
Total	99.92	99.38	99.36	99.97	99.94	100.00	99.67	99.37	98.87	100.01	100.01
SO3	0.08	0.62	0.64	0.03	0.06	0.00	0.33	0.63	1.13	0.00	0.00
As	-42.24	-34.92	-37.65	-36.22	-38.82	-40.86	-35.80	-33.12	-40.26	-38.45	
Ba	18.61	59.21	50.43	67.34	60.99	44.86	46.40	55.10	42.76	62.08	
Ce	-38.51	-116.12	28.54	-49.04	-22.83	-67.30	-28.09	34.08	-29.94	78.63	
Co	59.50	157.40	237.37	102.12	79.89	94.91	67.92	26.91	84.67	37.14	
Cr	1,910	3,449	1,857	1,358	2,445	2,248	990.33	324.26	249.20	35.44	
Cu	419.64	3,823.08	3,838.68	357.72	353.93	166.64	671.02	368.03	1,123.05	0.78	
Mo	0.78	0.79	0.81	0.80	0.78	0.77	0.83	0.81	0.73	6.31	
Nb	0.99	6.69	1.03	4.23	4.64	2.60	1.95	5.24	3.31	201.10	
Ni	672	7,017	7,715	1,399	956	658	1,019	364	1,789	0.03	
Pb	8.09	0.03	1.74	0.03	4.79	0.03	2.46	5.16	0.03	11.41	
Rb	0.09	19.86	2.25	4.80	10.94	10.19	0.71	20.08	0.09	191.57	
Sr	29.48	40.36	30.37	52.53	120.34	76.75	47.97	150.56	45.45	-19.83	
Th	-8.16	-10.29	-11.00	-3.77	-11.62	-11.76	-12.95	-6.25	-17.04	-9.13	
U	-40.35	-34.94	-38.11	-29.60	-20.91	-21.74	-35.75	-24.79	-42.21	133.72	

V	92.63	89.21	65.50	53.44	102.49	148.00	104.59	76.93	65.00	11.16
Y	9.21	9.84	9.76	9.02	8.39	8.92	12.68	13.27	21.64	87.38
Zn	72.97	88.82	102.95	101.79	117.26	113.52	76.81	74.99	43.57	49.70
Zr	34.82	41.18	36.88	35.77	37.48	40.26	39.04	49.82	43.00	
Au	47		117	33	73		129		45	
Pd	361		6,317	325	153		526	16	276	
Pt	316		1,457	280	109		384		114	

Table 14: Whole rock element geochemistry of samples from borehole ZF044.

Sample ID	**ZF045-46**	**ZF045-28**	**ZF045-44**	**ZF045-8**	**ZF045-27**
Lithology	**P**	**FH**	**FP**	**MN**	**MN**
Unit	**P1**	**P2**	**P3**	**P4**	**P4**
SiO2	43.099	35.01	46.20	46.01	45.96
Al2O3	2.864	6.39	9.02	5.88	5.63
Fe2O3	21.104	12.74	12.52	10.43	9.87
MnO	0.171	0.30	0.26	0.24	0.20
MgO	19.010	30.82	16.30	17.92	16.39
CaO	5.369	7.09	7.44	16.65	16.88
Na2O	0.412	0.11	1.48	0.43	0.70
K2O	0.152	0.69	0.74	0.03	0.30
TiO2	0.166	0.12	0.18	0.28	0.21
P2O5	0.037	0.01	0.01	0.03	0.02
LOI	5.547	6.57	5.39	2.09	3.12
Total	97.93	99.86	99.54	99.99	99.29
SO3	2.07	0.14	0.46	0.01	0.71
As	1.911	0.849	1.911	0.849	0.849
Ba	27.19	129.56	194.05	17.19	100.91
Ce	36.37	19.36	16.37	6.20	9.21
Co	307.31	64.68	67.75	51.01	107.76
Cr	5,060	164.27	1,205	82.84	1,006
Cu	1,419	588.94	1,035	129.32	2,779
Mo	0.807	0.764	0.793	0.806	0.796

Nb	6.844	2.627	5.716	4.217	2.405
Ni	8,401	1,440	915	364	4,612
Pb	0.073	3.980	5.215	2.283	0.317
Rb	0.16	78.10	44.29	1.94	8.82
Sr	40.39	69.40	196.26	64.85	72.69
Th	14.41	14.43	14.41	14.43	14.43
U	0.09	0.23	0.09	0.23	0.23
V	95.70	54.28	86.66	221.69	138.70
Y	13.97	14.77	17.33	17.66	14.26
Zn	101.60	206.33	159.16	91.90	54.14
Zr	36.93	33.24	45.79	43.40	48.12
Au	33	24	35		24
Pd	3,459	393	114		393
Pt	1,374	173	47		173

Table 15: Whole rock element geochemistry of samples from borehole ZF057.

Sample ID	ZF057-38	ZF057-53	ZF057-29	ZF057-30	ZF057-33	ZF057-40	ZF057-47	ZF057-46	ZF057-54	ZF057-44
Lithology	**P**	**C**	**SH**	**H**	**FH**	**SH**	**FH**	**FP**	**FP**	**FP**
Unit	**P1**	**P1**	**P2**	**P2**	**P2**	**P2**	**P2**	**P3**	**P3**	**P3**
SiO2	45.32	30.44	41.09	46.87	31.10	34.26	38.94	46.65	42.38	50.10
Al2O3	3.85	12.26	1.40	1.93	11.10	2.30	6.91	9.38	9.83	5.76
Fe2O3	18.12	32.70	16.64	17.01	10.05	9.57	8.41	12.01	15.69	13.07
MnO	0.35	-0.16	0.34	0.28	0.33	0.29	0.33	0.22	0.08	0.24
MgO	21.83	15.61	31.69	28.90	32.01	38.34	30.77	20.03	18.67	21.24
CaO	7.88	4.53	2.57	3.06	7.67	8.35	11.26	7.14	6.60	5.56
Na2O	0.39	0.95	0.00	0.15	0.21	-0.04	0.36	1.05	1.30	0.83
K2O	0.23	0.20	0.33	0.11	0.47	-0.01	0.15	0.22	0.65	0.39
TiO2	0.25	1.17	0.11	0.16	0.31	0.13	0.19	0.17	0.44	0.19
P2O5	0.02	0.04	0.01	0.01	0.13	0.01	0.02	0.02	0.10	0.01
LOI	1.40	1.41	5.60	0.70	6.60	7.37	2.74	2.99	2.68	2.69
Total	99.64	99.15	99.78	99.18	99.98	100.57	100.08	99.88	98.42	100.08
SO3	0.01	0.34	0.06	0.81	0.01	0.19	0.06	0.10	1.29	0.02
As										
Ba	48.2500	17.3010	127.9200	52.7500	47.1000	23.6800	72.6400	94.6000	142.3100	70.9800
Ce										
Co	77.67	109.03	216.52	187.80	61.25	73.16	38.86	72.65	312.51	74.43
Cr	2,318	114,005	2,699	4,524	233	352	304	2,163	46,961	2,379
Cu	158	1,252	2,718	2,951	180	552	138	519	2,239	267
Mo	0.74	0.83	0.76	0.78	0.94	0.78	0.86	0.79	0.82	0.78
Nb	3.08	9.50	3.70	0.87	1.63	4.87	3.95	2.21	6.41	1.68
Ni	772	1,479	4,986	4,213	286	915	142	1,192	2,141	706
Pb	4.89	0.66	1.96	2.04	7.46	0.66	0.53	13.33	4.55	0.66
Rb	30.45	0.01	30.62	6.73	34.85	15.06	20.72	13.68	0.01	15.71
Sr	55.21	42.81	27.87	30.71	74.43	30.51	103.35	132.93	97.47	87.19

Th										
U										
V	120.30	794.94	78.65	106.59	91.84	43.98	59.75	99.61	319.58	141.63
Y	11.41	5.99	10.07	7.94	15.74	14.58	11.89	7.98	10.10	13.84
Zn	121.20	211.52	155.60	145.80	331.82	74.60	147.34	165.50	170.78	149.84
Zr	37.96	36.78	32.44	36.42	73.83	35.53	62.03	42.23	45.90	42.56
Au			356	329		16		187		12
Pd			2,000	1,673		72	12	1,692		40
Pt			1,875	1,155		72	12	2,260		81

Table 16: Whole rock element geochemistry of samples from borehole ZF078.

Sample ID	ZF078-9	ZF078-17	ZF078-21	ZF078-22	ZF078-34	ZF078-42	ZF078-47	ZF078-49	ZF078-50	ZF078-52	ZF078-53	ZF078-15	ZF078-64	ZF078-39	ZF078-28	ZF078-30	ZF078-6
Lithology	**FP**	**FP**	**P**	**P**	**P**	**P**	**P**	**C**	**C**	**H**	**S**	**FP**	**FP**	**FP**	**FP**	**MN**	**MN**
Unit	**P1**	**P1**	**P1**	**P1**	**P1**	**P1**	**P1**	**P1**	**P1**	**P2**	**P2**	**P3**	**P3**	**P3**	**P3**	**P4**	**P4**
SiO2	46.92	45.81	42.63	44.48	45.17	45.01	43.72	44.73	31.78	41.95	16.07	46.33	52.44	50.03	40.37	44.67	46.22
Al2O3	5.19	5.12	1.70	2.46	1.69	3.53	3.42	2.16	13.70	3.74	1.17	7.26	7.00	5.96	6.06	2.34	14.74
Fe2O3	22.57	15.22	23.16	17.90	18.57	22.21	22.94	21.12	27.61	17.88	13.94	14.98	19.47	18.42	8.44	15.74	10.97
MnO	0.39	0.40	0.44	0.36	0.39	0.38	0.34	0.32	0.01	0.15	0.14	0.28	0.15	0.35	0.22	0.40	0.21
MgO	16.02	19.21	20.87	19.66	20.83	16.70	19.05	23.17	14.58	29.64	48.84	20.89	10.65	13.93	21.98	17.98	14.76
CaO	5.85	11.60	8.06	13.05	10.86	7.50	7.55	6.52	6.91	2.39	0.03	6.94	2.79	7.84	17.14	16.71	10.22
Na2O	0.61	0.34	0.11	0.20	0.13	0.61	0.42	0.18	0.66	0.02	0.01	0.67	1.75	1.09	0.15	0.11	1.04
K2O	0.42	0.35	0.16	0.18	0.12	0.44	0.11	0.09	0.80	0.00	0.00	0.21	0.46	1.14	0.70	0.04	0.15
TiO2	0.29	0.14	0.16	0.18	0.17	0.20	0.26	0.18	0.87	0.21	0.15	0.20	0.48	0.22	0.26	0.19	0.16
P2O5	0.03	0.01	0.01	0.01	0.01	0.03	0.01	0.03	0.02	0.01	0.01	0.02	0.02	0.05	0.03	0.02	0.01
LOI	1.40	1.39	1.60	1.00	1.80	2.00	0.80	0.40	0.20	3.39	18.96	1.99	2.40	0.20	4.19	1.40	1.39
Total	99.70	99.60	98.90	99.47	99.74	98.60	98.64	98.89	97.14	99.39	99.31	99.77	97.61	99.25	99.56	99.60	99.86
SO3	0.21	0.34	0.98	0.46	0.19	1.26	1.30	1.09	2.93	0.53	0.97	0.11	2.27	0.74	0.23	0.27	0.01
As	1.915	1.915	1.915	1.915	1.915	1.915	1.915	1.915	1.915	1.915	1.915	1.915	1.915	1.915	1.915	1.915	1.915
Ba	56.66	55.52	42.85	120.34	113.06	7.71	29.64	1.53	1.53	9.35	1.53	81.57	720.29	90.34	33.20	32.56	13.40
Ce	2.38	2.38	19.72	6.18	2.38	2.38	18.89	2.38	27.55	2.38	2.38	11.42	19.63	38.02	28.65	2.38	21.42
Co	101.3	160.42	100.97	65.30	91.73	149.58	171.46	205.96	177.38	102.20	98.92	78.15	2.35	128.31	72.89	77.90	91.51

Cr	2,230	1,591	1,440	255	1,276	4,742	2,522	103,07	29,262	0	475	2,044	70	1,752	1,340	1,387	1,232
Cu	568	2,383	1,677	388	1,129	1,876	1,892	2,918	1,287	4,467	3,404	1,290	56	5,035	996	934	1
Mo	0.78	0.83	0.81	0.87	0.85	0.82	0.81	0.82	0.81	0.83	0.89	0.75	0.81	0.82	0.84	0.84	4.78
Nb	2.76	4.40	4.50	3.95	6.46	2.49	5.15	7.34	2.52	5.39	4.25	4.92	6.08	5.59	1.81	2.51	917.3
Ni	1,331	4,190	2,120	1,794	3,259	4,844	5,729	7,155	2,886	5,164	6,030	1,572	7	3,162	1,545	1,176	0.08
Pb	0.08	0.32	0.08	15.20	9.54	0.87	5.59	0.08	0.08	9.29	8.06	0.08	56.74	0.08	12.32	0.08	9.54
Rb	12.09	0.01	3.08	46.99	22.74	0.01	0.01	0.01	0.01	15.77	0.01	16.48	83.91	2.57	0.01	0.01	63.11
Sr	89.79	34.33	41.30	114.70	74.78	51.60	33.68	79.89	36.27	24.03	84.17	57.90	789.17	55.05	30.73	34.62	14.47
Th	14.47	14.47	14.47	14.47	14.47	14.47	14.47	14.47	14.47	14.47	14.47	14.47	14.47	14.47	14.47	14.47	1.05
U	1.05	1.05	1.05	1.05	1.05	1.05	1.05	1.05	1.05	1.05	1.05	1.05	77.06	1.05	1.05	1.05	202.6
V	126.9	101.45	114.86	84.42	95.84	174.40	103.34	712.03	232.39	30.49	88.80	116.86	14.40	94.82	116.35	131.95	17.18
Y	9.23	7.06	13.04	19.55	17.53	8.65	10.04	8.01	5.80	3.42	12.36	13.75	17.89	11.33	12.04	13.40	170.6
Zn	169.3	118.32	93.15	67.68	3.00	114.86	101.51	248.71	216.81	110.73	36.36	93.15	114.38	113.42	106.79	57.31	38.67
Zr	40.91	37.29	38.27	64.29	48.94	39.15	36.77	38.85	35.66	47.16	57.08	34.63	92.83	43.31	47.53	35.46	
Au			166		113		358	1,398	77	114				977			
Pd			2,032		2,588		4,143	12,788	353	4,343				1,782			
Pt			1,685		2,257		2,978	10,288	158	2,118				1,493			

Table 17: Whole rock element geochemistry of samples from borehole ZF082.

Sample ID	ZF082-60	ZF082-37	ZF082-59
Lithology	**H**	**FP**	**FP**
Unit	**P2**	**P3**	**P3**
SiO2	41.25	45.77	44.71
Al2O3	2.34	7.42	12.25
Fe2O3	15.52	12.24	10.94
MnO	0.15	0.24	0.19
MgO	30.18	23.61	14.78
CaO	3.12	6.80	9.39
Na2O	0.04	0.42	1.03
K2O	0.55	0.31	0.72
TiO2	0.13	0.14	0.17
P2O5	0.02	0.01	0.02
LOI	6.48	2.82	5.04
Total	99.77	99.79	99.23
SO3	0.25	0.03	0.00
As	0.85	0.85	0.85
Ba	80	80	133
Ce	6	6	6
Co	141	84	52
Cr	718	2,410	1,171
Cu	333	487	112
Mo	0.77	0.77	0.78
Nb	4.01	6.84	0.73
Ni	1,362	1,083	413
Pb	-2.15	34.80	0.11
Rb	43.25	26.11	36.44
Sr	48.97	74.84	135.79
Th	0.01	0.01	0.01
U	0.23	0.23	0.23
V	62.06	109.63	114.03
Y	11.72	10.38	10.13
Zn	242.94	123.61	90.74

Zr	38.62	35.52	42.06
Au			
Pd			
Pt			

Table 18: Whole rock element geochemistry of samples from borehole ZF048.

Sample ID	**ZF048-48**	**ZF048-45**	**ZF048-46**	**ZF048-49**	**ZF048-50**	**ZF048-52**	**ZF048-44**
Lithology	**H**	**H**	**H**	**SH**	**SH**	**SH**	**FP**
Unit	**P2**	**P2**	**P2**	**P2**	**P2**	**P2**	**P3**
SiO2	44.45	47.65	48.16	34.05	34.40	31.83	45.99
Al2O3	2.18	3.00	4.88	1.90	1.14	1.58	9.14
Fe2O3	15.19	12.78	12.16	16.01	15.94	18.71	11.39
MnO	0.27	0.26	0.24	0.17	0.16	0.12	0.22
MgO	31.57	30.24	27.01	37.43	38.03	36.08	19.59
CaO	3.22	3.43	4.97	2.45	1.55	1.28	8.69
Na2O	0.084	0.142	0.325	0.092	0.018	0.003	0.755
K2O	0.029	0.162	0.123	0.102	0.000	0.048	0.060
TiO2	0.128	0.131	0.141	0.082	0.091	0.084	0.147
P2O5	0.006	0.006	0.006	0.005	0.008	0.011	0.007
LOI	2.55	2.20	1.98	7.56	8.65	10.08	2.19
Total	99.67	100.00	100.00	99.85	99.98	99.82	98.18
SO3	0.33	0.00	0.00	0.15	0.02	0.18	1.82
As	1.832	1.982	1.982	1.982	1.982	1.982	1.832
Ba	44.25	66.01	54.88	95.84	51.88	79.81	45.56
Ce	1.38	5.44	5.44	5.44	7.06	5.44	3.86
Co	121.13	95.86	89.12	178.92	229.08	171.07	62.73
Cr	3,641	3,883	3,117	449	3,905	987	1,698
Cu	1,085	162	129	528	247	1,025	162
Mo	0.765	0.764	0.748	0.738	0.794	0.776	0.782
Nb	3.986	1.591	0.037	2.442	6.835	4.402	0.083
Ni	1,799	986	781	1,988	2,196	2,012	562
Pb	3.719	1.785	1.785	3.806	1.785	5.823	0.271

Rb	10.53	22.49	18.84	11.35	4.36	6.61	16.75
Sr	34.20	57.71	64.85	42.64	32.72	44.46	105.34
Th	14.57	14.32	14.32	14.32	14.32	14.32	14.57
U	0.027	0.117	0.117	0.117	0.117	0.117	0.027
V	80.92	113.38	114.44	37.24	57.37	22.37	117.59
Y	6.20	9.00	6.39	6.05	7.19	6.32	7.62
Zn	153.30	144.94	116.98	77.97	81.23	34.82	136.38
Zr	33.10	32.64	39.30	33.27	33.16	34.95	40.88
Au	36	36	5	12		245	5
Pd	210	113	12	129		1,994	16
Pt	181	628	121	181		1,230	5

Table 18: Whole rock element geochemistry of a sample from borehole MO023.

Sample ID	**MO023-21**
Lithology	**MN**
Unit	**P4**
SiO2	50.97
Al2O3	7.15
Fe2O3	16.04
MnO	0.30
MgO	10.99
CaO	11.16
Na2O	1.0069
K2O	0.7962
TiO2	0.4574
P2O5	0.0995
LOI	0.70
Total	99.66
SO3	0.29
As	-33.978
Ba	26.3850
Ce	44.8040

Co	82.650
Cr	383.905
Cu	479.288
Mo	0.887
Nb	8.777
Ni	319.622
Pb	4.364
Rb	22.7550
Sr	82.945
Th	-10.6460
U	-38.327
V	206.752
Y	38.895
Zn	167.803
Zr	60.923
Au	
Pd	32
Pt	8

Appendix C: Normative mineral calculations.

Table 19 to 24 below shows the modal mineralogical compositions as quantified by the CIPW norm based upon available geochemical data for boreholes ZF044, ZF045, ZF057, ZF048, ZF078, ZF082 and MO023. The units and rock type short code are similar to those given in Appendix B.

Table 19: Normative mineralogical calculations of samples from borehole ZF044.

Sample ID	ZF044-47	ZF044-31	ZF044-32	ZF044-39	ZF044-51	ZF044-28	ZF044-43	ZF044-57	ZF044-58	ZF044-1	ZF044-16
Unit	**P1**	**P2**	**P2**	**P2**	**P3**	**P3**	**P4**	**P4**	**P4**	**P4**	**P4**
Lithology	**P**	**SH**	**SH**	**SH**	**FP**	**FP**	**MN**	**MN**	**MN**	**MN**	**MN**
Quartz	1.366	0	0	0	0	0	0	0	0	0	0
Corundum	0	0	0	0	0	0	0	0	0	0	0
Orthoclase	0.209	1.799	0.318	0	0.999	0.435	0.282	0	0	0.886	0.733
Albite	0.607	0.921	0.025	0	7.543	4.249	1.632	0	0	9.847	9.962
Anorthite	6.03	4.774	1.638	5.961	16.894	16.806	6.119	15.794	5.214	38.637	40.622
Leucite	0	0	0	25.898	0	0	0	51.35	69.212	0	0
Nepheline	0	0	0	0.225	0	0	0	3.927	2.851	1.187	0
Kaliopphilite	0	0	0	-18.541	0	0	0	-36.023	-50.038	0	0
Diopside	30.741	31.317	13.277	0	13.785	13.665	60.999	0	0	32.87	30.205
Hypersthene	39.135	1.049	8.005	0	39.763	47.127	0.717	0	0	0	0.918
Olivine	0	38.998	48.761	54.087	6.396	2.799	13.489	26.428	27.013	6.629	6.984
Dicalcium Silicate	0	0	0	10.15	0	0	0	25.763	28.78	0	0
Magnetite	0.792	0.215	0.336	0.785	0.356	0.326	0.708	0	0.235	0	0
Ilmenite	0.292	0.286	0.192	0.199	0.303	0.297	0.354	0.288	0.298	0.312	0.337
Hemaetite	17.48	12.793	18.024	14.646	13.146	12.477	12.899	7.391	11.339	7.32	7.892
Sphene	0	0	0	0	0	0	0	0	0	0	0.016
Perovskite	0	0	0	0	0	0	0	0.1	0	0.029	0
Rutile	0	0	0	0	0	0	0	0	0	0	0
Apatite	0.012	0.021	0.017	0.02	0.022	0.019	0.028	0.149	0.618	0.033	0.027
Sum	96.663	92.173	90.592	93.428	99.209	98.2	97.227	95.167	95.522	97.75	97.696

Table 20: Normative mineralogical calculations of samples from borehole ZF045.

Sample ID	ZF045-46	ZF045-28	ZF045-44	ZF045-8	ZF045-27
Unit	**P1**	**P2**	**P3**	**P4**	**P4**
Lithology	**P**	**FH**	**FP**	**MN**	**MN**
Quartz	4.888	0	0	0	0
Corundum	0	0	0	0	0
Orthoclase	0.899	0	4.403	0.203	1.749
Albite	3.488	0	12.538	3.62	5.937
Anorthite	5.516	14.867	15.771	14.023	11.333
Leucite	0	8.464	0	0	0
Nepheline	0	0.523	0	0	0
Kaliopphilite	0	-3.8	0	0	0
Diopside	16.251	0	16.388	53.212	56.258
Hypersthene	39.815	0	29.888	6.055	0.723
Olivine	0	53.788	2.183	9.753	9.829
Dicalcium Silicate	0	6.252	0	0	0
Magnetite	0.076	0.645	0.305	0	0.044
Ilmenite	0.316	0.226	0.348	0.508	0.4
Hemaetite	21.051	12.292	12.307	10.43	9.842
Sphene	0	0	0	0.042	0
Perovskite	0	0	0	0	0
Rutile	0	0	0	0	0
Apatite	0.088	0.032	0.024	0.062	0.057
Sum	92.39	93.289	94.155	97.907	96.171

Table 21: Normative mineralogical calculations of samples from borehole ZF057.

Sample ID	ZF057-38	ZF057-53	ZF057-29	ZF057-30	ZF057-33	ZF057-40	ZF057-47	ZF057-46	ZF057-54	ZF057-44
Unit	**P1**	**P1**	**P2**	**P2**	**P2**	**P2**	**P2**	**P3**	**P3**	**P3**
Lithology	**P**	**C**	**SH**	**H**	**FH**	**SH**	**FH**	**FP**	**FP**	**FP**
Quartz	0	0	0	0	0	0	0	0	0	3.831
Corundum	0	2.34	0	0	0	0	0	0	0	0
Orthoclase	1.359	1.182	1.95	0.65	0	0	0	1.3	3.841	2.305
Albite	3.3	8.039	0	1.269	0	0	0	8.885	11	7.023
Anorthite	8.075	22.213	2.845	4.268	27.957	6.171	16.796	20.231	19.067	10.839
Leucite	0	0	0	0	-24.847	-3.01	13.279	0	0	0
Nepheline	0	0	0	0	0.963	0.092	1.65	0	0	0
Kaliopphilite	0	0	0	0	19.585	2.198	-9.12	0	0	0
Diopside	24.043	0	7.659	8.444	0	0	0	11.723	9.189	12.983
Hypersthene	41.453	9.753	39.395	62.412	0	0	0	37.268	20.354	46.886
Olivine	1.244	20.412	25.219	3.965	55.872	66.921	53.708	5.037	15.339	0
Dicalcium Silicate	0	0	0	0	2.862	10.893	12.053	0	0	0
Magnetite	0.418	0	0.791	0.45	0.178	0.57	0.526	0.225	0	0.233
Ilmenite	0.475	0.171	0.209	0.304	0.589	0.247	0.361	0.323	0.171	0.361
Hemaetite	17.832	32.7	16.094	16.699	9.927	9.177	8.047	11.854	15.69	12.909
Sphene	0	0	0	0	0	0	0	0	0.859	0
Perovskite	0	0	0	0	0	0	0	0	0	0
Rutile	0	1.08	0	0	0	0	0	0	0	0
Apatite	0.047	0.095	0.024	0.024	0.308	0.024	0.047	0.047	0.237	0.024
Sum	98.246	97.984	94.186	98.485	93.394	93.282	97.348	96.895	95.747	97.394

Table 22: Normative mineralogical calculations of samples from borehole ZF078.

Sample ID	ZF078-9	ZF078-17	ZF078-21	ZF078-22	ZF078-34	ZF078-42	ZF078-47	ZF078-49	ZF078-50	ZF078-52	ZF078-53	ZF078-15	ZF078-64	ZF078-39	ZF078-28	ZF078-30	ZF078-6
Unit	**P1**	**P1**	**P1**	**P1**	**P1**	**P1**	**P1**	**P1**	**P1**	**P2**	**P2**	**P3**	**P3**	**P3**	**P3**	**P4**	**P4**
Lithology	**FP**	**FP**	**P**	**P**	**P**	**P**	**P**	**C**	**C**	**H**	**S**	**FP**	**FP**	**FP**	**FP**	**MN**	**MN**
Quartz	9.45	0	0.84	0	0.49	5.67	2.85	0.80	0	0	0	0	19.515	8.50	0	0	0
Corundum	0	0	0	0	0	0	0	0	0	0	1.111	0	0	0	0	0	0
Orthoclase	2.48	2.10	0.97	1.04	0.70	2.61	0.65	0.54	4.75	0.02	0.00	1.21	2.71	6.72	0.00	0.21	0.89
Albite	5.19	2.91	0.94	1.69	1.09	5.18	3.55	1.53	5.56	0.21	0.00	5.68	14.84	9.25	0.00	0.90	8.84
Anorthite	10.16	11.3	3.66	5.30	3.67	5.58	7.11	4.83	32.05	10.08	0.13	16.19	9.87	8.00	13.80	5.79	35.10
Leucite	0	0	0	0	0	0	0	0	0	0	-74.08	0	0	0	33.32	0	0
Nepheline	0	0	0	0	0	0	0	0	0	0	0.03	0	0	0	0.70	0	0
Kaliopphilite	0	0	0	0	0	0	0	0	0	0	53.69	0	0	0	-21.81	0	0
Diopside	14.50	35.9	28.19	46.22	39.05	24.47	23.56	21.28	0.00	1.24	0.00	14.10	2.13	23.78	0.00	59.91	12.08
Hypersthene	33.19	27.6	38.91	21.60	33.78	30.25	36.53	47.83	0.00	49.45	0.00	44.14	25.54	23.69	0.00	10.29	28
Olivine	0	2.50	0	4.17	0	0	0	0	25.45	16.68	85.24	0.95	0	0	38.37	4.72	2.21
Dicalcium Silicate	0	0	0	0	0	0	0	0	0	0	0	0	0	0	21.98	0	0
Magnetite	0.43	0.90	0.99	0.65	0.79	0.67	0.36	0.52	0	0	0.014	0.336	0	0.488	0	0.761	0.221
Ilmenite	0.55	0.26	0.30	0.34	0.32	0.37	0.50	0.35	0.02	0.32	0.29	0.38	0.33	0.43	0.48	0.35	0.30
Hemaetite	22.27	14.6	22.48	17.45	18.02	21.75	22.70	20.76	27.61	17.88	13.93	14.75	19.47	18.08	8.44	15.22	10.82
Sphene	0	0	0	0	0	0	0	0	0.57	0.094	0	0	0.757	0	0	0	0
Perovskite	0	0	0	0	0	0	0	0	0.63	0	0	0	0	0	0.006	0	0
Rutile	0	0	0	0	0	0	0	0	0.25	0	0	0	0	0	0	0	0
Apatite	0.08	0.01	0.03	0.03	0.03	0.06	0.03	0.06	0.05	0.03	0.01	0.05	0.05	0.13	0.08	0.06	0.03
Sum	98.31	98.21	97.31	98.48	97.94	96.61	97.84	98.50	96.94	96.00	80.36	97.78	95.21	99.06	95.37	98.21	98.48

Table 23: Normative mineralogical calculations of samples from borehole ZF082.

Sample ID	ZF082-60	ZF082-37	ZF082-59
Unit	**P2**	**P3**	**P3**
Lithology	**H**	**FP**	**FP**
Quartz	0	0	0
Corundum	0	0	0
Orthoclase	3.255	1.852	4.268
Albite	0.329	3.559	8.698
Anorthite	4.588	17.434	26.674
Leucite	0	0	0
Nepheline	0	0	0
Kaliopphilite	0	0	0
Diopside	8.377	12.636	15.423
Hypersthene	36.607	39.229	23.416
Olivine	24.301	9.611	4.372
Dicalcium Silicate	0	0	0
Magnetite	0.101	0.382	0.151
Ilmenite	0.254	0.272	0.316
Hemaetite	15.447	11.974	10.836
Sphene	0	0	0
Perovskite	0	0	0
Rutile	0	0	0
Apatite	0.04	0.025	0.041
Sum	93.299	96.976	94.195

Table 24: Normative mineralogical calculations of samples from borehole ZF048.

Sample ID	ZF048-48	ZF048-45	ZF048-46	ZF048-49	ZF048-50	ZF048-52	ZF048-44
Unit	**P2**	**P2**	**P2**	**P2**	**P2**	**P2**	**P3**
Lithology	**H**	**H**	**H**	**SH**	**SH**	**SH**	**FP**
Quartz	0	0	0	0	0	0	0
Corundum	0	0	0	0	0	0	0
Orthoclase	0.171	0.957	0.727	0.605	0.002	0.282	0.356
Albite	0.712	1.201	2.75	0.777	0.151	0.024	6.393
Anorthite	5.486	7.08	11.504	4.47	3.035	4.17	21.374
Leucite	0	0	0	0	0	0	0
Nepheline	0	0	0	0	0	0	0
Kaliopphilite	0	0	0	0	0	0	0
Diopside	8.139	7.699	10.215	5.95	3.58	1.647	16.878
Hypersthene	48.664	58.144	54.955	2.751	10.515	7.516	35.098
Olivine	18.353	9.541	5.318	61.466	57.84	57.171	4.124
Dicalcium Silicate	0	0	0	0	0	0	0
Magnetite	0.507	0.467	0.376	0.301	0.243	0.151	0.294
Ilmenite	0.243	0.248	0.268	0.156	0.173	0.159	0.278
Hemaetite	14.836	12.457	11.898	15.802	15.775	18.605	11.185
Sphene	0	0	0	0	0	0	0
Perovskite	0	0	0	0	0	0	0
Rutile	0	0	0	0	0	0	0
Apatite	0.014	0.014	0.013	0.012	0.019	0.026	0.017
Sum	97.125	97.809	98.023	92.29	91.334	89.751	95.997

Table 25: Normative mineralogical calculations of samples from borehole MO023.

Sample ID	MO023-21
Unit	**P4**
Lithology	**MN**
Quartz	11.135
Corundum	0
Orthoclase	4.705
Albite	8.52
Anorthite	12.635
Leucite	0
Nepheline	0
Kaliopphilite	0
Diopside	32.435
Hypersthene	12.333
Olivine	0
Dicalcium Silicate	0
Magnetite	0
Ilmenite	0.646
Hemaetite	16.04
Sphene	0.289
Perovskite	0
Rutile	0
Apatite	0.236
Sum	98.974

Appendix D: Mineral Chemistry data

Table D.1: Representative compositions for Olivine

SAMPLE ID	UNIT	SiO2	MgO	Mg	TiO2	CaO	Al2O3	Al	Cr2O3	Cr	FeO	Fe	MnO	NiO	Total	Mg#	Cr/ (Cr+Al)
zf048-50-OLIVINE2-CORE1	**P2**	39.19	42.9	25.88	0.04	0.06	-	0.00	0.04	0.03	18.14	16.32	0.31	0.10	100.77	0.61	
zf048-50-OLIVINE2-CORE2	**P2**	38.95	42.6	25.70	-	0.02	0.06	0.04	0.02	0.01	18.21	16.39	0.34	0.15	100.35	0.61	0.28
zf048-50-OLIVINE2-RIM1	**P2**	39.37	42.73	25.77	-	0.05	0.15	0.09	-		17.98	16.18	0.26	0.10	100.64	0.61	0.00
zf048-50-OLIVINE3-CORE1	**P2**	55.27	30.68	18.51	0.06	0.63	1.05	0.63	0.15	0.11	11.49	10.34	0.26	-	99.60	0.64	0.14
zf048-50-OLIVINE4-CORE1	**P2**	39.24	42.73	25.77	0.02	0.04	-		-		18.58	16.72	0.25	0.13	100.99	0.61	
zf048-50-OLIVINE4-CORE2	**P2**	39.25	42.4	25.57	0.02	0.06	0.03	0.02	-		18.38	16.54	0.26	0.16	100.55	0.61	0.00
zf048-50-OLIVINE4-CORE3	**P2**	39.09	42.54	25.66	-	0.02	0.04	0.03	0.02	0.01	18.45	16.60	0.24	0.11	100.51	0.61	0.35
zf048-50-OLIVINE4-RIM	**P2**	39.52	42.69	25.75	0.03	0.05	0.12	0.07	-		17.90	16.11	0.26	0.17	100.73	0.62	0.00
zf048-50-OLIVINE4-RIM1	**P2**	39.03	42.74	25.78	0.02	0.05	0.06	0.03	0.03	0.02	17.93	16.13	0.19	0.13	100.16	0.62	0.34
zf048-50-OLIVINE5-CORE1	**P2**	39.12	42.66	25.73	0.03	0.07	-		-		18.06	16.25	0.31	0.10	100.34	0.61	
zf048-50-OLIVINE5-CORE2	**P2**	39.05	42.73	25.77	0.01	0.05	-		0.01	0.01	18.00	16.20	0.29	0.15	100.29	0.61	
zf048-50-OLIVINE5-RIM1	**P2**	39.55	42.36	25.55	0.06	0.02	-		-		17.62	15.85	0.35	0.13	100.10	0.62	
zf048-50-OLIVINE5-RIM2	**P2**	39.46	42.3	25.51	0.01	0.00	-		0.02	0.01	17.93	16.13	0.26	0.13	100.11	0.61	
zf048-50-OLIVINE6-CORE1	**P2**	39.29	42.45	25.60	0.00	0.05	0.02	0.01	0.00	0.00	18.02	16.21	0.27	0.15	100.26	0.61	0.08
zf048-50-OLIVINE6-CORE2	**P2**	39.3	42.1	25.39	-	0.03	-		0.02	0.01	17.74	15.96	0.26	0.14	99.59	0.61	
zf048-50-OLIVINE6-RIM1	**P2**	39.09	42.74	25.78	0.02	0.05	0.05	0.03	-		18.03	16.22	0.24	0.08	100.29	0.61	0.00
zf048-50-OLIVINE6-RIM2	**P2**	39.56	42.45	25.60	0.01	0.03	0.00	0.00	0.01	0.01	18.17	16.35	0.27	0.15	100.65	0.61	0.83
zf044-39-OLIVINE1-CORE1	**P2**	42.11	38.01	22.93	-	0.10	0.04	0.03	0.02	0.01	3.25	2.92	0.11	0.04	83.69	0.89	0.34
zf044-39-OLIVINE1-CORE2	**P2**	38.57	39.24	23.67	0.00	0.05	0.06	0.04	-		22.11	19.89	0.47	0.08	100.59	0.54	0.00
zf044-39-OLIVINE1-CORE3	**P2**	38.71	39.02	23.54	-	0.07	-		0.02	0.01	22.14	19.92	0.51	0.09	100.55	0.54	
zf044-39-OLIVINE1-CORE4	**P2**	38.63	39.05	23.55	-	0.09	0.03	0.02	0.01	0.01	22.09	19.88	0.50	0.09	100.49	0.54	0.32
zf044-39-OLIVINE1-RIM	**P2**	38.82	38.93	23.48	-	0.06	-		-		22.25	20.02	0.43	0.11	100.60	0.54	
zf044-39-OLIVINE1-RIM1	**P2**	38.8	39.2	23.64	0.02	0.02	0.06	0.03	-		22.31	20.07	0.47	0.11	100.98	0.54	0.00

Table 27: Representative compositions for Orthopyroxene

SAMPLE I.D	UNIT	Al2O3	Al	SiO2	TiO2	CaO	MgO	Mg	Cr2O3	Cr	FeO	Fe	Na2O	MnO	Total	Mg#	Cr/ (Cr + Al)
zf048-46-opx1-core	**P1**	1.65	0.87	55.17	0.04	1.18	29.27	17.65	0.46	0.32	12.48	9.70	0.02	0.31	100.59	0.65	0.27
zf048-46-opx1-core2	**P1**	1.55	0.82	54.51	0.07	1.57	29.15	17.58	0.55	0.38	12.24	9.51	0.01	0.27	99.93	0.65	0.31
zf048-46-opx1-rim	**P1**	1.78	0.94	54.64	0.13	1.33	29.57	17.84	0.53	0.36	12.57	9.77	0.03	0.27	100.84	0.65	0.28
zf048-46-opx1-rim1	**P1**	1.65	0.87	55.15	0.08	1.95	28.71	17.32	0.50	0.34	11.23	8.73	0.04	0.28	99.59	0.66	0.28
zf048-46-opx2-core2	**P1**	1.70	0.90	54.14	0.13	6.05	26.28	15.85	0.52	0.36	9.72	7.56	0.08	0.27	98.90	0.68	0.28
zf048-46-opx2-core3	**P1**	1.90	1.01	53.85	0.12	0.59	29.19	17.61	0.63	0.43	11.63	9.04	0.02	0.24	98.16	0.66	0.30
zf048-46-opx3-CORE	**P1**	2.10	1.11	54.46	0.14	1.53	28.77	17.35	0.50	0.34	11.38	8.85	0.03	0.23	99.14	0.66	0.23
zf048-46-opx3-RIM	**P1**	1.15	0.61	55.02	0.20	0.77	29.70	17.91	0.52	0.36	11.95	9.29	0.03	0.29	99.63	0.66	0.37
zf044-47-opx1-CORE1	**P1**	1.54	0.81	53.76	0.14	1.22	24.53	14.80	0.31	0.21	17.28	13.43	0.03	0.42	99.23	0.52	0.21
zf044-47-opx1-RIM1	**P1**	1.29	0.68	53.43	0.16	1.17	24.37	14.70	0.19	0.13	17.61	13.69	0.05	0.48	98.75	0.52	0.16
zf044-47-opx1-RIM2	**P1**	1.44	0.76	53.18	0.19	1.92	24.18	14.58	0.27	0.19	17.40	13.53	0.04	0.44	99.06	0.52	0.20
zf078-34-opx1-CORE	**P1**	1.36	0.72	54.31	0.09	0.90	25.01	15.09	0.18	0.13	18.02	14.01	0.05	0.41	100.33	0.52	0.15
zf078-34-opx1-RIM2	**P1**	1.04	0.55	54.21	0.10	2.35	23.27	14.04	0.23	0.15	17.99	13.98	0.05	0.44	99.68	0.50	0.22
zf078-34-opx2-CORE1	**P1**	0.94	0.50	53.44	0.12	1.11	24.34	14.68	0.13	0.09	18.62	14.47	-	0.44	99.15	0.50	0.16
zf078-34-opx2-RIM1	**P1**	1.13	0.60	53.49	0.09	0.82	24.10	14.54	0.19	0.13	19.06	14.82	0.02	0.44	99.34	0.50	0.18
zf078-34-opx3-CORE1	**P1**	1.28	0.68	54.07	0.11	0.72	24.58	14.83	0.11	0.08	18.70	14.54	0.05	0.48	100.12	0.50	0.10
zf078-34-opx3-RIM1	**P1**	1.41	0.75	53.55	0.09	1.16	24.33	14.68	0.16	0.11	18.07	14.05	0.00	0.48	99.26	0.51	0.13
zf078-34-opx3-RIM2	**P1**	1.40	0.74	53.02	0.17	1.39	24.08	14.52	0.18	0.12	18.28	14.21	0.03	0.45	98.99	0.51	0.14
zf078-34-opx4-CORE	**P1**	1.39	0.74	53.03	0.10	0.89	24.56	14.81	0.30	0.21	18.34	14.26	0.07	0.46	99.13	0.51	0.22
zf078-34-opx4-RIM2	**P1**	1.19	0.63	53.42	0.11	2.03	23.74	14.32	0.19	0.13	18.20	14.15	0.06	0.42	99.35	0.50	0.17
zf078-34-opx5-CORE	**P1**	1.18	0.63	53.77	0.09	0.78	25.15	15.17	0.12	0.08	17.74	13.79	-	0.42	99.25	0.52	0.12
zf078-34-opx5-RIM1	**P1**	1.64	0.87	53.11	0.12	1.81	24.70	14.90	0.20	0.14	16.94	13.17	0.08	0.44	99.04	0.53	0.14
zf078-47-opx1-CORE1	**P1**	1.72	0.91	53.03	0.10	1.68	24.00	14.48	0.39	0.26	17.56	13.65	0.03	0.40	98.91	0.51	0.23
zf078-47-opx1-CORE2	**P1**	1.09	0.58	54.08	0.12	2.07	23.96	14.45	0.32	0.22	17.60	13.68	0.05	0.47	99.76	0.51	0.27
zf078-47-opx1-RIM	**P1**	1.11	0.59	53.59	0.19	2.40	23.84	14.38	0.23	0.16	17.31	13.46	0.05	0.47	99.20	0.52	0.21
zf048-48-opx1-core1	**P2**	1.82	0.96	55.23	0.07	3.44	28.48	17.18	0.60	0.41	9.26	7.20	0.10	0.26	99.25	0.70	0.30
zf048-48-opx3-core1	**P2**	1.83	0.97	55.57	0.08	2.24	29.26	17.65	0.60	0.41	10.18	7.91	0.08	0.28	100.12	0.69	0.30

zf048-48-opx3-core2	**P2**	1.70	0.90	55.81	0.06	1.19	29.67	17.90	0.49	0.33	10.41	8.09	0.05	0.26	99.64	0.69	0.27
zf048-48-opx3-rim	**P2**	1.60	0.85	55.30	0.16	0.59	30.48	18.38	0.46	0.32	10.46	8.13	0.05	0.29	99.39	0.69	0.27
zf048-48-opx4-core2	**P2**	1.54	0.82	56.80	0.04	2.50	28.69	17.30	0.51	0.35	9.42	7.32	0.10	0.22	99.82	0.70	0.30
zf048-48-opx4-rim1	**P2**	2.41	1.28	54.48	0.04	0.50	29.72	17.93	1.58	1.08	11.52	8.95	0.02	0.27	100.54	0.67	0.46
zf048-48-opx4-rim2	**P2**	1.62	0.86	56.42	0.06	1.28	29.59	17.85	0.50	0.35	9.85	7.66	0.04	0.32	99.69	0.70	0.29
zf048-48-opx5-core1	**P2**	1.76	0.93	55.47	0.14	2.41	28.91	17.44	0.62	0.43	9.89	7.69	0.08	0.31	99.59	0.69	0.31
zf048-48-opx5-rim1	**P2**	1.90	1.01	54.62	0.08	1.87	29.01	17.50	0.57	0.39	10.35	8.05	0.06	0.32	98.79	0.69	0.28
zf048-48-opx5-rim2	**P2**	1.65	0.87	55.25	0.04	2.53	29.12	17.56	0.63	0.43	9.78	7.60	0.05	0.36	99.41	0.70	0.33
zf048-48-opx6-core2	**P2**	1.72	0.91	55.44	0.07	0.34	30.16	18.19	0.51	0.35	10.74	8.35	0.02	0.25	99.26	0.69	0.28
zf048-48-opx6-core3	**P2**	1.69	0.89	55.64	0.07	0.42	30.03	18.11	0.50	0.34	10.78	8.38	0.03	0.28	99.44	0.68	0.28
zf048-48-opx6-rim1	**P2**	7.20	3.81	47.36	0.35	8.56	21.50	12.97	0.33	0.22	7.81	6.07	0.76	0.18	94.05	0.68	0.06
zf048-48-opx6-rim2	**P2**	1.39	0.73	55.81	0.21	0.59	30.30	18.28	0.41	0.28	11.00	8.55	0.01	0.27	99.98	0.68	0.27
zf048-48-opx6-rim3	**P2**	0.01	0.00	39.42	-	0.02	42.67	25.74	0.01	0.01	16.55	12.86	-	0.25	98.92	0.67	0.67
zf048-50-opx1-CORE1	**P2**	1.15	0.61	56.37	0.04	0.60	30.93	18.66	0.19	0.13	10.52	8.18	0.02	0.26	100.08	0.70	0.18
zf048-50-opx1-RIM1	**P2**	0.00	0.00	40.25	-	0.04	42.25	25.48	-		16.37	12.72	0.04	0.21	99.16	0.67	0.00
zf048-50-opx1-CORE3	**P2**	1.90	1.01	56.07	0.09	0.73	29.90	18.03	0.35	0.24	10.82	8.41	0.01	0.28	100.14	0.68	0.19
zf048-50-opx3-CORE4	**P2**	-		39.91	0.03	0.03	42.80	25.82	-		16.72	13.00	0.02	0.30	99.81	0.67	
zf048-50-opx3-RIM1	**P2**	0.03	0.02	39.98	0.03	0.05	42.73	25.77	0.02	0.01	16.65	12.94	-	0.22	99.70	0.67	0.46
zf048-50-opx4-CORE1	**P2**	-		40.20	-	0.06	42.13	25.41	0.04	0.03	16.45	12.79	0.04	0.23	99.15	0.67	1.00
zf044-39-opx1-CORE1	**P2**	2.18	1.15	53.34	0.28	22.51	15.65	9.44	0.44	0.30	5.36	4.17	0.31	0.27	100.35	0.69	0.21
zf048-45-opx1-CORE1	**P2**	1.60	0.85	55.26	0.09	0.43	30.34	18.30	0.53	0.36	11.22	8.72	0.03	0.26	99.76	0.68	0.30
zf048-45-opx1-rim1	**P2**	1.42	0.75	55.18	0.08	0.65	30.10	18.16	0.47	0.32	11.10	8.63	0.02	0.26	99.28	0.68	0.30
zf048-45-opx1-rim2	**P2**	1.73	0.91	55.17	0.14	3.88	28.24	17.03	0.67	0.46	9.85	7.66	0.08	0.24	100.00	0.69	0.34
zf048-45-opx2-core1	**P2**	1.56	0.83	55.27	0.10	1.12	30.24	18.24	0.53	0.36	10.71	8.32	0.04	0.18	99.75	0.69	0.30
zf048-45-opx2-rim1	**P2**	1.66	0.88	54.85	0.09	0.60	29.57	17.84	0.54	0.37	11.24	8.74	0.01	0.26	98.81	0.67	0.29
zf048-45-opx2-rim2	**P2**	1.50	0.79	55.41	0.10	0.48	30.17	18.20	0.54	0.37	11.15	8.67	0.03	0.28	99.65	0.68	0.32
zf048-45-opx4-core1	**P2**	0.85	0.45	55.89	0.18	0.75	29.55	17.82	0.45	0.31	11.02	8.57	0.02	0.28	99.00	0.68	0.41
zf048-45-opx4-core2	**P2**	1.16	0.61	55.24	0.15	1.51	29.54	17.82	0.53	0.36	11.03	8.57	0.00	0.27	99.44	0.68	0.37
zf048-45-opx4-rim1	**P2**	0.93	0.49	55.72	0.18	0.82	30.47	18.38	0.35	0.24	11.16	8.67	0.02	0.26	99.90	0.68	0.32
zf048-45-opx5-core1	**P2**	1.72	0.91	55.47	0.08	1.30	29.70	17.91	0.53	0.36	10.98	8.53	0.04	0.29	100.10	0.68	0.29

zf048-45-opx5-core2	**P2**	1.80	0.95	55.31	0.11	1.77	29.08	17.54	0.55	0.38	10.53	8.19	0.05	0.26	99.46	0.68	0.28
zf048-45-opx5-rim1	**P2**	1.04	0.55	56.26	0.16	1.38	29.93	18.05	0.52	0.36	10.73	8.34	0.04	0.28	100.35	0.68	0.39
zf048-45-opx5-rim2	**P2**	1.26	0.67	55.63	0.12	0.96	29.58	17.84	0.49	0.34	10.70	8.32	0.03	0.25	99.03	0.68	0.33
zf057-44-opx1-CORE1	**P3**	1.14	0.61	55.78	0.12	0.74	28.20	17.01	0.33	0.23	13.45	10.45	-	0.31	100.08	0.62	0.27
zf057-44-opx1-CORE2	**P3**	1.70	0.90	55.31	0.17	1.04	27.97	16.87	0.57	0.39	13.20	10.26	0.03	0.29	100.27	0.62	0.30
zf057-44-opx1-RIM1	**P3**	1.07	0.57	55.77	0.23	2.24	27.66	16.68	0.35	0.24	12.54	9.75	0.04	0.32	100.21	0.63	0.29
zf057-44-opx1-RIM2	**P3**	1.23	0.65	55.83	0.20	0.86	28.34	17.09	0.41	0.28	13.31	10.35	0.05	0.27	100.49	0.62	0.30
zf057-44-opx2-CORE1	**P3**	1.32	0.70	55.49	0.10	1.75	28.49	17.18	0.43	0.29	11.31	8.79	0.05	0.28	99.22	0.66	0.30
zf057-44-opx2-CORE2	**P3**	1.65	0.87	54.74	0.14	3.04	27.81	16.77	0.60	0.41	11.36	8.83	0.10	0.25	99.69	0.66	0.32
zf057-44-opx2-RIM1	**P3**	1.83	0.97	55.43	0.14	0.64	28.70	17.31	0.47	0.32	12.87	10.00	0.05	0.27	100.41	0.63	0.25
zf057-44-opx2-RIM2	**P3**	1.16	0.61	55.36	0.11	0.66	29.03	17.51	0.26	0.18	12.75	9.91	0.03	0.31	99.66	0.64	0.22
zf057-44-opx3-CORE1	**P3**	1.24	0.65	55.19	0.19	1.81	28.32	17.08	0.34	0.23	12.47	9.69	0.03	0.27	99.85	0.64	0.26
zf057-44-opx3-CORE2	**P3**	30.97	16.39	51.13	0.04	14.47	0.05	0.03	-		0.20	0.16	3.37	-	100.23	0.16	0.00
zf057-44-opx3-RIM1	**P3**	1.21	0.64	56.11	0.20	0.79	28.60	17.25	0.40	0.28	12.90	10.03	0.06	0.28	100.56	0.63	0.30
zf057-44-opx3-RIM2	**P3**	1.15	0.61	55.14	0.22	1.28	28.60	17.25	0.38	0.26	12.62	9.81	0.03	0.28	99.70	0.64	0.30
zf057-44-opx4-CORE1	**P3**	1.32	0.70	54.81	0.20	0.71	27.62	16.66	0.47	0.32	14.12	10.98	0.01	0.35	99.62	0.60	0.32
zf057-44-opx4-RIM1	**P3**	0.96	0.51	55.12	0.14	0.72	27.52	16.60	0.30	0.20	14.50	11.27	0.04	0.35	99.65	0.60	0.29
zf057-44-opx5-CORE1	**P3**	1.89	1.00	54.59	0.13	1.93	26.89	16.22	0.57	0.39	13.21	10.27	0.08	0.31	99.59	0.61	0.28
zf057-44-opx6-CORE1	**P3**	1.06	0.56	55.81	0.07	0.39	28.82	17.38	0.28	0.19	12.85	9.99	0.02	0.32	99.62	0.64	0.25
zf057-44-opx6-CORE2	**P3**	1.24	0.65	55.26	0.08	2.03	28.32	17.08	0.37	0.26	12.04	9.36	0.07	0.27	99.67	0.65	0.28
zf057-44-opx6-RIM1	**P3**	1.48	0.78	54.50	0.12	1.39	28.30	17.07	0.39	0.27	12.74	9.90	0.08	0.19	99.19	0.63	0.25
zf057-44-opx6-RIM2	**P3**	31.48	16.66	50.50	0.03	15.23	0.03	0.02	-		0.21	0.17	3.10	0.00	100.59	0.09	0.00
zf078-15-opx1-CORE1	**P3**	1.30	0.69	55.50	0.13	0.70	28.66	17.29	0.44	0.30	12.42	9.65	0.01	0.36	99.50	0.64	0.30
zf078-15-opx1-RIM1	**P3**	1.13	0.60	55.18	0.12	1.66	28.32	17.08	0.41	0.28	12.07	9.38	0.06	0.30	99.24	0.65	0.32
zf078-15-opx2-CORE1	**P3**	1.30	0.69	55.06	0.15	2.21	27.45	16.56	0.36	0.25	12.59	9.79	0.07	0.35	99.56	0.63	0.27
zf078-15-opx2-RIM1	**P3**	1.15	0.61	55.03	0.19	1.87	27.48	16.58	0.36	0.25	12.60	9.79	0.04	0.30	99.01	0.63	0.29
zf078-15-opx3-CORE1	**P3**	1.76	0.93	53.87	0.08	1.86	26.98	16.27	0.53	0.36	13.22	10.28	0.01	0.35	98.65	0.61	0.28
zf078-15-opx3-CORE2	**P3**	1.23	0.65	54.61	0.23	1.21	26.94	16.25	0.39	0.26	14.00	10.88	0.01	0.28	98.90	0.60	0.29
zf078-15-opx4-CORE1	**P3**	1.49	0.79	55.44	0.12	2.27	28.24	17.03	0.47	0.32	11.84	9.20	0.04	0.25	100.16	0.65	0.29
zf078-15-opx4-RIM1	**P3**	2.18	1.15	53.15	0.54	23.29	15.77	9.51	0.57	0.39	4.52	3.51	0.36	0.21	100.60	0.73	0.25
zf078-15-opx5-CORE1	**P3**	1.32	0.70	55.45	0.08	1.66	28.74	17.34	0.35	0.24	11.79	9.16	-	0.31	99.69	0.65	0.25

zf078-15-opx5-RIM1	**P3**	2.09	1.11	54.34	0.21	0.77	27.95	16.86	0.50	0.34	12.70	9.87	0.03	0.27	98.86	0.63	0.23
zf078-15-opx5-RIM2	**P3**	1.98	1.05	54.33	0.14	0.85	28.36	17.11	0.53	0.36	12.81	9.96	0.01	0.27	99.28	0.63	0.26
zf078-15-opx6-CORE1	**P3**	0.79	0.42	54.89	0.21	0.83	27.69	16.70	0.20	0.14	14.16	11.01	0.02	0.38	99.17	0.60	0.25
ZF078-6-opx1-CORE1	**P4**	0.64	0.34	52.98	0.22	1.07	20.27	12.23	0.01	0.01	24.40	18.97	0.03	0.69	100.31	0.39	0.02
ZF078-6-opx1-CORE2	**P4**	0.72	0.38	52.88	0.21	0.92	20.50	12.36	-		24.48	19.03	0.00	0.67	100.38	0.39	0.00
ZF078-6-opx1-RIM1	**P4**	0.62	0.33	53.53	0.17	1.07	20.27	12.23	0.01	0.01	23.96	18.62	0.02	0.66	100.30	0.40	0.03
ZF078-6-opx1-RIM2	**P4**	0.47	0.25	53.54	0.15	0.79	20.21	12.19	0.00	0.00	24.63	19.15	0.04	0.71	100.56	0.39	0.00
ZF078-6-opx2-CORE2	**P4**	0.65	0.34	52.84	0.20	0.77	19.34	11.67	0.05	0.04	24.70	19.20	-	0.70	99.25	0.38	0.10
ZF078-6-opx2-RIM1	**P4**	0.68	0.36	51.90	0.14	1.28	19.07	11.50	-		25.20	19.59	0.05	0.74	99.06	0.37	0.00

Table 28: Representative compositions for Clinopyroxene.

SAMPLE ID	UNIT	SiO2	Na2O	TiO2	FeO	Al2O3	MgO	Cr2O3	CaO	MnO	K2O	Total
ZF044-47	**P1**	51.38	0.312	0.299	9.800	2.690	15.500	0.525	19.800	0.285	0.007	100.597
ZF044-47	**P1**	51.26	0.435	0.289	9.320	2.720	15.580	0.565	20.170	0.264	0.006	100.608
ZF044-47	**P1**	51.61	0.380	0.290	9.310	2.720	15.990	0.556	19.660	0.301	-	100.817
ZF078-47-CPX1-CORE2	**P1**	51.75	0.374	0.299	8.560	2.610	16.430	0.749	19.240	0.198	0.016	100.225
ZF078-47-CPX1-CORE3	**P1**	51.36	0.463	0.351	7.550	2.760	15.020	0.881	21.790	0.211	0.013	100.399
ZF078-47-CPX1-RIM2	**P1**	52.7	0.321	0.188	7.390	0.933	15.570	0.250	23.080	0.197	0.055	100.684
ZF078-47-CPX2-RIM	**P1**	51.97	0.333	0.321	9.080	1.853	15.540	0.422	20.740	0.261	0.003	100.523
ZF078-47-CPX2-RIM1	**P1**	51.9	0.367	0.297	8.880	2.250	16.000	0.565	20.050	0.279	0.004	100.592
ZF078-47-CPX1-CORE2	**P1**	52.46	0.208	0.122	6.850	1.195	15.760	0.231	23.830	0.188	0.013	100.857
ZF078-47-CPX3-CORE1	**P1**	52.49	0.331	0.313	8.330	1.478	15.180	0.425	22.150	0.280	0.001	100.978
ZF078-47-CPX3-CORE2	**P1**	52.12	0.340	0.249	9.010	1.786	15.920	0.550	20.340	0.221	0.016	100.552
ZF048-48-CPX1-CORE1	**P2**	53.3	0.507	0.186	5.220	2.630	16.790	1.172	20.310	0.151	0.071	100.337
ZF044-39-CPX1-CORE1	**P2**	52.56	0.339	0.263	5.980	2.170	16.010	0.358	22.270	0.315	0.008	100.273
ZF044-39-CPX1-CORE2	**P2**	51.55	0.387	0.306	6.360	2.860	15.930	0.576	22.060	0.297	0.019	100.345
ZF044-39-CPX2-CORE1	**P2**	51.7	0.330	0.189	7.290	2.740	18.550	0.574	17.100	0.295	0.029	98.796
ZF044-39-CPX2-CORE2	**P2**	51.9	0.314	0.270	6.590	2.980	16.370	0.559	21.050	0.203	0.010	100.246
ZF044-39-CPX2-CORE3	**P2**	52.02	0.368	0.279	6.870	3.180	16.750	0.625	19.860	0.301	0.013	100.266
ZF044-39-CPX2-RIM1	**P2**	52.04	0.340	0.283	6.750	2.960	16.620	0.562	20.220	0.300	0.020	100.094
ZF044-39-CPX3-CORE1	**P2**	52.31	0.412	0.277	5.930	2.480	15.930	0.656	21.880	0.236	0.008	100.119
ZF044-39-CPX3-CORE2	**P2**	52.29	0.340	0.196	5.790	2.510	15.990	0.601	22.680	0.260	0.043	100.699
ZF044-39-CPX3-CORE3	**P2**	53.34	0.149	0.093	12.280	2.460	24.470	0.477	7.130	0.313	0.043	100.754
ZF044-39-CPX3-RIM1	**P2**	52.19	0.386	0.257	5.760	2.560	16.340	0.661	22.170	0.274	0.017	100.615
ZF044-39-CPX3-RIM2	**P2**	53	0.304	0.277	5.750	1.980	15.770	0.459	22.730	0.275	0.011	100.556
ZF044-39-CPX3-RIM3	**P2**	52.13	0.308	0.292	7.040	2.700	17.060	0.500	20.030	0.277	0.006	100.342
ZF044-39-CPX3-RIM4	**P2**	52.05	0.335	0.162	7.810	2.760	17.310	0.508	19.180	0.333	0.031	100.479
ZF044-39-CPX3-RIM5	**P2**	51.99	0.370	0.215	6.780	2.960	15.840	0.518	20.970	0.208	0.035	99.886
ZF057-25-CPX1-CORE1	**P3**	56.18	0.163	0.124	7.890	1.578	20.620	0.113	12.610	0.208	0.108	99.593

ZF057-25-CPX1-CORE2	**P3**	53.58	0.138	0.073	5.530	0.435	16.310	0.113	24.470	0.187	0.014	100.849
ZF057-25-CPX2-CORE2	**P3**	56.35	0.139	0.190	6.970	1.238	20.980	0.081	12.680	0.218	0.061	98.907
ZF078-15-CPX1-CORE1	**P3**	52.1	0.331	0.501	4.990	2.030	16.010	0.552	22.910	0.199	0.031	99.653
ZF078-15-CPX1-RIM1	**P3**	51.95	0.348	0.468	4.900	2.010	16.100	0.583	23.400	0.180	0.048	99.987
ZF078-6-CPX2-CORE3	**P4**	53.39	0.315	0.061	10.770	0.581	13.660	0.022	21.520	0.435	0.025	100.779
ZF078-6-CPX3-CORE1	**P4**	53.05	0.302	0.157	10.370	0.725	13.620	-	21.420	0.364	0.028	100.035
ZF078-6-CPX4-CORE1	**P4**	52.82	0.314	0.213	10.830	0.922	13.900	0.029	21.240	0.315	0.012	100.595
ZF078-6-CPX4-RIM1	**P4**	53.19	0.331	0.085	10.480	0.732	13.600	0.025	21.040	0.383	0.014	99.878
ZF078-6-CPX6-CORE1	**P4**	52.97	0.302	-	10.180	0.577	13.800	0.007	21.980	0.361	0.051	100.227
ZF078-6-CPX6-CORE2	**P4**	52.99	0.279	0.093	10.090	0.619	13.820	-	21.940	0.315	0.020	100.167
ZF078-6-CPX6-RIM1	**P4**	53.72	0.188	0.028	9.590	0.260	14.080	0.024	22.390	0.348	0.057	100.683
ZF078-6-CPX7-CORE1	**P4**	53.53	0.312	0.088	9.940	0.537	13.590	0.046	21.620	0.327	0.023	100.013
ZF078-6-CPX7-RIM1	**P4**	53.07	0.262	0.019	9.600	0.482	13.820	0.008	21.850	0.352	0.040	99.502

Table 29: Representative compositions for Plagioclase.

SAMPLE I.D	Unit	SiO2	Al2O3	TiO2	CaO	Ca	MgO	MnO	FeO	Na2O	Na	K2O	K	Total	An%
ZF057-44-PLAG1-CORE1	**P3**	51.94	30.68	0.0518	12.8	9.148032	0.008	0.0387	0.2281	3.65	2.707789	0.2781	0.230865	99.6748	75.68685
ZF057-44-PLAG1-RIM1	**P3**	53.67	29.78	0.0517	11.54	8.247523	0.0455	0.0349	0.2363	4.16	3.086138	0.3559	0.29545	99.8743	70.92135
ZF057-44-PLAG2-CORE1	**P3**	51.93	30.74	0.0331	12.82	9.162326	0.0275	0.0183	0.3641	3.52	2.611347	0.2489	0.206624	99.7019	76.47828
ZF057-44-PLAG2-RIM1	**P3**	51.88	30.35	0.0201	12.56	8.976506	-	0.0206	0.3088	3.83	2.841324	0.2882	0.239249	99.2578	74.45009
ZF057-44-PLAG3-RIM1	**P3**	52.11	30.32	0.0257	12.42	8.87645	0.005	0.074	0.2025	3.76	2.789394	0.233	0.193425	99.1503	74.84821
ZF057-46-PLAG1-RIM1	**P3**	52.14	30.67	0.0333	12.84	9.17662	-	0.0124	0.2336	3.67	2.722626	0.2577	0.21393	99.857	75.75734
ZF057-46-PLAG2-CORE1	**P3**	51.39	31.37	0.0194	13.64	9.748372	0.0041	0.0386	0.303	3.23	2.396208	0.2525	0.209613	100.2476	78.9074
ZF057-46-PLAG2-CORE2	**P3**	51.26	31.55	0.0067	13.42	9.59114	0.0012	0.016	0.2769	3.23	2.396208	0.2675	0.222065	100.0282	78.55529
ZF057-46-PLAG2-RIM1	**P3**	50.63	31.95	0.0041	13.92	9.948485	0.0037	0.1043	0.2073	3.16	2.344278	0.2199	0.18255	100.1992	79.74538
ZF057-46-PLAG2-RIM2	**P3**	51.87	30.89	0.0316	13.18	9.419614	0.0025	0.0511	0.2396	3.51	2.603929	0.3311	0.274863	100.1059	76.59216
ZF057-25-PLAG4-CORE1	**P3**	52.37	30.85	0.0039	12.63	9.026535	0.0036	0.0391	0.2453	3.88	2.878417	0.1526	0.126681	100.1744	75.02336
ZF078-15-PLAG1-CORE1	**P3**	54.53	29.07	0.1834	10.83	7.740093	0.0323	0.0644	0.149	4.6	3.412556	0.3964	0.329071	99.8556	67.41231
ZF078-6-PLAG4-CORE1	**P4**	49.37	32.7	-	14.57	10.41303	0.0395	0.0211	0.3105	2.36	1.75079	0.2023	0.167939	99.5735	84.44076
ZF078-6-PLAG4-RIM1	**P4**	51.87	31	0.0451	13.22	9.448202	0.042	0.0565	0.2036	3.16	2.344278	0.3263	0.270878	99.9236	78.32149
ZF078-6-PLAG5-CORE1	**P4**	48.84	32.19	-	14.96	10.69176	0.0329	-	0.2095	2.38	1.765627	0.176	0.146106	98.7885	84.83172
ZF078-6-PLAG5-CORE2	**P4**	49.32	32.76	-	14.88	10.63459	0.0367	-	0.2337	2.4	1.780464	0.2093	0.17375	99.8398	84.47657
ZF078-6-PLAG5-RIM1	**P4**	47.68	33.05	-	15.5	11.0777	0.09	0.0963	0.3244	2.32	1.721115	0.1378	0.114395	99.1985	85.78579
ZF078-6-PLAG5-RIM2	**P4**	49.41	33.06	0.0022	14.76	10.54882	0.0175	-	0.2814	2.32	1.721115	0.18	0.149427	100.0311	84.93851

Table 30: Representative compositions for Chromitite.

SAMPLE I.D	UNIT	MgO	TiO2	FeO	Al2O3	Al	Cr2O3	Cr	NiO	MnO	Total	Cr/ (Cr + AL)
ZF044-55	**P1**	4.8	1.95	52.66	9.46	5.01	29.68	20.31	0.17	0.45	99.17	0.80
ZF044-55	**P1**	4.76	1.8	53.48	9.41	4.98	29.93	20.48	0.20	0.56	100.14	0.80
ZF044-55	**P1**	4.94	1.79	52.8	9.6	5.08	29.75	20.36	0.25	0.51	99.64	0.80
ZF044-55	**P1**	4.84	1.97	53.42	9.1	4.82	29.18	19.97	0.17	0.46	99.14	0.81
ZF044-55	**P1**	4.85	1.94	53.6	9.24	4.89	29.16	19.95	0.12	0.48	99.39	0.80
ZF044-55	**P1**	4.95	1.98	53.67	9.47	5.01	28.9	19.77	0.07	0.53	99.57	0.80
ZF044-55	**P1**	4.95	1.86	53.17	9.38	4.96	29.82	20.40	0.13	0.53	99.84	0.80
ZF044-55	**P1**	4.75	2.08	54.24	9.03	4.78	29.42	20.13	0.16	0.43	100.12	0.81
ZF044-55	**P1**	4.47	1.81	53.82	9.18	4.86	29.51	20.19	0.12	0.47	99.38	0.81
ZFO78-49	**P1**	7.4	1.5477	36.95	14.96	7.92	39.35	26.93	0.15	0.56	100.91	0.77
ZFO78-49	**P1**	7.32	1.5054	37.05	14.63	7.74	39.57	27.08	0.05	0.49	100.61	0.78
ZFO78-49	**P1**	7.45	1.5333	36.89	14.93	7.90	39.1	26.75	0.02	0.59	100.51	0.77
ZFO78-49	**P1**	6.98	1.4652	37.45	13.22	7.00	40.83	27.94	0.04	0.58	100.57	0.80
ZFO78-49	**P1**	7.06	1.2978	37.64	13.57	7.18	40.15	27.47	0.04	0.54	100.29	0.79

Appendix E: Rare Earth Element Data

Table 31: Rare earth elements data for selected samples from Boreholes ZF044, ZF078 and MO023.

Sample ID	ZF044-47	ZF078-21	MO023-39	MO023-42	ZF078-34	ZF078-39	ZF078-49	ZF078-22	ZF044-32	ZF057-29	ZF078-52	MO023-46	MO023-47	ZF078-15	ZF057-54	ZF044-51	ZF044-43	ZF044-57	ZF044-58	ZF078-28	ZF044-34
Unit	**P1**	**P1**	**P1**	**P1**	**P1**	**P1**	**P1**	**P1**	**P2**	**P2**	**P2**	**P3**	**P3**	**P3**	**P3**	**P3**	**P4**	**P4**	**P4**	**P4**	**P4**
La	1.85	8.18	2.62	3.24	3.4	3.09	2.47	3.55	1.85	1.08	7.72	2.31	2.47	4.78	12.81	2.01	4.17	7.56	15.43	9.26	6.79
Ce	1.37	6.69	2.09	2.39	2.99	2.99	1.85	3.4	1.67	1.01	7.4	1.61	1.55	3.28	9.25	1.55	4	6.03	15.16	7.94	5.97
Pr	1.38	5.35	1.77	1.97	2.64	2.64	1.57	3.03	1.61	0.98	6.42	1.26	1.14	2.28	7.01	1.34	3.66	5.67	15.04	7.17	5.47
Nd	1.36	4.64	1.52	1.44	2.24	2	1.44	3.52	1.6	0.96	5.28	1.28	0.8	1.76	5.28	1.12	3.52	5.44	14	6.88	5.12
Sm	1.13	3.72	1.21	1.13	2.09	2.22	0.84	2.64	1.01	0.67	3.74	0.71	0.84	1.35	3.33	0.99	2.73	4.11	9.85	4.63	3.82
Eu	0.91	2.34	0.78	0.91	1.49	1.3	0.71	1.82	0.84	0.45	2.4	0.84	0.84	1.56	2.73	1.3	2.08	3.05	4.03	3.7	2.73
Gd	0.97	3.2	0.97	0.94	2.1	1.89	0.88	2.22	0.79	0.59	2.59	0.79	0.72	1.58	2.61	0.94	2.5	3.18	7.67	3.84	3.09
Tb	1.11	3.13	1.21	1.11	2.12	1.82	0.81	2.32	0.91	0.61	2.42	0.81	0.81	1.31	2.32	1.01	2.73	3.03	7.68	3.54	3.03
Dy	0.98	3	1.17	1.13	1.77	1.59	0.86	2.12	0.86	0.43	1.91	0.95	0.62	1.44	1.57	1.01	2.42	2.54	6.17	3.13	2.66
Ho	1.07	2.62	1.48	1.21	2.08	1.81	0.87	2.08	0.74	0.54	1.95	0.87	0.74	1.61	1.81	1.01	2.55	2.48	6.24	3.29	2.48
Er	1.21	2.79	1.64	1.16	2.03	1.64	0.96	2.21	0.78	0.64	1.96	0.8	0.75	1.42	1.89	1.19	2.01	2.6	5.96	2.79	2.42
Tm	1.03	2.94	1.91	1.32	2.06	1.76	1.03	2.06	0.74	0.74	1.91	1.03	0.88	1.62	1.76	1.18	2.35	2.06	5.59	2.79	2.35
Yb	1.25	3.27	2.04	1.66	2.24	1.56	1.02	2.22	0.73	1.02	1.84	1	0.98	1.86	2	1.34	2.02	2.24	5.71	2.52	2.27
Lu	1.62	3.09	2.21	1.47	2.21	2.06	1.18	2.21	0.59	0.74	1.76	1.03	1.03	1.91	1.91	1.18	1.91	1.91	5.29	2.79	2.21
Eu/Eu*	0.87	0.68	0.72	0.88	0.71	0.63	0.83	0.75	0.94	0.73	0.77	1.12	1.09	1.06	0.93	1.35	0.79	0.84	0.46	0.88	0.79
La/Yb	1.48	2.5	1.29	1.96	1.51	1.97	2.42	1.6	2.55	1.06	4.2	2.32	2.53	2.57	6.42	1.5	2.06	3.37	2.7	3.68	2.99
La/Sm	1.63	2.2	2.17	2.86	1.62	1.39	2.95	1.35	1.83	1.62	2.06	3.24	2.95	3.53	3.85	2.04	1.52	1.84	1.57	2	1.78
Ce/Yb	1.1	2.05	1.02	1.44	1.33	1.91	1.81	1.53	2.3	0.99	4.03	1.62	1.59	1.77	4.64	1.16	1.98	2.69	2.65	3.15	2.63
Ce/Sm	1.21	1.8	1.73	2.11	1.43	1.35	2.21	1.29	1.66	1.53	1.98	2.26	1.85	2.42	2.78	1.58	1.46	1.47	1.54	1.71	1.56
Eu/Yb	0.73	0.72	0.38	0.55	0.67	0.83	0.7	0.82	1.16	0.45	1.31	0.85	0.87	0.84	1.37	0.97	1.03	1.36	0.7	1.47	1.2
Sum_REE	8.87	33.06	11.72	11.99	16.77	15.49	9.64	19.94	8.91	5.77	32.67	8.75	7.85	16.05	38.89	8.95	21.86	31.89	77.23	39.92	30.67

Appendix F: Data Quality Control and Quality Assuarance

Table 32: Original and duplicate samples from borehole ZF082. Note that SA = Spotted Anothosite, FP= Feldspathic Pyroxenite, N=Norite, PP= Parapyroxenite.

Sample Id		**ZF082-S16**	**ZF082-S38**	**ZF082-S40**	**ZF082-S42**	**ZF082-14**	**ZF082-37**	**ZF082-52**	**ZF082-59**	**ZF082-60**
Lithology		**SA**	**FP**	**N**	**N**	**N**	**N**	**FP**	**FP**	**PP**
SiO_2 (wt.%)	**Original**	41.93	42.586	40.236	39.966	38.292	43.091	41.326	42.996	41.418
	Duplicate	42.66	42.623	40.162	39.936	38.329	43.25	41.297	42.94	41.312
Al_2O_3 (wt.%)	**Original**	23.84	15.028	9.82	16.872	11.54	6.986	10.448	26.438	2.351
	Duplicate	24.32	15.003	9.83	16.884	11.504	6.997	10.475	26.491	2.323
Fe_2O_3 (wt.%)	**Original**	5.03	7.536	12.218	9.557	11.976	11.521	11.716	1.857	15.579
	Duplicate	5.10	7.562	12.228	9.552	11.916	11.527	11.719	1.873	15.573
CaO (wt.%)	**Original**	17.41	12.719	6.942	10.403	9.325	6.402	9.798	14.616	3.129
	Duplicate	17.73	12.733	6.953	10.412	9.344	6.383	9.811	14.608	3.123
MgO (wt.%)	**Original**	4.58	13.522	17.403	9.646	11.677	22.225	14.232	1.343	30.3
	Duplicate	4.67	13.505	17.397	9.646	11.683	22.218	14.284	1.285	30.283
Cr (ppm)	**Original**	38.784	485.374	1466.821	753.2	63.276	2416.3	897.61	11.27	717.097
	Duplicate	29.56	497.938	1451.871	756.699	64.39	2410.257	901.904	18.427	717.734
Cu (ppm)	**Original**	74.426	75.574	1541.406	2833.042	99.883	494.645	1237.727	87.038	346.27
	Duplicate	73.228	81.074	1476.528	2847.929	95.684	486.594	1239.3	79.324	333.129
Ni (ppm)	**Original**	81.885	242.337	3442.647	6518.19	320.714	1103.209	2344.664	25.748	1363.557
	Duplicate	73.936	256.433	3458.327	6511.485	325.15	1082.775	2365.07	23.983	1361.689
Zn (ppm)	**Original**	64.705	108.039	82.577	62.207	112.939	133.309	102.659	37.802	254.759
	Duplicate	55.097	115.342	79.502	64.033	92.858	123.605	99.296	41.741	242.941